Nitrosyl complexes of Co(II) and Mn(II) porphyrins - Reactivity towards reactive oxygen species and utility as HNO donor

A dissertation submitted to the
Indian Institute of Technology Guwahati as
Partial fulfillment for the degree of
Doctor of Philosophy in Chemistry

Submitted by

Rakesh Mazumdar

(Roll No. 176122032)

Supervisor

Prof. Biplab Mondal

Department of Chemistry

Indian Institute of Technology Guwahati

June, 2022

Dedicated to My Parents
&
Teachers

STATEMENT

I hereby declare that this thesis entitled "**Nitrosyl complexes of Co(II) and Mn(II) porphyrins - Reactivity towards reactive oxygen species and utility as HNO donor**" is the outcome of research work carried out by me under the supervision of Prof. Biplab Mondal in the Department of Chemistry, Indian Institute of Technology Guwahati, India.

In keeping with the general practice of reporting scientific observations, due acknowledgements have been made wherever the work described is based on the findings of other investigators.

June, 2022 **Rakesh Mazumdar**

IIT Guwahati

भारतीय प्रौद्योगिकी संस्थान गुवाहाटी
INDIAN INSTITUTE OF TECHNOLOGY GUWAHATI
North Guwahati, Assam – 781039, India

Prof. Biplab Mondal
Department of Chemistry

Phone: + 91-361-258-2317
Fax: + 91-361-258-2349
E-mail: biplab@iitg.ernet.in

Certificate

This is to certify that **Mr. Rakesh Mazumdar** has been working under my supervision since July, 2017 as a regular Ph.D. student in the Department of Chemistry, Indian Institute of Technology Guwahati. I am forwarding his thesis entitled **"Nitrosyl complexes of Co(II) and Mn(II) porphyrins - Reactivity towards reactive oxygen species and utility as HNO donor"** being submitted for the Ph.D. degree.

I certify that he has fulfilled all the requirements according to the ordinance of this Institute regarding the investigations embodied in his thesis and this work has not been submitted elsewhere for a degree.

June, 2022

Biplab Mondal

Acknowledgement

At the outset, I would like to mention that behind the success of this wonderful expedition lies the contribution of many people I have come across at different stages of life. This is a humble attempt on my part to gracefully thank all such people who have stood by me during this odyssey. My sincere apologies in advance to those I failed to mention at this moment.

I want to express my most profound appreciation to my PhD supervisor, Prof. Biplab Mondal, for his unremitting guidance and support throughout my time at IIT Guwahati. Without his immense knowledge, motivation and patience, completing this endeavor would have been beyond possible. Apart from research, his ideas and wisdom will continue to succor in the hardship of life. Words cannot suffice the thankfulness I owe to him.

I'm incredibly grateful to my doctoral committee members, Prof. Gopal Das, Prof. Debasis Manna, and Dr. Animesh Das. Their guidance and constructive criticism helped pave the way for writing this thesis.

I would like to thank the Department of Chemistry and Central Instrument Facility, IITG, for providing instrument facilities and IITG for the financial support. My sincere thanks to all the faculty members and non-teaching staff of the Department of Chemistry, IITG, for their unrestrained help.

I have spent my most wonderful five years working in the CHEL004 lab. Thanks to my ever so helpful and cooperative seniors and labmates Kuldeep da, Soumen da, Baishakhi di, Dibya da, Sukanya, Shankhadeep, Bapan, Riya, Sayani and Bristi. You are always going to hold a special place in my heart. It would be unfair if I did not mention all the M.Sc. and summer project students who joined our lab for a short time but left lasting impressions.

My deepest gratitude to all my PhD colleagues for their help and support. Special mention to Arpita, Monikha, Shilpa ba and Sourav da. You made IITG more enjoyable and more memorable.

To all my teachers at every stage of life, I can never ever thank them enough for my words. Their teachings and guidance have helped me reach the stage where I belong today.

I would like to take this opportunity to thank the peoples with whom I grew up through the childhood and adulthood and remained friends till today. I am also very much thankful to the friends I made during my days at Cotton College and Gauhati University.

It is impossible to find words that would have been sufficient to thank my parents. Nothing can ever be at par with their sacrifice while raising me to this point in life. I love you. The same goes for my family members. Thank you for believing in me. I am lucky to have you all in my life.

I am incredibly honored and grateful for the successful submission of my thesis. It has been a beautiful life venture on the beautiful campus of IITG that will be cherished forever.

Rakesh Mazumdar

Indian Institute of Technology Guwahati

Contents

Synopsis

The thesis entitled "**Nitrosyl complexes of Co(II) and Mn(II) porphyrins - Reactivity towards reactive oxygen species and utility as HNO donor**" is divided into five chapters.

Chapter 1: Introduction

Peroxynitrite

Nitric oxide (NO) mediates several physiological processes ranging from regulation of cardiovascular function to signal transduction and defense processes of the immune system at a very low concentration. In contrast, slightly higher concentration may result in serious pathological consequences.[1-3] *In vivo*, NO is produced *via* oxidation of L-arginine to L-citrulline by nitric oxide synthase (NOS) enzyme or by reduction of nitrite (NO_2^-) by nitrite reductase (NiR) enzyme. NO, by virtue of its unpaired electron at π^* orbital, can react with reactive oxygen species (ROS) such as superoxide ion (O_2^-) to produce secondary reactive nitrogen species (RNS) like peroxynitrite ($ONOO^-$, PN).[4-6] Biologically, the concentration of O_2^- is kept low to a nanomolar or picomolar level by superoxide dismutase (SOD) enzyme. When NO is produced at a sufficiently higher concentration to outcompete SOD, it reacts with O_2^- at a diffusion-controlled rate to form PN, which is known to show many adverse effects, e.g., oxidation or nitration of proteins, lipids and DNA.[7,8]

The protein tyrosine nitration is one of the key events of PN cytotoxicity and has been suggested as a specific biomarker for the presence of PN in biological systems.[9] This event can significantly disrupt functions of many enzymes having a redox active metal and a nearby tyrosine group. Studies have suggested that this particular process proceeds through a radical mechanism where NO_2 forms as an intermediate (Scheme S1).[10] The process is often mimicked using electron rich phenols such as 2,4-di-*tert*-butyl-phenol.

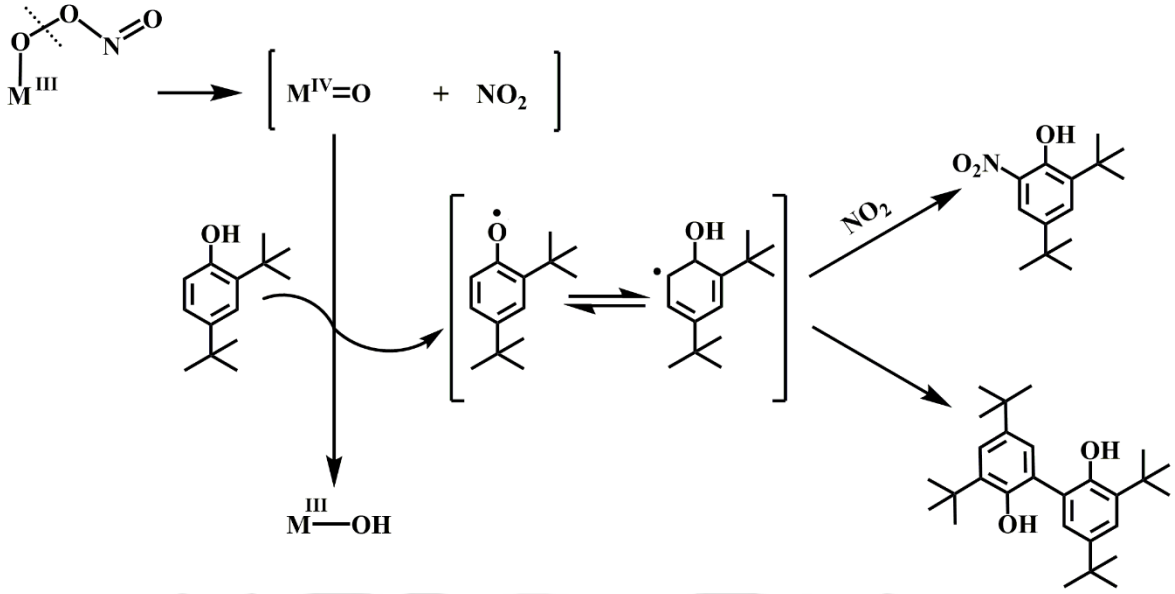

Scheme S1. Nitration of phenol ring by metal-PN complex.

The intracellular concentration of NO in biological systems is regulated by an enzyme called nitric oxide dioxygenase (NOD). In NOD activity, a [Fe(III)-O_2^-] complex reacts with NO to result in a biologically benign nitrate (NO_3^-) ion. This reaction is proposed to proceed *via* a [Fe(III)-PN] intermediate. The PN intermediate further gives an oxo-ferryl, [Fe(IV)=O] species and NO_2 *via* homolytic cleavage of O−O bond, followed by recombination to give NO_3^- (Scheme S2).[11]

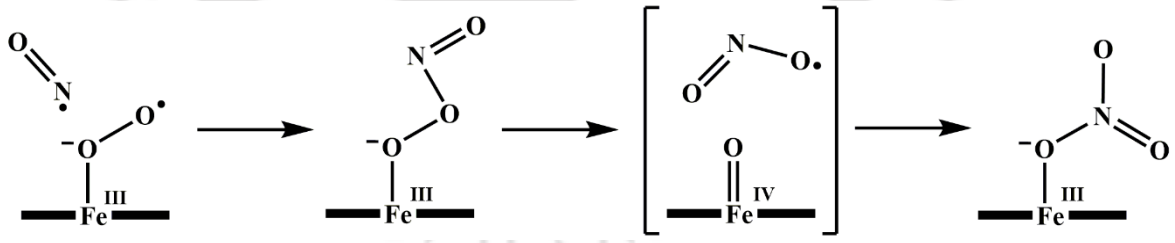

Scheme S2. Mechanism of nitric oxide dioxygenase.

Although a few studies have shown reaction of hemoglobin/myoglobin with PN resulting phenol ring nitration, in most of the reports, one or another synthetic PN complexes has been used to study metal center assisted phenol ring nitration. A metal PN complex may be synthesized *via* two pathways, either by the reaction of a metal nitrosyl complex with

reactive oxygen species (ROS); or a metal superoxo or peroxo complex may react with NO to give corresponding metal PN complex.[12] Limited numbers of PN complexes of transition metals have been exemplified in literature and spectroscopically characterized discrete PN complexes is scarce.

Nitroxyl

Nitroxyl or HNO is one electron reduced counterpart of NO which takes part in physiological processes like bacterial nitric oxide reductase, mitochondrial aldehyde dehydrogenase and thiol oxidation etc. HNO is highly reactive and undergoes spontaneous dimerization to produce nitrous oxide (N_2O) and water.[13] It reacts with thiols to give disulphide or sulphinamide;[14] with phosphines to produce phosphine oxide and aza-ylide;[15] and with metals and metalloproteins to result in reductive nitrosylation.[16]

Direct reduction of NO to HNO is a highly energy demanding process {$E(NO/NO^-) = -0.8$ ($\pm$ 0.2) V *vs.* NHE}. Endogenous production of HNO involves reduction of NO by cytochrome *c* oxidase, xanthine oxidase and hemoglobin, reaction of S-nitrosothiol with excess thiol and mostly NOS mediated oxidation of L-arginine in absence of tetrahydrobiopterin.[17] In laboratory, it is synthesized from common precursors like Angeli's salt, Piloty's acid, acyl or acyloxy nitroso compounds and cyanamide.[18] Another pathway of HNO production involves reduction of NO *via* a proton coupled electron transfer pathway involving a transition metal ion (Scheme S3). Such a process involves formation of a metal nitrosyl complexes of {M(NO)}$^{7-9}$ configuration and requires metal ion with higher 'd' electron density.[19]

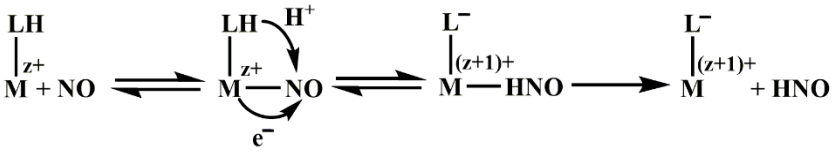

Scheme S3. Reduction of NO to HNO *via* proton couple electron transfer.

The present thesis originates from our interest to explore the reactivity of transition metal nitrosyl complexes with reactive oxygen species and their utility as HNO donor. The second chapter describes the reaction of a $\{Co(NO)\}^8$ complex with O_2^- which gives a $[Co^{II}(NO)(O_2^-)]$ intermediate followed by a [Co(II)-PN]. In the third chapter, formation of Co(III)-porphyrin cation radical was evidenced spectroscopically which confirms the involvement of a [Co(IV)=O] in the decomposition of a [Co(III)-PN] intermediate. In the fourth chapter, we got direct spectroscopic evidence for a [Mn(IV)=O] which forms in the decomposition of a [Mn(III)-PN] intermediate. In the final chapter, we reported the first example of a $\{Mn(NO)\}^6$ complex which has HNO donation ability.

Chapter 2: Reaction of a nitrosyl of Co(II) porphyrin complex with superoxide: Formation of a six coordinated $[Co^{II}(NO)(O_2^-)]$ species followed by peroxynitrite intermediate

A Co(II) porphyrinate complex, $[Co^{II}(F_{20}TPP^{2-})]$, **1** {$F_{20}TPPH_2$ = 5,10,15,20-*tetrakis*(pentafluorophenyl)porphyrin} was synthesized and characterized both spectroscopically and structurally.[20] The corresponding nitrosyl complex $[Co(F_{20}TPP^{2-})(NO)]$, **2** was synthesized by bubbling NO gas through a dry and degassed CH_2Cl_2 solution of complex **1**. The UV-visible, FT-IR and ^1H NMR spectroscopic characterization suggested that it has $\{Co(NO)\}^8$ electronic configuration. The characteristic nitrosyl stretching frequency for complex **2** appears at 1713 cm^{-1} in FT-IR spectrum.[21] X-ray crystal structure revealed that it is a bent cobalt nitrosyl with Co-N-O bond angle of 123(2)°; and N-O and Co-N bond distances of 1.01(3) Å and 1.97(2) Å, respectively (Figure S1). The bond distances are slightly deviated from previously reported analogous compounds owing to the presence of highly electron withdrawing ligand framework.[12c,e] The NO group exhibits eight-fold degeneracy around the C_4 symmetry axis and above and below

the σ_h plane, which was observed in some earlier examples.

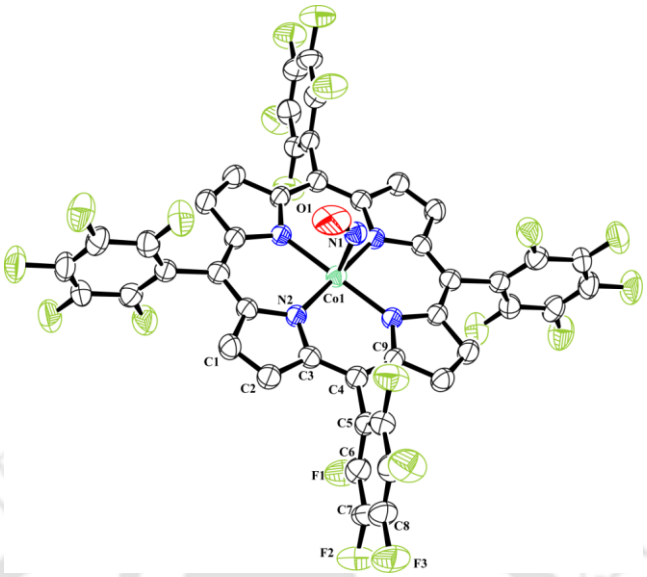

Figure S1. ORTEP diagram of complex **2** (30% thermal ellipsoid plot, H-atoms and solvent molecules are omitted for clarity; only one of the eight equivalent positions of NO groups are shown).

When complex **2** was made to react with superoxide, O_2^- at −40 ºC in CH_2Cl_2 the corresponding Co(III) nitrito complex [$Co^{III}(F_{20}TPP^{2-})(NO_2)$], **3** was obtained along with O_2. Formation of complex **3** was confirmed in UV-visible, FT-IR, ^{1}H NMR spectroscopy and ESI-MS. The single crystal X-ray structure of the complex was also obtained (Figure S2). Formation of O_2 was confirmed by alkaline pyrogallol test.

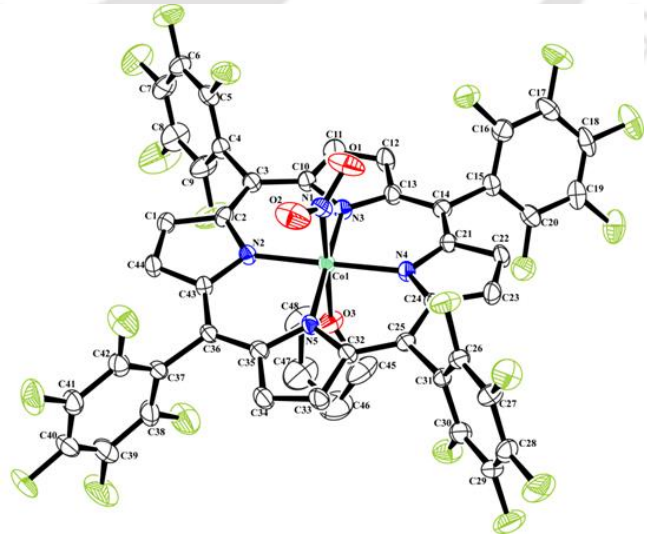

Figure S2. ORTEP diagram of complex **3** (30% thermal ellipsoid plot, H-atoms and solvent molecules are omitted for clarity).

When the reaction was monitored in UV-visible spectroscopy at −40 ºC, the Soret band of complex **2** at 394 nm gradually diminished with concomitant generation of a new Soret band at 425 nm which finally shifted to 433 nm corresponding complex **3** (Figure S3). The intermediate peak at 425 nm is attributed to a six coordinated [$Co^{II}(NO)(O_2^-)$] species **2a** (Scheme S4).[22] This species has odd number of electrons and accordingly EPR active. Moreover, a peak at m/z 1092.83 (Calcd. m/z 1076.97) corresponding to [$Co(F_{20}TPP^{2-})(NO)(O_2^-)$] was detected in ESI-MS.

Decomposition of **2a** to **3** is expected to proceed *via* a [Co(II)-PN] intermediate. However, no spectroscopic evidence could be obtained owing to the high instability of the proposed intermediate. Therefore, the formation of the same was confirmed by customary phenol ring nitration test. In principle, a [Co(II)-PN] should give [Co(II)-NO_2^-] and O_2. But [Co(II)-NO_2^-] is thermally unstable and oxidizes to [Co(III)-NO_2^-] during work-up at room temperature (Scheme S4).

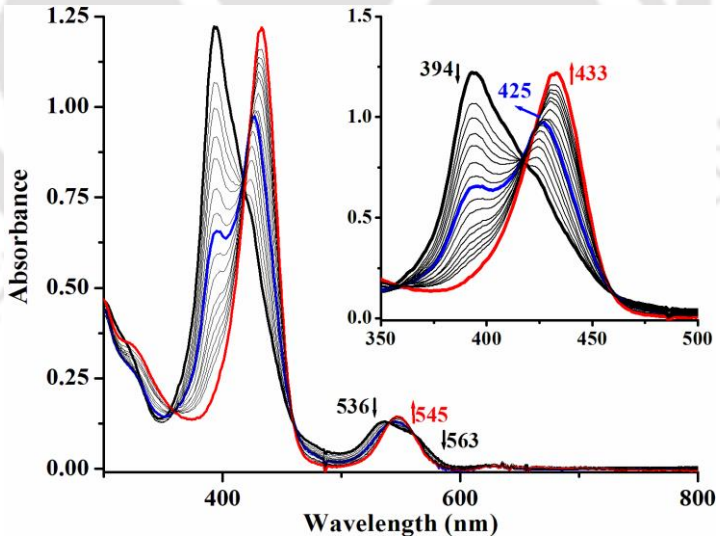

Figure S3. UV-visible spectral monitoring of complex **2** (black) and after addition of KO_2 to result in intermediate **2a** (blue) and complex **3** (red) at −40 °C in CH_2Cl_2 (scan rate 0.5 s/scan, only a few selected spectra were shown for clarity).

In conclusion, a nitrosyl complex of Co(II) porphyrinate, **2** reacts with O_2^- to result in a six-

coordinated [$Co^{II}(NO)(O_2^-)$] species, which then decomposes to the corresponding nitrito complex **3** *via* a putative [Co(II)-PN] intermediate.

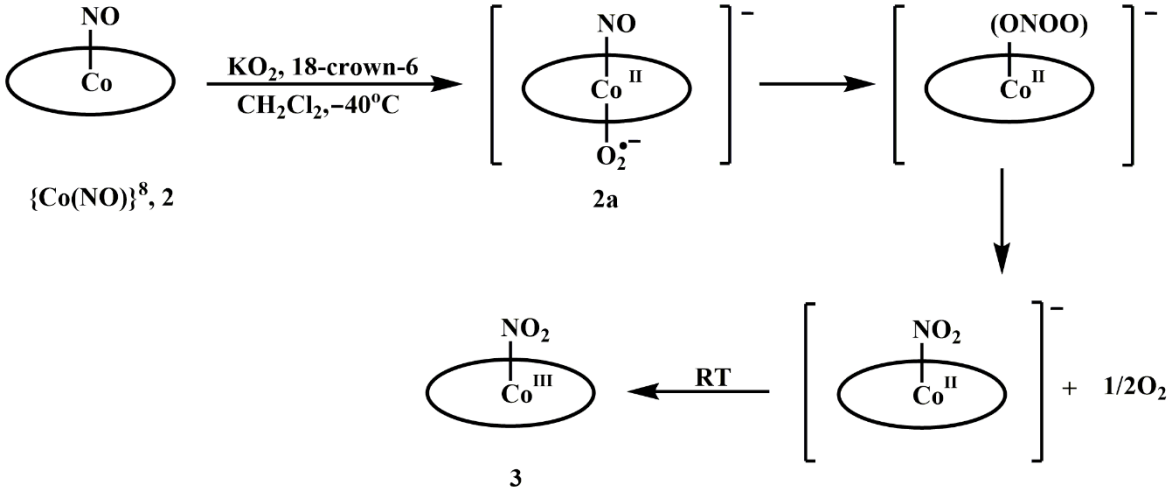

Scheme S4. Reaction of complex **2** with O_2^-.

Chapter 3: Reaction of nitrosyls of Co(II) porphyrins with H_2O_2: Formation of Co(III) porphyrin radical cation

Two Co(II) porphyrinate complexes [$Co^{II}(MPTPP^{2-})$], **5** {$MPTPPH_2$ = 5-(4-methoxyphenyl)-10,15,20-triphenylporphyrin} and [$Co^{II}(TMPP^{2-})$], **6** {$TMPPH_2$ = 5,10,15,20-*tetrakis*(4-methoxyphenyl)porphyrin} are prepared following reported procedures and characterized using various spectroscopic techniques.[20] The nitrosyl complexes [$Co(MPTPP^{2-})(NO)$], **7** and [$Co(TMPP^{2-})(NO)$], **8** are synthesized bubbling NO gas through CH_2Cl_2 solutions of **5** and **6**, respectively. X-ray diffraction studies revealed complex **8** as a bent nitrosyl with Co-N-O bond angle 119.1(9)°. The complex is in square pyramidal geometry and NO moiety is bonded axially. N-O bond length is 1.166(6) Å (Figure S4). These values are in accordance with the reported ones.[22] The nitrosyl stretching frequencies for complex **7** and **8** appear at 1683 cm^{-1} and 1696 cm^{-1}, respectively. These values are well in the reported ranges of values for bent cobalt nitrosyls.[12c,e,22] Both the complexes are diamagnetic due to antiferromagnetic coupling between unpaired '*d*' electron

of cobalt and odd electron in NO and displays well resolved ^{1}H NMR spectra which is in agreement with {Co(NO)}^{8} assignment.

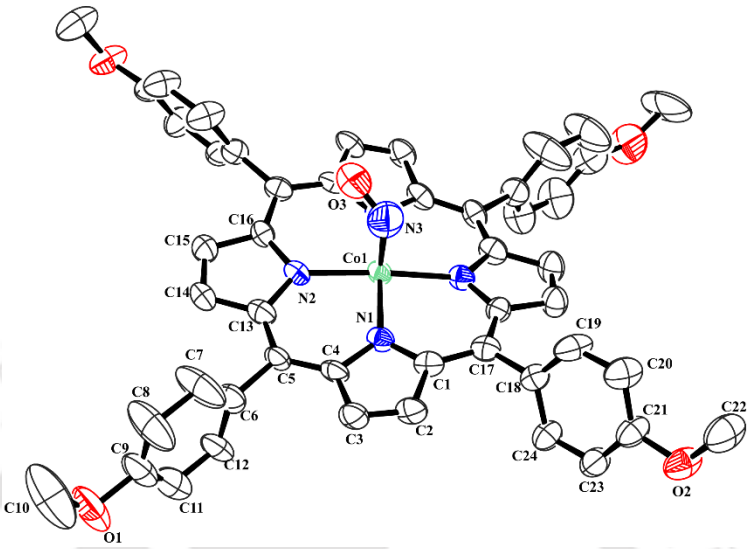

Figure S4. ORTEP diagram of complex **8** (30% thermal ellipsoid plot, H-atoms are omitted for clarity).

Reaction of complexes **7** and **8** with H_2O_2 at −40 ºC in CH_2Cl_2 resulted in complexes [Co^{III}($MPTPP^{2-}$)(NO_3)]; **9** and [Co^{III}($TMPP^{2-}$)(NO_3)]; **10**, respectively. The presence of 1384 cm^{-1} band in FT-IR spectra of both the complexes suggested that these are corresponding nitrato complexes.[12e] This is further confirmed in ESI-mass spectrometry where we got peak at m/z 764.25 (Calcd. m/z 763.16) for **9** and at m/z 854.24 (Calcd. m/z 853.19) for **10**. EPR silent nature as well as well resolved NMR spectra suggested that cobalt is in +3 oxidation state in both the complexes.

In UV-visible spectroscopy complex **7** shows characteristic absorption peaks at 414 and 536 nm in CH_2Cl_2 solution at −80 ºC. Upon addition of H_2O_2 these bands immediately shift to 431 and 540 nm, respectively. After that intensity of the Soret band decreases gradually and it further shifts to 441 nm. Two new bands at 827 nm and 928 nm appears in the meantime (Figure S5a). The peaks at 431 nm and 540 nm may be assigned to a high valent [Co(IV)=O]

species. However, this species was transient and converts rapidly to a Co(III)-porphyrin radical cation species as suggested by the significant quenching of characteristic Soret band (Scheme S5). In X-band EPR, addition of H_2O_2 to EPR silent complex **7** at −80 ºC resulted in a sharp singlet at g ~ 2.001 which confirms the generation of a radical species in the course of the reaction (Figure S5b). ESI-mass spectrum of the crude reaction mixture showed a peak at m/z 718.26 which may be assignable to the moiety [Co(MPTPP^{2-})(O)] (Calcd. m/z 717.17).

Similar results were observed in the reaction of complex **8** with H_2O_2. In UV visible spectroscopy, 420 nm and 540 nm bands shifted to 435 nm and 544 nm, respectively, after addition of H_2O_2 (Figure S6a). A peak at m/z 808.23 in mass spectrum suggested presence of [Co(TMPP^{2-})(O)] moiety (Calcd. m/z 807.20). This species is transient like the former case and rapidly isomerizes to a porphyrin cation radical species as suggested by decay of the Soret band in UV-visible spectroscopy as well as a sharp singlet at g ~ 2.002 in X-band EPR spectroscopy.

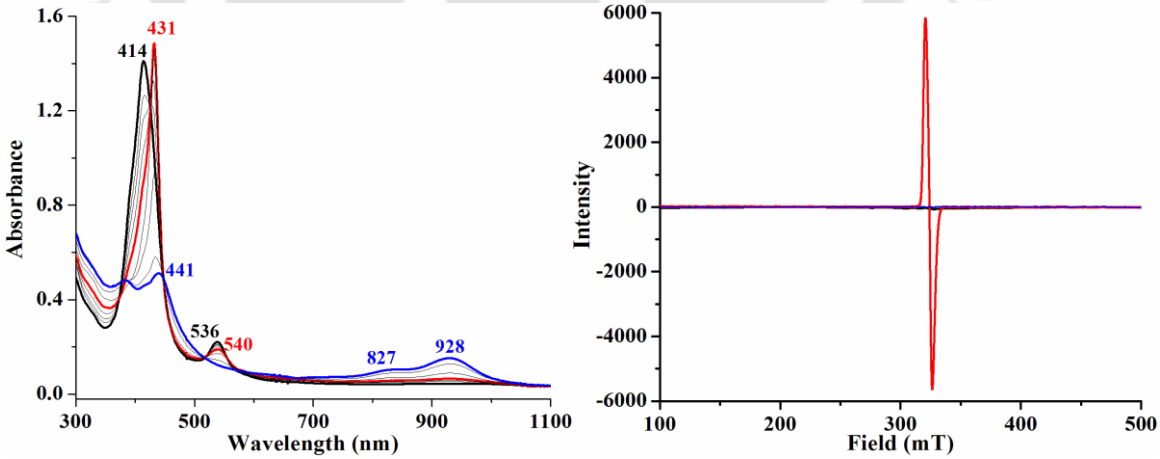

(a) **(b)**

Figure S5. (a) UV-visible and (b) X-band EPR spectral monitoring of **7** (black) and after addition of H_2O_2 (red) and final (blue) at −80 °C in CH_2Cl_2.

To confirm involvement of PN intermediate, complexes **7** and **8** were further made to react with H_2O_2 in presence of 2,4-di-*tert*-butylphenol. Appreciable amount (~60-65%) of 2,4-di-*tert*-butyl-6-nitrophenol was obtained from the final reaction mixture along with corresponding [Co^{III}-OH^-] (**11**, **12**) complexes.

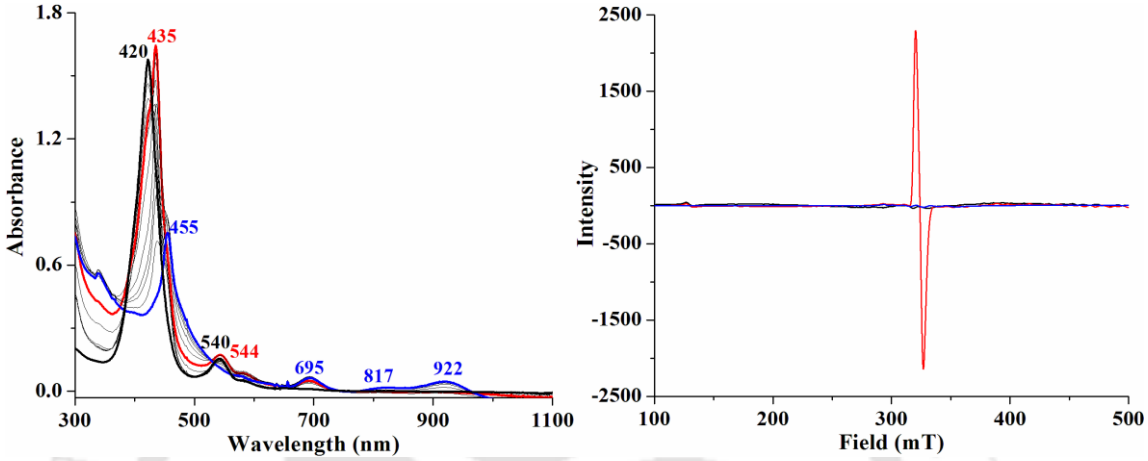

Figure S6. (a) UV-visible and (b) X-band EPR spectral monitoring of **8** (black) and after addition of H_2O_2 (red) and final (blue) at −80 °C in CH_2Cl_2.

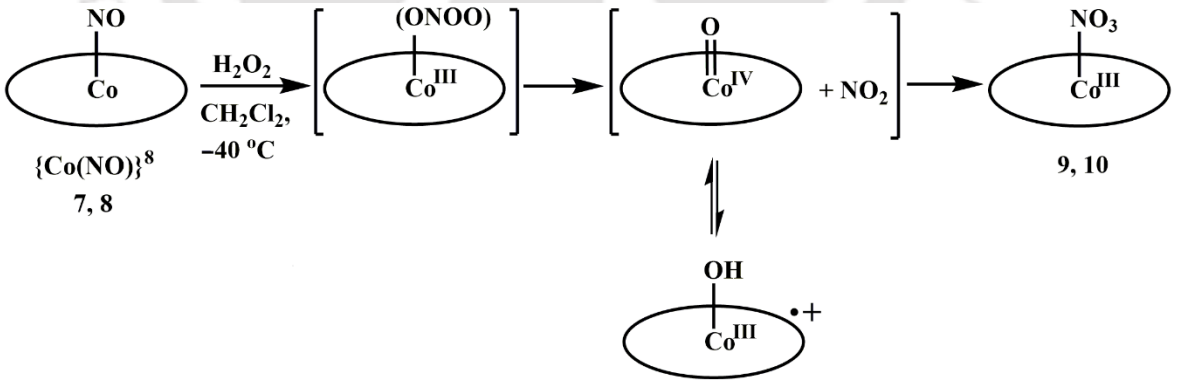

Scheme S5. Reaction of {Co(NO)}^{8} complexes with H_2O_2.

Summarizing the above results, two cobalt nitrosyl complexes react with H_2O_2 to give corresponding Co(III)-nitrato complexes. The reaction proceeds *via* putative [Co(III)-PN] intermediates.

Chapter 4: Reaction of a nitrosyl complex of Mn(II) porphyrin with superoxide: Formation of a Mn(IV)-oxo species

A Mn(III) porphyrinate complex [$Mn^{III}(TMPP^{2-})(Cl)$], **13** was synthesized following reported procedure.[20,12f] Crystal structure of **13** confirms that it is in square pyramidal geometry. CH_2Cl_2 solution of **13** absorbs at 475, 530, 583 and 621 nm in UV-visible spectroscopy and does not show any peak in X-band EPR spectroscopy as expected.

Reductive nitrosylation of **13** with hydroxylamine results in complex [$Mn(TMPP^{2-})(NO)$], **14**.[23] This complex was previously reported by Kubiak *et al.* as a five coordinated nitrosyl complex of Mn(II) porphyrinate with $\{Mn(NO)\}^6$ configuration.[24] It shows FT-IR stretching frequency at around 1755 cm^{-1}. Complex **14** is diamagnetic due to antiferromagnetic coupling between unpaired '*d*' electron of manganese and the antibonding electron of NO and displays well resolved ^1H NMR spectrum.

Complex **14** reacts with KO_2 in THF solution to give complex [$Mn^{III}(TMPP^{2-})(OH)$], **15** and NO_2 (Scheme S6). Complex **15** was characterized spectroscopically as well as structurally. The crystal structure reveals it as five coordinated square planar complex with hydroxo ligand at the axial position (Figure S7).

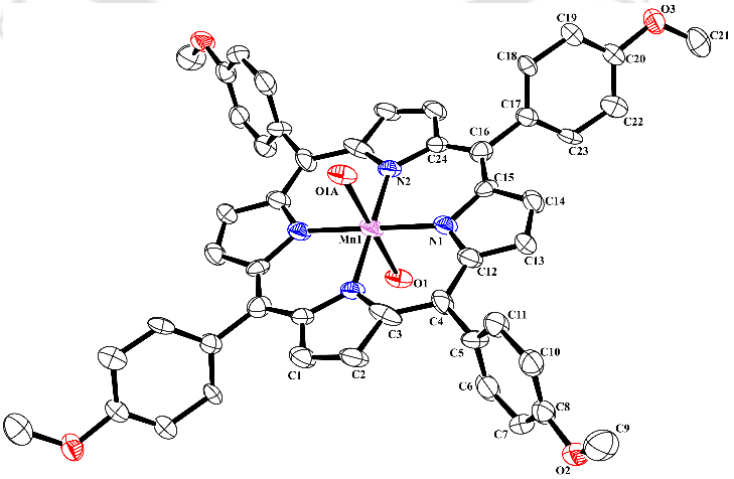

Figure S7. ORTEP diagram of complex **15** (30% thermal ellipsoid plot, H-atoms are omitted for clarity).

When the reaction of **14** and O_2^- in THF at room temperature was monitored in UV-visible spectroscopy, it was observed that the intensity of the Soret band of **14** at 427 nm gradually decreased and a new transient peak at 475 nm appeared which subsequently shifted to 470 nm which corresponds to complex **15** (Figure S8). The transient peak at 475 nm corresponds to generation of an intermediate, **14a** in the course of the reaction. The same reaction was then monitored in FT-IR spectroscopy where after the addition of O_2^-, nitrosyl stretching frequency of **14** in THF at 1739 cm^{-1} immediately shifted to 1776 cm^{-1}, indicative of the oxidation of the metal center, with the generation of a new peak at 1194 cm^{-1} which can be attributed to a metal bound superoxide stretching frequency (Figure S8). Finally, both the peaks disappeared simultaneously indicating that these two peaks are associated to the same intermediate species **14a** which is $[Mn^{III}(TMPP^{2-})(NO)(O_2^-)]$ (Scheme S6). The decomposition of **14a** to **15** is presumed to be occurred *via* a [Mn(III)-PN] intermediate. To confirm our presumption the reaction of complex **14** and KO_2 was done in presence of 2,4-di-*tert*-butylphenol. Appreciable amount of 2,4-di-*tert*-butyl-6-nitrophenol was obtained from the reaction confirming the involvement of [Mn(III)-PN] species in the reaction.

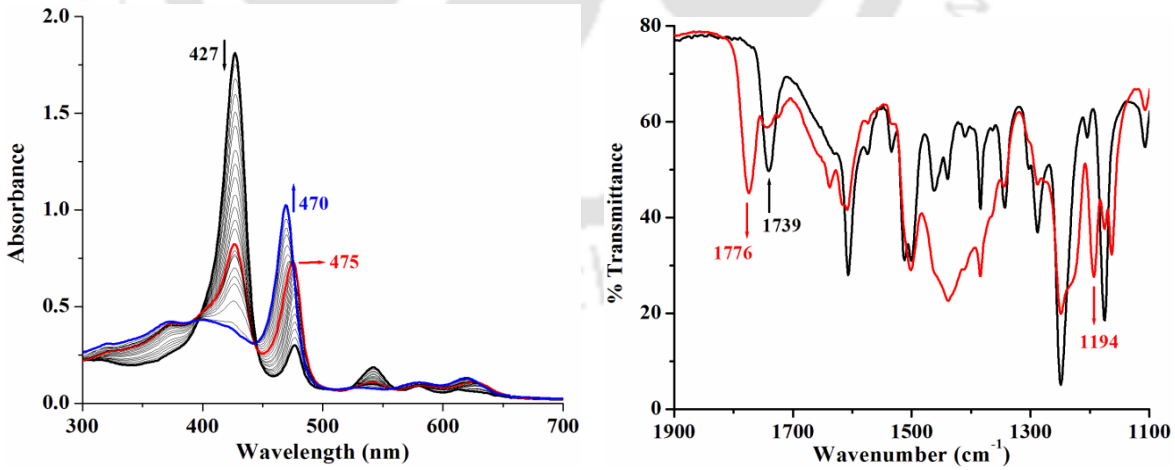

(a) **(b)**

Figure S8. (a) UV-visible and (b) FT-IR spectra of complex **14** (black); after addition of KO_2 (red); and complex **15** (blue) in THF at room temperature.

The proposed decomposition pathway of a metal PN intermediates involves a high valent metal oxo complex formed *via* homolytic fission of O−O bond of PN. In this case, the presumed [Mn(III)-PN] complex is believed to give [Mn(IV)=O] and NO_2 in the process (Scheme S6). Formation of complex **15** as final product suggest that it might be the decomposition product of [Mn(IV)=O], which in turn confirms the validity of our presumption. Hence, more evidence towards formation of [Mn(IV)=O] was sought. When the UV-visible spectroscopic study of the reaction was repeated at –40 °C, a new intermediate species was identified by the formation of new Soret band at 435 nm (Figure S9). The appearance of this band has been attributed to the formation of a high valent oxo intermediate [Mn^{IV}($TMPP^{2-}$)(O)].[26] In X-band EPR spectroscopy, frozen reaction mixture of complex **14** and KO_2 in THF showed a peak at g ~ 2.05 which is supposedly because of a [Mn(IV)=O] species (Figure S9).[27] In case of [Mn^{IV}($F_{20}TPP^{2-}$)(O)], similar EPR signal was reported. The other proposed intermediate **14a** is an even electron species and therefore, is not expected to show any signal in X-band EPR.

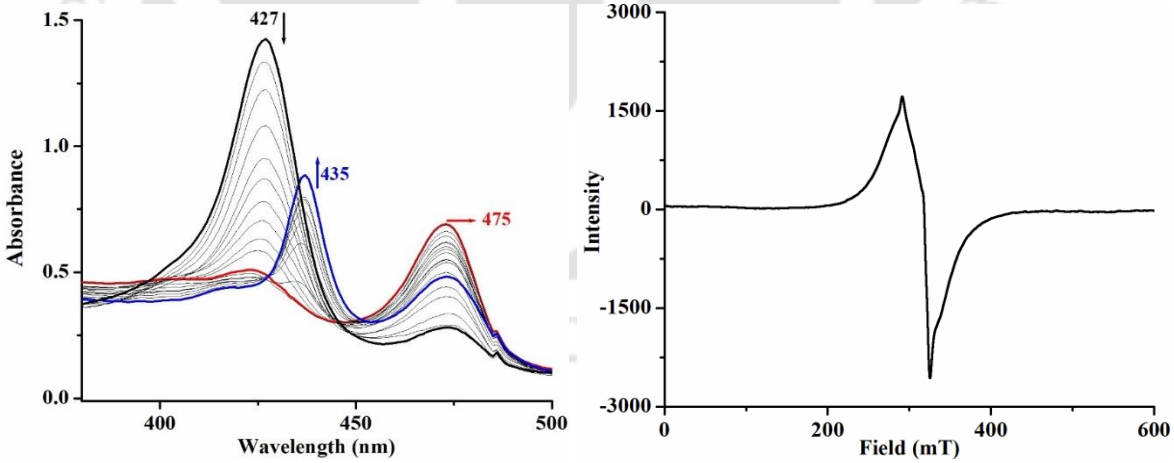

(a) **(b)**

Figure S9. (a) UV-visible spectral monitoring of the reaction of complex **14** (black) and KO_2 to give **14a** (red) and Mn^{IV}=O (blue) in THF at –40 °C. (b) X-band EPR spectrum of the frozen reaction mixture of complex **14** and KO_2 in THF at 77 K.

To further confirm the formation of [Mn(IV)=O], we introduced fluorene in the reaction mixture. Formation of 9-fluorenone as one of the products supports the presence of a metal oxo species in the course of the reaction. It is worth mentioning that KO_2 alone cannot oxidise fluorene to 9-fluorenone.

Conversion of a [Mn(III)-PN] to [Mn(III)-OH^-] involves loss of one NO_2 molecule which must be present in the reaction vessel at the end. (2,2,6,6-tetramethylpiperdin-1-yl)oxyl (TEMPO) was previously used to detect the presence of with NO_2. When TEMPO was introduced in the reaction of complex **14** and KO_2, 2,2,6,6-tetramethylpiperidin-1-yl nitrate was isolated as one of the final products confirming the release of NO_2 in the reaction.

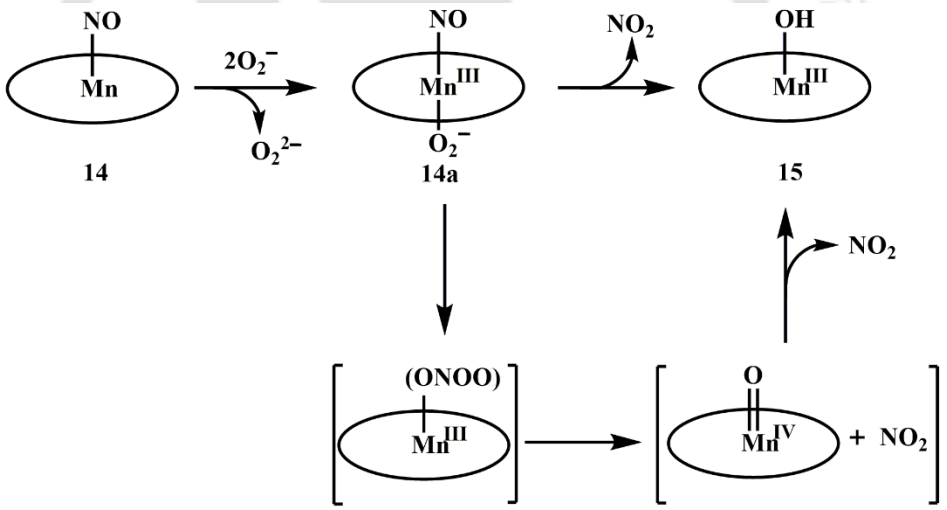

Scheme S6. Reaction of complex **14** with O_2^-.

Chapter 5: Can a nitrosyl complex of Mn(II) porphyrin release nitroxyl/HNO?

Spectroscopic characterizations of complex **14** suggest that it has [Mn(I)-NO^+] character and is not expected to behave as a nitroxyl/HNO donor. However, in the reaction of **14** and [$Co^{II}(TMPP^{2-})$], **6** in CH_2Cl_2, appearance of a new peak at 1696 cm^{-1} in FT-IR spectroscopy suggests formation of [$Co(TMPP^{2-})(NO)$], **8**.

$$[Mn(TMPP^{2-})(NO)] + [Co(TMPP^{2-})] \longrightarrow [Mn(TMPP^{2-})] + [Co(TMPP^{2-})(NO)]$$

Addition of 1 equivalent of HBF_4 as H^+ donor to a CH_2Cl_2 solution of **14** resulted in formation of new complex **16**, $[Mn^{III}(TMPP^{2-})(H_2O)_2](BF_4)$ along with the release of HNO. Formation of complex **16** was detected in UV-visible and FT-IR spectroscopy. In UV-visible spectroscopy, shift of Soret band from 429 nm to 452 nm through a transient intermediate band at 475 nm was observed (Figure S10a). This intermediate band is attributed to a [Mn(III)-NO^-] species that forms in the reaction course (Scheme S7). The ORTEP diagram of the complex **16** is shown in the figure S10b.

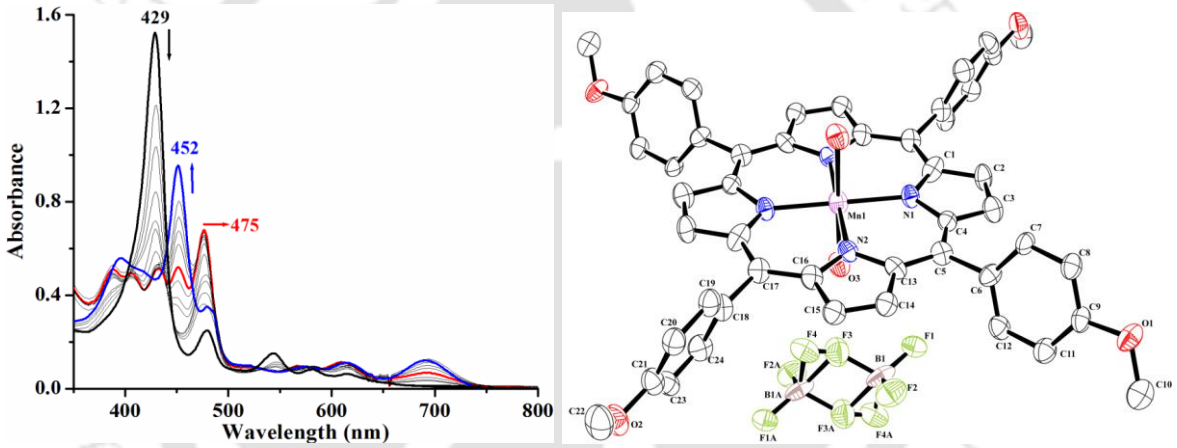

(a) **(b)**

Figure S10. (a) UV-visible spectral monitoring of the reaction of complex **14** (black) and after addition of HBF_4 (red) and final product $[Mn(TMPP^{2-})(H_2O)_2](BF_4)$, **16** (blue) in CH_2Cl_2 at −40 °C. (b) ORTEP diagram of complex **16** (30% thermal ellipsoid plot, H atoms are omitted for clarity).

The generation of HNO in the reaction was confirmed by its characteristic reaction with phosphine (R_3P), which react selectively with HNO donors to result in the corresponding phosphine oxide (R_3P=O) and aza-ylide (R_3P=NH). The reaction mixture of complex **14** with HBF_4 in presence of Ph_3P was subjected to ^{31}P NMR, where the presence of peaks for Ph_3P=O (δ = 44.1 ppm), Ph_3P=NH (δ = 36.5 ppm) and unreacted Ph_3P (δ = – 6.4 ppm) was

detected.[29]

HNO is known to undergo spontaneous dimerization followed by decomposition to give H_2O and N_2O.[13] The presence of the N_2O in the reaction vessel was detected by subjecting the headspace gas into gas chromatography.

$[Fe^{III}(TPP^{2-})(Cl)]$ (TPP^{2-} = tetraphenylporphyrinate) serves as an acceptor for HNO. When $[Fe^{III}(TPP^{2-})(Cl)]$ was introduced in the reaction of complex **14** and HBF_4, reductive nitrosylation occurred to result in $[Fe(TPP^{2-})(NO)]$. This was confirmed by the corresponding nitrosyl peak at 1698 cm^{-1} in FT-IR.[29]

Further, nitroxyl release from complex **14** was evidenced from its reaction with $[Fe^{III}(dtc)_3]$, (dtc = diethyldithiocarbamate anion), where nitroxyl transfer from complex **14** to $[Fe^{III}(dtc)_3]$ resulted in the formation of $[Fe(dtc)_2(NO)]$ and $[Mn^{III}(TMPP^{2-})]^+$. Formation of $[Fe(dtc)_2(NO)]$ was detected in FT-IR and X-band EPR spectroscopy. In FT-IR spectroscopy the peak of **14** at 1734 cm^{-1} gradually disappeared and a new peak at 1708 cm^{-1} (in CH_2Cl_2) corresponding to $[Fe(dtc)_2(NO)]$ appeared (Figure S11). In X-band EPR spectroscopy, the reaction mixture of **14** and $[Fe^{III}(dtc)_3]$ in DMSO showed a sharp triplet at g ~ 2.05 corresponding to $[Fe(dtc)_2(NO)]$.

$$\mathbf{[Mn^{II}(TMPP^{2-})(NO)] + [Fe^{III}(dtc)_3] \longrightarrow [Mn^{III}(TMPP^{2-})](dtc^{-}) + [Fe(dtc)_2(NO)]}$$

Considering the redox potential for the corresponding Mn^{III}/Mn^{II} couple, direct reduction of the NO group by the Mn(II) moiety through an outer-sphere mechanism is not feasible. However, an inner-sphere electron transfer from the metal ion to the coordinated NO group in the presence of electron rich ligand (as sixth ligand) will consequently increase the electron density on the central metal atom which, in turn, stabilizes [Mn(III)-NO^-] form and contributes to the HNO/NO^- donation. In case of HBF_4, it acts as H^+ source to polarize the

NO group as well as the BF_4^- donates electron density to the metal center to get stabilized in Mn(III) form (Scheme S7).

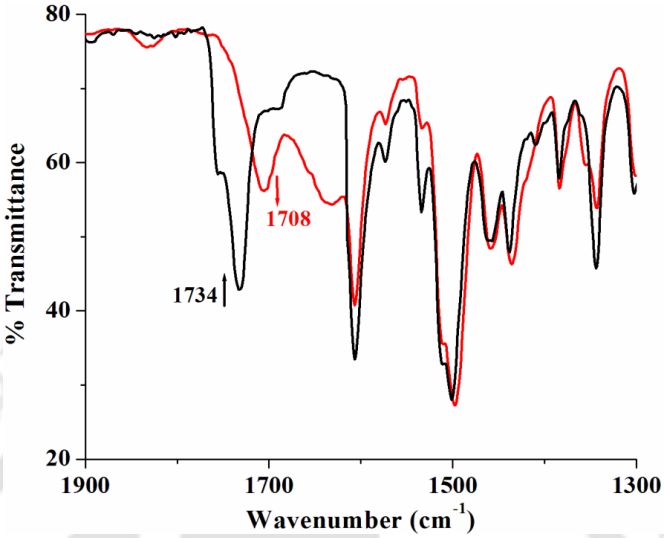

Figure S11. FT-IR spectral monitoring of the reaction of complex **14** (black) and $[Fe(dtc)_3]$ to give $[Fe(dtc)_2(NO)]$ and $[Mn(TMPP^{2-})](dtc)$ (red) in CH_2Cl_2.

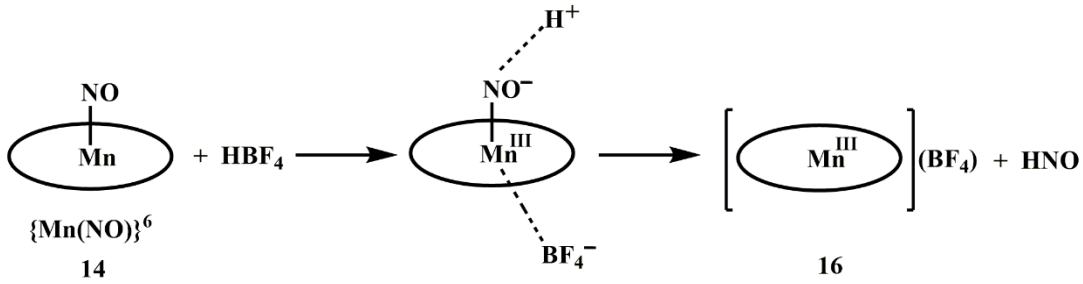

Scheme S7. Reaction of complex **14** with HBF_4.

On the other hand, $[Fe(dtc)_3]$ is known to equilibrate between $[Fe(dtc)_2]^+$ and dtc^- in solution. dtc^- unit provides the extra electron density to stabilize the corresponding Mn(III) form of the complex whereas the positively charged $[Fe(dtc)_2]^+$ helps in polarizing the coordinated NO group and the cooperative effect of these two results in NO^- release from complex **14**.

Conclusion and Future Prospect

Through chapters 2 to 4 we have discussed a few nitrosyl complexes of Co(II) and Mn(II) porphyrins and their reactivity with reactive oxygen species in an attempt to mimic the NOD

activity. In each case we observed formation of a PN intermediate in the reaction course and some of the associated intermediates that form during its formation and decomposition. For instance in chapter 2, formation of a $[Co^{II}(NO)(O_2^-)]$ species was evidenced spectroscopically prior to formation of a [Co(II)-PN]. In chapter 3, a Co(III) porphyrin cation radical species has been detected in the decomposition of a [Co(III)-PN], which in turn confirms the involvement of a [Co(IV)=O] intermediate in the reaction. In chapter 4, we could prove the involvement of [Mn(IV)=O] in the decomposition of a [Mn(III)-PN] intermediate both spectroscopically and chemically. A $[Mn^{III}(NO)(O_2^-)]$ species was also observed prior to formation of the [Mn(III)-PN].

Although we could get some significant evidence on the involvement of a high valent metal oxo species in the decomposition of PN, efforts to characterize the PN itself was not very successful because of its unstable nature.

In chapter 5, we explored the HNO donation ability of a nitrosyl of Mn(II)-porphyrin complex in presence of HBF_4. Previously, $\{Mn(NO)\}^6$ complexes were not considered as HNO/NO^- donors due to their $[Mn(I)\text{-}NO^+]$ nature. However, we have shown that presence of electron donating ligand environment along with an electron rich sixth ligand may induce $[Mn(III)\text{-}NO^-]$ character and result in release of HNO. This is a new type of reactivity for such complexes and definitely needs more investigation in future. The mechanism of the process needs further experimental support which may be achieved by tuning the ligand framework with appropriate electron donating groups.

References

1. *Nitric Oxide: Biology and Pathobiology*; Ignarro, L. J., Ed.; Academic Press: San Diego, **2000**.

2. *Nitric Oxide and Infection*; Fang, F. C., Ed.; Kluwer Academic/ Plenum Publishers: New York, **1999**.
3. Bourassa, J. L.; Ives, E. P.; Marqueling, A. L.; shimanovich, R.; Groves, J. T. *J. Am. Chem. Soc.* **2001**, *123*, 5142.
4. Furchgott, R. F. *Angew. Chem. Int. Ed.* **1999**, *38*, 1870.
5. Ignarro, L. J. *Angew. Chem. Int. Ed.* **1999**, *38*, 1882.
6. Murad, F. *Angew. Chem. Int. Ed.* **1999**, *38*, 1856.
7. Pacher, P., Beckman, J. S., Liaudet, L. *Physiol. Rev.* **2007**, *87*, 315.
8. Beckman, J. S.; Koppenol, W. H. *Am. J. Physiol.* **1996**, *271*, 1424.
9. Vliet, A. V.; Eiserich, J. P.; Halliwell, B.; Cross, C. E. *J. Biol. Chem.* **1997**, *272*, 7617.
10. Radi, R. *Proc. Natl. Acad. Sci. U. S. A.* **2004**, *101*, 4003.
11. Schopfer, M. P.; Mondal, B.; Lee, D. -H.; Sarjeant, A. A. N.; Karlin, K. D. *J. Am. Chem. Soc.* **2009**, *131*, 11304.
12. (a) Kalita, A.; Kumar, P.; Mondal, B. *Chem. Commun.* **2012**, *48*, 4636. (b) Saha, S.; Ghosh, S.; Gogoi, K.; Deka, H.; Mondal, B.; Mondal, B. *Inorg. Chem.* **2017**, *56*, 10932. (c) Saha, S.; Gogoi, K.; Mondal, B.; Ghosh, S.; Deka, H.; Mondal, B. *Inorg. Chem.* **2017**, *56*, 7781. (d) Gogoi, K.; Saha, S.; Mondal, B.; Deka, H.; Ghosh, S.; Mondal, B. *Inorg. Chem.* **2017**, *56*, 14438. (e) Mondal, B.; Saha, S.; Borah, D.; Mazumdar, R.; Mondal, B. *Inorg. Chem.* **2019**, *58*, 1234. (f) Mondal, B.; Borah, D.; Mazumdar, R.; Mondal, B. *Inorg. Chem.* **2019**, *58*, 14701.
13. Shafirovich, V.; Lymar, S. V. *Proc. Natl. Acad. Sci. U. S. A.* **2002**, *99*, 7340.
14. (a) Fukuto, J. M.; Millikin R. J.; *The Chemistry and Biology of Nitroxyl (HNO)*; Doctorovich, F., Farmer, P. J., Marti, M. A., Eds.; Elsevier, **2017**, 321. (b) Sherman, M. P.; Grither, W. R.; McCulla, R. D. *J. Org. Chem.* **2010**, *75*, 4014.

15. Reisz, J. A.; Klorig, E. B.; Wright, M. W.; King, S. B. *Org. Lett.* **2009**, *11*, 2719.
16. Miranda, K. M.; Yamada, K.; Espey, M. G.; Thomas, D. D.; DeGraff, W.; Mitchell, J. B.; Krishna, M. C.; Colton, C. A.; Wink, D. A. *Arch. Biochem. Biophys.* **2002**, *401* , 134.
17. (a) Rusche, K. M.; Spiering, M. M.; Marletta, M. A. *Biochemistry* **1998**, *37*, 15503. (b) Adak, S.; Wang, Q.; Stuehr, D. J. *J. Biol. Chem.* **2000**, *275*, 33554.
18. Miao, Z.; King, S. B. *Nitric Oxide* **2016**, *57*, 1.
19. Ivanovic-Burmazovic, I.; *The Chemistry and Biology of Nitroxyl (HNO)* Doctorovich, F.; Farmer, P. J.; Marti, M. A. Eds.; Elsevier, **2017**, 67.
20. (a) Adler, A. D.; Longo, F. R.; Finarelli, J. D.; Goldmacher, J.; Assour, J.; Korsakoff, L. *J. Org. Chem.* **1967**, 32, 476. (b) Rothemund, P.; Menotti, A. R. *J. Am. Chem. Soc.* **1948**, *70*, 1808.
21. Soldatova, A. V.; Ibrahim, M.; Spiro, T. G. *Inorg. Chem.* **2013**, *52*, 7478.
22. Kurtikyan, T. S.; Gulyan, G. M.; Dalaloyan, A. M.; Kidd, B. E.; Goodwin, J. A. *Inorg. Chem.* **2010**, *49*, 7793.
23. Richter-Addo, G. B.; Hodge, S. J.; Yi, G. B.; Khan, M. A.; Ma, T.; Caemelbecke, E. V.; Guo, N.; Kadish, K. M. *Inorg. Chem.* **1996**, *35*, 6530.
24. Choi, In-K.; Liu, Y.; Wei, Z.; Ryan, M. D. *Inorg. Chem.* **1997**, *36*, 3113.
25. Zavarine, I. S.; Kini, A. D.; Morimoto, B. H.; Kubiak, C. P. *J. Phys. Chem. B* **1998**, *102*, 7287.
26. Zhang, R.; Horner, J. H.; Newcomb, M. *J. Am. Chem. Soc.* **2005**, *127*, 6573.
27. Schappacher, M.; Weiss R. *Inorg. Chem.* **1987**, *26*, 1189.
28. Zhang, Z.-Q.; Chen, T.; Zhang F.-M. *Org. Lett.* **2017**, *19*, 1124.
29. Rhine, M. A.; Rodrigues, A. V.; Bieber Urbauer, R. J.; Urbauer, J. L.; Stemmler, T. L.; Harrop, T. C. *J. Am. Chem. Soc.* **2014**, *136*, 12560.

30. Ileperuma, O. A.; Feltham, R. D. *Inorg. Chem.* **1977**, *16*, 1876.

31. Komarov, A. M.; Reef, A.; Schmidt, H. H. H. W.; *Methods in Enzymology*, vol 359, Cadenas, E.; Packer, L. Eds. Academic Press; **2002**, 18.

Chapter 1

Introduction

1.1 Nitric oxide

Nitric oxide (NO) is a ubiquitous diatomic molecule which mediates several physiological processes ranging from regulation of cardiovascular function to signal transduction and defense processes of the immune system at a very low concentration. In contrast, slight imbalance in NO concentration may result in serious pathological consequences.[1-3] *In vivo*, NO is produced *via* oxidation of L-arginine to L-citrulline by nitric oxide synthase (NOS) enzyme.[4] In biological denitrification process, NO is produced from reduction of nitrite (NO_2^-) by nitrite reductase enzyme (NiR).[5] Most of its physiochemical/biochemical activities are mainly due to its interaction with various metalloenzymes. For example, NO binding to the soluble isoform of guanylate cyclase (sGC), significantly weakens the proximal Fe-His bond, breakage of which results activation of the enzyme for catalytic formation of the secondary messenger cyclic-guanylyl monophosphate (cGMP) from guanylyl triphosphate (GTP). This leads to relaxation of smooth muscle tissue of blood vessels and regulation blood pressure.[6,7] Interaction of NO with fully oxidized states of copper containing enzymes, laccase or cytochrome *c* oxidase causes fast reduction of copper centre from +2 to +1 oxidation state. The reduction of Cu_B(II) in cytochrome *c* oxidase to Cu(I) is believed to play key role in control of the activity of the enzyme.[8]

NO is radical in nature with the unpaired electron at π* orbital, which makes it very reactive. It immediately reacts with molecular oxygen to form nitrogen dioxide (NO_2). Inside living bodies, excess production of NO can cause oxidative and nitrosative stress,

inhibit various metalloenzymes *via* reversible or irreversible binding to metal centers in enzyme active sites. For example, NO binds reversibly with the Fe(II) centre of cytochrome P-450 and thereby competitively inhibits O_2 binding and disrupts enzymatic activity.[9] Similarly, activity of catalase is completely inhibited when NO interacts with the [Fe(V)=O] intermediate in its reaction pathway and forms a ferric nitrosyl complex, which prevents further binding of H_2O_2 and breaks the catalytic cycle.[10] NO oxidizes DNAs and lipids, reacts with thiols to produce S-nitrosothiols *via* free radical or metal mediated mechanism. One of the major toxicities arises from its diffusion-controlled reaction with superoxide (O_2^-), which produces peroxynitrite ($ONOO^-$, PN). PN is known to be responsible for nitration of protein tyrosine group.

In the redox series of related nitrogen oxides, NO occupies the central position and can be conveniently oxidized or reduced. For this reason, both oxidative and reductive pathways for NO exist in physiological system. In mammals, an enzyme called nitric oxide dioxygenase (NOD) is responsible for regulation of NO concentration. NOD catalytically oxidizes NO to atoxic nitrate (NO_3^-). In lower organisms, nitric oxide reductase (NOR) enzyme reduces toxic NO, generated in biological denitrification, to benign nitrous oxide (N_2O).

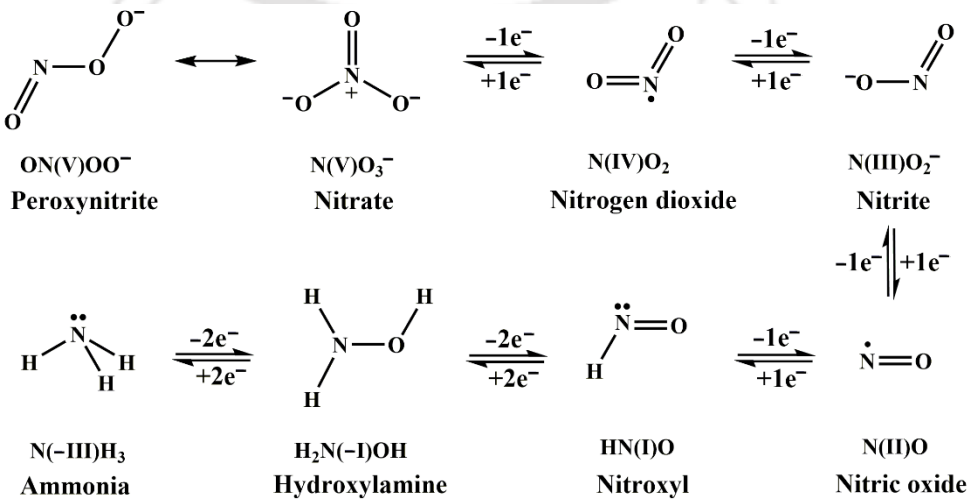

Figure 1.1. Redox relationship of NO with other nitrogen species.

1.2 Peroxynitrite

Excess production of NO is associated with cell and tissue pathology. One of the common routes to NO dependent pathology involves PN, which is formed *via* reaction of NO and O_2^{-}. *In vivo*, O_2^{-} is produced by enzymes like NADPH oxidase and xanthine oxidase. This O_2^{-} is consumed by superoxide dismutase (SOD) catalyzed conversion to hydrogen peroxide (H_2O_2) and O_2. This process is faster than most of the other reactions of O_2^{-} and due to this preferential reaction with SOD; its concentration is kept low to a picomolar level. However, during certain biological conditions like sepsis, inflammation, excitotoxicity, and ischemia-reperfusion of tissues when there are high intracellular fluxes of O_2^{-} and significantly high concentration of NO to outcompete SOD, these two reacts at diffusion-controlled rate and produces PN.[11] The rate of the reaction is reported to a value of 1.9×10^{10} $M^{-1}s^{-1}$.[12]

$$NO + O_2^{-} \longrightarrow ONOO^{-} \qquad \text{----------(Eq. 1.1)}$$

PN and its protonated form, peroxynitrous acid, are highly reactive and considered as strong biological oxidants due to its very high reduction potential [$E°'(ONOO^{-}, 2H^{+}/NO_2, H_2O) = +1.6 \pm 0.1$ V and $E°'(ONOO^{-}, 2H^{+}/NO_2^{-}, H_2O) = +1.3 \pm 0.1$ V *vs.* NHE].[13] The anionic form is relatively stable. However fast decomposition occurs in presence of H^{+} or Lewis acids. Peroxynitrous acid quickly decomposes to $^{\bullet}OH$, NO_2. Reaction of CO_2 and PN results in NO_2 and $CO_3^{\bullet-}$. In presence of metal ions, it quickly isomerizes to nitrate or nitrite. It reacts with a number of biomolecules including proteins (*via* nitration of tyrosine, tryptophan residues; oxidation of methionine residue), DNA, lipids etc. The reaction of PN with carbohydrates may degrade sugars to aldehyde products or alternatively oxidize to organic nitrates/nitrites. Similarly, thiols can be either oxidized to a higher oxidation state

or converted to S-nitrosothiols.[14-17]

The protein tyrosine nitration is one of the key events of PN activity and has been suggested as a specific biomarker for the presence of PN in biological systems.[18] This event can significantly disrupt functions of many metalloenzymes having a redox active metal and a nearby tyrosine group. Studies have suggested that this particular process proceeds *via* a radical mechanism where NO_2 forms as an intermediate.[19] Crucial role of the metal ion in the mechanism is also implicated. For example, Mn superoxide dismutase losses its activity on interaction with PN because of the nitration of a tyrosine residue in the protein chain. Radi *et al.* proposed that PN first binds to the Mn ion which in turn facilitate the homolytic cleavage of the O−O bond in the PN group. This leads to the formation of a [Mn(IV)=O] species and NO_2 which are actually responsible for nitration reaction.[20]

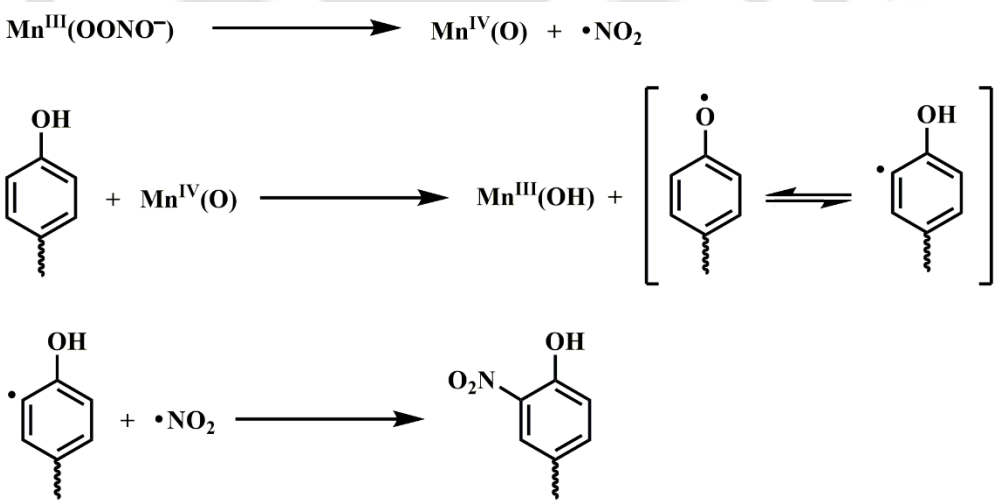

Scheme 1.1. Protein tyrosine nitration.

Nitric oxide dioxygenase (NOD) enzyme is responsible for maintaining an optimum concentration of NO in the mammals. The enzymatic active core consists of a [Fe(III)-O_2^-] species which reacts with NO and converts it to biologically benign NO_3^- ion. The proposed mechanistic pathway involves a [Fe(III)-PN] intermediate which upon O−O bond

homolysis gives an oxo-ferryl, [Fe(IV)=O] moiety and NO_2. The mechanism is elusive since none of the intermediates are well characterized owing to their highly unstable nature in biological systems.

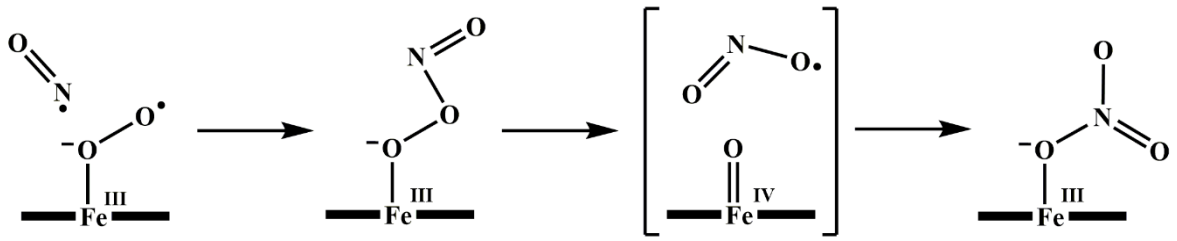

Scheme 1.2. Mechanistic pathway for NOD activity.

1.2.1 Transition metal peroxynitrite complexes and their synthesis

As discussed in the previous section, PN ion plays key roles in many biological events; for example, NOD activity and protein tyrosine nitration etc. Consequently, there is an immense demand for synthetic PN complexes for the sake of better understanding of the chemistry. There have been several reports to gain insights on their formation and decomposition pathways. However, much to the dismay of the scientific community this chemistry is still elusive in terms of proper spectroscopic evidence.

There are mainly two routes to synthesize a metal-PN complex, (i) reaction of a metal-nitrosyl complex with reactive oxygen species (ROS) such as O_2, O_2^-, O_2^{2-} etc. (ii) reaction of metal-superoxo/peroxo complex with NO.

1.2.2 Reaction of nitrosyl complexes with ROS

Basolo and Clarkson reported the formation of a cobalt-PN intermediate in the reaction of a cobalt nitrosyl complex with molecular oxygen. This intermediate upon spontaneous reaction with a second equivalent of nitrosyl complex gives the corresponding nitrito product in the next step.[21] This is the first report where formation of a metal-PN

intermediate is implicated. However, the mechanism is quite speculative and no direct or indirect proof for the proposed intermediate has been provided (Scheme 1.3).

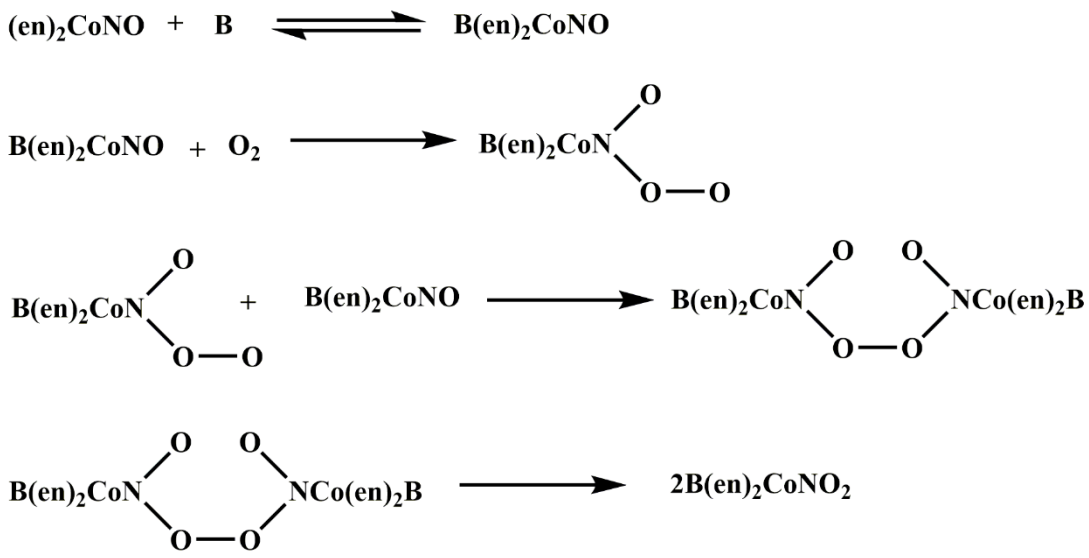

Scheme 1.3. Mechanistic pathway for the formation and decomposition of [Co-PN] proposed by Basolo *et al.*

Karlin group has reported a Cu(I) nitrosyl complex of a tridentate alkylamine ligand which on reaction with O_2 at –80 ºC in THF medium to give [Cu(II)-PN] intermediate which they postulated by means of UV-visible and EPR spectroscopic observation as well as theoretical calculations. In the calculated lowest energy structure, the PN ligand binds to the Cu center in a κ^2 fashion. This unstable intermediate complex thermally decomposes to give a nitrito-Cu(II) complex and half molecule of oxygen gas.[22] They further commented on the decomposition pathway of the said PN complex which involves a 'oxo-cupryl' or rather a Cu(II)-oxyl species and NO_2. This Cu(II)-oxyl moiety subsequently reacts with another equivalent of [Cu(II)-PN] to give corresponding nitrito product and O_2 (Scheme 1.4). Their results are further supported by the phenol ring nitration experiment which is similar to the nitration of tyrosine ring in the biological systems.

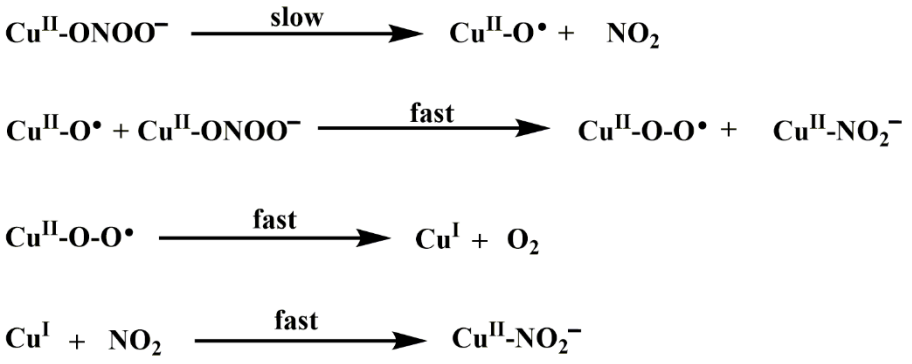

Scheme 1.4. Proposed decomposition pathway of the Cu(II)-PN intermediate.

Kim *et al.* reported a $\{Fe(NO)_2\}^{10}$ dinitrosyliron complex (DNIC), $[Fe(TMEDA)(NO)_2]$ (TMEDA = N,N,N′,N′-tetramethylethylenediamine) which acts as a nitrating agent in presence of O_2 and converts 2,4-di-*tert*-butylphenol to 2,4-di-*tert*-butyl-6-nitrophenol. A five-coordinated κ^2-peroxynitrito-iron nitrosyl complex, [Fe(TMEDA)(NO)(PN)] was proposed having IR stretching at 1805 and 1589 cm^{-1} corresponding to the NO and a *trans*-PN ligands respectively. These results were also supported by EPR and EXAFS studies (Scheme 1.5).[23]

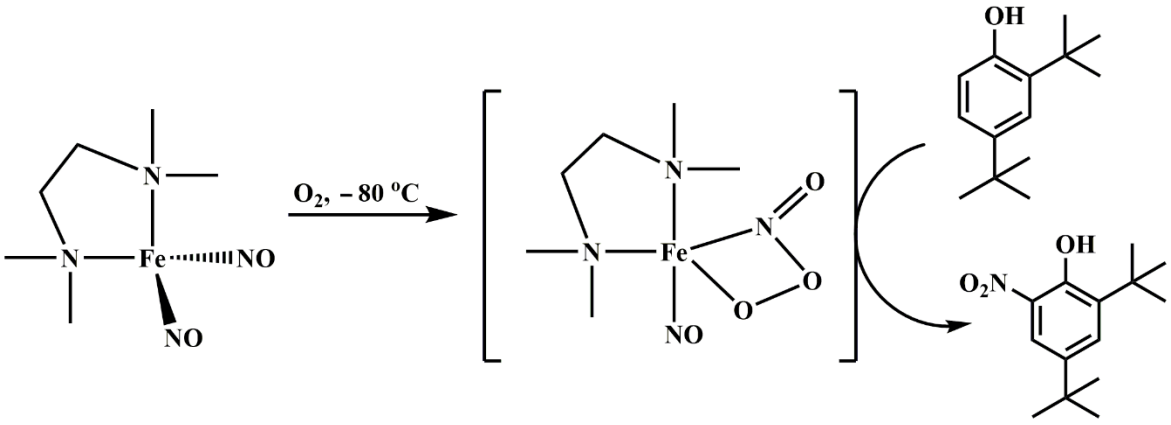

Scheme 1.5. Phenol ring nitration by DNIC.

Karlin *et al.* reported a mixed valent dicopper system $[Cu^{I,II}_2(UN\text{-}O^-)]^{2+}$, which reacts with NO at −80 ºC to in CH_2Cl_2 results in the corresponding μ-nitrosyl complex $[Cu^{I,II}_2(UN\text{-}O^-)(\mu\text{-}NO)]^{2+}$. This nitrosyl complex reacts with O_2 give $[Cu^{II}_2(UN\text{-}O^-)(NO)(O_2^-)]^{2+}$ intermediate. Low temperature IR monitoring of this reaction at −80 ºC revealed shifting of

NO stretching frequency from 1670 cm^{-1} to 1859 cm^{-1} indicating the oxidation of one Cu center. This new IR band is transient and disappears to give another set of bands at 1640 and 1520 cm^{-1} assignable to *cis* and *trans* isomers of the PN ligand of a μ-peroxynitrito dicopper complex respectively (Scheme 1.6). This binuclear system is of much importance in terms of the mechanism of formation of the PN intermediate from the reaction of NO and O_2^- groups in close proximity.[24]

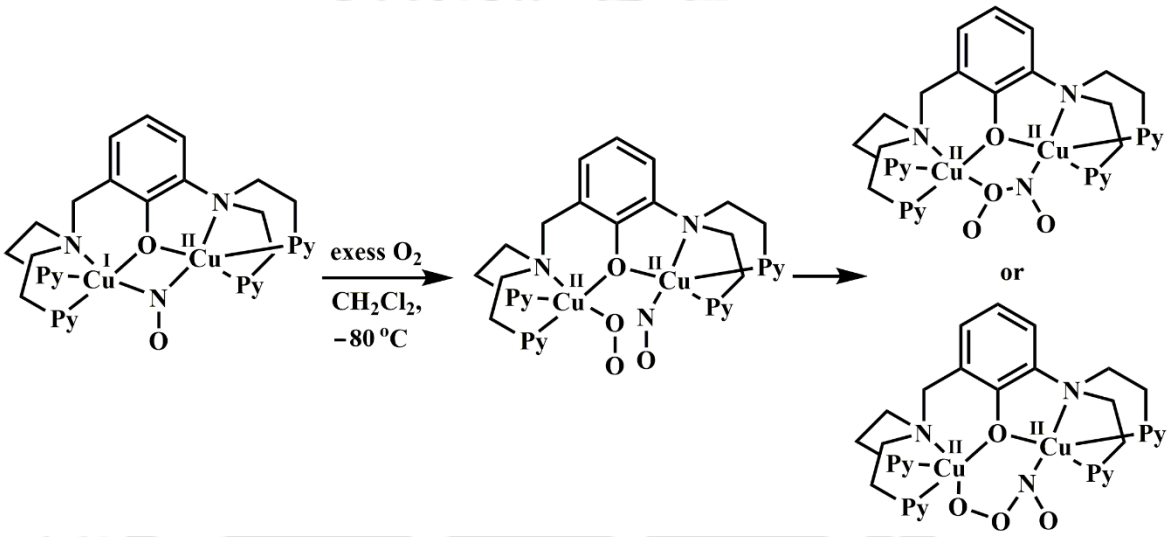

Scheme 1.6. Reaction of mixed-valent dicopper nitrosyl with O_2 to give *cis*- and *trans*-PN.

Our group reported the example of a $\{Co(NO)\}^8$ complex which reacts with O_2 to give a putative [Co(III)-PN] intermediate followed by its decomposition to corresponding [Co(III)-NO_2^-] (Scheme 1.7). In the FT-IR monitoring of the reaction a six-coordinated [$Co^{III}(NO)(O_2^-)$] species was detected.[25]

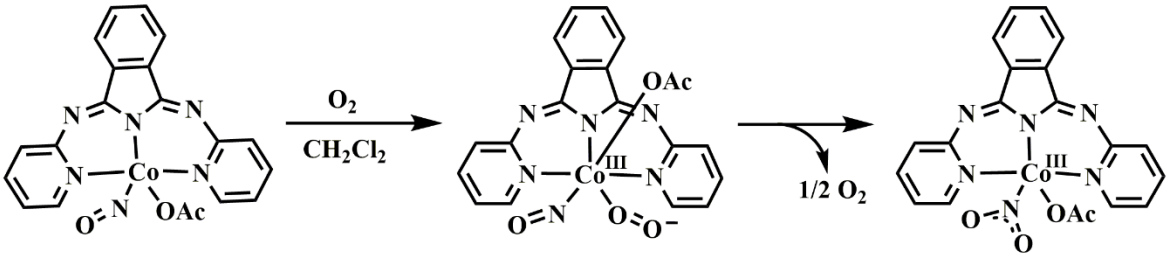

Scheme 1.7. Reaction of $\{Co(NO)\}^8$ complex with O_2 to give a [$Co^{III}(NO)(O_2^-)$] species.

In another report, a copper nitrosyl complex $[L_2Cu(NO)(ClO_4)]$ (L = *bis*(2-ethyl-4-methyl-imidazol-5-yl)methane), reacts with hydrogen peroxide (H_2O_2) at −20 ºC in CH_3CN to give a Cu(I)-nitrato complex *via* a Cu(I)-PN intermediate.[26] Formation of PN intermediate was confirmed by characteristic phenol ring nitration experiment as well as the isolation of $[Cu(I)\text{-}NO_3^-]$. The $[Cu(I)\text{-}NO_3^-]$ complex converts to $[Cu(II)\text{-}NO_3^-]$ *via* aerial oxidation (Scheme 1.8).

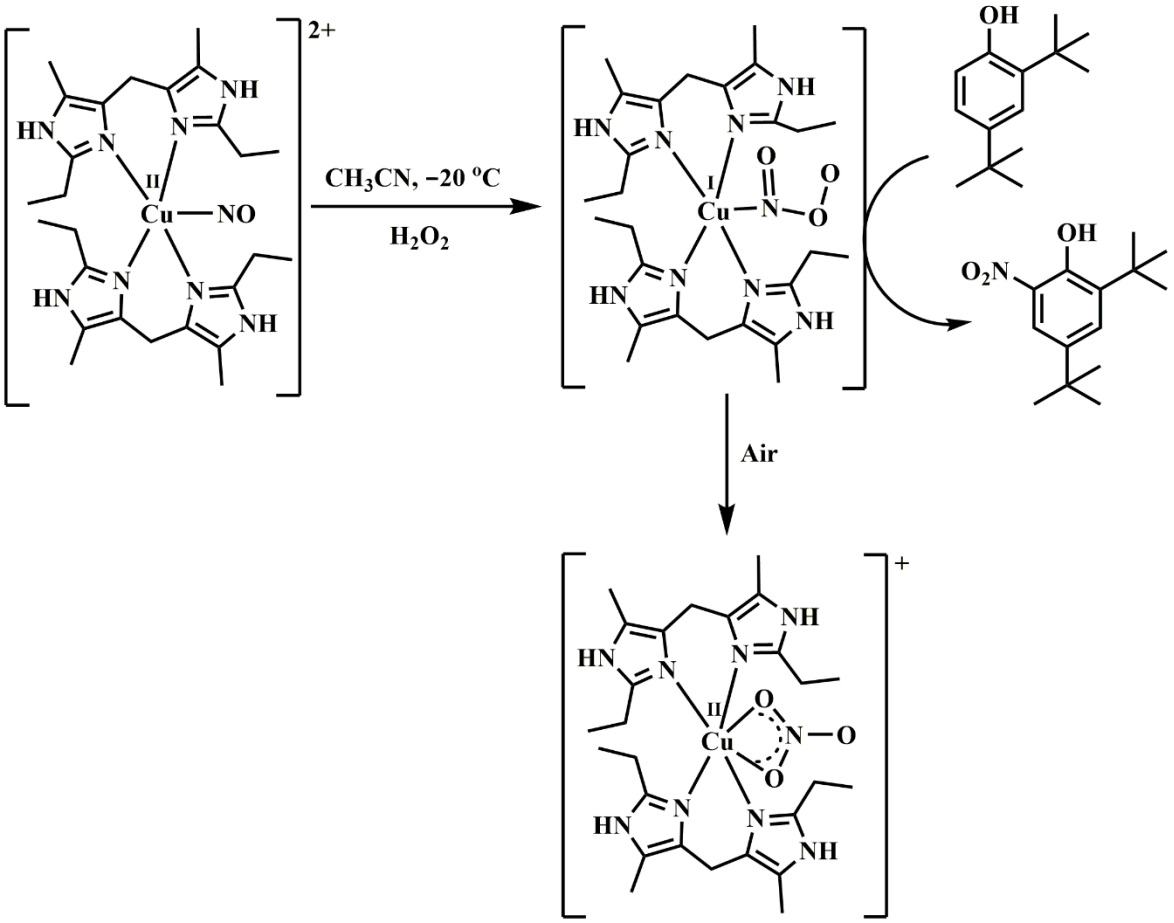

Scheme 1.8. Formation of a [Cu(I)-PN] complex.

Nam group reported two Co(III)-nitrosyls of N-tertamethylatedcyclam, *viz.* $[(12\text{-}TMC)Co(NO)]^{2+}$ and $[(13\text{-}TMC)Co(NO)]^{2+}$ which do not react with O_2, but react with O_2^- to form the corresponding Co(II)-nitrito complexes and O_2 *via* a presumed [Co(II)-PN] intermediate (Scheme 1.9).[27] While the nitrito complexes were well characterized, no spectroscopic evidence is given in support of the PN intermediate.

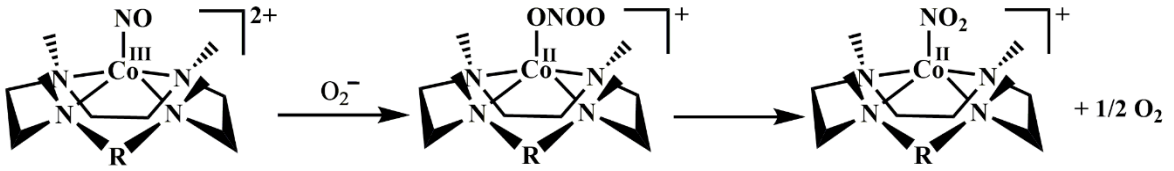

Scheme 1.9. Reaction of Co(III)-nitrosyls with O_2^- to give [Co(II)-PN].

Reaction of nitrosyl of Co(II) porphyrin complexes having {Co(NO)}^{8} configuration with H_2O_2, may result in the corresponding Co(III)-nitrito or -nitrato complex depending upon the ligand environment. For example, [Co(Cl_4TPP^{2-})(NO)] {Cl_4TPPH_2 = 5,10,15,20-*tetrakis*(4-chlorophenyl)porphyrin} gives a [Co(III)-NO_2^-],[28] whereas [Co(F_8TPP^{2-})(NO)] {F_8TPPH_2 = 5,10,15,20-*tetrakis*(2,6-difluorophenyl)porphyrin} gives the [Co(III)-NO_3^-] complex.[29] In both the cases involvement of putative [Co(III)-PN] intermediate was proposed. In the latter case involvement of an oxyl radical species [Co(III)-O$^\bullet$], generated from the homolysis of O−O bond of the PN ligand, was implicated by means of EPR spectroscopy and ESI-mass spectrometry at −40 ºC (Scheme 1.10).

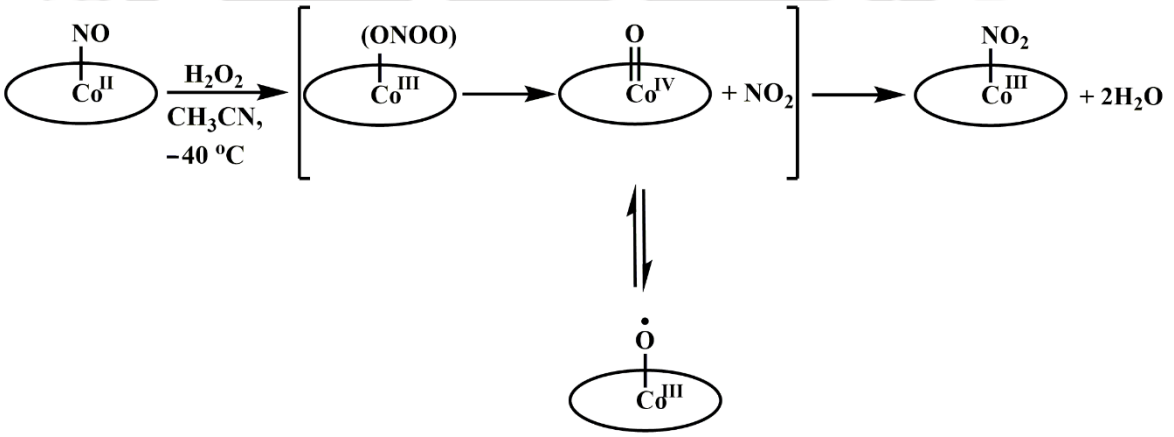

Scheme 1.10. Reaction of porphyrnato Co(II) nitrosyl with H_2O_2.

A nitrosyl of Mn(II) porphyrin, {Mn(NO)}^{6} complex [Mn($F_{20}TPP^{2-}$)(NO)] {$F_{20}TPPH_2$ = 5,10,15,20-*tetrakis*(pentafluorophenyl)porphyrin} reacts with O_2^- to give [Mn(III)-NO_3^-] *via* putative [Mn(III)-PN] intermediate (Scheme 1.11).[30] Presence of the PN intermediate was confirmed by the exclusive nitration of 2,4-di-*tert*-butylphenol. Similar to the previous

example here also involvement of a high-valent [Mn(IV)=O] species, in the decomposition pathway of the PN, was observed in UV-visible and EPR spectroscopy at −80 ºC which was further confirmed in ESI-MS. Resonance Raman study was precluded because of the photodecomposition of the intermediate.

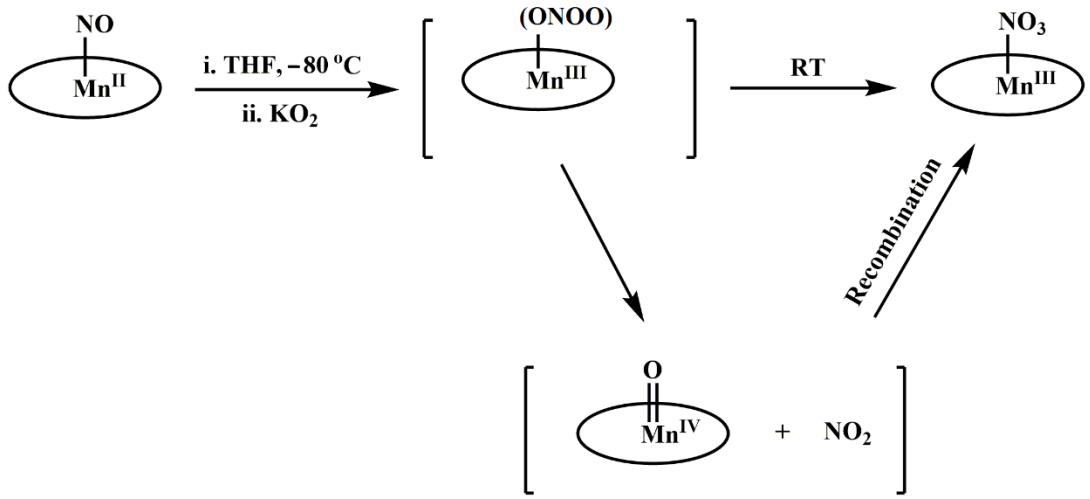

Scheme 1.11. Formation of [Mn(III)-PN] complex.

1.2.3 Reaction of metal superoxo and peroxo complexes with NO

Koppenol group reported the only example of stable, discrete cobalt-PN complex, *tris*(tetraethylammonium) pentacyanoperoxynitritocobaltate(III), $[Co^{III}(CN)_5(ONOO^-)]^{3-}$ from the reaction of corresponding solid pentacyanosuperoxocobaltate(III), $[Co^{III}(CN)_5(O_2^-)]^{3-}$ and NO in CH_3CN. The complex results nitrated and hydroxylated product in presence of phenol and isomerizes within the coordination sphere to NO_3^- complex in absence of light. However, upon irradiation of light it releases NO_2. Despite of their claims, these evidences were not enough to characterize the said complex, even their results were not reproducible.[31]

Theopold *et al.* reported the formation of a cobalt PN complex in the reaction of a [Co(III)-O_2^-] complex with NO in a sterically hindered hydro-*tris*(3-*tert*-butyl-5-

methylpyrazole)borate framework. In the IR experiment at −78 °C an intermediate species having stretching frequency at 1598 cm^{-1} and 1301 cm^{-1} was detected which, as they proposed, is attributed to a PN moiety bonded to cobalt center. Decomposition of this intermediate results in formation of equimolar amount nitrito and nitrato products. A homolytic cleavage of O−O bond of [Co(III)-PN] to yield [Co(IV)=O] and NO_2 followed by recombination is proposed for the former case. However, for the latter case they proposed formation of a binuclear [Co(N(O)OO(O)N)Co] moiety and subsequent O−O bond decomposition.[32]

Karlin group provided an example of Cu(II)-PN complex which forms in the reaction of [Cu^{II}(TMG_3tren)(O_2^-)] with NO {TMG_3tren = 1,1,1-*tris*{2-[N2-(1,1,3,3-tetramethyl-guanidino)]ethyl}amine; Scheme 1.12}. They supported their results with a ^{18}O labelling experiment and showed a four unit shift in the mass spectrum of the species which they claimed to be a Cu(II) PN complex.[33]

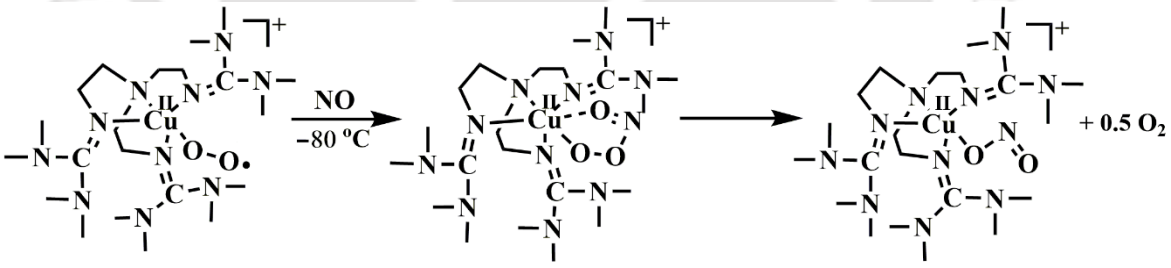

Scheme 1.12. Formation of [Cu(II)-PN] complex.

Subsequent report at a much later time provided the resonance Raman spectroscopic study of the complex [Cu^{II}(TMG_3tren)(ONOO)]. They proposed that there are two types of PN complexes involved in the reaction pathway, *viz.* [Cu^{II}(TMG_3tren)(κ^1-ONOO)] (PN1) and [Cu^{II}(TMG_3tren)(κ^2-O,O′-ONOO)] (PN2); former is more stable than the latter at −125 °C (Scheme 1.13). Resonance Raman bands at 1545, 929 and 658 cm^{-1} are assigned to N=O, O−O and N−O stretching vibration of a *cis* PN ligand of [Cu^{II}(TMG_3tren)(κ^1-ONOO)].[34]

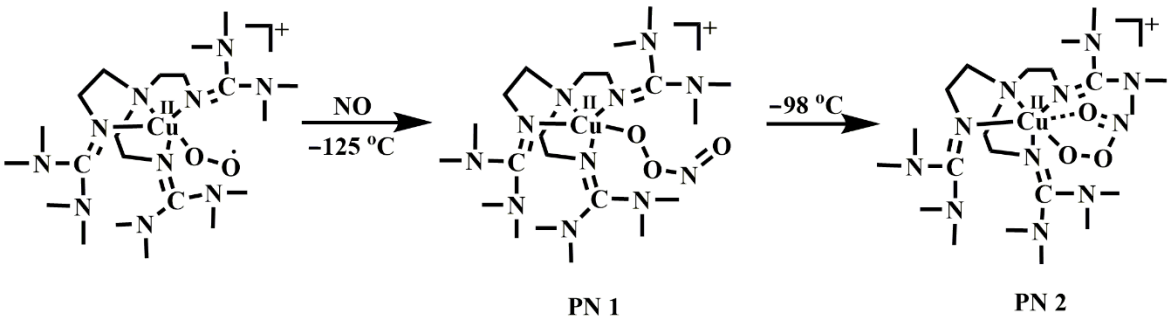

Scheme 1.13. Conversion between two types of [Cu(II)-PN] complexes.

A stable Fe(III)-superoxo complex, $[Fe^{III}(F_8TPP^{2-})(THF)(O_2^{-})]$ reacts with NO in THF medium at −80 °C giving $[Fe^{III}(F_8TPP^{2-})(NO_3^{-})]$ *via* a [Fe(III)-PN] intermediate (Scheme 1.14).[35] This study offers comparative comprehension between two major events, *viz.* NOD activity and tyrosine ring nitration. Experimental result shows that ring nitration is a much faster event than isomerization to NO_3^{-}.

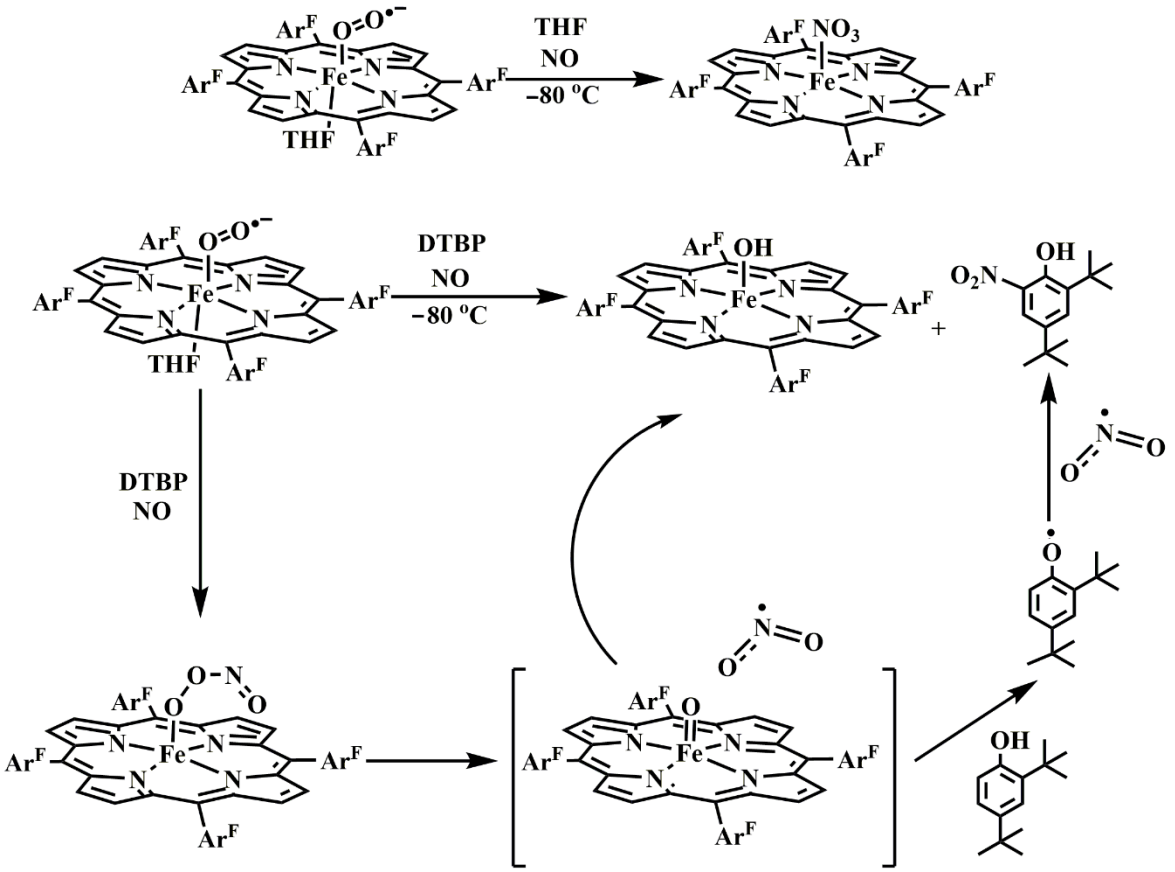

Scheme 1.14. NOD activity by a heme superoxo complex.

Kurtikyan group reported oxy-coboglobin model compounds [(Py)Co(Por)(O_2)] {por = *meso*-tetraphenyl- and *meso*-tetra(*p*-tolyl)porphyrinato dianions}, which react with NO at low temperature to form a six coordinated nitrato complex [(Py)Co(Por)(η^1-ONO_2)] *via* initial formation of a six-coordinate PN intermediate [(Py)Co(Por)(η^1-OONO)] (Scheme 1.15). They characterized the Co-PN complexes by FT-IR spectroscopy.[36]

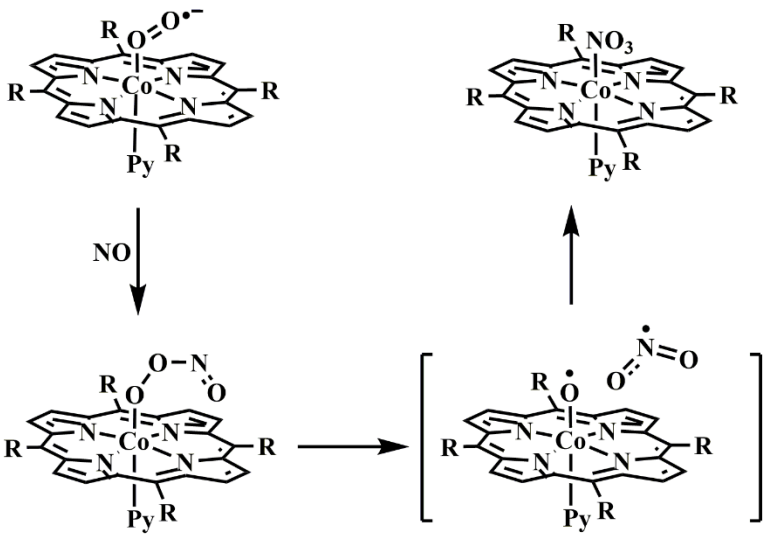

Scheme 1.15. NOD activity of oxy-coboglobin model complexes.

Very recently the same group reported the reactions of Mn(II)-porphyrin O_2 adducts [Mn^{IV}(por)(η^2-O_2)] with NO. In all the cases they ended up with six-coordinated peroxynitrito Mn(III)-nitrosyl complexes (Scheme 1.16).[37]

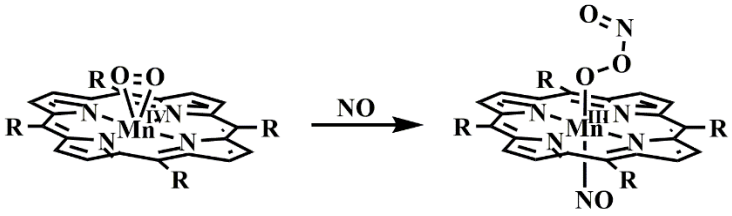

Scheme 1.16. Formation of six-coordinated peroxynitrito Mn(III) nitrosyls.

Not only metal-superoxo, but metal-peroxo complexes are also known to display NOD activity. The reaction of a [Co(III)-O_2^{2-}] complex of *bis*(2-ethyl-4-methyl-imidazol-5-yl)methane ligand with NO at −40 ºC results in corresponding Co(II)-nitrato complex.[38]

The presence of a [Co(II)-PN] intermediate was confirmed by characteristic phenol ring nitration experiment (Scheme 1.17).

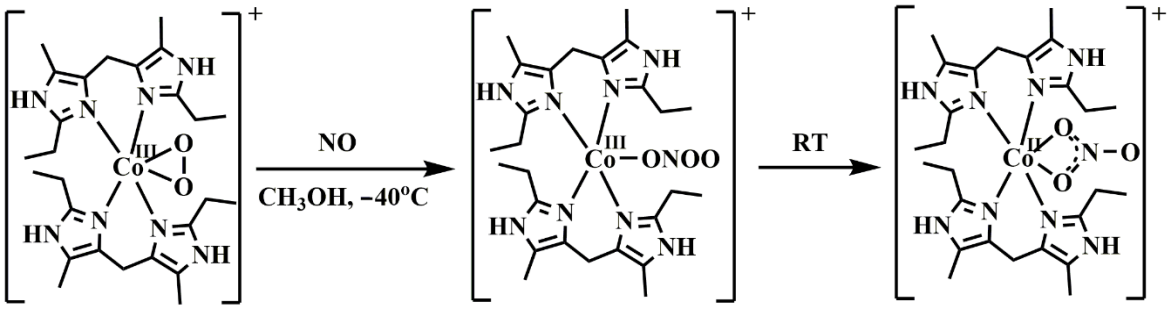

Scheme 1.17. NOD activity of a Co(III) peroxo complex.

TMC ligated Cr(IV)-peroxo complex, $[Cr^{IV}(12\text{-TMC})(O_2^{2-})(Cl)]^+$ reportedly reacts with NO to form a Cr(III)-nitrato complex which is most likely to form *via* a [Cr(III)-PN] intermediate (Scheme 1.18).[39] They proposed subsequent dissociation to [Cr(IV)=O] and NO_2 through homolytic cleavage of O−O bond in PN followed by recombination which yield the NO_3^- complex. However, the mechanism is purely speculative and no effort was made to identify the proposed intermediates.

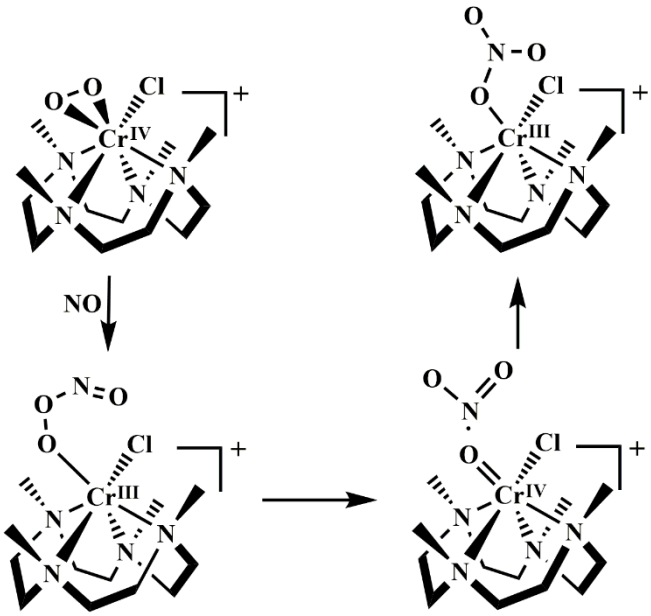

Scheme 1.18. Reaction of a Cr(IV) peroxo complex with NO.

A Cr(III)-superoxo complex $[(14\text{-TMC})Cr(O_2^{-})(Cl)]^{+}$ reacts with NO to result in the $[Cr(III)\text{-}NO_2^{-}]$ complex *via* [Cr(III)-PN] intermediate (Scheme 1.19). In this case, however, involvement of a stable [Cr(IV)=O] species, $[(14\text{-TMC})Cr(O)(Cl)]^{+}$, was seen in EPR spectroscopy and ESI-MS.[40]

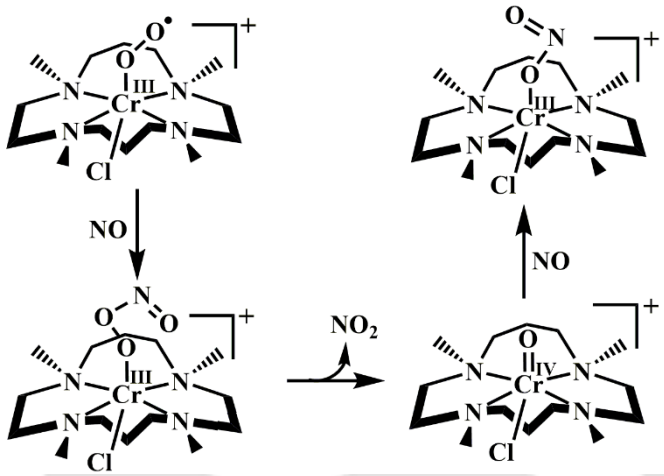

Scheme 1.19. Formation of a stable [Cr(IV)=O] in the reaction of $[Cr(III)\text{-}O_2^{-}]$ and NO.

Most recently, Kumar group reported the formation of [Ni(II)-PN] complexes generated in the reaction of a Ni(III)-peroxo complex, $[Ni^{III}(12\text{-TMC})(O_2^{2-})]$ and NO. The unstable intermediate readily isomerizes to a stable $[Ni(II)\text{-}NO_3^{-}]$ complex (Scheme 1.20).[41]

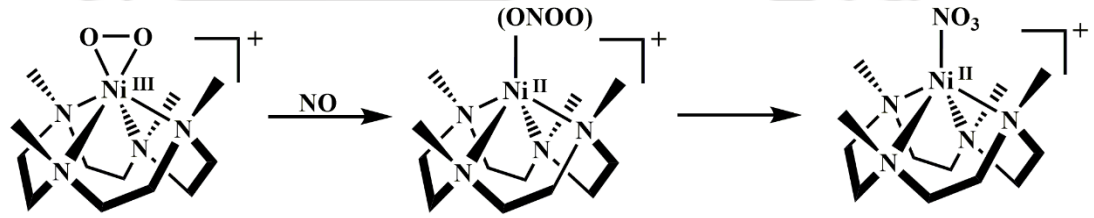

Scheme 1.20. Formation of a [Ni(II)-PN] intermediate in the reaction of $[Ni(III)\text{-}O_2^{2-}]$ and NO.

1.3 Nitroxyl

Nitroxyl (HNO or NO^{-}; also known as azanone, nitrosyl hydride, hydrogen oxonitrate, nitroso hydrogen, monomeric hyponitrous acid etc.) is one electron reduced species of NO which is believed to have a diverse range of physiochemical activity.[42] It has chemical

properties and chemicophysical properties distinct from NO and many of those are not well established and quite controversial.[43] HNO is reported to take part in assimilatory nitrite reductase, and cytochrome P450 nitric oxide reductase; to act as an irreversible inhibitor of mitochondrial aldehyde dehydrogenase and glyceraldehydes-3-phosphate dehydrogenase through cystein modification; and as an oxidant to thiols.[44] Recently, HNO has shown to have potential pharmacological properties including maintaining vascular tone, preventing myocardial diseases as well as anti-oxidant and anticancer activities etc.[45]

The production, detection and investigation of HNO have been extremely complicated due to its high reactivity, which often raises questions about the validity of any chemical or biochemical investigation. It readily undergoes dehydrative dimerisation to form H_2O and N_2O *via* the formation of hyponitrous acid ($H_2N_2O_2$).[46] It reacts with thiols at an even faster rate to produce either sulfinamide or disulfide and hydroxylamine.[47]

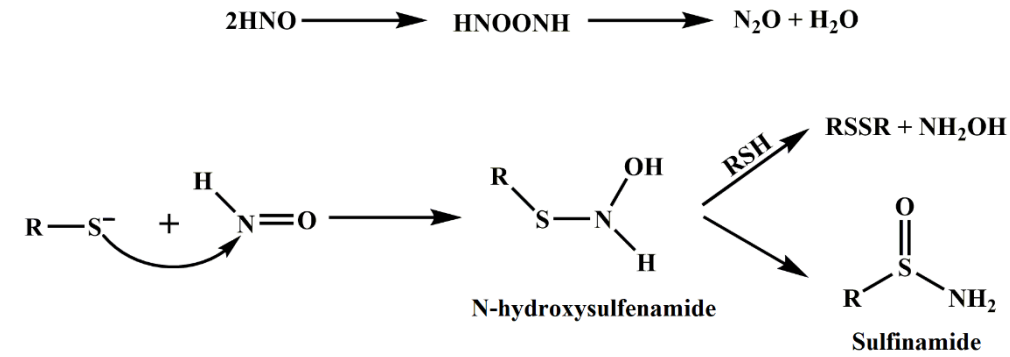

Scheme 1.21. Decomposition pathways of HNO.

Another important property of HNO is its reactivity towards phosphines to produce phosphine oxide and aza-ylide. This is a very specific reaction and often used as a marker for in situ detection of HNO.[48]

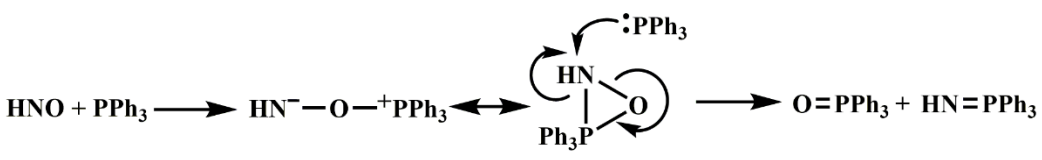

Scheme 1.22. Reaction of HNO with phosphines.

Metal complexes with metal in higher oxidation state undergo reductive nitrosylation on reacting with HNO. This reaction is biologically important because HNO can interact with oxidized state of various hemeproteins to form corresponding ferrous nitrosyls *via* one step reduction. Examples include methemoglobin (metHb), metmyoglobin (metMb), ferric-cytochromes, and peroxidases etc. Moreover, it oxidises oxyhemoglobin and oxymyoglobin to their ferric form. HNO reacts with O_2 to form a reactive nitrogen species (RNS), which is not PN, but has similar cytotoxic effects and can cause oxidation of DNA even in milimolar concentration.[49,50]

Scheme 1.23. General reaction of HNO with ferric hemeproteins.

Endogenously, HNO is generated from reduction of NO by cytochrome *c* oxidase, xanthine oxidase and hemoglobin, reaction of S-nitrosothiol with excess thiol and mostly *via* NOS mediated oxidation of L-arginine in absence of tetrahydrobiopterin.[51]

First reported attempt of laboratory synthesis of HNO was reported by Harteck where he tried to react H atom with NO at cryogenic temperatures of liquid air (~ −196 °C). He got a hygroscopic yellow transparent solid product which was described as $[HNO]_n$.[52] Commonly, HNO is synthesized from photochemical or thermal decomposition of organic compounds like nitromethane, N-hydroxybenzensulfonamide (Piloty's acid), cyanamide, acyl or acyloxy nitroso compounds or inorganic salts $Na_2N_2O_3$ (Angeli's Salt) and transition metal nitrosyl complexes suitable electronic configurations, {M(NO)}[7,8,9]. Among those Angeli's salt or sodium trioxodinitrate (sodium salt of N-nitrohydroxylamate) is the most extensively studied. The conventional mechanism of decomposition above pH 4 involves protonation of the dianion at the nitroso oxygen

followed by tautomerization and heterolytic cleavage of the N-N bond to produce HNO and nitrite.[53]

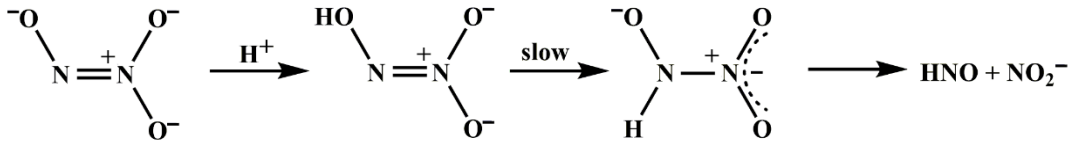

Scheme 1.24. Generation of HNO from Angeli's salt.

N-hydroxysulfonamides or Piloty's acid has almost similar mechanism to Angeli's salt in terms pH dependency and reversibility. The decomposition pathway includes base catalyzed deprotonation mechanism followed by S−N bond heterolysis.[54]

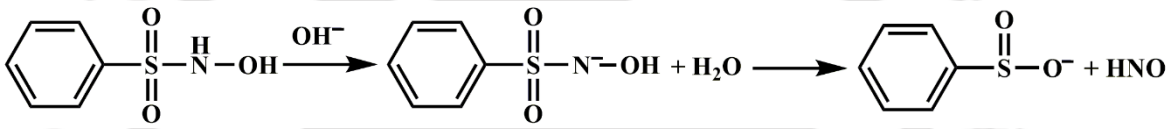

Scheme 1.25. Generation of HNO from Piloty's acid.

Among the HNO donors, cyanamide is the only clinically approved drug used for anti-alcoholism. Cyanamide is oxidized by the catalase enzyme to N-hydroxy cyanamide which then spontaneously decomposes to HNO and cyanide, CN^-.[55]

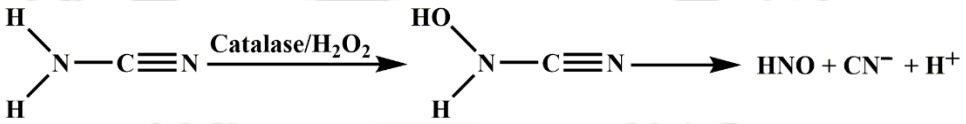

Scheme 1.26. Bioactivation of cyanamide to release HNO.

1.3.1 Transition metal mediated formation of HNO/NO^-

Direct reduction NO to $^3NO^-$ is highly energy demanding process as redox potential for the NO/$^3NO^-$ couple is −0.8 (± 0.2) V *vs.* NHE. Hence, outer sphere electron transfer from metal to NO is quite difficult, but an inner sphere process is attainable when coupled with a proton coupled electron transfer pathway (Scheme 1.27). A few examples of outer sphere

reduction is still available in literature. For example, Leipoldt *et al.* reported direct reduction of NO to NO^- by $[Ru(NH_3)_6]^{2+}$.[56] Lehnert *et al.* reported another outer sphere reaction by a $[Fe(Por)NO]^-$ species.[57]

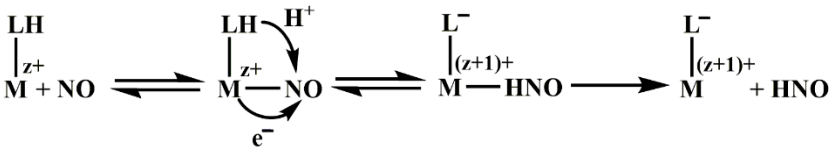

Scheme 1.27. Mechanism for inner sphere proton coupled electron transfer process.

The ferric heme enzyme in NOS is known to produce NO^- in absence of tetrahydrobiopterin (H_4B). It is reported that in an H_4B free reduction of N-hydroxy-L-arginine (NHA) with H_2O_2 or $NADPH/O_2$ resulted release of NO^- as one of the inorganic products which was confirmed by the reduction of the ferric NOS to give a ferrous nitrosyl complex.[58,59]

In denitrifying bacteria *Fusarium oxysporum* an enzyme called cytochrome P450 nitric oxide reductases (P450nor) eliminates toxic nitric oxide by reducing it to N_2O (Scheme 1.28). The active site, a heme *b* group with axially bound proximal cystein residue, reacts with NO to give a ferric nitrosyl complex which is then reduced by NADPH to give an intermediate complex, I which is a proposed Fe^{III}-nitroxyl complex.[60]

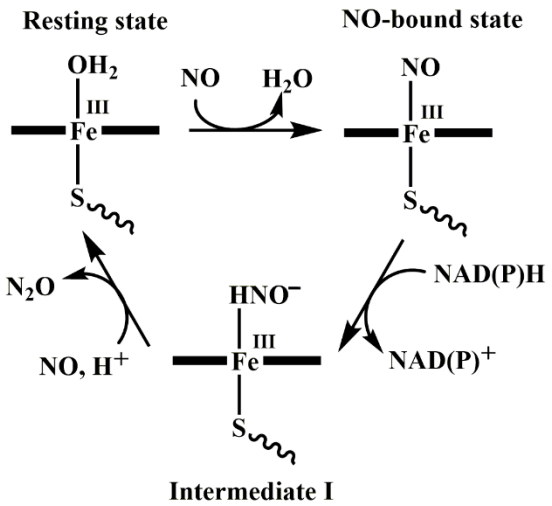

Scheme 1.28. Bacterial nitric oxide reduction by P450nor.

In assimilatory nitrite reductase (NiR) catalyzed reduction of nitrite to ammonia in plants involvement of a Fe(III)-nitroxyl intermediate is proposed. This is a six electron process which involves a Fe_4S_4/siroheme active site; nonetheless the exact mechanism is still unknown. In the proposed mechanistic pathway dehydration of a ferrous nitrite adduct produces a [Fe(III)-NO] intermediate which was further reduced by the Fe_4S_4 cluster to give a [Fe(III)-NO^-] species.[61]

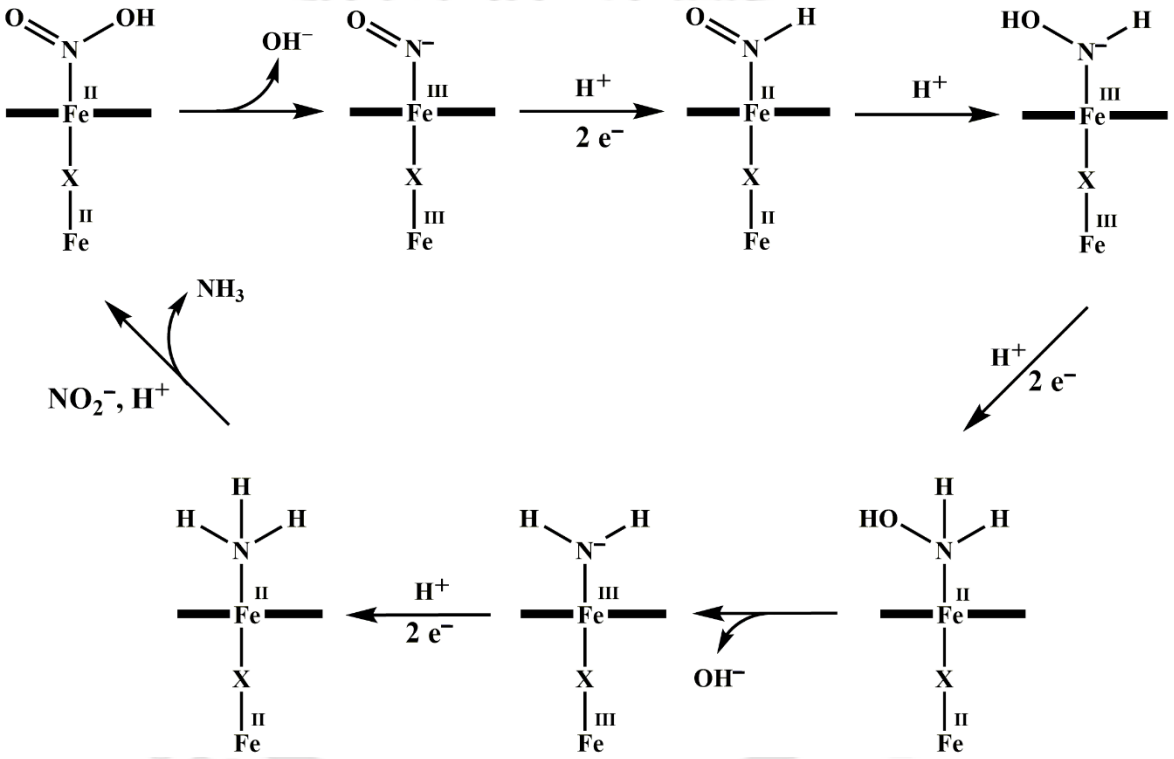

Scheme 1.29. Mechanism of assimilatory nitrite reductase.

Goldberg group reported a non-heme high-spin $\{Fe(NO)\}^8$ complex, that they synthesized by reducing the corresponding $\{Fe(NO)\}^7$ precursor with decamethylcobaltocene ($Co(Cp^*)_2$), which spontaneously releases N_2O (Scheme 1.30). This observation is in agreement with the proposed mechanism of NOR. DFT calculation suggested the electronic structure of the reduced complex as [Fe^{II}-NO^-]. However, the release of N_2O is attributed to reductive N-N coupling of two nitrosyl groups rather than release of HNO and its subsequent dimerization to N_2O.[62]

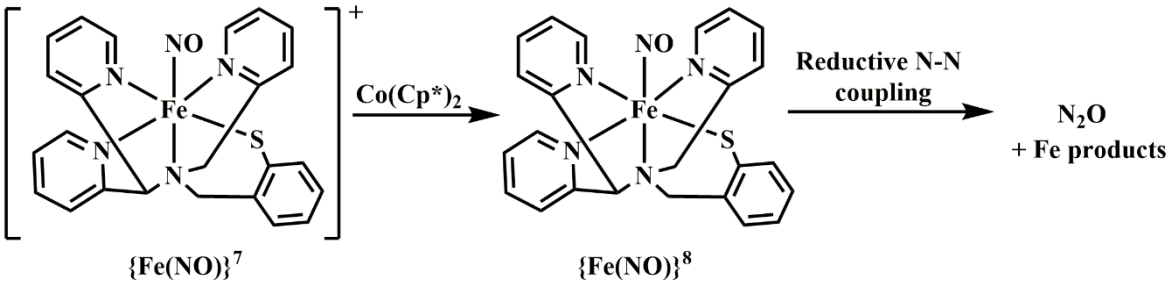

Scheme 1.30. Spontaneous release of N_2O by an $\{Fe(NO)\}^8$ complex.

Enemark and Feltham reported $\{Co(NO)\}^8$ complex of type $[Co(NO)(das)_2X_2]$ (das = o-phenylene-*bis*(dimethylarsine); X= ClO_4^-, NCS^-) where they showed two electron reduction from NO^+ to NO^- upon change of the coordination environment. Crystal structure revealed that $[Co(NO)(das)_2](ClO_4)_2$ is a 5-coordinated linear nitrosyl complex with NO^+ character ($\angle$Co-N-O = 178°; ν_{NO} = 1852 cm^{-1}). But in case of $[Co(NO)(das)_2(NCS)](NCS)$, when NCS^- is present as sixth ligand bond angle decreases to 132° and IR stretch of 1587 cm^{-1} suggests NO^- character.[63]

Harrop *et al.* reported a thermally stable $\{Fe(NO)\}^8$ complex $[Co(Cp^*)_2][Fe(LN_4)(NO)]$ (H_2LN_4 = (N^1E,N^2E)-N^1,N^2-*bis*((1H-pyrrol-2-yl)methylene)-propane-1,3-diamine) which was obtained from the reduction of corresponding $\{Fe(NO)\}^7$ complex with $(Co(Cp^*)_2)$. This complex reportedly reacts with metMb to produce MbNO *via* reductive nitrosylation, which suggests presence of a Fe(III)-HNO/NO^- form (Scheme 1.31).[64]

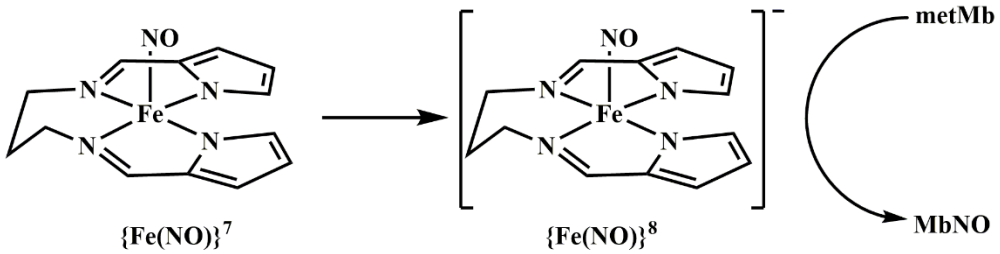

Scheme 1.31. Nitroxyl release from a thermally stable $\{Fe(NO)\}^8$ complex.

The same group reported a proton induced release of NO^- from a $\{Co(NO)\}^8$ system $[Co(LN_4^{PhCl})(NO)]$ ($H_2LN_4^{PhCl}$ = (N^1E,N^2E)-N^1,N^2-*bis*((1H-pyrrol-2-yl)methylene)-4,5-dichlorobenzene-1,2-diamine). Otherwise stable, this complex acts as HNO/NO^- donor upon addition of HBF_4 and readily reacts with $[Fe^{III}(TPP^{2-})Cl]$ to produce the corresponding $\{Fe(NO)\}^7$ complex or reacts with PPh_3 to yield $Ph_3P{=}O$ and $Ph_3P{=}NH$. In absence of any HNO acceptor, it disproportionate to give $\{Co(NO)_2\}^{10}$ complex (Scheme 1.32).[65]

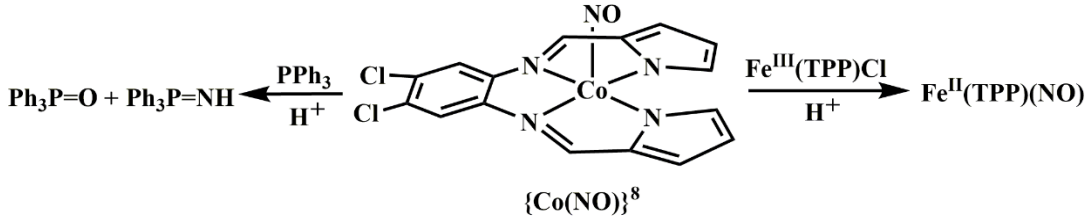

Scheme 1.32. Proton induced NO^- release from $\{Co(NO)\}^8$ complex.

Later, they reduced the same complex using KC_8 in 18-crown-6 ether (18C6) to generate corresponding $\{Co(NO)\}^9$ system $[K(18C6)][Co(LN_4^{PhCl})(NO)]$ which has NO stretch at 1617 cm^{-1} (Scheme 1.33). This complex releases HNO upon addition of H^+ in water which was confirmed by detection of N_2O as one of the decomposition products. Moreover, this complex reacts with PPh_3 to give $Ph_3P{=}O$ and $Ph_3P{=}NH$; $[Mn^{III}(Por)]$ to give $[(Por)Mn^{II}$-NO]; and metMb to give MbNO confirming its role as HNO donor.[66]

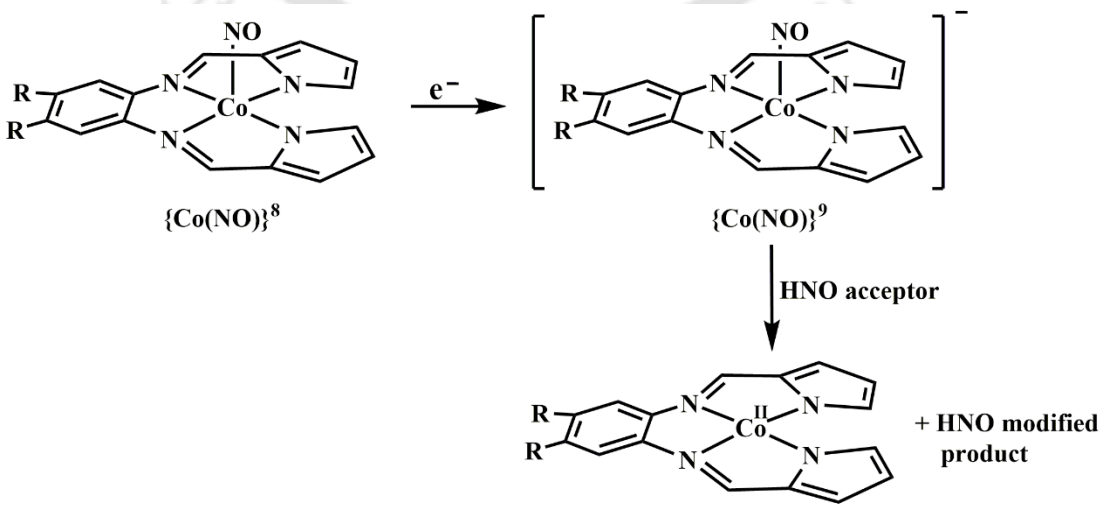

Scheme 1.33. $\{Co(NO)\}^9$ complex as HNO donor.

Photo-induced HNO release from $\{Fe(NO)\}^6$ complexes is reported by Lee *et al.* Fe-nitrosyl complex, $[Fe(NO)(^{TMS}PS_2)(^{TMS}PS_2H)]$, ($^{TMS}PS_2H_2$ = 2,2′-dimercapto-3,3′-*bis*(trimethylsilyl)diphenyl)phenylphosphine) with a pendant thiol in the ligand releases HNO on irradiation of visible light (Scheme 1.34). This was confirmed by detection of N_2O in the reaction vessel as well as its reaction with a Mn(III) nitroxyl trap giving $\{Mn(NO)\}^6$. Replacement of the thiol proton by a methyl group resulted release NO rather than HNO, which confirms that the process occurs only in the presence of thiol proton.[67]

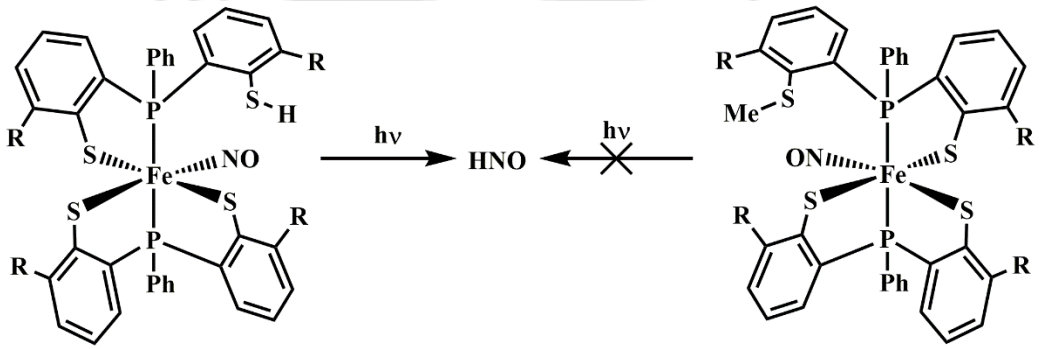

Scheme 1.34. Photo-induced release of HNO from $\{Fe(NO)\}^6$ complex.

1.4 Scope of the thesis

The biochemical metabolism of excess NO broadly follows two pathways *viz.* oxidative and reductive. The oxidative pathway, found in mammals, involves NOD enzyme which converts NO to benign NO_3^-. The proposed mechanism of NOD includes the formation of an [Fe(III)-PN] intermediate followed by its decomposition to an oxo-ferryl intermediate and NO_2. However, owing to their high instability explicit spectroscopic characterization of neither of the intermediates could be done till date; thereby making the mechanism an elusive one. The reductive pathway is seen in lower organisms where NO is reduced to N_2O by NOR enzymes like bacterial P450nor. Here also, in most of the cases involvement of an unstable metal-nitroxyl intermediate complex is often implicated.

The idea of the thesis originates from our interest in mimicking these enzymatic processes using small molecule models. First-row transition metal complexes were used for their more biological relevancy. Both the oxidative and reductive pathways were explored and attempts of identifying and characterizing the intermediates were made. The main objective briefly includes,

1. Synthesis and characterization of first-row transition metal nitrosyl complexes bearing substituted porphyrin ligands.
2. Study of the reactivity of these complexes towards reactive oxygen species (ROS) leading to the formation of metal-PN intermediates and their decomposition in pursuit of a well characterized high valent metal oxo species along the mechanistic pathway.
3. Exploring the mechanism of metal mediated reduction of the bonded NO and finding utility of the metal nitrosyl complexes as HNO donors.

1.5 References

1. *Nitric Oxide: Biology and Pathobiology*; Ignarro, L. J., Ed.; Academic Press: San Diego, **2000**.
2. *Nitric Oxide and Infection*; Fang, F. C., Ed.; Kluwer Academic/ Plenum Publishers: New York, **1999**.
3. Bourassa, J. L.; Ives, E. P.; Marqueling, A. L.; shimanovich, R.; Groves, J. T. *J. Am. Chem. Soc.* **2001**, *123*, 5142.
4. Marietta, M. A.; Yoon, P. S.; Iyengar, R.; Leaf, C. D.; Wishnok, J. S. *Biochemistry* **1988**, *27*, 8706.
5. Averill, B. A. *Chem. Rev.* **1996**, *96*, 2951.
6. Torres, J.; Cooper, C. E.; Wilson, M. T. *J. Biol. Chem.* **1998**, *273*, 8756.

7. Cooper, C. E.; Torres, J.; Sharpe, M. A.; Wilson, M. T. *FEBS Letters* **1997**, *414*, 281.
8. Torres, J.; Svistunenko, D.; Karlsson, B.; Cooper, C. E.; Wilson, M. T. *J. Am. Chem. Soc.* **2002**, *124*, 963.
9. Stadler, J.; Trockfeld, J.; Schmalix, W. A.; Brill, T.; Siewert, J. R.; Greim, H.; Doehmer, J. *Proc. Natl. Acad. Sci. U.S.A.* **1994**, *91*, 3559.
10. Brown, G. C. *Eur. J. Biochem.* **1995**, *232*, 188.
11. Gross, S. S.; Wolin, M. S. *Annu. Rev. Physiol.* **1995**, *57*, 737.
12. Kissner, R.; Nauser, T.; Bugnon, P.; Lye, P. G.; Koppenol, W. H. *Chem. Res. Toxicol.* **1997**, *10*, 1285.
13. Koppenol, W. H.; Kissner, R. *Chem. Res. Toxicol.* **1998**, *11*, 87.
14. Marletta, M. A.; Yoon, P. S.; Iyengar, R; Leaf, C. D; Wishnok, J. S. *Biochemistry* **1988**, *27*, 8706.
15. Szabó, C.; Ischiropoulos, H.; Radi, R. *Nat. Rev. Drug. Discov.* **2007**, *6*, 662.
16. Beal, M. F. *Free Radical Biol. Med.* **2002**, *32*, 797.
17. Radi, R.; Cassina, A.; Hodara, R.; Quijano, C.; Castro, L. *Free Radical Biol. Med.* **2002**, *33*, 1451.
18. (a) Vliet, A. V.; Eiserich, J. P.; Halliwell, B.; Cross, C. E. *J. Biol. Chem.* **1997**, *272*, 7617. (b) Bartesaghi, S.; Radi, R. *Redox Biol.* **2018**, *14*, 618.
19. Radi, R. *Proc. Natl. Acad. Sci*. U. S. A. **2004**, *101*, 4003.
20. Quijano, C.; Hernandez-Saavedra, D.; Castro, L.; McCord, J. M.; Freeman, B. A.; Radi, R. *J. Biol. Chem.* **2001**, *276*, 11631.
21. (a) Clarkson, S. G.; Basolo, F. *J. Chem. Soc. Chem. Commun.* **1972**, *11*, 670; (b) Clarkson, S. G.; Basolo, F. *Inorg. Chem.* **1973**, *12*, 1528.
22. Park, G. Y.; Deepalatha, S.; Puiu, S. C.; Lee, D.-H.; Mondal, B.; Sarjeant, A. A. N.;

del Rio, D.; Pau, M. Y. M.; Solomon, E. I.; Karlin, K. D. *J. Biol. Inorg. Chem.* **2009**, *14*, 1301.

23. (a) Tran, N. G.; Kalyvas, H.; Skodje, K. M.; Hayashi, T.; Moënne-Loccoz, P.; Callan, P. E.; Shearer, J.; Kirschenbaum, L. J.; Kim, E. *J. Am. Chem. Soc.* **2011**, *133*, 1184. (b) Skodje, K. M.; Williard, P. G.; Kim, E. *Dalton Trans.* **2012**, *41*, 7849.
24. Cao, R.; Elrod, L. T.; Lehane, R. L.; Kim, E.; Karlin, K. D. *J. Am. Chem. Soc.* **2016**, *138*, 16148.
25. Gogoi, K.; Saha, S.; Mondal, B.; Deka, H.; Ghosh, S.; Mondal, B. *Inorg. Chem.* **2017**, *56*,14438.
26. Kalita, A.; Kumar, P.; Mondal, B. *Chem. Commun.* **2012**, *48*, 4636.
27. Kumar, P.; Lee, Y.-M.; Park, Y. J.; Siegler, M. A.; Karlin, K. D.; Nam, W. *J. Am. Chem. Soc.* **2015**, *137*, 4284.
28. Saha, S.; Gogoi, K.; Mondal, B.; Ghosh, S.; Deka, H.; Mondal, B. *Inorg. Chem.* **2017**, *56*, 7781.
29. Mondal, B.; Saha, S.; Borah, D.; Mazumdar, R.; Mondal, B. *Inorg. Chem.* **2019**, *58*, 1234.
30. Mondal, B.; Borah, D.; Mazumdar, R.; Mondal, B. *Inorg. Chem.* **2019**, *58*, 14701.
31. (a) Wick, P.K., Kissner R., Koppenol, W. H., *Helv. Chim. Acta.* **2000**, *83*, 748. (b) Wick, P. K.; Kissner, R.; Koppenol, W. H. *Helv. Chim. Acta*. **2001**, *84*, 3057.
32. Thyagarajan, S.; Incarvito, C.; Rheingold, A. L.; Theopold, K. H. *Inorg. Chim. Acta.* **2003**, *345*, 333.
33. Maiti, D.; Lee, D.-H.; Sarjeant, A. A. N.; Pau, M. Y. M.; Solomon, E. I.; Gaoutchenova, K.; Sundermeyer, J.; Karlin, K. D. *J. Am. Chem. Soc.* **2008**, *130*, 6700.
34. Liu, J. J.; Siegler, M. A.; Karlin, K. D.; Moënne-Loccoz, P. *Angew. Chem. Int. Ed.*

2019, *58*, 10936.

35. Schopfer, M. P.; Mondal, B.; Lee, D.-H.; Sarjeant, A. A. N.; Karlin, K. D. *J. Am. Chem. Soc*. **2009**, *131*, 11304.
36. (a) Kurtikyan, T. S.; Eksuzyan, S. R.; Hayrapetyan, V. A.; Martirosyan, G. G.; Hovhannisyan, G. S.; Goodwin, J. A. *J. Am. Chem. Soc.* **2012**, *134*, 13861. (b) Kurtikyan, T. S.; Eksuzyan, Sh. R.; Goodwin, J. A.; Hovhannisyan, G. S.; *Inorg. Chem.* **2013**, *52*, 12046.
37. Kurtikyan, T. S.; Hayrapetyan, V. A.; Hovhannisyan, A. A.; Martirosyan, G. G.; Hovhannisyan, G. S.; Iretskii, A. V.; Ford, P. C. *Inorg. Chem.* **2020**, *59*, 17224.
38. Saha, S.; Ghosh, S.; Gogoi, K.; Deka, H.; Mondal, B.; Mondal, B. *Inorg. Chem*. **2017**, *56*, 10932.
39. Yokoyama, A.; Han, J. E.; Cho, J.; Kubo, M.; Ogura, T.; Siegler, M. A.; Karlin, K. D.; Nam, W. *J. Am. Chem. Soc.* **2012**, *134*, 15269.
40. Yokoyama, A.; Cho, K.-B.; Karlin, K. D.; Nam, W. *J. Am. Chem. Soc.* **2013**, *135*, 14900.
41. Yenuganti, M.; Das, S.; Kulbir, Ghosh, S.; Bhardwaj, P.; Pawar, S. S.; Sahoo, S. C.; Kumar, P. *Inorg. Chem. Front.* **2020**, *7*, 4872.
42. Miranda, K. M. *Coord. Chem. Rev.* **2005**, *249*, 433.
43. Paolocci, N.; Jackson, M. I.; Lopez, B. E.; Miranda, K.; Tocchetti, C. G.; Wink, D. A.; Hobbs, A. J.; Fukuto, J. M. *Pharmacol. Ther.* **2007**, *113*, 442.
44. Fukuto, J. M.; Bartberger, M. D.; Dutton, A. S.; Paolocci, N.; Wink, D. A.; Houk, K. N. *Chem. Res. Toxicol* **2005**, *18*, 790.
45. (a) Paolocci, N.; Katori, T.; Champion, H. C.; St. John, M. E.; Miranda, K. M.; Fukuto, J. M.; Wink, D. A.; Kass, D. A. *Proc. Natl. Acad. Sci. U.S.A.* **2003**, *100*, 5537. (b) Pagliaro, P.; Mancardi, D.; Rastaldo, R.; Penna, C.; Gattullo, D.;

Miranda, K. M.; Feelisch, M.; Wink, D. A.; Kass, D. A.; Paolocci, N. *Free Radical Biol. Med.* **2003**, *34*, 33. (c) Wink, D. A.; Miranda, K. M.; Katori, T.; Mancardi, D.; Thomas, D. D.; Ridnour, L.; Espey, M. G.; Feelisch, M.; Colton, C. A.; Fukuto, J. M.; Pagliaro, P.; Kass, D. A.; Paolocci, N. *Am. J. Physiol. Heart Circ. Physiol.* **2003**, *285*, H2264.

46. Shafirovich, V.; Lymar, S. V. *Proc. Natl. Acad. Sci. U. S. A.* **2002**, *99*, 7340.
47. (a) Fukuto, J. M.; Millikin R. J.; *The Chemistry and Biology of Nitroxyl (HNO)*; Doctorovich, F.; Farmer, P. J.; Marti, M. A.; Eds.; Elsevier, **2017**; 321. (b) Sherman, M. P.; Grither, W. R.; McCulla, R. D. *J. Org. Chem.* **2010**, *75*, 4014.
48. Reisz, J. A.; Klorig, E. B.; Wright, M. W.; King, S. B. *Org. Lett.* **2009**, *11*, 2719.
49. Miranda, K. M.; Espey, M. G.; Yamada, K.; Krishna, M.; Ludwick, N.; Kim, S.; Jourd'heuili, D.; Grishami, M. B.; Feelischi, M.; Fukuto, J. M.; Wink, D. A. *J. Biol. Chem.* **2001**, *276*, 1720.
50. Miranda, K. M.; Yamada, K.; Espey, M. G.; Thomas, D. D.; DeGraff, W.; Mitchell, J. B.; Krishna, M. C.; Colton, C. A.; Wink, D. A. *Arch. Biochem. Biophys.* **2002**, *401*, 134.
51. (a) Rusche, K. M.; Spiering, M. M.; Marletta, M. A. *Biochemistry* **1998**, *37*, 15503. (b) Adak, S.; Wang, Q.; Stuehr, D. J. *J. Biol. Chem.* **2000**, *275*, 33554.
52. Harteck, P. *Berichte der Deutschen Chemischen Gesellschaft* **1933**, *66*, 423.
53. (a) King, S. B.; Nagasawa, H. T. *Methods Enzymol.* **1999**, *301*, 211. (b) Hughes, M. N.; Wimbledon, P. E. *J. Chem. Soc. Dalton Trans.* **1976**, 703.
54. (a) Piloty, O. *Ber. Dtsch. Chem. Ges.* **1896**, *29*, 1559. (b) Bonner, F.; Ko, Y. *Inorg. Chem.* **1992**, *31*, 2514. (c) Zamora, R.; Grzesiok, A.; Weber, H.; Feelisch, M. *Biochem. J.* **1995**, *312*, 333.
55. (a) Nagasawa, H. T.; DeMaster, E. G.; Redfern, B.; Shirota, F. N.; Goon, D. J. W.

J. Med. Chem. **1990**, *33*, 3120. (b) Shirota, F. N.; Goon, D. J. W.; DeMaster, E. G.; Nagasawa, H. T. *Biochem. Pharmacol.* **1996**, *52*, 141.

56. Leipoldt, J. G.; Eldik, R.; Basson, S. S.; Roodt, A. *Inorg. Chem.* **1986**, *25*, 4639.
57. Goodrich, L. E.; Roy, S.; Alp, E. E.; Zhao, J.; Hu, M. Y.; Lehnert, N. *Inorg. Chem.* **2013**, *52*, 7766.
58. Rusche, K. M.; Spiering, M. M.; Marletta, M. A. *Biochemistry* **1998**, *37*, 15503.
59. Adak, S.; Wang, Q.; Stuehr, D. J. *J. Biol. Chem.* **2000**, *275*, 33554.
60. (a) McQuarters, A. B.; Wirgau, N. E.; Lehnert, N. *Current Opinion in Chemical Biology* **2014**, *19*, 82. (b) Tosha, T.; Nomura, T.; Nishida, T.; Saeki, N.; Okubayashi, K.; Yamagiwa, R.; Sugahara, M.; Nakane, T.; Yamashita, K.; Hirata, K.; Ueno, G.; Kimura, T.; Hisano, T.; Muramoto, K.; Sawai, H.; Takeda, H.; Mizohata, E.; Yamashita, A.; Kanematsu, Y.; Takano, Y.; Nango, E.; Tanaka, R.; Nureki, O.; Shoji, O.; Ikemoto, Y.; Murakami, H.; Owada, S.; Tono, K.; Yabashi, M.; Yamamoto, M.; Ago, H.; Iwata, S.; Sugimoto, H.; Shiro, Y.; Kubo, M. *Nat. Commun.* **2017**, *8*, 1585.
61. Lui, S. M.; Liang, W.; Soriano, A.; Cowan, J. A. *J. Am. Chem. Soc.* **1994**, *116*, 4531.
62. Confer, A. M.; McQuilken, A. C.; Matsumura, H.; Moënne-Loccoz, P.; Goldberg, D. P. *J. Am. Chem. Soc.* **2017**, *139*, 10621.
63. Enemark, J. Feltham, R. D.; Riker-Nappier, J.; Bizot, K. F. *Inorg. Chem.* **1975**, *14*, 624.
64. Patra, A. K.; Dube, K. S.; Sanders, B. C.; Papaefthymiou, G. C.; Conradie, J.; Ghosh, A.; Harrop T. C. *Chem. Sci.* **2012**, *3*, 364.
65. Rhine, M. A.; Rodrigues, A. V.; Bieber Urbauer, R. J.; Urbauer, J. L.; Stemmler, T. L.; Harrop, T. C. *J. Am. Chem. Soc.* **2014**, *136*, 12560.

66. Walter, M. R.; Dzul, S. P.; Rodrigues, A. V.; Stemmler, T. L.; Telser, J.; Conradie, J.; Ghosh, A.; Harrop, T. C. *J. Am. Chem. Soc.* **2016**, *138*, 12459.

67. Chiang, C.-K.; Chu, K.-T.; Lin, C.-C.; Xie, S.-R.; Liu, Y.-C.; Demeshko, S.; Lee, G.-H.; Meyer, F.; Tsai, M.-L.; Chiang, M.-H.; Lee, C.-M. *J. Am. Chem. Soc.* **2020**, *142*, 8649.

Chapter 2

Reaction of a $\{Co(NO)\}^8$ complex with superoxide: Formation of a six coordinated $[Co^{II}(NO)(O_2^-)]$ species followed by peroxynitrite intermediate

Abstract

A nitrosyl complex of Co(II) porphyrinate, $[Co(F_{20}TPP^{2-})(NO)]$, [$F_{20}TPPH_2$ = 5,10,15,20-*tetrakis*(pentafluorophenyl)porphyrin] having $\{Co(NO)\}^8$ configuration was synthesized and characterized by means of spectroscopic and structural analyses. Single crystal X-ray structure of the complex revealed the square pyramidal geometry around the cobalt center with a bent nitrosyl group. It reacts with superoxide (O_2^-) ion in CH_2Cl_2 at –40 °C to result in the corresponding nitrite (NO_2^-) complex. Involvement of a [Co(II)-PN] intermediate is proposed in the course of the reaction. Moreover, spectroscopic studies suggested the formation of a transient six-coordinated $[Co^{II}(NO)(O_2^-)]$ species.

2.1 Introduction

Nitric oxide (NO) is a ubiquitous molecule in mammalian system and takes part in various physiological processes ranging from regulation of cardiovascular function to signal transduction and defense processes of the immune system.[1-3] Though a sub-micromolar concentration of NO is required for smooth functioning of these physiological processes, higher concentration has detrimental effects due to its high reactivity. By virtue of its radical nature NO is known to cause oxidative or nitrosative stress through direct or transition metal mediated pathways. A number of NO-dependent toxicity often arises from the generation of secondary reactive nitrogen species like nitrogen dioxide (NO_2), PN ($ONOO^-$) etc. PN, formed in the reaction of superoxide (O_2^-) and NO, has a half-life period of few milliseconds, is highly reactive and can cause nitration of protein tyrosine and tryptophan residues and oxidation of DNA molecules.[4-10] Further, when bonded to a transition metal ion its activity increases by many folds. Such a species is very likely to form inside the body through interaction of NO with metalloenzymes-dioxygen adducts. For more than a decade researcher have been trying to get insights on the formation and decomposition pathways of transition metal-PN complexes. However, elevated reactivity of these complexes is a big challenge for such studies. In this direction, Karlin's group reported some of the earliest examples of iron and copper superoxo complexes which react with NO to give respective PN intermediate complexes in both heme and non-heme ligand frameworks.[11] Similarly, Kurtikyan's group reported that an oxy-coboglobin complex reacts with NO to give [Co(III)-PN] complex.[12] Nam's group also reported reaction of NO with chromium superoxo and peroxo complexes to give chromium PN complexes.[13] In all these examples, PN complexes are found to be highly unstable and rapidly convert to corresponding nitrates or nitrites.

Transition metal PN complexes are also reported to form in the reactions of metal nitrosyls

with superoxides/peroxides. For example, a $\{Co(NO)\}^8$ complex of N-tetramethylated cyclam reacts with superoxide to give [Co(II)-PN].[14] Recently, our group reported a few cobalt and manganese PN complexes formed in the reactions of respective nitrosyl complexes and reactive oxygen species.[15-18] Despite of numerous attempts, the mechanism of formation of the metal-PNs is still unclear and lacks proper spectroscopic evidence.

Herein, we report a nitrosyl complex of Co(II) 5,10,15,20-*tetrakis*(pentafluorophenyl)porphyrinate, which upon reaction with potassium superoxide (KO_2) gives [Co(III)-NO_2^-]. The reaction presumably proceeds *via* a [Co(II)-PN] intermediate as evident from phenol ring nitration test and decomposition product analysis. In the mechanistic pathway, prior to the PN intermediate, the involvement of a [$Co^{II}(NO)(O_2^-)$] species is suggested from UV-visible and X-band EPR spectroscopy as well as in ESI-mass spectrometry.

2.2 Results and Discussion

The ligand, 5,10,15,20-*tetrakis*(pentafluorophenyl)porphyrin ($F_{20}TPPH_2$) was synthesized according to previously reported procedure (Appendix I, Figures A1.1-A1.4).[16] The precursor complex [$Co^{II}(F_{20}TPP^{2-})$], **1** was synthesized following standard protocol [17] and characterized using UV-visible, FT-IR, EPR and mass spectrometry as well as single crystal X-ray structure determination (Experimental Section and Appendix I, Figures A1.5-A1.8). The perspective ORTEP view is shown in figure 2.1. The X-ray structure of the complex revealed it as a square planar complex with cobalt in +2 oxidation state. In ESI-mass spectrometry complex **1** displays molecular ion peak at m/z 1030.92 (calculated m/z 1030.98) (Appendix I, Figure A1.6). In UV-visible spectroscopy, a CH_2Cl_2 solution of complex **1** shows absorption maxima at 404 nm (Soret) along with absorptions at 525 and 555 nm (Appendix I, Figure A1.7). The X-band EPR spectrum exhibits high g_x and g_y and

low g_z values (g_x, g_y ~2.40; g_z ~2.02) which are characteristic of four coordinated Co(II) complexes of symmetrical porphyrins (Appendix I, Figure A1.8).[19a] Hyperfine splitting from Co(II) center and in-plane nitrogen atoms of the porphyrin ring is not observed distinctly at 77 K.[19]

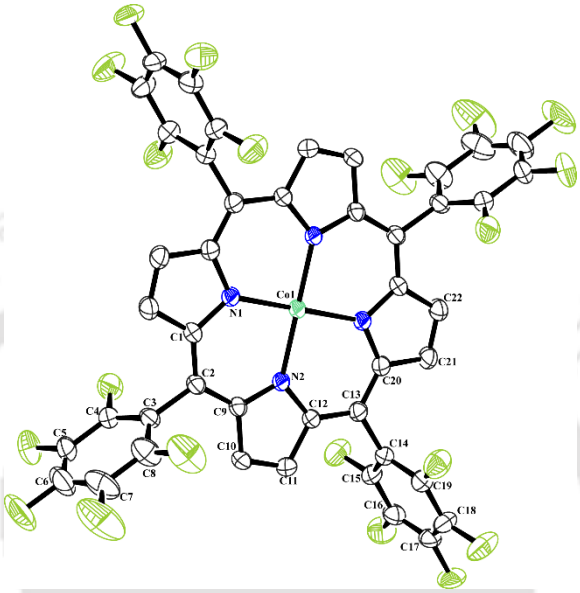

Figure 2.1. ORTEP diagram of complex **1** (30% thermal ellipsoid plot, H-atoms are omitted for clarity).

The nitrosyl complex [Co(F_{20}TPP^{2-})(NO)], **2** was prepared by bubbling NO gas through a dry and degassed CH_2Cl_2 solution of complex **1**. This complex was characterized both spectroscopically and structurally (Experimental Section and Appendix I, Figures A1.9-A1.11). It is worth mentioning that complex **2** was previously reported by Spiro and co-workers as five-coordinated {Co(NO)}^{8} complex.[20] However, they did not isolate the compound from solution. Single crystal of the complex was grown from THF solution. The X-ray crystal structure confirms that complex **2** is a five coordinated cobalt nitrosyl complex with square pyramidal geometry. The nitrosyl ligand occupies the axial positions while the four nitrogen atoms from porphyrin ring occupy the equatorial positions. The ORTEP view is shown in figure 2.2 and the crystallographic data and metric parameters are listed in appendix I, tables A1.1-A1.3. The crystal was solved in tetragonal symmetry;

where the nitrosyl group has two equivalent positions above and below the symmetry plane containing the porphyrin ring and the oxygen atom of the nitrosyl occupies eight equivalent positions around the four-fold axis. This type of disorder was previously reported in case of iron nitrosyl, [Fe(TPP^{2-})(NO)] (TPPH$_2$= *meso*-tetraphenylporphyrin).[21] The Co-N$_{NO}$, N-O bond distance and the Co-N-O bond angle are 1.97(2) Å, 1.01(3) Å and 123(2)°, respectively. These values appeared to be in the reported range of analogous complexes. For instance, in case of [Co(F$_8$TPP^{2-})(NO)] {F$_8$TPPH$_2$ = 5,10,15,20-*tetrakis*(2,6-difluorophenyl)porphyrin} these values are reported to be 1.894(10) Å, 1.158(13) Å and 127.40(14)°, respectively.[17] Similarly, for [Co(TMPP^{2-})(NO)] {TMPPH$_2$ = 5,10,15,20-*tetrakis*(4-methoxyphenyl)porphyrin}, these values are 1.855(6) Å, 1.159(8) Å and 120.6(5)°, respectively.[22] Slightly larger Co-N$_{NO}$ and smaller N-O bond length may be attributed to the presence of electron withdrawing fluorine atoms in the ligand which may affect the back donation of electron density from cobalt to nitrosyl. Other metric parameters are in well agreement with the reported values of {Co(NO)}^{8} complexes.[17]

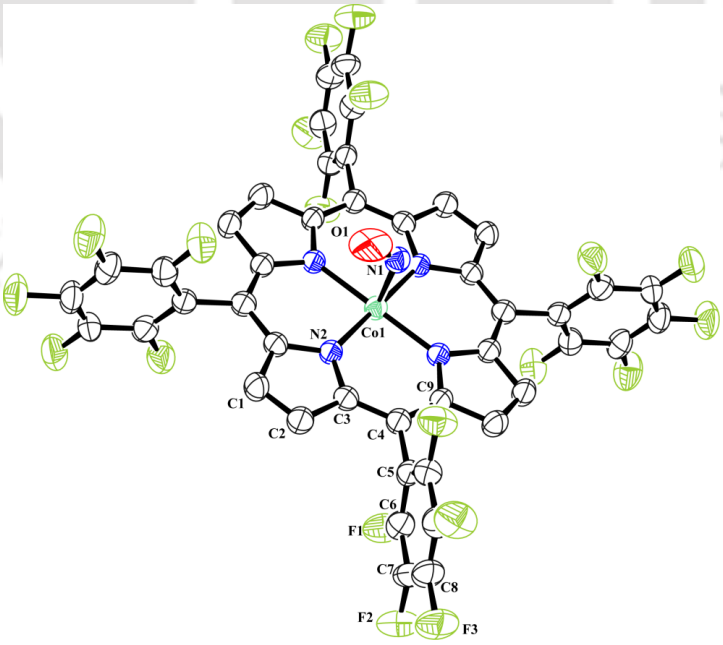

Figure 2.2. ORTEP diagram of complex **2** (30% thermal ellipsoid plot, H-atoms and solvent molecules are omitted for clarity). Among all the eight equivalent positions of the NO group only one is shown here.

In UV-visible spectroscopy, complex **2** in CH_2Cl_2 solution displays the Soret band at 394 nm along with absorptions at 536 and 563 nm, respectively (Appendix I, Figure A1.9). In FT-IR spectrum, a strong, sharp signal at 1713 cm^{-1} is attributed to N-O stretch of a nitrosyl group bonded to cobalt center (Figure 2.3). This value is in the assigned range of the previously reported bent $\{Co(NO)\}^8$ complexes.[17,18,22] Also, Spiro group reported the Resonance Raman frequency for the nitrosyl stretching in CH_2Cl_2 solution appeared at 1709 cm^{-1}.[20]

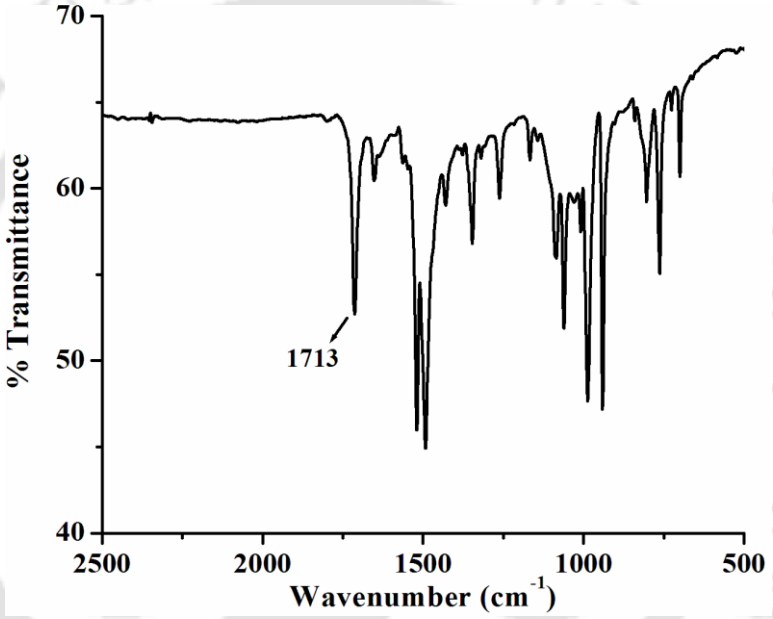

Figure 2.3. FT-IR spectrum of complex **2** in KBr.

The ESI-mass spectrum of the complex is populated by a peak at m/z 1030.86 (calculated m/z 1030.98 for $[Co(F_{20}TPP^{2-})]$), which is attributed to the facile loss of axially bound labile NO moiety. This was observed in case of some of the previously reported square pyramidal cobalt nitrosyl complexes where nitrosyl ligand was axially bound.[17, 18] Like other $\{Co(NO)\}^8$ complexes, complex **2** is diamagnetic owing to antiferromagnetic coupling between antibonding π* electron of nitrosyl and unpaired '*d*' electron of cobalt. In ^{1}H-NMR spectroscopy a sharp singlet appeared at δ = 8.98 ppm for pyrrole protons (Appendix I, Figures A1.10-A1.11).

2.2.1 Reactivity with superoxide ion

Complex **2** is inert towards O_2, but reacts with KO_2 in CH_2Cl_2 at −40 °C to give the corresponding Co(III)-nitrito complex [$Co^{III}(F_{20}TPP^{2-})(NO_2)$], **3** and O_2 (Scheme 2.1).

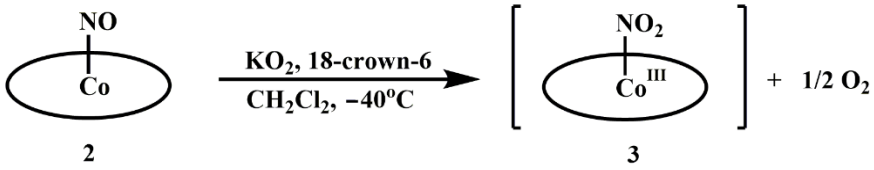

Scheme 2.1. Reaction of complex **2** with KO_2.

Complex **3** was isolated and characterized using various spectroscopic techniques. In FT-IR, a peak at 1295 cm^{-1} is attributed to nitrite stretching.[14a, 18, 23] A sharp singlet at δ = 9.16 ppm in ^{1}H-NMR as well as EPR silent nature suggested diamagnetic nature of the complex which is in agreement with the assignment of +3 oxidation state to cobalt (Appendix I, Figures A1.12-A1.15). Further, formation of a [Co(III)-NO_2^-] complex was confirmed by single crystal X-ray structure determination. The ORTEP diagram is shown in figure 2.4 and metric parameters are listed in appendix I, tables A1.1-A1.3. X-ray quality crystals were obtained from slow evaporation of THF solution, the coordinated THF must have come during crystallization.

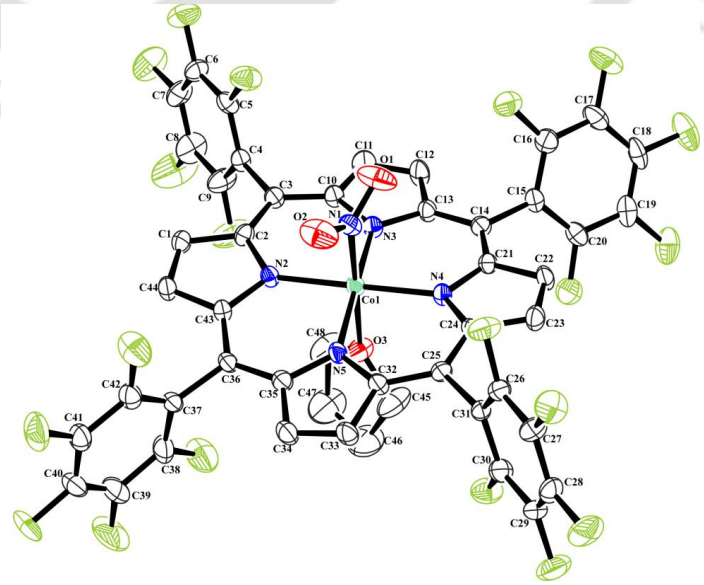

Figure 2.4. ORTEP diagram of complex **3** (30% thermal ellipsoid plot, H-atoms and solvent molecules are omitted for clarity).

In UV-visible spectroscopy, upon addition of 1 equivalent of KO_2 in a CH_2Cl_2 solution of complex **2**, the Soret band at 394 nm gradually diminished and a new peak at 425 nm appeared. This peak was transient and further shifted to 433 nm which is attributed to complex **3** (Figure 2.5). In literature, six-coordinated Co(II)-nitrosyls are reported to show Soret band in the region of 420-430 nm. For example, six-coordinated Co(II)-nitrosyl of *meso*-tetratolylporphyrin absorbs at 427 nm.[24] In the present case it is logical to assume that the superoxo, O_2^- ion binds to the Co(II) center to result in a six-coordinated nitrosyl; $[Co(F_{20}TPP^{2-})(NO)(O_2^-)]^-$, **2a** which absorbs at 425 nm. To further confirm our proposition we reacted complex **2** with imidazole to produce the corresponding six-coordinated species, $[Co(F_{20}TPP^{2-})(NO)(Im)]$. The formation of this complex was confirmed by shift in nitrosyl stretching frequency in FT-IR from 1713 to 1669 cm^{-1}. This complex also absorbs at 425 nm in UV-visible which renders validity to our assignment (Appendix I, Figures A1.16-A1.17).

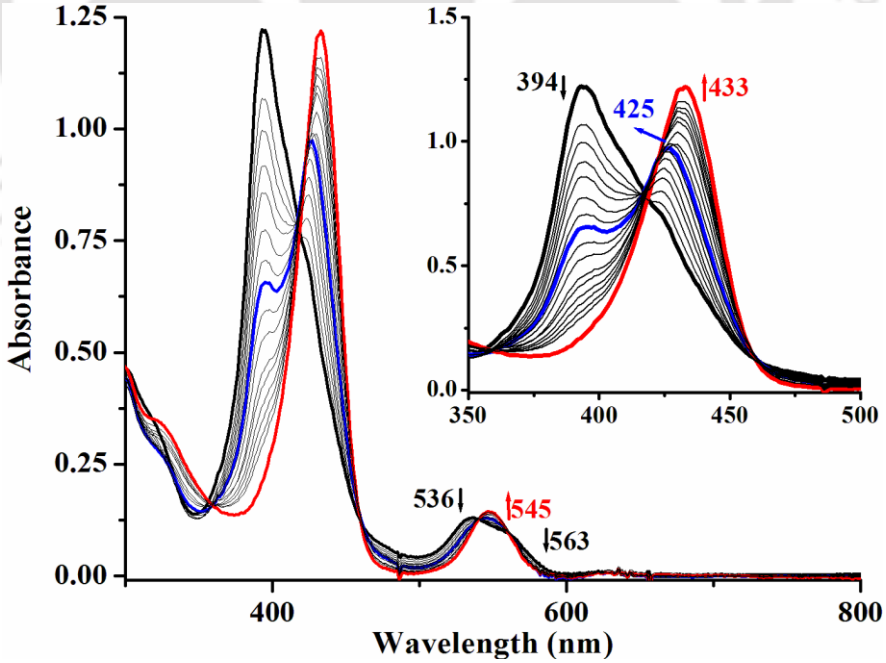

Figure 2.5. UV-visible spectral monitoring of complex **2** (black, 0 s) and after addition of KO_2 to result in intermediate **2a** (blue, 120 s) and complex **3** (red, 600 s) at −40 °C in CH_2Cl_2 (scan rate 0.5 s/scan, only a few selected spectra were shown for clarity).

The proposed intermediate **2a** is essentially a [$Co^{II}(NO)(O_2^-)$] species with odd number of electrons and expected to be EPR active. Accordingly, in X-band EPR spectrum of the frozen reaction mixture a peak at g ~ 2.06 was observed (Appendix I, Figure A1.18). More evidence of formation of **2a** came from ESI-mass spectrometry of the reaction mixture, where a peak at m/z 1092.83 corresponding to [$Co(F_{20}TPP^{2-})(NO)(O_2^-)$] appeared (Calcd. m/z 1092.96) (Appendix I, Figure A1.19). In FT-IR spectrum, the presence of other broad and intense bands near ~1100 cm^{-1} precluded the identification of any new band due to the formation of complex **2a**.

Conversion of complex **2a** to **3** is proposed to proceed *via* a [Co(II)-PN] intermediate. This type of intermediate have been evidenced earlier in the reaction of [(BPI)Co(NO)(OAc)] {BPI = 1,3-*bis*(2′-pyridylimino)isoindol} with dioxygen in CH_2Cl_2 solution.[23] Another example of such intermediate was reported by Theopold *et al.* in the reaction of a hydro-*tris*(3-tert-butyl-5-methylpyrazole)borate ligand derived [Co(III)-O_2^-] complex with NO at −78 °C.[25] A nitrosyl complex of a di-copper system, $[Cu^{I,II}_2(UN\text{-}O^-)(\mu\text{-}NO)]^{2+}$ in CH_2Cl_2 solution, was reported to result in the formation of $[Cu^{II}_2(UN\text{-}O^-)(NO)(O_2^-)]^{2+}$ upon addition of O_2 gas.[11d] These species are decomposed to the respective nitrate or nitrite complex through a corresponding putative PN intermediate. Considering the very short-life of the PN intermediates, no spectroscopic evidence could be obtained in support of the [Co(II)-PN]. However, when we performed the reaction in presence of 2,4-di-*tert*-butylphenol, formation of 2,4-di-*tert*-butyl-6-nitrophenol was observed (Appendix I, Figure A1.20-A1.22). A high valent [Co(III)=O] species and NO_2, generated from O-O bond homolysis of PN, are believed to be the cause of the nitration. Complex [$Co^{III}(F_{20}TPP^{2-})(OH)$], **4** was obtained as decomposition product of [Co(III)=O] along with the nitrated product. This reaction is extensively used as a chemical evidence for the formation of metal PN intermediate in the course of a reaction. The ESI mass spectral

analysis of the reaction mixture revealed a peak at m/z 1075.90 corresponding to the molecular ion peak (M−1) of $[Co^{II}(F_{20}TPP^{2-})(NO_2)]^-$ (Calcd. m/z 1076.97) (Appendix I, Figure A1.19). However, we could not isolate this in its Co(II)-nitrite form, rather we got Co(III)-nitrite. In principle, decomposition of [Co(II)-PN] should produce Co(II)-nitrite and half equivalent of O_2. In the present case, $[Co^{II}(F_{20}TPP^{2-})(NO_2)]^-$ would be thermally and kinetically unstable and during work-up and crystallization process, it gets oxidized to the corresponding Co(III) complex. The formation of the O_2 in the reaction was confirmed by alkaline pyrogallol test of the headspace gas.

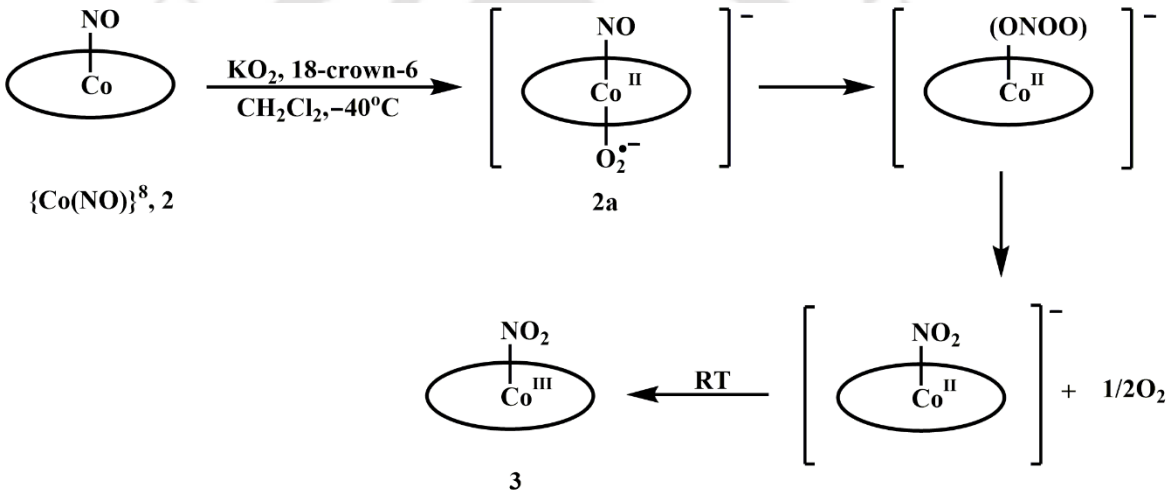

Scheme 2.2. Plausible reaction mechanism.

2.3 Experimental Section

2.3.1 Materials and Methods

All the chemicals were purchased from commercial sources and used without purification unless specified. CH_2Cl_2 was dried over calcium hydride, followed by distillation under N_2. KO_2 with 96.5% purity was brought from Alfa Aesar Chemicals and was standardized using reported procedure by colorimetric Nitro Blue Tetrazolium (NBT) assay.[26] All the reactions were performed under inert condition. UV-visible spectra were recorded either at room temperature or at −40 °C on an Agilent Cary 8454 spectrophotometer equipped with

Unisoku cryostat USP- 203 B and thermostated cell holder. FT-IR spectra were recorded in a PerkinElmer Spectrum Two spectrophotometer as KBr pellets. ^{1}H and ^{19}F NMR experiments were performed in a 500 MHz Bruker AVANCE NEO 500 FTNMR spectrophotometer. ^{1}H NMR peaks were referenced from either tetramethylsilane or residual solvent peaks; while hexafluorobenzene was used as internal standard for ^{19}F NMR. X-band EPR spectra were recorded on a JEOL JES-FA200 ESR spectrophotometer with microwave power, 0.998 mW; microwave frequency, 9.14 GHz; modulation frequency, 100 KHz and modulation amplitude, 1. All the EPR spectra were recorded at 77K. ESI-mass spectra were recorded in a Waters, Q-TOF premier instrument. Elemental analyses were obtained from a Perkin Elmer Series II Analyzer.

Single crystals were grown from the respective CH_2Cl_2 or THF solutions using slow evaporation technique. The intensity data were collected using a Bruker SMART APEX-II CCD diffractometer, equipped with a fine focus 1.75 kW sealed tube MoK_α radiation (λ = 0.71073 Å) at 293(3) K, with increasing ω (width of 0.3° per frame) at a scan speed of 3 s/frame. The SMART software was used for data acquisition. Data integration and reduction were undertaken with SAINT and XPREP software.[27] Structures were solved by direct methods using SHELXS-2016 and refined with full-matrix least squares on F^2 using SHELXL-2016/6.[28a] Structural illustrations have been drawn with ORTEP-3 for Windows.[28b]

2.3.2 Syntheses

5,10,15,20-*tetrakis*(pentafluorophenyl)porphyrin ($F_{20}TPPH_2$). The ligand $F_{20}TPPH_2$ was prepared using previously reported procedure.[16]

Complex 1. A mixture of $F_{20}TPPH_2$ (0.5 g, 0.5 mmol) and $Co(OAc)_2.4H_2O$ (1.25 g, 5 mmol) was refluxed in $CHCl_3$ (10 mL) and acetic acid (10 mL) for 24 h. The reaction was

stopped and 100 mL water was added. The crude product was extracted with $CHCl_3$ and dried *in vacuo*. Recrystallization from CH_2Cl_2 resulted red crystals of complex **1**. Yield: 0.4 g (~75%). Elemental analyses for $C_{44}H_8N_4F_{20}Co$, Calcd. (%):C, 51.24; H, 0.78; N, 5.43, found (%): C, 51.15; H, 0.76; N, 5.37. UV-visible (CH_2Cl_2): 404 nm ($\varepsilon/M^{-1}cm^{-1}$, 2.06×10^5); 525 nm ($\varepsilon/M^{-1}cm^{-1}$, 1.14×10^4) and 555 nm ($\varepsilon/M^{-1}cm^{-1}$, 9.53×10^3). FT-IR (in KBr): 1522, 1495, 1431, 1349, 1262, 1083, 1057, 990, 942, 807, 764 and 706 cm^{-1}. ESI-mass (m/z): Calcd. 1030.98; found: 1030.92 (molecular ion peak).

Complex 2. Complex **1** (0.1 g, 0.1 mmol) was dissolved in dry and degassed CH_2Cl_2. NO gas was bubbled for ~10 minutes to this solution. After a few days purple crystals of complex **2** appeared. Yield: 0.08 g (~80%). FT-IR (in KBr): 1713, 1520, 1492, 1347, 1262, 1089, 1061, 987, 941, 804, 763 and 700 cm^{-1}. UV-visible (CH_2Cl_2): 394 nm ($\varepsilon/M^{-1}cm^{-1}$, 1.13×10^5), 536 nm ($\varepsilon/M^{-1}cm^{-1}$, 1.15×10^4) and 563 nm ($\varepsilon/M^{-1}cm^{-1}$, 7.79×10^3). ^1H NMR (500 MHz, $CDCl_3$): δ_{ppm}, 8.98 (s). ESI-mass (m/z): Calcd. 1030.98; found 1030.86 for $[Co(F_{20}TPP^{2-})]$. X-ray quality single crystals were obtained from slow evaporation of a THF solution at 0 ºC.

2.3.3 Reaction of complex 2 with KO_2

Complex **2** (0.53 g, 0.5 mmol) was taken in 10 mL of dry and degassed CH_2Cl_2 and cooled to −40 ºC. Pre-cooled CH_2Cl_2 solution of KO_2 (96.5 %, 36.8 mg, 0.5 mmol) in 18-crown-6 was added to this cold solution and stirred for 6 h. The solution was warmed up to room temperature and dried under reduced pressure, Recrystallization from $CHCl_3$ resulted complex **3** (0.35 g, ~70% yield).

Complex 3. Elemental analyses for $C_{44}H_8N_5F_{20}O_2Co$, Calcd. (%): C, 49.05; H, 0.75; N, 6.50, found (%): C, 49.11; H, 0.79; N, 6.56. FT-IR (in KBr): 1520, 1492, 1355, 1295, 1262, 1087, 1064, 985, 941, 802, 769 and 695 cm^{-1}. UV-visible (CH_2Cl_2): 433 nm

($\varepsilon/M^{-1}cm^{-1}$, 1.40 × 10^5) and 545 nm ($\varepsilon/M^{-1}cm^{-1}$, 1.43 × 10^4). ^{1}H NMR (500 MHz, CD_3CN): δ_{ppm}, 9.16 (s). X-ray quality crystals were obtained by re-dissolving complex **3** in THF followed by slow evaporation.

2.3.4 Reaction of complex 2 with KO_2 in presence of 2,4-di-*tert*-butylphenol

To a dry and degassed CH_2Cl_2 solution of complex **2** (1.06 g, 1 mmol) and 2,4-di-*tert*-butylphenol (1.03 g, 5 mmol), solution of KO_2 (96.5 %, 73.6 mg, 1 mmol) in 18-crown-6 was added at −40 °C and stirred for 2 h at the same temperature. The reaction mixture was then brought to room temperature and dried *in vacuo*. Purification of the crude mass through column chromatography resulted in pure 2,4-di-*tert*-butyl-6-nitrophenol and [$Co^{III}(F_{20}TPP^{2-})(OH)$], **4**.

2,4-di-*tert*-butyl-6-nitrophenol. Yield: 0.17 g (~70%). Elemental analyses for $C_{14}H_{21}NO_3$, Calcd. (%): C, 66.91; H, 8.42; N, 5.57, found (%):C, 67.07; H, 8.40; N, 5.68. ^{1}H NMR (500 MHz, $CDCl_3$): δ_{ppm}, 11.44 (s, 1H), 7.96 (s, 1H), 7.65 (s, 1H), 1.45 (s, 9H), 1.32 (s, 9H). ^{13}C NMR (125 MHz, $CDCl_3$): δ_{ppm}, 153.0, 142.0, 139.9, 133.7, 132.6, 118.8, 35.7, 34.5, 31.1, 29.4. ESI-mass (m/z): Calcd: 251.15, found: 250.19 (M−1).

Complex 4. Elemental analyses for $C_{44}H_9N_4F_{20}OCo$, Calcd. (%): C, 50.40; H, 0.87; N, 5.34, found (%): C, 50.61; H, 0.89; N, 5.26. FT-IR (in KBr): 3426, 1652, 1522, 1498, 1383, 1326, 1261, 1229, 1121, 991, 935 and 795 cm^{-1}. UV-visible (CH_2Cl_2): 421 nm and 540 nm.

2.4 Conclusion

In conclusion, a Co(II) porphyrinate, **1** reacts with NO to give corresponding nitrosyl complex **2**. This complex was characterized both spectroscopically and structurally as a bent $\{Co(NO)\}^8$ complex. Complex **2**, upon reaction with O_2^-, gives [Co(III)-NO_2^-]

complex. A transient intermediate [$Co^{II}(NO)(O_2^-)$], **2a** was detected in UV-visible spectroscopy and further confirmed by X-band EPR spectroscopy and ESI-mass spectrometry. This intermediate complex further decomposes to the nitrite complex through a highly unstable [Co(II)-PN] intermediate. Although no spectroscopic evidence could be obtained for the formation of PN, it was chemically confirmed by the customary phenol ring nitration test.

2.5 References

1. *Nitric Oxide: Biology and Pathobiology*; Ignarro, L. J., Ed.; Academic Press: San Diego, **2000**.
2. *Nitric Oxide and Infection*; Fang, F. C., Ed.; Kluwer Academic/ Plenum Publishers: New York, **1999**.
3. Bourassa, J. L.; Ives, E. P.; Marqueling, A. L.; Shimanovich, R.; Groves, J. T. *J. Am. Chem. Soc.* **2001**, *123*, 5142.
4. Pacher, P.; Beckman, J. S.; Liaudet, L. *Physiol. Rev.* **2007**, *87*, 315.
5. Beckman, J. S.; Koppenol, W. H. *Am. J. Physiol.* **1996**, *271*, 1424.
6. Marletta, M. A.; Yoon, P. S.; Iyengar, R.; Leaf, C. D.; Wishnok, J. S. *Biochemistry* **1988**, *27*, 8706.
7. Szabó, C.; Ischiropoulos, H.; Radi, R. *Nat. Rev. Drug Discov.* **2007**, *6*, 662.
8. Beal, M. F. *Free Radical Biol. Med.* **2002**, *32*, 797.
9. Radi, R.; Cassina, A.; Hodara, R.; Quijano, C.; Castro, L. *Free Radical Biol Med.* **2002**, *3*, 1451.
10. Vliet, A. V.; Eiserich, J. P.; Halliwell, B.; Cross, C. E. *J. Biol. Chem.* **1997**, *272*, 7617.
11. (a) Park, G. Y.; Deepalatha, S.; Puiu, S. C.; Lee, D.-H.; Mondal, B.; Sarjeant, A. A.

N.; del Rio, D.; Pau, M. Y. M.; Solomon, E. I.; Karlin, K. D. *J. Biol. Inorg. Chem.* **2009**, *14*, 1301. (b) Maiti, D.; Lee, D.-H.; Sarjeant, A. A. N.; Pau, M. Y. M.; Solomon, E. I.; Gaoutchenova, K.; Sundermeyer, J.; Karlin, K. D. *J. Am. Chem. Soc.* **2008**, *130*, 6700. (c) Schopfer, M. P.; Mondal, B.; Lee, D.-H.; Sarjeant, A. A. N.; Karlin, K. D. *J. Am. Chem. Soc.* **2009**, *131*, 11304. (d) Cao, R.; Elrod, L. T.; Lehane, R. L.; Kim, E.; Karlin, K. D. *J. Am. Chem. Soc.* **2016**, *138*, 16148.

12. (a) Kurtikyan, T. S.; Eksuzyan, S. R.; Hayrapetyan, V. A.; Martirosyan, G. G.; Hovhannisyan, G. S.; Goodwin, J. A. *J. Am. Chem. Soc.* **2012**, *134*, 13861. (b) Kurtikyan, T. S.; Eksuzyan, S. R.; Goodwin, J. A.; Hovhannisyan, G. S. *Inorg. Chem.* **2013**, *52*, 12046.
13. (a) Yokoyama, A.; Han, J. E.; Cho, J.; Kubo, M.; Ogura, T.; Siegler, M. A.; Karlin, K. D.; Nam, W. *J. Am. Chem. Soc.* **2012**, *134*, 15269. (b) Yokoyama, A.; Cho, K.-B.; Karlin, K. D.; Nam, W. *J. Am. Chem. Soc.* **2013**, *135*, 14900.
14. (a) Kumar, P.; Lee, Y.-M.; Park, Y. J.; Siegler, M. A.; Karlin, K. D.; Nam, W. *J. Am. Chem. Soc.* **2015**, *137*, 4284. (b) Kumar, P.; Lee, Y.-M,; Hu, L.; Chen, J.; Park, Y. J.; Yao, J.; Chen, H.; Karlin, K. D.; Nam, W. *J. Am. Chem. Soc.* **2016**, *138*, 7753.
15. (a) Saha, S.; Ghosh, S.; Gogoi, K.; Deka, H.; Mondal, B.; Mondal, B. *Inorg. Chem*, **2017**, *56*, 10932. (b) Kalita, A.; Kumar, P.; Mondal, B. *Chem. Commun.* **2012**, *48*, 4636.
16. Mondal, B.; Borah, D.; Mazumdar, R.; Mondal, B. *Inorg. Chem.* **2019**, *58*, 14701.
17. Mondal, B.; Saha, S.; Borah, D.; Mazumdar, R.; Mondal, B. *Inorg. Chem.* **2019**, *58*, 1234.
18. Saha, S.; Gogoi, K.; Mondal, B.; Ghosh, S.; Deka, H.; Mondal, B. *Inorg. Chem.* **2017**, *56*, 7781.

19. (a) Ozarowski, A.; Lee, H. M.; Balch, A. L. *J. Am. Chem. Soc.* **2003**, *125*, 12606. (b) Van Doorslaer, S.; Schweiger, A. *Phys. Chem. Chem. Phys.* **2001**, *3*, 159.
20. Soldatova, A. V. Ibrahim, M.; Spiro, T. G. *Inorg. Chem.* **2013**, *52*, 7478.
21. Scheidt, W. R.; Frisse, M. E. *J. Am. Chem. Soc.* **1975**, *97*, 17.
22. (a) Richter-Addo, G. B.; Hodge, S. J.; Yi, G. B.; Khan, M. A.; Ma, T.; Caemelbecke, E. V.; Guo, N.; Kadish, K. M. *Inorg. Chem.* **1996**, *35*, 6530. (b) Richter-Addo, G. B.; Hodge, S. J.; Yi, G. B.; Khan, M. A., Ma, T.; Caemelbecke, E. V.; Guo, N.; Kadish, K. M. *Inorg. Chem.* **1997**, *36*, 2696.
23. Gogoi, K.; Saha, S.; Mondal. B.; Deka, H.; Ghosh, S.; Mondal, B. *Inorg. Chem.* **2017**, *56*, 14438.
24. Kurtikyan, T. S.; Gulyan, G. M.; Dalaloyan, A. M.; Kidd, B. E.; Goodwin, J. A. *Inorg. Chem.* **2010**, *49*, 7793.
25. Thyagarajan, S.; Incarvito, C. D.; Rheingold, A. L.; Theopold, K. H. *Inorg. Chim. Acta*. **2003**, *345*, 333.
26. Hayyan, M.; Hashim, M. A.; AlNashef, I. M. *Chem. Rev.* **2016**, *116*, 3029.
27. SMART, SAINT and XPREP, Siemens Analytical X-ray Instruments Inc., Madison, Wisconsin, USA, **1995**.
28. (a) Sheldrick, G. M. SHELXS-2014, University of Gottingen, Germany. (b) Farrugia, L. J. ORTEP-3 for Windows - a version of ORTEP-III with a Graphical User Interface (GUI) *J. Appl. Crystallogr.* **1997**, *30*, 565.

Chapter 3

Reaction of nitrosyls of Co(II) porphyrins with H_2O_2: Formation of Co(III) porphyrin radical cation

Abstract

Two Co(II) porphyrin complexes, *viz.* [$Co^{II}(MPTPP^{2-})$], **5** {$MPTPPH_2$ = 5-(4-methoxyphenyl)-10,15,20-triphenylporphyrin} and [$Co^{II}(TMPP^{2-})$], **6** {$TMPPH_2$ = 5,10,15,20-*tetrakis*(4-methoxyphenyl)porphyrin} were made to react with NO to yield the bent nitrosyl complexes [$Co^{II}(MPTPP^{2-})(NO)$], **7** and [$Co(TMPP^{2-})(NO)$], **8**; having $\{Co(NO)\}^8$ description. Both the complexes were characterized spectroscopically and structurally. Complex **7** and **8** react with H_2O_2 to give the corresponding [Co(III)-NO_3^-] complexes, [$Co^{III}(MPTPP^{2-})(NO_3)$], **9** and [$Co^{III}(TMPP^{2-})(NO_3)$], **10**. The reaction is believed to proceed *via* a [Co(III)-PN] intermediate as evident from phenol ring nitration experiment. Also, involvement of a [Co(IV)=O] intermediate, followed by a Co(III) porphyrin π-cation radical species was observed in UV-visible and X-band EPR spectroscopy as well as in ESI-mass spectrometry.

3.1 Introduction

Nitric oxide (NO) is a signal transducer molecule that plays the key roles in various physiological processes, for instance cellular signaling, vasodilation, neurotransmission etc.[1-3] A sub-micromolar concentration NO is required for its activity and over production often leads to toxic effects. The concentration of NO in biological systems is regulated by nitric oxide dioxygenase (NOD) enzymes. In NOD activity, an [Fe(III)-O_2^-] complex reacts with NO to result in biologically benign nitrate (NO_3^-) ion. This reaction is proposed to proceed *via* the formation of a peroxynitrite ($ONOO^-$, PN) intermediate. It is believed that the PN intermediate breaks up to an oxo-ferryl, [Fe(IV)=O] species and NO_2 through the homolytic cleavage of the O−O bond, followed by a recombination to form NO_3^- ion. High instability of the PN intermediate makes it hard to be traced or to back up this proposition with spectroscopic evidence. Only a well-established phenol ring nitration test is used in almost all the cases where the involvement of PN is proposed. Although the homolytic cleavage of O−O bond of PN is proposed to yield the high-valent metal oxo intermediate, identification is restricted only to a handful of examples because of its fast recombination with NO_2 in the reaction cage to give the NO_3^- ion.[4-7]

A number of examples have been reported since the first report by Basolo, where the involvement of a Co-PN intermediate is implicated.[8] The reactions of NO with superoxo and peroxo complexes iron, cobalt, and chromium with NO are shown to involve the formation of the metal-PN intermediate.[8-15] For example, the reaction of a [Fe(III)-O_2^-] complex with NO gives the corresponding nitrate through a PN intermediate.[6] A Cr(IV)-peroxo complex of N-tetramethylatedcyclam, $[Cr^{IV}(12\text{-TMC})(O_2^{2-})(Cl)]^+$ upon reaction with NO results in a Cr(III)-nitrate complex, $[Cr^{III}(12\text{-TMC})(NO_3^-)(Cl)]^+$. However, the Cr(III)-superoxo analogue, $[Cr^{III}(14\text{-TMC})(O_2^-)(Cl)]^+$, reacts with NO to give Cr(IV)-oxo complex, [Cr^{IV}(14-

TMC)(O)(Cl)]$^{+}$ and NO_2. In both the cases, the formation of a [Cr(III)-PN] intermediate was proposed.[13,14] The reaction of Fe(III)-peroxo complex, [Fe^{III}(14-TMC)(O_2^{2-})]$^{+}$, with NO^{+} was reported to proceed through the PN intermediate. Our group reported the reaction of cobalt peroxo complex [$L_2Co^{III}(O_2^{2-})$] (L = *bis*(2-ethyl-4-methyl-imidazol-5-yl)methane), with NO to give [Co(II)-NO_3^{-}] complex *via* a putative [Co(II)-PN] intermediate.[15]

In addition, the reactions of metal nitrosyl complexes with reactive oxygen species are also known to result in the corresponding nitrate through the formation of a PN intermediate. A non-heme dinitrosyliron complex upon reaction with O_2 was found to afford the corresponding nitrate complex.[16] Similarly, a copper nitrosyl complex with H_2O_2 gives presumed [Cu(I)-PN] intermediate.[17] Two recent examples of {Co(NO)}^{8} complexes, *viz.* [Co(Cl_4TPP^{2-})(NO)] {Cl_4TPPH_2 = 5,10,15,20-*tetrakis*(4-chlorophenyl)porphyrin} and [Co(F_8TPP^{2-})(NO)] {F_8TPPH_2 = 5,10,15,20-*tetrakis*(2,6-difluorophenyl)porphyrin} are shown to react with H_2O_2 to give corresponding nitrito and nitrato products respectively and the reaction proceeds *via* putative PN intermediates.[18,19] Another {Mn(NO)}^{6} complex [Mn($F_{20}TPP^{2-}$)(NO)] {$F_{20}TPPH_2$ = 5,10,15,20-*tetrakis*(pentafluorophenyl)porphyrin} reacts with superoxide to form a unstable [Mn(IV)=O] complex *via* homolytic cleavage of a proposed PN intermediate.[20] Hence the reaction of metal nitrosyl with reactive oxygen species is important to study to understand the PN chemistry.

Co-porphyrin complexes are known as the better models for the heme-iron systems and relatively better stability compared to the iron analogues also encourage their use for reactivity studies in biological systems. Herein, we report the NOD activity of nitrosyl complexes of two Co(II)-porphyrins [Co($MPTPP^{2-}$)(NO)], **7** {$MPTPPH_2$ = 5-(4-methoxyphenyl)-10,15,20-triphenylporphyrin} and [Co($TMPP^{2-}$)(NO)], **8** {$TMPPH_2$ = 5,10,15,20-*tetrakis*(4-methoxyphenyl)porphyrin} in the presence of H_2O_2 where the

formation of a presumed PN intermediate is implicated. Earlier with [Co(Cl_4TPP^{2-})(NO)] and [Co(F_8TPP^{2-})(NO)], it has been observed that the reaction of H_2O_2 results in the formation of corresponding nitrito and nitrato products, respectively and the reaction is proposed to proceed through putative PN intermediate. In case of [Co(F_8TPP^{2-})(NO)], the spectral studies suggested the involvement of a [Co(IV)=O] intermediate; however, for [Co(Cl_4TPP^{2-})(NO)], no such intermediate was evidenced. The present study has been done with an electron donating substituent, −OMe, on the phenyl group of the ligand to see the effect of it on the overall reactivity as well as on the formation, stability and decomposition of the PN intermediate. The spectral studies indicate the involvement of a porphyrin cation radical during the reaction.

3.2 Results and Discussion

The ligands, 5-(4-methoxyphenyl)-10,15,20-triphenylporphyrin ($MPTPPH_2$) and 5,10,15,20-*tetrakis*(4-methoxyphenyl)porphyrin ($TMPPH_2$) were synthesized following Adler's method,[21a] which was then characterized using ESI-mass, FT-IR, ^1H and ^{13}C NMR (Appendix II, Figures A2.1-A2.9). The complexes [$Co^{II}(MPTPP^{2-})$], **5** and [$Co^{II}(TMPP^{2-})$], **6** were prepared following reported procedures and characterized using various spectroscopic techniques (Appendix II, Figures A2.10-A2.17).[21] The crystal structure of **6** was reported earlier and it shows that the Co center is in square planar geometry where cobalt atom is coordinated to four nitrogen atoms of the porphyrin ring (Appendix II, Figure A2.18). Crystal structure as well as X-band EPR studies showed that cobalt is in +2 oxidation state in complex **6**.

The nitrosyl complexes, [$Co^{II}(MPTPP^{2-})(NO)$], **7** and [$Co^{II}(TMPP^{2-})(NO)$], **8** have been synthesized by bubbling NO gas through a degassed CH_2Cl_2 solutions of **5** and **6**, respectively (Experimental Section). The complex **8** was reported earlier by Kadish *et al.*[22]

Both the complexes have been isolated as solid and characterized using UV-visible, FT-IR, ^{1}H-NMR spectroscopy as well by single crystal structure determination (Appendix II, Figures A2.19-A2.27). The perspective ORTEP view is shown in figure 3.1. X-ray diffraction studies revealed that in complex **8**, Co center is in square pyramidal geometry where the four nitrogen atoms of the porphyrin ring formed the square plane and NO moiety is bonded axially. N-O bond length is 1.166(6) Å and the Co-N-O bond angle is 119.1(9)º. These values are in accordance with the reported one.[22] The observed metric parameters of complex **8** are in accord with the bent nitrosyls having {Co(NO)}^{8} configuration (Appendix II, Tables A2.1-A2.3).[18,19]

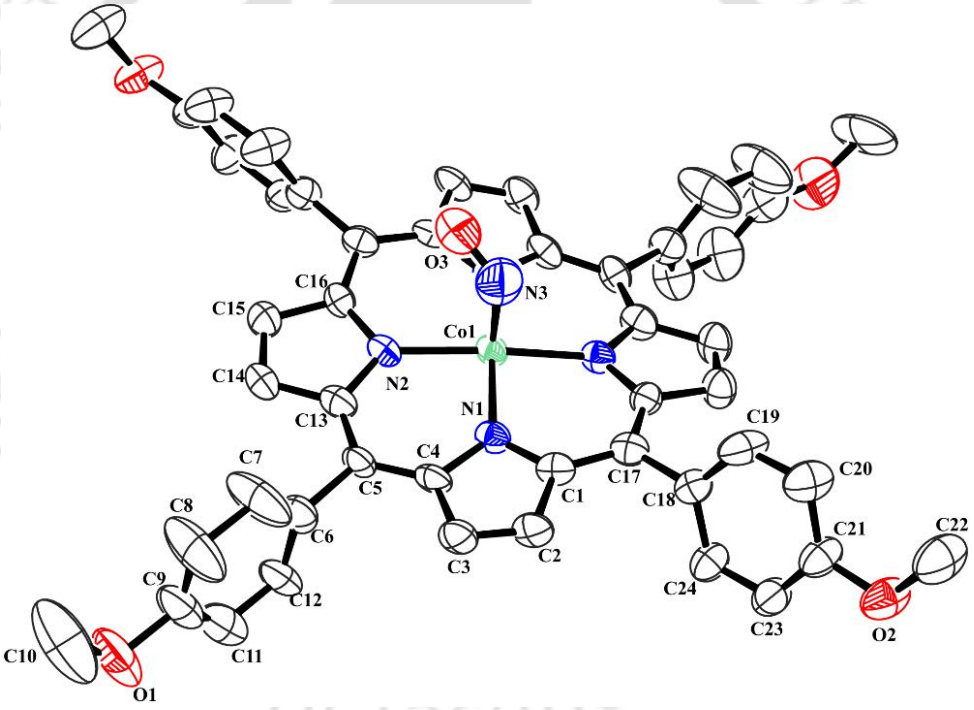

Figure 3.1. ORTEP diagram of complex **8** (30% thermal ellipsoid plot, H-atoms are omitted for clarity).

In FT-IR spectroscopy, along with the others, the nitrosyl stretching frequency for complex **8** appears at 1696 cm^{-1} (Figure 3.2); whereas the same frequency for complex **7** appears at 1682 cm^{-1} (Appendix II, Figure A2.19). In case of [Co(F_8TPP^{2-})(NO)] the NO stretching appears at 1692 cm^{-1} in KBr (1699 cm^{-1} in CH_2Cl_2) whereas in [Co(Cl_4TPP^{2-})(NO)], it shifts

to 1701 cm^{-1} (in KBr).[18,19] In other examples such as [Co(TPP^{2-})(NO)] {$TPPH_2$ = *meso*-tetraphenylporphyrin} and [Co(OEP^{2-})(NO)] {$OEPH_2$ = octaethylporphyrin}, it appear at 1689 cm^{-1}(in KBr) and 1675 cm^{-1}(in CH_2Cl_2), respectively.[12] Further, the nitrosyl complexes of cobalt porphyrins having general formula [{T(*p*/*m*-X)PP^{2-}}Co(NO)] [*p*/*m*-X = *p*-CH_3, *m*-CH_3, *p*-H, *m*-OCH_3, *p*-OCF_3, *p*-CF_3, *p*-CN etc.] in CH_2Cl_2, this frequency appear in the range of 1681-1695 cm^{-1}.[23-25] The observed NO stretching also suggests the existence of bent nitrosyl with {Co(NO)}^{8} configuration. In ESI-mass spectrometry, complex **7** shows molecular ion peak at m/z 732.205 (Calcd. m/z 732.173 (M+1); Appendix II, Figure A2.20). The ESI-mass spectrum of complex **8** is populated with a peak at m/z 791.163 corresponding to [Co($TMPP^{2-}$)] (Calcd. m/z 791.207). This is attributed to facile loss of axial NO group, which have been observed in some earlier cases, too (Appendix II, Figure A2.24).

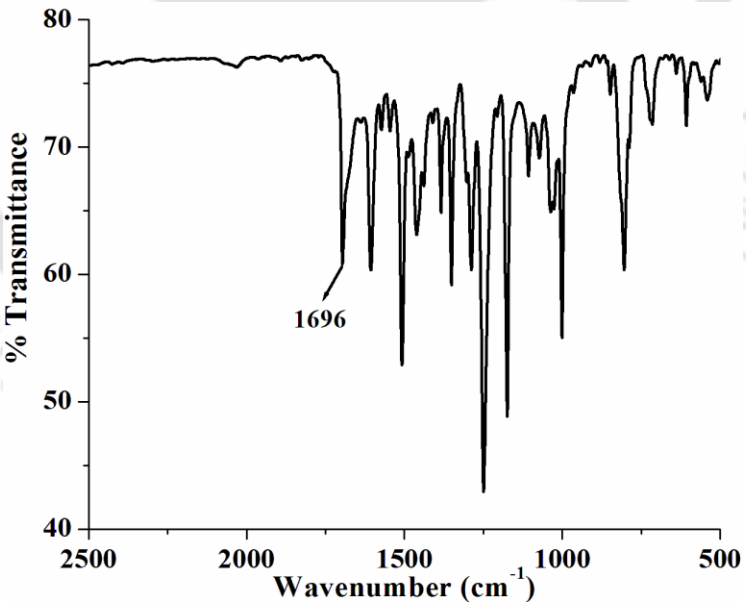

Figure 3.2. FT-IR spectrum of **8** in KBr.

Both the nitrosyl complexes are EPR silent owing to the anti-ferromagnetic coupling between the Co(II) and NO and show well resolved peaks in ^{1}H-NMR suggesting diamagnetic nature (Appendix II, Figures A2.22-A2.23; A2.26-A2.27).

Reaction of complex **7** and **8** with H_2O_2 at −40 ºC in CH_2Cl_2 resulted in complexes $[Co^{III}(MPTPP^{2-})(NO_3)]$, **9** and $[Co^{III}(TMPP^{2-})(NO_3)]$, **10** respectively (Scheme 3.1). These were isolated and characterized spectroscopically. The presence of 1384 cm^{-1} band in FT-IR spectra of both the complexes suggests the presence of the corresponding nitrato complexes (Appendix II, Figures A2.37; A2.41). This is further confirmed by ESI-mass spectrometry where the peak at m/z 764.248 {Calcd. m/z 763.163 for $[Co(MPTPP^{2-})(NO_3)]$} for complex **9**; m/z 854.240 {Calcd. m/z 853.195 for $[Co(TMPP^{2-})(NO_3)]$} for complex **10** was observed (Appendix II, Figures A2.38; A2.42). EPR silent nature as well as well resolved NMR spectra suggested that cobalt is in +3 oxidation state (Appendix II, Figures A2.40 and A2.44).

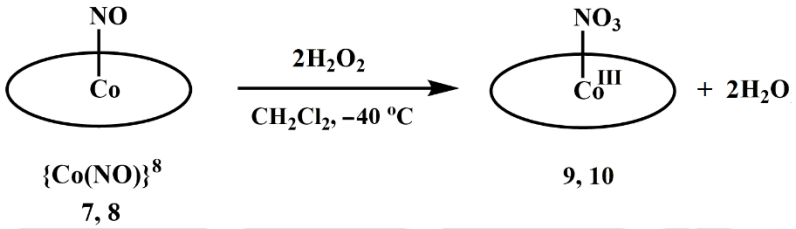

Scheme 3.1. Reaction of complexes **7** and **8** with H_2O_2 to give **9** and **10**, respectively.

In UV-visible spectroscopy complex **8** shows characteristic absorption peaks at 420 nm and 540 nm in CH_2Cl_2 solution at −80 ºC. Upon addition of H_2O_2, these bands immediately shift to 435 nm and 545 nm, respectively. Then the intensity of these bands decreases gradually and 435 nm band further shifts to 455 nm. Two new bands at 695 nm and 922 nm appeared in the meantime (Figure 3.3). These absorption bands correspond to the final decomposition product, complex **10**. It has been reported earlier that the reaction of metal-nitrosyls with H_2O_2 led to the formation of nitrate product though the corresponding PN intermediate. For instance, $[Co(F_8TPP^{2-})(NO)]$, upon reaction with H_2O_2 results in $[Co^{III}(F_8TPP^{2-})(NO_3)]$ and the reaction was shown to proceed through a PN intermediate.[19] It is known that metal PN complexes undergoes homolytic cleavage at O−O site to result in high valent metal-oxo

species and NO_2. It has been reported earlier that heme [Co(IV)=O] species absorb at 430 nm and 550 nm. Keeping the reaction pathway in mind, thus, the transient absorptions at 435 nm and 545 nm are assigned to a [Co(IV)=O] species. To confirm this assignment an authentic sample was prepared by reacting complex **6** with 4-chloroperbenzoic acid (*m*CPBA) which shows absorption bands at 438 nm and 548 nm (Apeendix II, Figure A2.34). However, this species was thermally unstable and converts rapidly to a Co(III)-porphyrin radical cation species as suggested by the significant quenching of characteristic Soret band (Figure 3.3).

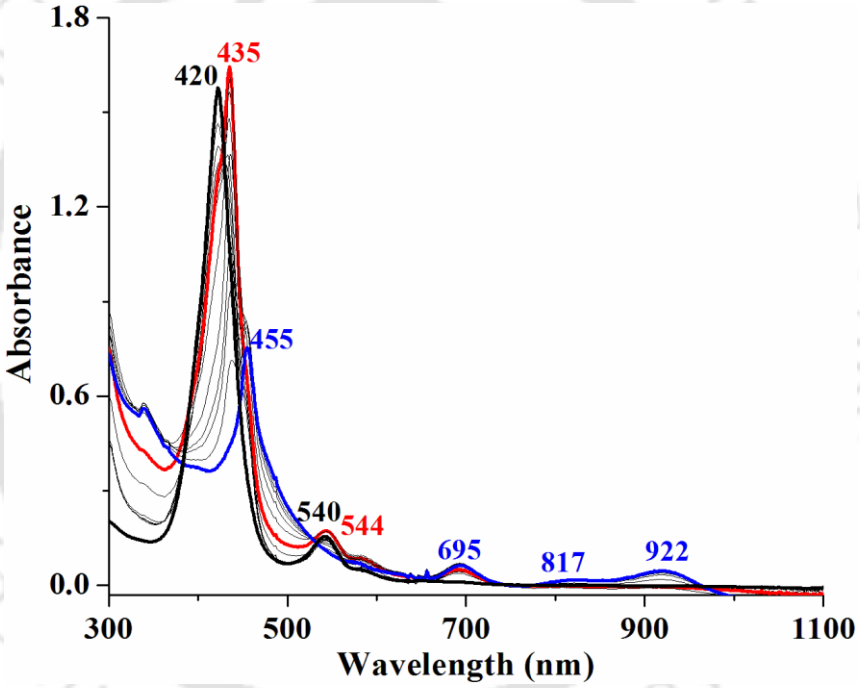

Figure 3.3. UV-visible spectral monitoring of **8** (black) and after addition of H_2O_2 (red) and final (blue) at −80 °C in CH_2Cl_2 (scan rate 0.5 s/scan, only a few selected spectra were shown for clarity).

In X-band EPR study, the frozen intermediate which formed upon addition of H_2O_2 to complex **8** at −40 ºC displayed a sharp isotropic signal at g ~ 2.002. This suggests the formation of a radical species in the course of the reaction. In the present case, the appearance of the isotropic signal at g, 2.002 is actually suggestive to the formation of a [Co(IV)=O] species and NO_2 (Scheme 3.2) because NO_2 at 77 K dimerizes to form

diamagnetic N_2O_4. ESI-mass spectrum of the crude reaction mixture showed a peak at m/z 808.231 which may be assignable to the moiety [Co(TMPP^{2-})(O)] (Calcd. m/z 807.202).

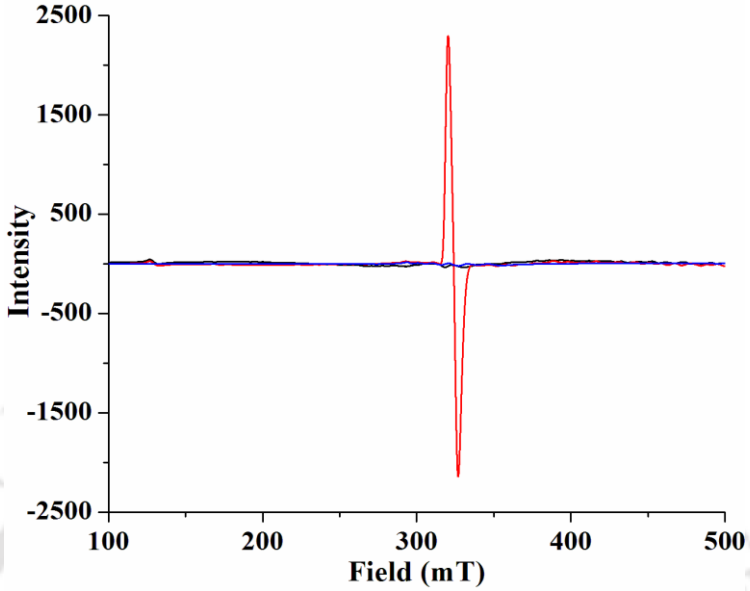

Figure 3.4. X-band EPR spectra of **8** (black), the intermediate (red) and **10** (blue) in CH_2Cl_2 at 77K.

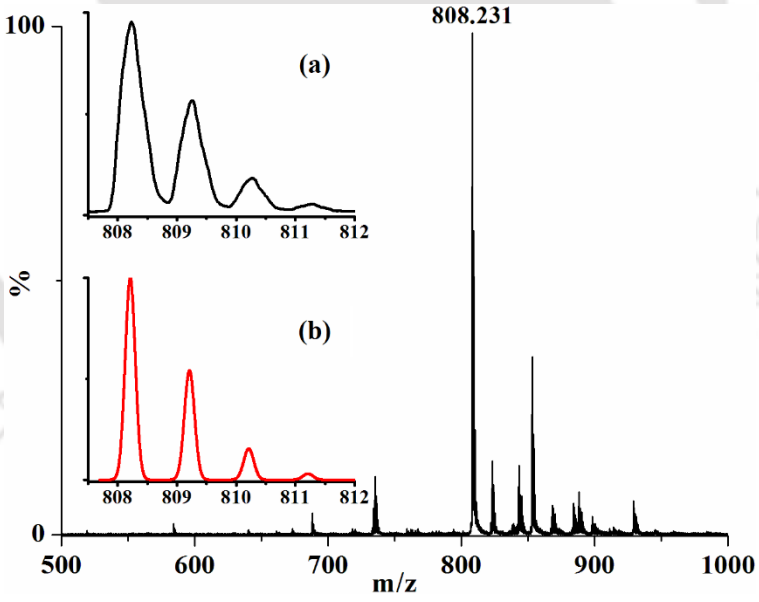

Figure 3.5. ESI-mass spectrum of the reaction mixture obtained from the reaction of **8** and H_2O_2 (in CH_2Cl_2 at −40 °C) in CH_3CN. [Inset: (a) experimental and (b) simulated isotopic distribution pattern].

Similar observations were noticed in case of the reaction of complex **7** and H_2O_2 in UV-visible, X-band EPR spectroscopy and ESI-mass spectrometry. In UV-visible spectroscopy, 414 nm and 536 nm bands shifted to 431 nm and 540 nm, respectively, after addition of

H_2O_2. Authentic sample prepared from the reaction of complex **5** with *m*CPBA showed bands at 429 nm and 541 nm. A peak at m/z 718.261 in mass spectrum suggested presence of [Co(MPTPP^{2-})(O)] moiety (Calcd. m/z 717.170). This species is also transient like the former case and rapidly isomerizes to a porphyrin cation radical species as suggested by decay of the Soret band in UV-visible spectroscopy as well as a sharp singlet at g ~ 2.001 in X-band EPR spectroscopy (Appendix II, Figure A2.28-A2.33).

These results collectively suggest the formation of a [Co(IV)=O] intermediate which then coverts into another species which is also radical in nature. The quenched Soret band and the radical nature can be attributed to the formation of a corresponding porphyrin cation radical from the [Co(IV)=O] intermediate.

It has been reported by Winkler and Gray that for oxo-metal complexes having d^5 configuration, the [M(III)-O$^{\bullet}$] is more likely than [M(IV)=O] configuration.[26] It is to be noted that in case of [Co(F_8TPP^{2-})(NO)], similar reaction resulted in the formation of (Porphyrin)Co(III)-O$^{\bullet}$ owing to its d^5 configuration. It was evidenced by the appearance of sharp EPR signal at g, 2.002 and non-observance of the quenching of Soret band in UV-visible spectroscopy. However, in the present study, it is observed that the porphyrin radical cation is more stable than the (Porphyrin)Co(III)-O$^{\bullet}$. The (Porphyrin)Co(III)-O$^{\bullet}$ in the presence of NO_2 undergoes fast decomposition to the final product, complex **9** and **10**. In the ESI mass spectrum of this reaction mixture, a molecular ion peak (m/z) was observed at 808.231 (Calcd. 807.202) which is assignable to the (Porphyrin)Co^{III}-O$^{\bullet}$ (Figure 3.5). It has been shown earlier that with [Co(F_8TPP^{2-})(NO)] and [Mn(F_{20}TPP^{2-})(NO)], the corresponding [Co(IV)=O] or [Mn(IV)=O] species do not isomerise to the respective porphyrin cation radical. This is probably because of the presence of electron donating substituents in the phenyl ring of ligand $TMPPH_2$. In addition, it is observed that in cases where the proposed PN afforded the corresponding nitrite complex and oxygen, oxo-

intermediate was not evidenced; only in cases which results in the formation of nitrate as the end decomposition product, the spectroscopic evidence of the formation of oxo-intermediate was observed.

The theoretical studies and thermos-kinetic evidence suggests that the PN complexes are too short lived to be characterized using spectroscopic methods. Because of very short lifetime of the proposed Co-PN, no direct spectroscopic evidence has been observed and indirect chemical evidence for the postulated species has been sought. It is to be noted that commonly a phenol nitration reaction is used to provide an evidence in support of the presence of metal-PN. In case of NOD, it is proposed that the presumed [Fe(III)-PN] intermediate decomposes to a [Fe(IV)=O] species and NO_2 *via* homolytic cleavage of O−O bond. In the present case, the $\{Co(NO)\}^8$ complex upon reaction with H_2O_2 gives a [Co(III)-PN] intermediate. This decomposes rapidly to [Co(IV)=O] and NO_2 followed by either recombination to give a [Co(III)-NO_3^-] complex or converts to a more stable porphyrin radical cation species.

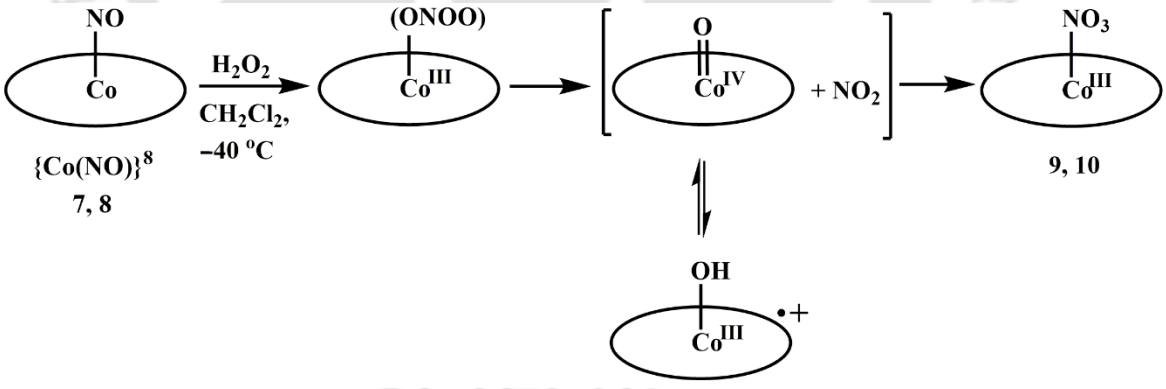

Scheme 3.2. Plausible reaction mechanism.

To confirm involvement of PN intermediate, complex **7** and **8** was further made to react with H_2O_2 in presence of 2,4-di-*tert*-butylphenol (DTBP). Appreciable amount (~60-65%) of 2,4-di-*tert*-butyl-6-nitrophenol was obtained from the final reaction mixture along with corresponding [Co^{III}-OH^-] complexes, **11** and **12** (Appendix II, Figures A2.45-A2.51).

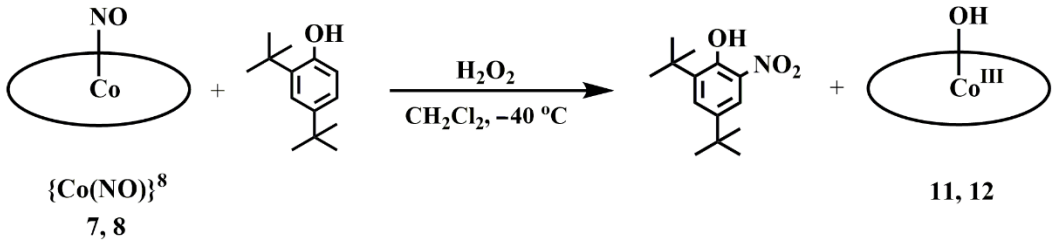

$\{Co(NO)\}^8$
7, 8

11, 12

Scheme 3.3. Reaction of complexes **7** and **8** with H_2O_2 in presence of DTBP.

Recently, $[Co(Cl_4TPP^{2-})(NO)]$ complex in the presence of H_2O_2 in CH_3CN at −40 °C was exemplified to result in the corresponding nitrite complex, $[Co(Cl_4TPP^{2-})(NO_2)]$ and the formation of a PN intermediate was implicated.[18]

3.3 Experimental Section

3.3.1 Materials and methods

All the reagents and solvents were purchased from commercial sources and used as received unless specified. All the reactions were carried out under Ar or N_2 atmosphere. Repeated vacuum/purge cycles or bubbling with Ar was used to remove the oxygen from the solvents and solutions. CH_3CN was distilled over calcium hydride. UV-visible spectra were recorded on Agilent Cary 8454 UV-visible spectrophotometer using Chemstation software. FT-IR spectra were taken on a Perkin Elmer spectrophotometer with samples prepared as KBr pellets or in solutions using KBr cell having 1 cm pathlength. ^{1}H-NMR spectra were recorded on a 600 MHz Varian FT spectrometer. Chemical shifts (ppm) were referenced with respect to Me_4Si as internal standard for organic compounds or to the residual solvent peaks. Elemental analyses were done on a Perkin Elmer Series II Analyzer. Mass spectra were recorded on a Waters, Model: Q-Tof Premier instrument with ESI mode of ionization. The X-band Electron Paramagnetic Resonance (EPR) spectra were recorded on a JES-FA200 ESR spectrometer, at room temperature or at 77 K with microwave power, 0.998 mW; microwave frequency, 9.14 GHz and modulation amplitude, 2.

Single crystals were grown from the respective CH_2Cl_2 and $CHCl_3$ solutions using slow evaporation technique. The intensity data were collected using a Bruker SMART APEX-II CCD diffractometer, equipped with a fine focus 1.75 kW sealed tube MoK_α radiation (λ = 0.71073 Å) at 293(3) K, with increasing ω (width of 0.3° per frame) at a scan speed of 3 s/frame. The SMART software was used for data acquisition. Data integration and reduction were undertaken with SAINT and XPREP software.[27] Structures were solved by direct methods using SHELXS-2016 and refined with full-matrix least squares on F^2 using SHELXL-2016/6.[28a] Structural illustrations have been drawn with ORTEP-3 for Windows.[28b]

3.3.2 Syntheses

5-(4-methoxyphenyl)-10,15,20-triphenylporphyrin (MPTPPH_2). To a solution of 3.18 g (30 mmol) benzaldehyde and 0.41 g (3 mmol) 4-methoxybenzladehyde in 150 mL propionic acid, a solution of 2.76 g (40 mmol) freshly distilled pyrrole in 10 mL propionic acid was added dropwise over a period of 30 min at reflux temperature. The reaction mixture was further refluxed for another 3 h. After that neutralization was done using aqueous Na_2CO_3 solution to obtain dark colored precipitate which was then washed thoroughly and extracted with $CHCl_3$. Elution of this crude mixture with 20% $CHCl_3$ in hexane in a silica gel column resulted pure compound (0.19 g, ~10% yield). Elemental analyses for $C_{45}H_{32}N_4O$. Calcd. (%): C, 83.83; H, 5.00; N, 8.69, found (%): C, 83.92; H, 5.10; N, 8.56. ^{1}H NMR (400 MHz, $CDCl_3$): δ_{ppm}, 8.90-8.86 (m, 8H), 8.24-8.22 (dd, 6H), 8.15-8.13 (dd, 2H), 7.79-7.74 (m, 9H), 7.30-7.28 (dd, 2H), 4.10 (s, 3H), −2.74 (br, 2H). ^{13}C NMR (100 MHz, $CDCl_3$): δ_{ppm}, 159.4, 142.2, 135.6, 134.6, 127.7, 126.7, 120.1, 112.2, 55. 6. ESI-mass (m/z): Calcd: 644.258, found: 645.277 (M+1).

5,10,15,20-*tetrakis*(4-methoxyphenyl)porphyrin (TMPPH_2). 4-methoxybenzaldehyde (

2.72 g, 20 mmol) and freshly distilled pyrrole (1.34 g, 20 mmol) were refluxed in 50 mL of propionic acid for 3 hours. The solution was cooled to room temperature and neutralized by aqueous Na_2CO_3. A precipitate appeared and it was filtered off. The crude mass was subjected to silica gel column to afford the desired ligand as purple solid (1.1 g, ~30% yield). Elemental analyses for $C_{48}H_{38}N_4O_4$. Calcd. (%): C, 78.45; H, 5.21; N, 7.62, found (%): C, 78.38; H, 5.20; N, 7.68. ^{1}H-NMR (400 MHz, $CDCl_3$): δ_{ppm}, 8.86 (s, 8H), 8.13-8.11(d; 8H), 7.29-7.28 (d; 8H), 4.10 (s, 12H), −2.73 (s, 2 H). ^{13}C NMR (100 MHz, $CDCl_3$): δ_{ppm}, 159.5, 135.6, 134.7, 119.7, 112.2, 55.6. ESI-mass (m/z): Calcd: 734.289, found: 735.291 (M+1).

Complex 5. A mixture of the ligand $MPTPPH_2$ (0.13 g, 0.2 mmol), $Co(OAc)_2.4H_2O$ (0.5 g, 2 mmol) in $CHCl_3$ (10 mL) and acetic acid (10 mL) was refluxed overnight. The reaction mixture was cooled and 60 mL of water was added. The solution was then extracted with $CHCl_3$ (3 × 30 mL). The crude mass was column chromatographed to result in complex **5** as red solid. Yield: ~85%. Elemental analyses for $C_{45}H_{30}N_4OCo$, Calcd. (%): C, 77.03; H, 4.31; N, 7.98, found (%): C, 77.15; H, 4.36; N, 7.87. UV-visible (CH_2Cl_2): 411 nm ($\varepsilon/M^{-1}cm^{-1}$, 1.20×10^5) and 528 nm ($\varepsilon/M^{-1}cm^{-1}$, 0.93×10^4). FT-IR (in KBr): 1606, 1540, 1509, 1440, 1349, 1245, 1176, 1002, 794, 747, 716 and 699 cm^{-1}. ESI-mass (m/z): Calcd. 701.175, found: 701.188 (molecular ion peak).

Complex 6. Complex **6** was synthesized following similar procedure as above using the ligand $TMPPH_2$ (0.15 g, 0.2 mmol). Yield: 0.14g (~90%). Elemental analyses for $C_{48}H_{36}N_4O_4Co$, Calcd. (%): C, 72.81; H, 4.58; N, 7.08, found (%): C, 72.85; H, 4.46; N, 7.07. UV-visible (CH_2Cl_2): 415 nm ($\varepsilon/M^{-1}cm^{-1}$, 2.12×10^5) and 529 nm ($\varepsilon/M^{-1}cm^{-1}$, 2.14×10^4). FT-IR (in KBr): 1607, 1506, 1461, 1352, 1289, 1248, 1172, 1039, 999 and 807 cm^{-1}. ESI-mass (m/z): Calcd: 791.207, found: 791.205 (molecular ion peak).

Complex 7. Complex **5** (0.08 g, 0.1 mmol) was dissolved in dry and degassed CH_2Cl_2. NO

gas was bubbled for ~10 minutes to this solution. The color of the solution changes from orange to dark red. After removal of the excess NO, the product was isolated by continuous argon flash with 85% yield (0.06 g). Elemental analyses for $C_{45}H_{30}N_5O_2Co$, Calcd. (%): C, 73.87; H, 4.13; N, 9.57, found (%): C, 73.98; H, 4.15; N, 9.49. FT-IR (in KBr): 1682, 1605, 1575, 1511, 1454, 1440, 1345, 1298, 1248, 1174, 1004, 751 and 700 cm^{-1}. UV-visible (CH_2Cl_2): 414 nm ($\varepsilon/M^{-1}cm^{-1}$, 0.89×10^5), 536 nm (ε/M^{-1} cm^{-1}, 1.29×10^4). ^1H NMR (400 MHz, $CDCl_3$): δ_{ppm}, 8.96-8.85 (m, 8H), 8.18-8.14 (dd, 6H), 8.09-8.06 (dd, 2H), 7.76-7.73 (m, 9H), 7.29-7.27 (d, 2H), 4.09 (s, 3H). ESI-mass (m/z): Calcd: 731.173; found: 732.205 (M+1).

Complex 8. Complex **8** was synthesized from direct reaction of **6** (0.08 g, 0.1 mmol) with NO following the same procedure described above. Yield: 0.07 g (~80%). Elemental analyses for $C_{48}H_{36}N_5O_5Co$, Calcd. (%): C, 70.16; H, 4.42; N, 8.52, found (%): C, 70.08; H, 4.45; N, 8.49. FT-IR (in KBr): 1696, 1607, 1508, 1462, 1351, 1289, 1249, 1174, 1001 and 805 cm^{-1}. UV-visible (CH_2Cl_2): 420 nm ($\varepsilon/M^{-1}cm^{-1}$, 1.28×10^5) and 540 nm ($\varepsilon/M^{-1}cm^{-1}$, 1.31×10^4). ^1H NMR (400 MHz, $CDCl_3$): δ_{ppm}, 8.93 (s, 8H), 8.09-8.07 (d, 8H), 7.28-7.26 (d, 8H), 4.08 (s, 12H). ESI-mass (m/z): Calcd: 791.207; found: 791.163 (molecular ion peak for [Co($TMPP^{2-}$)]).

3.3.3 Reaction of complex 7 with H_2O_2

Complex **7** (0.37 g, 0.5 mmol) was taken in 10 mL of dry and degassed CH_2Cl_2 and cooled to −40 ºC. Pre-cooled hydrogen peroxide (50% v/v, 1 mmol) in CH_3CN was added to this cold solution and stirred for 2 h. The solution was warmed up to room temperature and dried under reduced pressure.

Complex 9. Yield: 0.23 g (~60%). Elemental analyses for $C_{45}H_{30}N_5O_4Co$, Calcd. (%): C, 70.77; H, 3.96; N, 9.17, found (%): C, 70.71; H,3.21; N, 9.06. FT-IR (in KBr): 1636, 1528,

1441, 1384, 1342, 1300, 1022 and 807 cm^{-1}. UV-visible (CH_2Cl_2): 441 ($\varepsilon/M^{-1}cm^{-1}$, 0.32 × 10^5), 546 ($\varepsilon/M^{-1}cm^{-1}$, 0.41 × 10^4) and 579 ($\varepsilon/M^{-1}cm^{-1}$, 0.34 × 10^4) nm. ^{1}H NMR (400 MHz, CD_3CN): δ_{ppm}, 9.22-9.17 (m, 8H), 8.22-8.21 (d, 6H), 8.13-8.12 (d, 2H), 7.85-7.81 (m, 9H), 7.38-7.36 (d, 2H), 4.07 (s, 3H). ESI-mass (m/z): Calcd: 763.163, found: 764.248 (M+1).

3.3.4 Reaction of complex 8 with H_2O_2

Complex **8** (0.41 g, 0.5 mmol) was reacted with H_2O_2 in CH_2Cl_2 at −40 ºC under similar reaction condition to get complex **10**.

Complex 10. Yield: 0.23 g (~55%). Elemental analyses for $C_{48}H_{36}N_5O_7Co$, calcd. (%): C, 67.53; H, 4.25; N, 8.20, found (%): C, 67.50; H, 4.31; N, 8.16. FT-IR (in KBr): 1603, 1510, 1462, 1440, 1384, 1355, 1303, 1255, 1176, 1025 and 815 cm^{-1}. UV-visible (CH_2Cl_2): 455 nm ($\varepsilon/M^{-1}cm^{-1}$, 1.02 × 10^5) and 695 nm ($\varepsilon/M^{-1}cm^{-1}$, 1.20 × 10^4). ^{1}H NMR (400 MHz, CD_3CN): δ_{ppm}, 9.24 (s, 8H), 8.15-8.13 (d, 8H), 7.41-7.39 (d, 8H), 4.10 (s, 12H). ESI-mass (m/z): Calcd: 853.195, found: 854.240 (M+1).

3.3.5 Reaction of complex 7 with H_2O_2 in presence of 2,4-di-*tert*-butylphenol

To a dry and degassed CH_3CN solution of complex **7** (0.73 g, 1 mmol), precooled 2,4-di-*tert*-butylphenol (1.03 g, 5 mmol) was added followed by pre-cooled H_2O_2 (50% v/v, 2 mmol) in CH_3CN at −40 °C and stirred for 2 h at the same temperature. The reaction mixture was then brought to room temperature and dried in a rotavapor. Purification of the crude mass through column chromatography resulted in pure 2,4-di-*tert*-butyl-6-nitrophenol (Yield: 0.16 g, ~65%) and complex **11** (Yield: 0.48 g, ~67%).

2,4-di-*tert*-butyl-6-nitrophenol. Elemental analyses for $C_{14}H_{21}NO_3$, Calcd. (%): C, 66.91; H, 8.42; N, 5.57, found (%):C, 67.07; H, 8.40; N, 5.68. ^{1}H NMR (400 MHz, $CDCl_3$): δ_{ppm}, 11.44 (s, 1H), 7.96 (s, 1H), 7.65 (s, 1H), 1.45 (s, 9H), 1.32 (s, 9H). ^{13}C NMR (100 MHz,

$CDCl_3$): δ_{ppm}, 152.7, 141.6, 139.5, 133.4, 132.2, 118.5, 35.4, 34.2, 30.8, 29.1. ESI-mass (m/z): Calcd: 251.15, found: 250.08 (M−1).

Complex 11. Elemental analyses for $C_{45}H_{31}N_4O_2Co$, Calcd. (%): C, 75.20; H, 4.35; N, 7.80, found (%): C, 75.36; H, 4.45; N, 7.78. FT-IR (in ATR): 3528, 1607, 1509, 1440, 1349, 1246, 1176, 1069, 1003 and 795 cm^{-1}. ESI-mass (m/z): Calcd: 718.178, found: 719.048 (M+1).

3.3.6 Reaction of complex 8 with H_2O_2 in presence of 2,4-di-*tert*-butylphenol

Reaction of complex **8** (0.82 g, 1 mmol) and H_2O_2 in presence of 2,4-di-*tert*-butylphenol in a similar condition gave 2,4-di-*tert*-butyl-6-nitrophenol and complex **12**.

Complex 12. Yield: 0.55 g (~70%). Elemental analyses for $C_{48}H_{37}N_4O_5Co$, Calcd. (%):C, 71.28; H, 4.61; N, 6.93, found (%):C, 71.25; H, 4.64; N, 6.95. FT-IR (in KBr): 3418, 2924, 2853, 1597, 1574, 1511, 1417, 1304, 1262, 1169, 1073, 1023, 898, 849, 808, 750 and 719 cm^{-1}. ESI-mass (m/z): Calcd: 808.210, found: 809.566 (M+1).

3.4 Conclusion

Two stable $\{Co(NO)\}^8$ complexes (**7** and **8**) have been synthesized and characterized. These complexes react with H_2O_2 to give corresponding [Co(III)-NO_3^-] complexes, **9** and **10**. The reaction is proposed to proceed *via* putative [Co(III)-PN] intermediate. UV-visible, X-band EPR spectroscopic studies suggested involvement of a Co(III) porphyrin cation radical in the reaction pathway. Detection of the porphyrin radical cation is the indirect evidence for a [Co(IV)=O] intermediate that forms in the decomposition of a [Co(III)-PN].

3.5 References

1. *Nitric Oxide: Biology and Pathobiology*; Ignarro, L. J., Ed.; Academic Press: San Diego, **2000**.

2. *Nitric Oxide and Infection*; Fang, F. C., Ed.; Kluwer Academic/ Plenum Publishers: New York, **1999**.
3. Bourassa, J. L.; Ives, E. P.; Marqueling, A. L.; shimanovich, R.; Groves, J. T. *J. Am. Chem. Soc.* **2001**, *123*, 5142.
4. Goldstein, S.; Lind, J.; Merenyi, G. *Chem. Rev.* **2005**, *105*, 2457.
5. Gardner, P. R.; Gardner, A. M.; Martin, L. A.; Salzman, A. L. *Proc. Natl. Acad. Sci. U. S. A.* **1998**, *95*, 10378.
6. Schopfer, M. P.; Mondal, B.; Lee, D.-H.; Sarjeant, A. A. N.; Karlin, K. D. *J. Am. Chem. Soc*. **2009**, *131*, 11304.
7. Ford, P. C.; Lorkovic, I. M. *Chem. Rev*. **2002**, *102*, 993.
8. (a) Clarkson, S. G.; Basolo, F. *J. Chem. Soc. Chem. Commun.* **1972**, *11*, 670. (b) Clarkson, S. G.; Basolo, F. *Inorg. Chem*. **1973**, *12*, 1528.
9. (a) Wick P. K.; Kissner R.; Koppenol W. H. *Helv. Chim.Acta.* **2000**, *83*, 748. (b) Wick, P. K.; Kissner, R.; Koppenol, W. H. *Helv. Chim.Acta*. **2001**, *84*, 3057.
10. Thyagarajan, S.; Incarvito, C.; Rheingold, A. L.; Theopold, K. H. *Inorg. Chim. Acta.* **2003**, *345*, 333.
11. Maiti, D.; Lee, D.-H.; Sarjeant, A. A. N.; Pau, M. Y. M.; Solomon, E. I.; Gaoutchenova, K.; Sundermeyer, J.; Karlin, K. D. *J. Am. Chem. Soc.* **2008**, *130*, 6700.
12. (a) Kurtikyan, T. S.; Eksuzyan, S. R.; Hayrapetyan, V. A.; Martirosyan, G. G.; Hovhannisyan, G. S.; Goodwin, J. A. *J. Am. Chem. Soc.* **2012**, *134*, 13861. (b) Kurtikyan, T. S.; Eksuzyan, Sh. R.; Goodwin, J. A.; Hovhannisyan, G. S. *Inorg. Chem.* **2013**, *52*, 12046.
13. Yokoyama, A.; Han, J. E.; Cho, J.; Kubo, M.; Ogura, T.; Siegler, M. A.; Karlin, K. D.; Nam, W. *J. Am. Chem. Soc.* **2012**, *134*, 15269.

14. Yokoyama, A.; Cho, K.-B.; Karlin, K. D.; Nam, W. *J. Am. Chem. Soc.* **2013**, *135*, 14900.

15. Saha, S.; Ghosh, S.; Gogoi, K.; Deka, H.; Mondal, B.; Mondal, B. *Inorg. Chem.* **2017**, *56*, 10932.

16. (a) Tran, N. G.; Kalyvas, H.; Skodje, K. M.; Hayashi, T.; Moënne-Loccoz, P.; Callan, P. E.; Shearer, J.; Kirschenbaum, L. J.; Kim, E. *J. Am. Chem. Soc.* **2011**, *133*, 1184. (b) Skodje, K. M.; Williard, P. G.; Kim, E. *Dalton Trans*. **2012**, *41*, 7849.

17. Kalita, A.; Kumar, P.; Mondal, B. *Chem. Commun.* **2012**, *48*, 4636.

18. Saha, S.; Gogoi, K.; Mondal, B.; Ghosh, S.; Deka, H.; Mondal, B. *Inorg. Chem.* **2017**, *56*, 7781.

19. Mondal, B.; Saha, S.; Borah, D.; Mazumdar, R.; Mondal, B. *Inorg. Chem.* **2019**, *58*, 1234.

20. Mondal, B.; Borah, D.; Mazumdar, R.; Mondal, B. *Inorg. Chem.* **2019**, *58*, 14701.

21. (a) Adler, A. D.; Longo, F. R.; Finarelli, J. D.; Goldmacher, J.; Assour, J.; Korsakoff, L. *J. Org. Chem.* **1967**, *32*, 476. (b) Rothemund, P.; Menotti, A. R. *J. Am. Chem. Soc.* **1948**, *70*, 1808. (c) Tong, S. L.; Zhang, J.; Yan, Y.; Hua, S.; Yu, J.; Yu, L. *Solid State Sciences* **2011**, *13*, 1320.

22. Richter-Addo, G. B.; Hodge, S. J.; Yi, G. B.; Khan, M. A.; Ma, T.; Caemelbecke, E. V.; Guo, N.; Kadish, K. M. *Inorg. Chem.* **1996**, *35*, 6530.

23. Fujita, E.; Chang, C. K.; Fajer, J. *J. Am. Chem. Soc.* **1985**, *107*, 7665.

24. Wayland, B. B.; Minkiewicz, J. V.; Abd-Elmageed, M. E. *J. Am. Chem. Soc.* **1974**, *96*, 2795.

25. Fujita, E.; Fajer, J. *J. Am. Chem. Soc.* **1983**, *105*, 6743.

26. Winkler, J. R.; Gray, H. B. *Struct. Bonding (Berlin, Ger.)* **2011**, *142*, 17.

27. SMART, SAINT and XPREP, Siemens Analytical X-ray Instruments Inc., Mad-

ison, Wisconsin, USA, **1995**.

28. (a) Sheldrick, G. M. SHELXS-2014, University of Gottingen, Germany. (b) Farrugia, L. J. *J. Appl. Crystallogr.* **1997**, *30*, 565.

Chapter 4

Reaction of a nitrosyl complex of Mn(II) porphyrin with superoxide: Formation of a Mn(IV)-oxo species

Abstract

A five-coordinated $\{Mn(NO)\}^6$ complex of Mn(II)-porphyrinate, $[Mn(TMPP^{2-})(NO)]$, **14** {$TMPPH_2$ = 5,10,15,20-*tetrakis*(4-methoxyphenyl)porphyrin}, reacts with superoxide (O_2^-) in THF at −40 °C to result in the corresponding [Mn(III)-OH^-] complex $[Mn^{III}(TMPP^{2-})(OH)]$, **15** *via* the formation of a putative Mn(III)-PN intermediate. Nitrogen dioxide (NO_2) is released in the reaction as a side product. UV-visible and X-band EPR spectroscopic studies suggest the involvement of a [Mn(IV)=O] species in the reaction, which forms through the O−O bond homolysis of the PN ligand. Moreover, formation of the [Mn(III)-PN] is further supported by the well-eshtablished phenol ring nitration experiment.

4.1 Introduction

Nitric oxide (NO) plays diverse role in mammalian biochemistry *via* its involvement in signal transduction and a number of regulatory processes. Contrarily, its toxicological effects are observed at elevated concentration in the forms of oxidative or nitrosative stress and metallo-enzyme activity inhibition.[1] One of the major pathological effects of NO involves its reaction with superoxide, O_2^- resulting in peroxynitrite, $ONOO^-$ (PN),[2] a potent biological oxidant. PN forms when intracellular concentration of both the reactants increases as a result of events like sepsis, inflammation, excitotoxicity, and ischemia-reperfusion and associated with a number of mitochondrial injuries including disruption of Fe-S clusters, inactivation of aconitase, superoxide dismutase etc. PN attacks protein tyrosine, tryptophan, phenylalanine residues, causes oxidation of thiols, forms nitro, nitrito or nitroperoxo products with lipids and responsible for deoxyribose oxidation and cleavage.[2,3] *In vivo*, superoxide dismutase (SOD) enzymes maintain optimal physiological concentration of O_2^-.[4] On contrary, PN inactivates the enzyme *via* nitration of a tyrosine residue in the protein chain.[5] Radi *et al.* reported the involvement of a high valent metal oxo species and NO_2 in the nitration event.[5a] Similar mechanism is proposed in case of nitric oxide dioxygenase (NOD), an enzyme that metabolizes NO to more benign nitrate, NO_3^-. NO reacts with the [Fe(III)-O_2^-] species present in the active site of NO to generate a [Fe(III)-PN] intermediate which then decomposes to give an oxo-ferryl, [Fe(IV)=O] and NO_2. This mechanism is, however, elusive and not much evidence can be found in support of the proposed intermediates owing to their high instability. In fact, presence of a Lewis acid, such as transition metal ion, increases the rate of decomposition of PN by many folds by facilitating the homolytic cleavage of O−O bond. Hence, understanding this chemistry has always been a challenge to the researchers and growing interest for trapping the intermediate demanded

a range of small molecule bio-mimics. Basolo and Clarkson were the firsts to report the formation of Co-PN intermediate in the reaction of Co-NO and O_2.[6] Following this, a number of both heme and non-heme model PN complexes of Fe, Co, Mn, Cr, Cu were reported in literature. These complexes are synthesized mainly using two routes, reaction of metal nitrosyls with reactive oxygen species and reaction of metal-superoxo/peroxo/hydroperoxo complexes with NO. However, examples of well characterized discrete PN complexes are very rare. Karlin's group being one of the pioneers in the field reported a few Fe and Cu PN complexes which form in the reaction of NO with respective peroxo/superoxo complexes.[7] Similarly, Kurtikyan's group and Nam's group reported some of the important examples of Co and Cr PN complexes.[8] Reaction of a [Cr(IV)-O_2^{2-}] complex with NO resulted [Cr(III)-NO_3^-] complex,[8c] while the reaction of NO with a [Cr(III)-O_2^-] complex resulted corresponding [Cr(III)-NO_2^-]. Both the reaction involve [Cr(III)-PN] intermediate followed by [Cr(IV)=O] species.[8d] Kurtikyan's group also reported examples of [Mn(III)-PN] complexes that forms in the reaction of Mn-porphyrin dioxygen adducts with NO.[9] Very recently Kumar and co-workers reported example of [Ni(II)-PN] complex which forms in the reaction of [Ni^{III}-O_2^{2-}] with NO.[10] A few examples of Co and Mn PN complexes were also reported from our group.[11] A {Co(NO)}^{8} complex in porphyrin ligand framework reacts with H_2O_2 to give Co^{III}-PN intermediate which then decomposes to [Co(III)-NO_3^-] *via* a [Co(III)-$O^{\bullet}$] species.[11e] Similarly a {Mn(NO)}^{6} complex upon reacting with O_2^- yielded a very unstable [Mn(IV)=O] species *via* the formation of [Mn(III)-PN].[11f]

Herein, we report an example of {Mn(NO)}^{6} complex [Mn($TMPP^{2-}$)(NO)], **14** {$TMPPH_2$ = 5,10,15,20-*tetrakis*(4-methoxyphenyl)porphyrin} which on reaction with O_2^- gives the corresponding [Mn(III)-OH^-] complex [Mn^{III}($TMPP^{2-}$)(OH)], **15** with the release of NO_2. The reaction is proposed to proceed *via* a putative [Mn(III)-PN] intermediate. Formation of

[Mn(IV)=O] intermediate by O−O bond homolysis of PN is proposed in the plausible reaction pathway. Isolation of [Mn(III)-OH^-] and NO_2 as final products validates the proposition. Moreover, involvement of [Mn(IV)=O] species is also confirmed spectroscopically and chemically.

4.2 Results and Discussion

The Mn(III) complex [$Mn^{III}(TMPP^{2-})(Cl)$], **13** was synthesized following reported procedure and characterized both spectroscopically and structurally (Appendix III, Figures A3.1-A3.5).[12] Complex **13** is a low spin d^4 complex and hence, in CH_2Cl_2 solution of it does not show any signal in X-band EPR even at 77 K. In UV-visible spectroscopy, the same solution displays Soret band at 475 nm and Q bands at 530, 583 and 621 nm, which is typical of Mn(III)-porphyrin complexes.[13] Crystal structure of **13** confirms that it is a five-coordinated square pyramidal complex with manganese at the center of the square plan formed by the porphyrin nitrogens and chloride as the axial ligand (Appendix, Figure A3.5). The Mn-N_{por} and Mn-Cl bond lengths are consistent with the previously reported analogous compounds. The crystallographic data and metric parameters are listed in appendix III, tables A3.1-A3.3.

Complex **13** upon reaction with hydroxylamine undergoes reductive nitrosylation to yield the nitrosyl complex [$Mn(TMPP^{2-})(NO)$], **14** (Experimental Section).[14] Kubiak *et al.* reported complex **14** as the five coordinated nitrosyl complex of $\{Mn(NO)\}^6$ configuration; which they synthesized by bubbling excess NO gas through a CH_3OH solution of complex **13** in presence of $NaBH_4$.[15] Complex **14** shows FT-IR stretching frequency at around 1755 cm^{-1} in KBr which matches with the reported one (Appendix III, Figure A3.6). The same peak was found to shift to 1739 cm^{-1} in THF solution. In UV-visible spectrum of complex **14** in THF, the characteristic Soret band appears at 427 nm along with which multiple Q

bands at 542, 579 and 613 nm can be observed (Appendix III, Figure A3.8). The complex is diamagnetic due to antiferromagnetic coupling between unpaired '*d*' electron of manganese and the antibonding π* electron of NO and hence EPR silent. Moreover, it displays well resolved ^{1}H NMR peaks at 8.67 (pyrrole), 8.07-8.06 (ortho), 7.96-7.95 (ortho), 7.33 (meta), 4.03 (−CH_3) (Appendix III, Figure A3.9). Even after several attempts we could not grow X-ray quality crystals.

Complex **14** reacts with KO_2 in THF at −40 ºC to give complex [Mn^{III}($TMPP^{2-}$)(OH)], **15** and NO_2 (Scheme 4.1). Complex **15** was characterized spectroscopically as well as structurally. In THF solution complex **15** absorbs at 470 (Soret), 530, 581 and 619 nm and is silent in X-band EPR spectroscopy (Appendix III, Figures A3.15-A3.16). These spectroscopic observations confirms that complex **15** is a low spin Mn(III) complex. Moreover, in ESI-mass spectrometry, a peak at m/z 787.225 was observed which corresponds to the [Mn($TMPP^{2-}$)]$^{+}$ ion (Calcd. 787.211). Further information on complex **15** came from single crystal X-ray structure which reveals it as [Mn(III)-OH^{-}] complex with hydroxo ligand occupying the axial position (Figure 4.1). However, in the crystal structure,

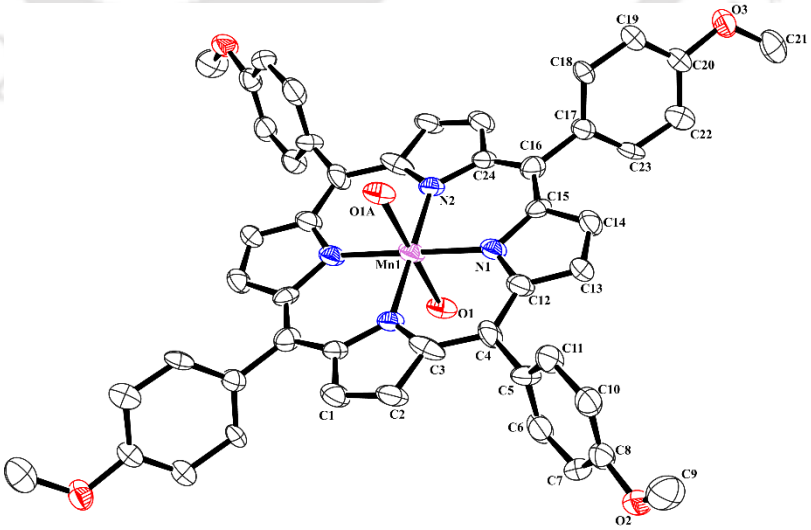

Figure 4.1. ORTEP diagram of complex **15** (30% thermal ellipsoid plot, H atoms are omitted for clarity).

the hydroxo group occupies two symmetry equivalent positions and this disorder could not be corrected even at 100 K.

When the reaction of **14** and KO_2 in THF at room temperature was monitored in UV-visible spectroscopy it was observed that the intensity of Soret band of **14** at 427 nm gradually decreased and a new transient peak at 475 nm appeared which subsequently shifted to 470 nm corresponding to complex **15** (Figure 4.2). The transient peak at 475 nm attributed to the generation of an intermediate, **14a** in the course of the reaction. Kaddish *et al.* previously reported that on one electron oxidation of [Mn(TPP^{2-})(NO)] (TPP^{2-} = *meso*-tetraphenylporphyrinate) results similar shifting of Soret band.[17] In a recent report from Galinato *et al.*, it is reported that in case of Mn(III) porphyrinates, the Soret band appears around ~475 nm.[13]

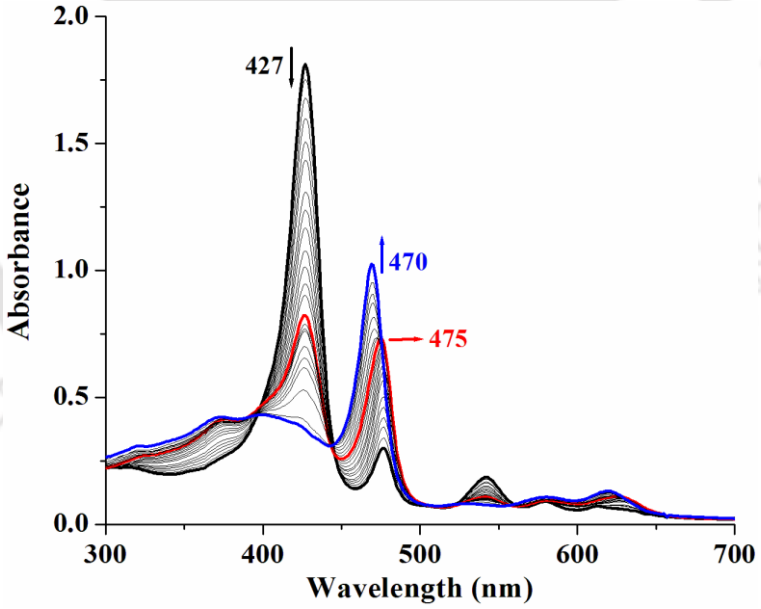

Figure 4.2. UV-visible spectral monitoring of complex **14** (black); after addition of KO_2 to result in the intermediate **14a** (red) and complex **15** (blue) in THF at room temperature.

For more insights the same reaction was then monitored in FT-IR spectroscopy; where after the addition of KO_2 nitrosyl stretching frequency of **14** in THF at 1739 cm^{-1} immediately shifted to 1776 cm^{-1} (Figure 4.3). Previous attempts to oxidize (Porphyrin)Mn(II)-NO

electrochemically, led to the loss of nitrosyl stretching frequency in FT-IR.[18] However, in case of (Porphyrin)Co(II)-NO, one electron oxidation of the metal center resulted ~ 40 cm^{-1} shift in nitrosyl stretching frequency.[19] Along with this shift, a concomitant generation of a new peak at 1194 cm^{-1} was observed. Finally, both the peaks at 1776 and 1194 cm^{-1} disappeared simultaneously indicating that these two peaks are associated to the same intermediate species **14a**. In literature, the range of ~ 1100-1250 cm^{-1} is attributed for the metal bound superoxide stretching frequency.[20] It is important to note that KO_2 gives signal at 1146 cm^{-1}.[21] In the present case, the appearance of 1194 cm^{-1} peak is best assigned to a Mn(III)-superoxide complex. Thus, from the above discussion intermediate **14a** can be formally designated as a [Mn^{III}($TMPP^{2-}$)(NO)(O^{2-})] species (Scheme 4.1).

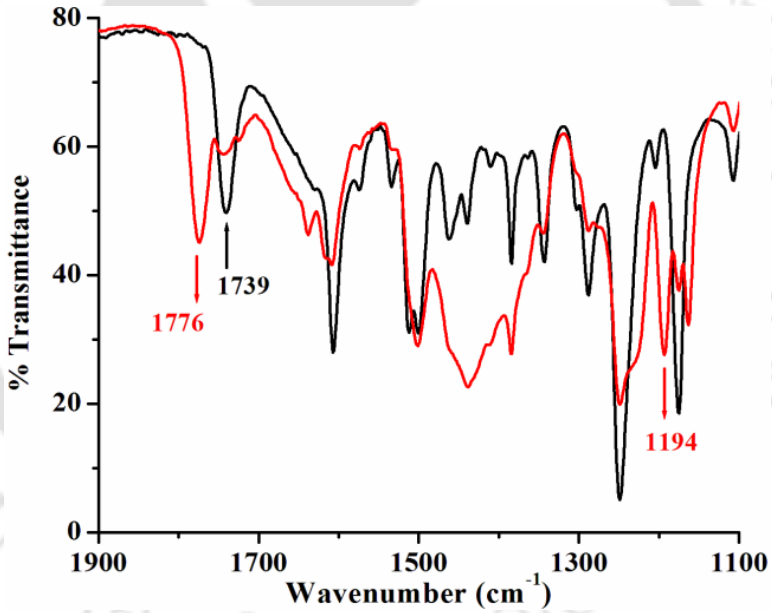

Figure 4.3. FT-IR spectra of complex **14** (black) and after addition of KO_2 (red) in THF.

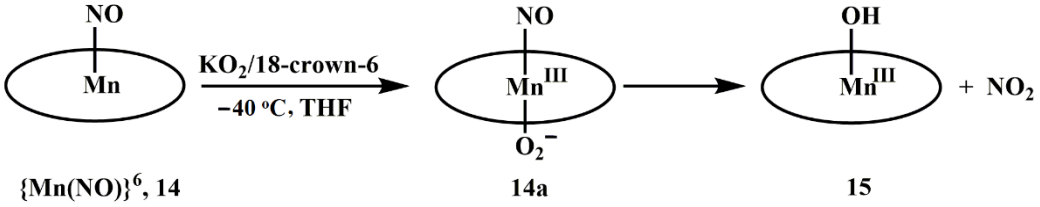

Scheme 4.1. Reaction of complex **14** with KO_2.

This type of intermediate was previously reported by our group where a cobalt nitrosyl complex [Co^{II}(NO)(BPI)(OAc)] (BPI = 1,3-*bis*(2′-pyridylimino)isoindol anion) reacts with O_2 to give intermediate, [Co^{III}(NO)(O_2^-)(BPI)(OAc)] which finally decomposes to [Co^{III}(NO_2^-)(BPI)(OAc)] *via* formation of a putative [Co(III)-PN] intermediate.[11d] Similarly, Theopold *et al.* reported in the reaction of a *tris*(3-*tert*-butyl-5-methylpyrazole)borate ligand derived Co(III) superoxo complex with NO at −78 °C.[22] A nitrosyl complex of a di-copper system, [$Cu^{I,II}_2$(UN-O^-)(μ-NO)]$^{2+}$ in CH_2Cl_2 solution, was reported to results in the formation of [Cu^{II}_2(UN-O^-)(NO)(O_2^-)]$^{2+}$ upon addition of O_2 gas.[7d]

Quantitative titration in FT-IR with increasing amount of KO_2 revealed that complete conversion of **14** to **14a** did not occur until the ratio of O_2^- to complex **14** do not exceed two. Therefore, two equivalents of O_2^- are believed to be taking part in the reaction, one equivalent oxidizing the metal centre and the other equivalent subsequently binding to it. However, UV-visible and FT-IR spectroscopic evidences suggest that these two processes occur parallelly rather than a stepwise manner. In a hypothetical first step, the reaction of Mn(II)-porphyrinate and O_2^- yields corresponding Mn(III)-porphyrinate and O_2^{2-} similar to what occurs in the superoxide dismutase (SOD) activity (Eq. 4.1). Formation of the later was detected by the standard protocol using potassium iodide and starch. In the next step, the said Mn(III)-porphyrinate reacts with a second equivalent of O_2^- and forms a Mn(III)-superoxo complex **14a** (Eq. 4.2).

$$[Mn^{II}(TMPP^{2-})(NO)] + O_2^- \longrightarrow [Mn^{III}(TMPP^{2-})(NO)]^+ + O_2^{2-} \quad \text{---------- (Eq. 4.1)}$$

$$[Mn^{III}(TMPP^{2-})(NO)]^+ + O_2^- \longrightarrow [Mn^{III}(TMPP^{2-})(NO)(O_2^-)] \quad \text{---------- (Eq. 4.2)}$$

Based on earlier reports, the decomposition of **14a** to **15** is presumed to occur *via* a [Mn(III)-PN] intermediate. But the formation of a PN intermediate could not be traced by any

spectroscopic techniques. However, when the reaction of complex **14** and KO_2 was done in presence of 2,4-di-*tert*-butylphenol (DTBP), an appreciable amount of 2,4-di-*tert*-butyl-6-nitrophenol was obtained (Appendix III, Figure A3.17-A3.19). This reaction is often used as a marker for presence of a PN species in the course of a reaction.[7] Here also the formation of the nitration product serves as an indirect evidence for involvement of [Mn(III)-PN] intermediate in the reaction.

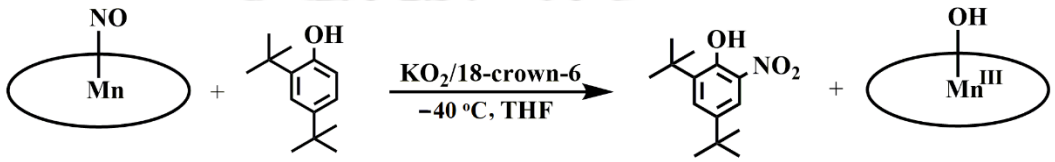

{Mn(NO)}^{6}, 14 15

Scheme 4.2. Reaction of complex **14** with KO_2 in presence of DTBP.

The proposed decomposition pathway of a Metal PN intermediates involves a high valent metal oxo complex formed *via* homolytic fission of O−O bond of PN. In this case, the presumed Mn(III)-PN complex is believed to give [Mn(IV)=O] and NO_2 in the process. Formation of complex **15** as final product suggest that it might be the decomposition product of [Mn(IV)=O], which confirms the validity of our presumption.

Hence, more evidence towards formation of [Mn(IV)=O] was sought. When the UV-visible spectroscopic study of the reaction was repeated at −40 °C, a new intermediate species was identified by the formation of new Soret band at 435 nm (Figure 4.4). The appearance of this band is attributed to the formation of a high valent oxo intermediate [Mn^{IV}($TMPP^{2-}$)(O)]. In an earlier report, it has been observed that [Mn($F_{20}TPP^{2-}$)(NO)] reacts with KO_2 to give corresponding nitrato product and this reaction goes *via* [Mn^{IV}($F_{20}TPP^{2-}$)(O)] intermediate. The characteristic Soret band for this intermediate appeared at 426 nm.[11f] Similarly, two other complexes [Mn^{IV}(TPP^{2-})(O)] and [Mn^{IV}($TMPyP^{2-}$)(O)] {$TMPyPH_2$ = 5,10,15,20-

tetrakis(4-methylpyridinium)porphyrin} are reported to show Soret band at 425 and 438 nm, respectively.[23] The shifts in the values may be because of differences in substitutions and solvents. Noteworthy that, UV-visible absorption pattern for [$Mn^{II}(TMPP^{2-})$] is different from the observed intermediate ruling out the possibility of probable reduction of Mn(III) to Mn(II) by O_2^{-}.[24]

Reaction of Mn(III)-porphyrinate with *tert*-butyl hydroperoxide (*t*BuOOH) gives [Mn(IV)=O].[25] Complex **13** was made to react with *t*BuOOH in THF and was monitored in UV-visible spectroscopy. The resulting reaction mixture showed shifting of Soret band to 433 nm which is due to the formation of [$Mn^{IV}(TMPP^{2-})(O)$] (Appendix III, Figure A3.12). This confirms that our assignment of the intermediate as [Mn(IV)=O] is appropriate.

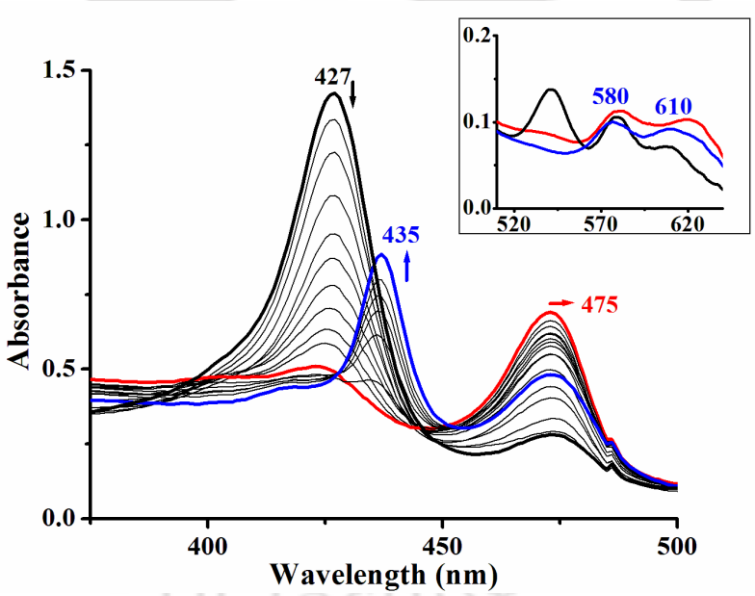

Figure 4.4. UV-visible spectral monitoring of the reaction of complex **14** (black) and KO_2 to give **14a** (red) and [Mn(IV)=O] (blue) in THF at −40 °C .

In X-band EPR spectroscopy, frozen reaction mixture of complex **14** and KO_2 in THF showed a peak at g = 2.05 which is supposedly because of a [Mn(IV)=O] species (Figure 4.5). In case of [$Mn^{IV}(F_{20}TPP^{2-})(O)$], similar EPR signal was reported.[26] The other proposed intermediate **14a** is an even electron species and therefore is not expected to show any signal

in X-band EPR.

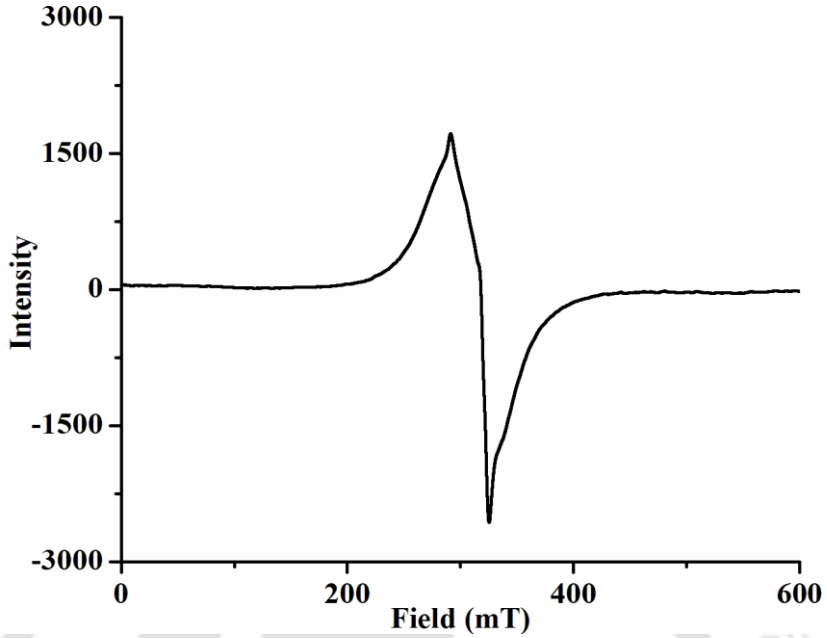

Figure 4.5. X-band EPR spectrum of reaction mixture of complex **14** and KO_2 in THF at 77K.

To further confirm the formation of [Mn(IV)=O], we introduced fluorene in the reaction mixture. Formation of 9-fluorenone as one of the products was confirmed by ESI-mass, ^{1}H- and ^{13}C-NMR (Appendix III, Figures A3.20-A3.22). It has been reported earlier that [Mn(IV)=O] complexes can take part in H-atom abstraction reaction from common organic substrates.[27] These results supports the presence of a metal oxo species somewhere in the course of the reaction. It is worth mentioning that KO_2 alone could not oxidize fluorene to 9-fluorenone.

Conversion of a [Mn(III)-PN] to Mn(III)-OH involves loss of one NO_2 molecule which must be present in the reaction vessel at the end. (2,2,6,6-tetramethylpiperdin-1-yl)oxyl (TEMPO) was previously used to detect the presence of with NO_2.[28] When TEMPO was introduced in the reaction of complex **14** and KO_2, 2,2,6,6-tetramethylpiperidin-1-yl nitrate ($tmpNO_3$) was isolated as one of the final product confirming the release of NO_2 in the reaction (Appendix III, Figure A3.23-A3.26).

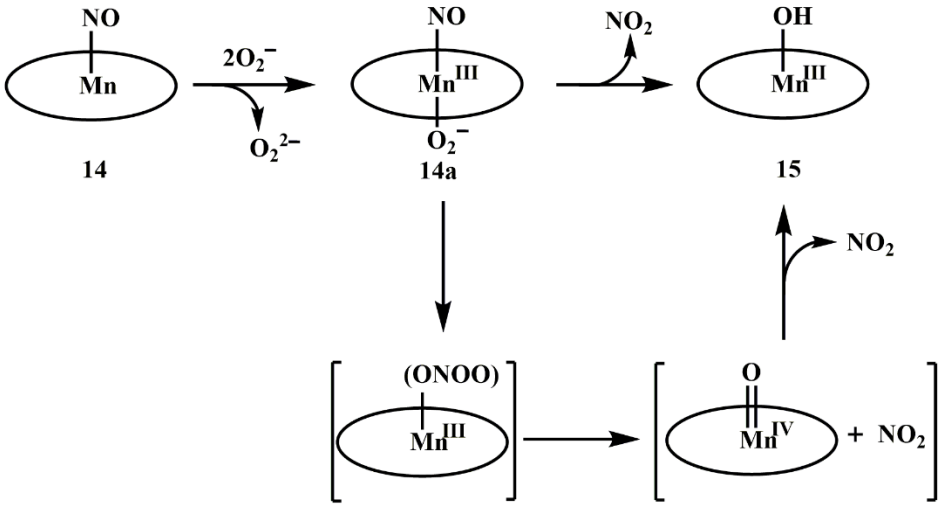

Scheme 4.3. Overall reaction mechanism.

In the mechanistic pathway of Mn-SOD the dismutation is proposed to occur *via* two consecutive redox steps involving the Mn^{III}/Mn^{II} redox couple (Scheme 4.4). A similar mechanism can be employed for the oxidation of complex **14** by O_2^- in the first step. However, subsequent reduction of Mn(III) by a second equivalent of O_2^- was not observed. Rather it interacted with the NO, which led to the formation of a putative PN species. In other words, SOD activity of a Mn-porphyrin complex, **14** was inhibited in presence of the bonded NO group. Noteworthy that, the standard reduction potentials for O_2/O_2^- and O_2^-/O_2^{2-} couples against NHE are −0.16 V and +0.94 V respectively.[29] In the cyclic voltammogram of complex **14**, an irreversible oxidation at +1.07 V against NHE (+0.88 V against Ag/AgCl) is assigned for the oxidation of Mn(II) to Mn(III). In terms of redox potential complex **14** is not expected to be reduced by O_2^-, which is indeed the case.

$$Mn^{II}\text{-SOD} + O_2^- \longrightarrow Mn^{III}\text{-SOD} + O_2^{2-}$$

$$Mn^{III}\text{-SOD} + O_2^- \longrightarrow Mn^{II}\text{-SOD} + O_2$$

Scheme 4.4. Mechanism Mn-SOD enzyme.

Radi *et al.* reported that interaction of PN with Mn-SOD leads to the nitration of a nearby tyrosine residue. Control experiments showed that the mechanism involved a [Mn(IV)=O] species and NO_2 generated from homolytic O−O cleavage of PN induced by manganese ion.[5a] In our case nitration reaction was observed when DTBP was present in the reaction mixture. Similar reactions was previously observed in case of [Mn($F_{20}TPP^{2-}$)(NO)] where O_2^- directly attacks the axial NO group without even interacting with the metal centre.[11f] But in this case O_2^- first binds to the manganese center then reacts with the NO group. It is logical to assume that either of the axial ligand dissociates from the metal center before the formation of the PN intermediate. In most cases the axial NO groups of Mn(III)-porphyrins are very labile and likely to be lost spontaneously.[18] Here also, the NO group presumably dissociates from the manganese center and consecutively reacts with the O_2^- to result in the PN intermediate.

4.3 Experimental Section

4.3.1 Materials and methods

All the reagents and chemicals were purchased from commercial sources and used without further purification. THF was distilled over sodium/benzophenone under N_2. Inert atmosphere was maintained while performing the reactions. UV-visible studies were done either at room temperature or at −40 ºC in an Agilent Cary 8454 spectrophotometer equipped with Unisoku cryostat USP- 203 B and thermostated cell holder using chemstation software. FT-IR spectra were taken as KBr pellets or in a KBr cell using a PerkinElmer Spectrum two spectrophotometer. ^1H and ^{13}C NMR spectra were recorded in 400 MHz Bruker AVANCE 400 and 500 MHz Bruker AVANCE NEO 500 FTNMR spectrophotometers. The chemical shifts were referenced either from an internal standard, i.e. tertramethylsilane or from a residual solvent peak. X-band EPR spectra were recorded on a JES-FA200 ESR

spectrophotometer with microwave power, 0.998 mW; microwave frequency, 9.14 GHz; modulation frequency, 100 KHz and modulation amplitude, 1. Elemental analyses were obtained from a Perkin Elmer Series II Analyzer. Cyclic voltammograms were recorded on CH instrument CHI660A machine with a glassy carbon working electrode, a platinum wire counter electrode, and an Ag/AgCl reference electrode. CH_2Cl_2 solutions of complexes containing 0.10 M $[(^nBu)_4N]ClO_4$ as supporting electrolyte, were used for the measurements. ESI-mass spectra were collected on an Waters, Q-TOF premier instrument.

Single crystals were grown from the respective CH_2Cl_2-hexane solutions. The intensity data were collected using a Bruker SMART APEX-II CCD diffractometer, equipped with a fine focus 1.75 kW sealed tube MoK_α radiation (λ = 0.71073 Å) at either 293 K or 100 K, with increasing ω (width of 0.3° per frame) at a scan speed of 3 s/frame. The SMART software was used for data acquisition. Data integration and reduction were undertaken with SAINT and XPREP software.[30] Structures were solved by direct methods using SHELXS-2016 and refined with full-matrix least squares on F^2 using SHELXL-2016/6.[31a] Structural illustrations have been drawn with ORTEP-3 for Windows.[31b]

4.3.2 Syntheses

Complex 13. The ligand $TMPPH_2$ (0.37 g, 0.5 mmol), $Mn(OAc)_2.4H_2O$ (0.61 g, 2.5 mmol) and NaCl (0.15 g, 2.5 mmol) were dissolved in $CHCl_3$ (25 mL) and acetic acid (25 mL) and the resulting mixture was refluxed overnight. The reaction mixture was cooled and washed with 100 mL of water and extracted with $CHCl_3$ (3 × 30 mL). The crude mass was subjected to neutral alumina column to get **13** as green solid. Yield: 0.33 g (*ca.* 80%). Elemental analyses for $C_{48}H_{36}N_4O_4MnCl$, Calcd. (%):C, 70.03; H, 4.41; N, 6.81, found (%): C, 70.05; H, 4.39; N, 6.80. FT-IR (in KBr): 1606, 1572, 1513, 1497, 1463, 1441, 1341, 1288, 1248, 1176, 1106, 1021, 1005, 808, and 603 cm^{-1}. UV-visible (CH_2Cl_2): 475 nm ($\varepsilon/M^{-1}cm^{-1}$, 1 × 10^5), 530 nm ($\varepsilon/M^{-1}cm^{-1}$, 0.82 ×

10^4), 583 nm (ε/$M^{-1}cm^{-1}$, 1.04 × 10^4) and 621 nm (ε/$M^{-1}cm^{-1}$, 1.43 × 10^4). ESI-mass (m/z): Calcd. 787.211, found: 787.243 for $[(TMPP^{2-})Mn]^+$.

Complex 14. Complex **13** (0.08 g, 0.1 mmol) was dissolved in dry and degassed CH_2Cl_2 and cooled to −20 °C. To this solution a freshly prepared hydroxylamine solution in methanol was added (2.5 eq). The color of the solution changed from green to red. Addition of excess dry and degassed methanol yielded purple color precipitate of complex **14** with *ca.* 80% yield (0.06 g). Elemental analyses for $C_{48}H_{36}N_5O_5Mn$, Calcd. (%):C, 70.50; H, 4.44; N, 8.56, found (%): C, 70.48; H, 4.45; N, 8.54. FT-IR (in KBr): ν_{NO}=1755 cm^{-1}, also 1605, 1534, 1511, 1499, 1463, 1439, 1343, 1286, 1247, 1176, 1000, 804 and 607 cm^{-1}. FT-IR (in THF): ν_{NO}=1739 cm^{-1}. FT-IR (in CH_2Cl_2): ν_{NO}=1734 cm^{-1}. UV-visible (CH_2Cl_2): 429 nm (ε/$M^{-1}cm^{-1}$, 1.81 × 10^5), 545 nm (ε/$M^{-1}cm^{-1}$, 1.70 × 10^4), 582 nm (ε/$M^{-1}cm^{-1}$, 1.04 × 10^4) and 618 nm (ε/$M^{-1}cm^{-1}$, 0.81 × 10^4). ^{1}H NMR (400 MHz, $CDCl_3$): δ_{ppm}, 8.67 (s, 8H), 8.07-8.06 (d, 4H), 7.96-7.95 (d, 4H), 7.33 (s, 8H), 4.03 (s, 12H). ESI-mass (m/z): Calcd. 787.211; found 787.253 for $[(TMPP^{2-})Mn]^+$ (M−NO).

4.3.3 Reaction of complex 14 with KO_2

Complex **14** (0.41 g, 0.5 mmol) was taken in 10 mL of dry and degassed THF and cooled to −20 ºC. Pre-cooled THF solution of KO_2 in 18 crown 6 (1.1 mmol) was then added and stirred for 2 h. The solution was warmed up to room temperature and dried under reduced pressure and subjected to column chromatography to get complex **15** (0.28 g, ~70% yield).

Complex 15. Elemental analyses for $C_{48}H_{37}N_4O_5Mn$, Calcd. (%):C, 71.64; H, 4.63; N, 6.96, found (%): C, 71.71; H, 4.61; N, 6.91. FT-IR (in KBr): 3431, 1606, 1513, 1497, 1461, 1440, 1342, 1289, 1249, 1175, 1005 and 804 cm^{-1}. UV-visible (THF): 470 nm (ε/$M^{-1}cm^{-1}$, 1.12 × 10^5), 530 nm (ε/ $M^{-1}cm^{-1}$, 1.15 × 10^4), 581 nm (ε/ $M^{-1}cm^{-1}$, 1.43 × 10^4) and 619 nm (ε/ $M^{-1}cm^{-1}$, 2.06 × 10^4). ESI-mass (m/z): Calcd: 787.211; found: 487.225 for $[(TMPP^{2-})Mn]^+$.

4.3.4 Reaction of complex 14 with KO_2 in presence of 2,4-di-*tert*-butylphenol

To a dry and degassed THF solution of complex **14** (0.82 g, 1 mmol), precooled 2,4-di-*tert*-butylphenol (1.03 g, 5 mmol) was added followed by pre-cooled THF solution of KO_2 in 18-crown-6 at −20 °C and stirred for 2 h at the same temperature. The reaction mixture was then brought to room temperature and dried in a rotavapor. Purification of the crude mass through column chromatography resulted in pure 2,4-di-*tert*-butyl-6-nitrophenol.

2,4-di-*tert*-butyl-6-nitrophenol. Yield: 0.15 g (~60%). Elemental analyses for $C_{14}H_{21}NO_3$, Calcd. (%): C, 66.91; H, 8.42; N, 5.57, found (%):C, 67.11; H, 8.45; N, 5.46. ^{1}H NMR (400 MHz, $CDCl_3$): δ_{ppm}, 11.45 (s, 1H), 7.95 (s, 1H), 7.65 (s, 1H), 1.45 (s, 9H), 1.32 (s, 9H). ^{13}C NMR (150 MHz, $CDCl_3$): δ_{ppm}, 152.0, 140.9, 138.9, 132.7, 131.6, 117.8, 34.7, 33.5, 30.1, 28.4. ESI-mass (m/z): Calcd: 251.15, found: 250.16 (M−1).

4.3.5 Reaction of complex 14 with KO_2 in presence of fluorene

Complex **14** (0.4 g, 0.5 mmol) and fluorene (0.33 g, 2 mmol) was dissolved in THF and cooled to −20 °C. Pre-cooled THF solution of KO_2 in 18-crown-6 was then added and stirred for 5 h at the same temperature. The reaction mixture was then brought to room temperature and solvent was removed *in vacuo*. The reaction mixture was extracted with 3×20 mL hexane which contained 9-fluorenone along with unreacted fluorene.

9-fluorenone. Yield: 27 mg (~30%). Elemental analyses for $C_{13}H_8O$, Calcd. (%):C, 86.65; H, 4.47, found (%): C, 86.77; H, 4.44. ^{1}H NMR (500 MHz, $CDCl_3$): δ_{ppm}, 7.67-7.65 (d, 2H), 7.53-7.47 (m, 4 H), 7.31-7.28 (t, 2H). ^{13}C NMR (126 MHz, $CDCl_3$): δ_{ppm}, 193.9, 144.5, 134.7, 134.2, 129.1, 124.3,120.3. ESI-mass (m/z): Calcd: 180.057, found: 181.101 (M+1).

4.3.6 Reaction of complex 2 with KO_2 in presence of TEMPO

To a dry and degassed THF solution of complex **14** (0.16 g, 0.2 mmol) at −20 °C, pre-cooled THF solution of KO_2 in 18 crown 6 was added followed by addition of TEMPO (0.16 g, 1

mmol in THF) and stirred for 1 h at the same temperature. The reaction mixture was then brought to room temperature allowed to stand overnight. Isolation and characterization of final products revealed formation of 2,2,6,6-tetramethylpiperidin-1-yl nitrate among others.

2,2,6,6-tetramethylpiperidin-1-yl nitrate, tmpNO$_3$. Yield: 10 mg (~25%). Elemental analyses for $C_9H_{18}N_2O_3$, Calcd. (%):C, 53.45; H, 8.97; N, 13.85, found (%): C, 53.37; H, 9.04; N, 13.78. ^{1}H NMR (500 MHz, $CDCl_3$): δ_{ppm}, 1.74 (s, 6H), 1.47 (s, 12H). ^{13}C NMR (126 MHz, $CDCl_3$): δ_{ppm}, 56.7, 34.8, 27.3, 16.1. ESI-mass (m/z): Calcd: 140.144, found: 140.164 for tmp^+.

4.4 Conclusion

In this work, interaction of the superoxide ion with a five coordinated nitrosyl complex of a manganese porphyrin was investigated. When two equivalents of superoxide was made to react with a $\{Mn(NO)\}^6$ complex [$Mn(TMPP^{2-})(NO)$], **14**, oxidation of the metal center followed by formation of a intermediate complex [$Mn^{III}(TMPP^{2-})(NO)(O_2^-)$], **14a** was postulated on the basis of FT-IR and UV-visible spectroscopic studies. In subsequent steps **14a** gives a putative Mn(III)-PN intermediate followed by its decomposition to a high-valent [Mn(IV)=O] species with the loss of NO_2. Existence of the [Mn(IV)=O] intermediate was detected in UV-visible as well as X-band EPR spectroscopy. Further evidence of this intermediate complex was obtained from the isolation of [Mn(III)-OH^-] as end product; and its oxo transfer activity towards organic substrate, e.g. fluorene. This reaction is interesting because of its contrast to the SOD activity shown by most of the manganese porphyrins. Unlike other manganese porphyrin complexes, reaction of O_2^- with a oxidized (porphyrinato)Mn(III)-nitrosyl does not lead to reduction of the metal centre with the release of O_2. Formation of a reactive intermediate **14a** followed by a [Mn(IV)=O] species and NO_2 is the more preferred pathway here.

4.5 References

1 (a) *Nitric Oxide: Biology and Pathobiology*; Ignarro, L. J.; Ed.; Academic Press: San Diego, **2000**. (b) *Nitric Oxide and Infection*; Fang, F. C.; Ed.; Kluwer Academic/ Plenum Publishers: New York, **1999**. (c) Bourassa, J. L.; Ives, E. P.; Marqueling, A. L.; Shimanovich, R.; Groves, J. T. *J. Am. Chem. Soc.* **2001**, *123*, 5142. (d) Richter-Addo, G. B.; Legzdins, P.; Burstyn, J. *Chem. Rev.* **2002**, *102*, 857. (e) Bogdan, C. *Nat. Immunol.* **2001**, *2*, 907. (f) Jia, L.; Bonaventura, C.; Bonaventura, J.; Stamler, J. S. *Nature* **1996**, *380*, 221. (g) Furchgott, R. F. *Angew. Chem. Int. Ed.* **1999**, *38*, 1870. (h) Ignarro, L. J. *Biosci. Rep.* **1999**, *19*, 51.

2 (a) Gross, S. S.; Wolin, M. S. *Annu. Rev. Physiol.* **1995**, *57*, 737. (b) Kissner, R.; Nauser, T.; Bugnon, P.; Lye, P. G.; Koppenol, W. H. *Chem. Res. Toxicol.* **1997**, *10*, 1285.

3 (a) Stadler, J.; Trockfeld, J.; Schmalix, W. A.; Brill, T.; Siewert, J. R.; Greim, H.; Doehmer J. *Proc. Natl. Acad. Sci. U.S.A.* **1994**, *91*, 3559. (b) Brown, G. C. *Eur. J. Biochem.* **1995**, *232*, 188. (c) Koppenol, W. H.; Kissner, R. *Chem. Res. Toxicol.* **1998**, *11*, 87. (d) Pacher, P.; Beckman, J. S.; Liaudet, L. *Physiol. Rev.* **2007**, *87*, 315. (e) Beckman, J. S.; Koppenol, W. H. *Am. J. Physiol.* **1996**, *271*, 1424. (f) Radi, R.; Cassina, A.; Hodara, R.; Quijano, C.; Castro, L. *Free Radical Biol. Med.* **2002**, *33*, 1451. (g) Vliet, A. V.; Eiserich, J. P.; Halliwell, B.; Cross, C. E. *J. Biol. Chem.* **1997**, *272*, 7617.

4 Miriyala, S.; Spasojevic, I.; Tovmasyan, A.; Salvemini, D.; Vujaskovic, Z.; St. Clair, D.; Batinic-Haberle, I. *Biochim. Biophys. Acta Mol. Basis. Dis.* **2012**, *1822*, 794.

5 (a) Quijano, C.; Hernandez-Saavedra, D.; Castro, L.; McCord, J. M.; Freeman, B. A.; Radi, R. *J. Biol. Chem.* **2001**, *276*, 11631. (b) Filipović, M. R.; Stanić, D.; Raičević, S.; Spasić, M.; Niketic, V. *Free Radic. Res.* **2007**, *41*, 62.

6 (a) Clarkson, S. G.; Basolo, F. *J. Chem. Soc. Chem. Commun.* **1972**, *11*, 670. (b) Clarkson, S. G.; Basolo, F. *Inorg. Chem*. **1973**, *12*, 1528.

7 (a) Park, G. Y.; Deepalatha, S.; Puiu, S. C.; Lee, D.-H.; Mondal, B.; Sarjeant, A. A. N.; del Rio, D.; Pau, M. Y. M.; Solomon, E. I.; Karlin, K. D. *J. Biol. Inorg. Chem.* **2009**, *14*, 1301. (b) Maiti, D.; Lee, D.-H.; Sarjeant, A. A. N.; Pau, M. Y. M.; Solomon, E. I.; Gaoutchenova, K.; Sundermeyer, J.; Karlin, K. D. *J. Am. Chem. Soc.* **2008**, *130*, 6700. (c) Schopfer, M. P.; Mondal, B.; Lee, D.-H.; Sarjeant, A. A. N.; Karlin, K. D. *J. Am. Chem. Soc.* **2009**, *131*, 11304. (d) Cao, R.; Elrod, L. T.; Lehane, R. L.; Kim, E.; Karlin, K. D. *J. Am. Chem. Soc.* **2016**, *138*, 16148.

8 (a) Kurtikyan, T. S.; Eksuzyan, S. R.; Hayrapetyan, V. A.; Martirosyan, G. G.; Hovhannisyan, G. S.; Goodwin, J. A. *J. Am. Chem. Soc.* **2012**, *134*, 13861. (b) Kurtikyan, T. S.; Eksuzyan, S. R.; Goodwin, J. A.; Hovhannisyan, G. S. *Inorg. Chem.* **2013**, *52*, 12046. (c) Yokoyama, A.; Han, J. E.; Cho, J.; Kubo, M.; Ogura, T.; Siegler, M.A.; Karlin, K.D.; Nam, W. *J. Am. Chem. Soc.* **2012**, *134*, 15269. (d) Yokoyama, A.; Cho, K.-B.; Karlin, K.D.; Nam, W. *J. Am. Chem. Soc.* **2013**, *135*, 14900. (e) Kumar, P.; Lee, Y. -M.; Park, Y. J.; Siegler, M. A.; Karlin, K. D.; Nam, W. *J. Am. Chem. Soc.* **2015**, *137*, 4284. (f) Kumar, P.; Lee, Y.-M.; Hu, L.; Chen, J.; Park, Y. J.; Yao, J.; Chen, H.; Karlin, K.D.; Nam, W. *J. Am. Chem. Soc.* **2016**, *138*, 7753.

9 Kurtikyan, T. S.; Hayrapetyan, V. A.; Hovhannisyan, A. A.; Martirosyan, G. G.; Hovhannisyan, G. S.; Iretskii, A. V.; Ford, P. C. *Inorg. Chem.* **2020**, *59*, 17224.

10 Yenuganti, M.; Das, S.; Kulbir; Ghosh, S.; Bhardwaj, P.; Pawar, S. S.; Sahoo, S. C.; Kumar, P. *Inorg. Chem. Front.* **2020**, *7*, 4872.

11 (a) Kalita, A.; Kumar, P.; Mondal, B. *Chem. Commun.* **2012**, *48*, 4636. (b) Saha, S.; Ghosh, S.; Gogoi, K.; Deka, H.; Mondal, B.; Mondal, B. *Inorg. Chem.* **2017**, *56*, 10932. (c) Saha, S.; Gogoi, K.; Mondal, B.; Ghosh, S.; Deka, H.; Mondal, B. *Inorg.*

Chem. **2017**, *56*, 7781. (d) Gogoi, K.; Saha, S.; Mondal, B.; Deka, H.; Ghosh, S.; Mondal, B. *Inorg. Chem.* **2017**, *56*, 14438. (e) Mondal, B.; Saha, S.; Borah, D.; Mazumdar, R.; Mondal, B. *Inorg. Chem.* **2019**, *58*, 1234. (f) Mondal, B.; Borah, D.; Mazumdar, R.; Mondal, B. *Inorg. Chem.* **2019**, *58*, 14701.

12 (a)Yadava, S.; Bharati, S. L. *J. Coord. Chem.* **2011**, *64*, 3950. (b) Tong, S. L.; Zhang, J.; Yan, Y.; Hu, S.; Yu, J.; Yu L. *Solid State Sci.* **2011**, *13*, 1320. (c) da Silva, V. S.; Vieira, W. C d. S.; Meireles, A. M.; Ucoski, G. M.; Nakagaki, S.; Idemoria, Y. M.; DeFreitas-Silva G. *New J. Chem.* **2017**, *41*, 997.

13 Galinato, M. J. I.; Brocious, E. P.; Paulat, F.; Martin, S.; Skodack, J.; Harland, J. B.; Lehnert, N. *Inorg. Chem.* **2020**, *59*, 2144.

14 Choi, In-K.; Liu, Y.; Wei, Z.; Ryan, M. D. *Inorg. Chem.* **1997,** *36*, 3113.

15 Zavarine, I. S.; Kini, A. D.; Morimoto, B. H.; Kubiak, C. P. *J. Phys. Chem. B* 1998, *102*, 7287.

16 Zahran, Z. N.; Lee, J.; Alguindigue, S. S.; Khan, M. A.; Richter-Addo G. B. *Dalton Trans*. **2004**, *2004*, 44.

17 Kelly, S.; Lancon, D.; Kadish, K. M. *Inorg. Chem.* **1984**, *23*, 1451.

18 Zahran, Z. N.; Shaw, M. J.; Khan, M. A.; Richter-Addo, G. B. *Inorg. Chem.* **2006**, *45*, 2661.

19 Kini, A. D.; Washington, J.; Kubiak, C. P.; Morimoto B. H. *Inorg. Chem.* **1996,** *35*, 6904.

20 (a) Liu, L.-L.; Li, H.-X.; Wan, L.-M.; Ren, Z.-G.; Wanga, H.-F.; Lang, J.-P. *Chem. Commun.* **2011**, *47*, 11146. (b) Lin, Y.-H.; Kutin, Y.; van Gastel, M.; Bill, E.; Schnegg, A.; Ye, S.; Lee, W.-Z. *J. Am. Chem. Soc.* **2020**, *142*, 10255. (c) Lin, Y-H.; Cramer, H. H.; van Gastel, M.; Tsai, Y.-H.; Chu, C.-Y.; Kuo, T.-S.; Lee, I.-R.; Ye, S.; Bill, E.; Lee, W.-Z. *Inorg. Chem.* **2019**, *58*, 9756. (d) Kim, H.; Rogler, P. J.;

Sharma, S. K.; Schaefer, A. W.; Solomon, E. I.; Karlin, K. D. *J. Am. Chem. Soc.* **2020**, *142*, 3104. (e) Cheung, S. K.; Grimes, C. J.; Wong, J.; Reed, C. A. *J. Am. Chem. Soc.* **1976**, *98*, 5028. (f) Collman, J. P.; Brauman, J. I.; Halbert, T. R.; Suslick, K. S. *Proc. Natl. Acad. Sci. U.S.A.* **1976**, *73*, 3333. (g) Kozuka, M.; Nakamoto, K. *J. Am. Chem. Soc.* **1981**, *103*, 2162.

21 Blunt, F. J.; Hendra, P. J.; Mackenzie, J. R. *J. Chem. Soc. D* **1969**, *1969*, 278.

22 Thyagarajan, S.; Incarvito, C. D.; Rheingold, A. L.; Theopold, K.H. *Inorg. Chim. Acta* **2003**, *345*, 333.

23 Zhang, R.; Horner, J. H.; Newcomb, M. *J. Am. Chem. Soc.* **2005**, *127*, 6573.

24 Jones, R. D.; Summerville, D. A.; Basolo F. *J. Am. Chem. Soc.* **1978**, *100*, 4416.

25 Nam, W.; Kim, I.; Lim, M. H.; Choi, H. J.; Lee, J. S.; Jang, H. G. *Chem. Eur. J.* **2002**, *8*, 2067.

26 Schappacher, M.; Weiss R. *Inorg. Chem.* **1987**, *26*, 1189.

27 Garcia-Bosch, I.; Company, A.; Cady, C. W.; Styring, S.; Browne, W. R.; Ribas, X.; Costas, M. *Angew. Chem. Int. Ed.* **2011**, *50*, 5648.

28 Zhang, Z.-Q.; Chen, T.; Zhang F.-M. *Org. Lett.* **2017**, *19*, 1124.

29 Krumova, K.; Cosa, G.; *Singlet Oxygen: Applications in Biosciences and Nanosciences*; Nonell, S.; Flors, C.; Eds.; The Royal Society of Chemistry: Cambridge, UK, **2016**, 1.

30 SMART, SAINT and XPREP, Siemens Analytical X-ray Instruments Inc., Madison, Wisconsin, USA, **1995**.

31 (a) Sheldrick, G. M. SHELXS-2014, University of Gottingen, Germany. (b) Farrugia, L. J. *J. Appl. Crystallogr.* **1997**, *30*, 565.

Chapter 5

Can a nitrosyl complex of Mn(II)-porphyrin release nitroxyl/HNO?

Abstract

In general, the nitrosyl complexes of Mn(II)-porphyrinate having $\{Mn(NO)\}^6$ configuration are not considered as HNO or nitroxyl (NO^-) donors because of $[Mn^I\text{-}NO^+]$ nature. A nitrosyl complex of Mn(II)-porphyrin, $[Mn(TMPP^{2-})(NO)]$, **14** [$TMPPH_2$ = 5,10,15,20-*tetrakis*(4-methoxyphenyl)porphyrin] is shown to release HNO in the presence of HBF_4. It is evidenced from the characteristic reaction of HNO with triphenylphosphine and isolation of the $[Mn^{III}(TMPP^{2-})(H_2O)_2](BF_4)$, **16**. This is attributed to the fact that H^+ from HBF_4 polarizes the NO group whereas the BF_4^- interacts with metal ion to stabilize the Mn(III) form. These two effects cooperatively result in the release of HNO from complex **14**. In addition, complex **14** behaves as a nitroxyl (NO^-) donor in the presence of $[Fe^{III}(dtc)_3]$ (dtc = diethyldithiocarbamate) and $[Fe^{III}(TPP^{2-})(Cl)]$ ($TPPH_2$ = 5,10,15,20-tetraphenylporphyrin) to result in $[Fe(dtc)_2(NO)]$ and $[Fe(TPP^{2-})(NO)]$, respectively.

5.1 Introduction

The interest in HNO chemistry has increased considerably due to its chemical properties and biological relevance.[1,2] Over the decade, a great advancement has been made towards direct methods of detection and quantification of HNO.[1-8] However, the examples of HNO donors still remain restricted to only a few such as Angeli's Salt, Piloty's acid or acyl and acyloxy nitroso derivatives.[9] The metal bound nitrosyl complexes with suitable electronic configuration could be an efficient HNO donor. It has been found that though the direct reduction of NO to HNO is less viable, the intramolecular reduction of NO while coordinated to a metal center would be a preferable one. The coordination of NO to a transition metal ion in combination with a proton coupled electron transfer agent (HX) would considerably facilitate the HNO formation. Thus, $\{MNO\}^8$ complexes, being electron rich in nature, are potential candidates to be considered as HNO donor and the HNO releasing ability of those complexes can be modulated by the presence of electron donating groups in ligand. In this direction, Harrop and co-workers reported the examples of $\{Co(NO)\}^8$ complexes and their $\{Co(NO)\}^9$ analogues.[10] $\{MNO\}^7$ complexes, for example, the high spin Fe(II)-NO complexes, are having M-NO bond with very high degree of covalency and thus stable.[11] Addition of an electron *via* chemical or electrochemical reduction of these complexes results into a $\{MNO\}^8$ species and then only they may behave as a HNO donor.[12] On the other hand, examples of heme $\{Fe(NO)\}^7$ systems, without being reduced, are known to release HNO in the presence of appropriate sixth ligand. This sixth ligand actually can induce an inner-sphere electron transfer to stabilize the Fe^{III}-NO^- form which in the presence of H^+ generates HNO.[13] Ford's group reports that $[Fe^{II}(TPPS^{2-})(NO)]$ [$TPPSH_2$ = *meso-tetrakis*(4-sulfonatophenyl)porphyrin] in slightly acidic medium and in the presence of *tris*(3-sulfonatophenyl)phosphine as reductant forms HNO. However, the rate of the reaction is reported to be slow.[13b] In

$\{MNO\}^6$ complexes, the NO has typically a nitrosonium character and the Mn-NO bonds are shown to be quite strong, hence they normally cannot be considered as direct HNO donor.[14a] However, one electron or two electron reduction to $\{MNO\}^7$ or $\{MNO\}^8$ systems may result into a HNO donor.[14b] Interestingly, the five-coordinated nitrosyl complex Mn(II)-tropocoronand, [Mn(THF)(TC-5,5)], has been reported to have characteristics of high spin Mn^{III}-NO^- configuration.[15] However, the electron releasing character of TC-5,5 ligand actually favours the nitroxyl character of the coordinated nitrosyl, [Mn(NO)(TC-5,5)] does not release HNO, but reacts with excess NO to result in N_2O and O_2.[15] On the other hand, in case of Mn(II)-porphyrin complexes, the nitrosyls are in general low-spin and having a Mn^{I}-NO^+ configuration.[15,16] In fact, that is why the example of nitrosyl complex of Mn-porphyrin releasing HNO is not known. We report herein a nitrosyl complex of Mn(II)-porphyrin, **14**, which in presence of HBF_4 shows HNO releasing ability. In addition, the complex **14** displays NO^- transfer to $[Fe^{III}(dtc)_3]$ and $[Fe^{III}(TPP^{2-})(Cl)]$ complexes. These examples clearly demonstrate the utilization of nitrosyl complex of Mn(II)-porphyrin as nitroxyl donor.

5.2 Results and Discussion

The Spectroscopic studies suggest $[Mn^{I}$-$NO^+]$ as the formal assignment for complex **14**. As a consequence, the complex **14** is not expected to behave as HNO donor. However, Kubiak *et al.* reported that complex **14** can transfer NO group to $[Co^{II}(TPP^{2-})]$ in THF.[17] The reaction of NO transfer to $[Co^{II}(TMPP^{2-})]$, **6** from complex **14** has been observed in CH_2Cl_2. The reaction was monitored using FT-IR spectrum, and the nitrosyl stretching of complex **14** diminishes with a concomitant growth of new band at 1696 cm^{-1} characteristic of $[Co(TMPP^{2-})(NO)]$, **8** along with the formation of $[Mn^{II}(TMPP^{2-})]$ (Appendix IV, Figure A4.1) (Eq. 5.1).

Kubiak *et al.* attributed the NO transfer between complex **14** and [$Co^{II}(TPP^{2-})$] to the denitrosylation of complex **14** and very fast recombination of NO with [$Co^{II}(TPP^{2-})$] in THF. However, in the present case, complex **14** was found to be stable in degassed CH_2Cl_2 solution for more than 12 h. As no observable change in the FT-IR spectrum of the CH_2Cl_2 solution of complex **14** was found during this period, the denitrosylation of complex **14** in CH_2Cl_2 may be ruled out.

$$[Mn(TMPP^{2-})(NO)] + [Co(TMPP^{2-})] \longrightarrow [Mn(TMPP^{2-})] + [Co(TMPP^{2-})(NO)]$$

----- (Eq. 5.1)

Addition of one mole equivalent of HBF_4 as H^+ donor, results in the shift of Soret band from 429 nm to 452 nm through a transient intermediate band at 475 nm (Figure 5.1). It has been reported earlier that the Soret band of Mn(III)-porphyrin complexes appear in the range of ~475 nm.[18] Thus, it is logical to assume that addition of HBF_4 leads to the formation of a Mn(III) intermediate which results into the final compound having absorption at 452 nm (Scheme 5.1).

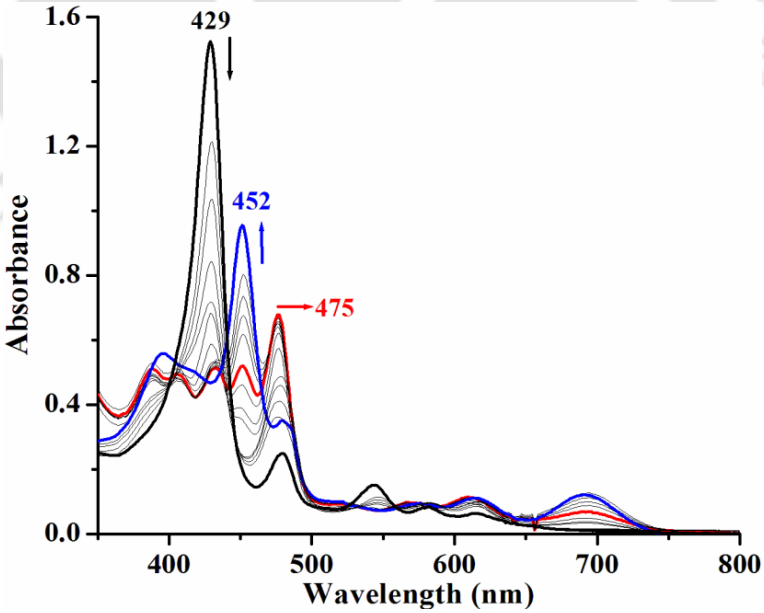

Figure 5.1. UV-visible spectral monitoring of the reaction of complex **14** (black) and after addition of HBF_4 (red) and final product [$Mn^{III}(TMPP^{2-})(H_2O)_2$]($BF_4$), **16** (blue) in CH_2Cl_2 at −40 °C.

X-band EPR study of the frozen reaction mixture reveals the presence of Mn(III) species (Appendix IV, Figure A4.2). In FT-IR spectrum, the addition of HBF_4 results in the disappearance of the 1734 cm^{-1} stretching frequency (Appendix IV, Figure A4.3). However, no spectrum corresponding to an intermediate was observed. This is perhaps because of the fact that the FT-IR was recorded at room temperature and the intermediate is thermally unstable. Isolation and characterization of the product reveals the formation of complex **16**, $[Mn^{III}(TMPP^{2-})(H_2O)_2](BF_4)$. From equation 5.2, it is expected to get $[Mn^{III}(TMPP^{2-})](BF_4)$ instead of complex **16**. However, the self-reaction of HNO produces water (*vide infra*) which leads to the formation of complex **16** during crystallization. Single crystal structure determination supports the formulation. The perspective ORTEP view is shown in figure 5.2. The crystal structure has some intrinsic disorder which has not been corrected even after growing the crystals in several batches. In the reaction the formation of HNO is suggested (Eq. 5.2).

$$[Mn^{II}(TMPP^{2-})(NO)] + HBF_4 \longrightarrow [Mn^{III}(TMPP^{2-})](BF_4) + HNO$$

----- (Eq. 5.2)

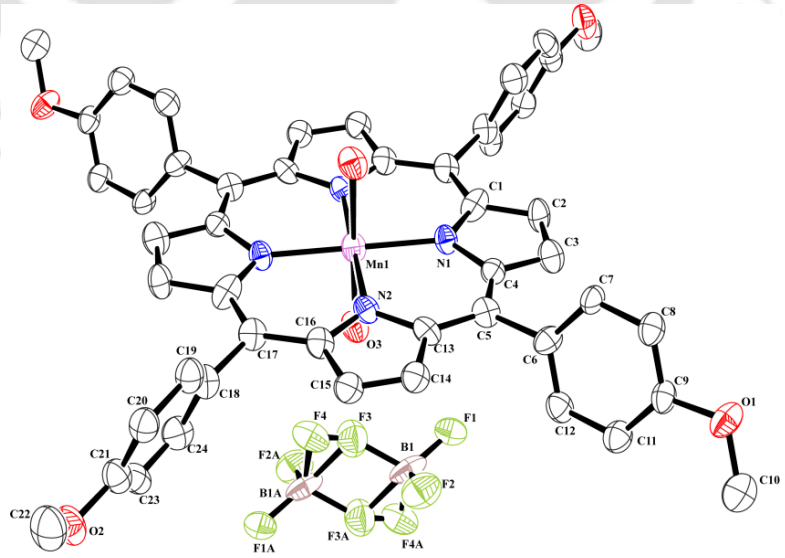

Figure 5.2. ORTEP diagram of complex **16** (30% thermal ellipsoid plot, H-atoms are omitted for clarity).

It has been confirmed by its characteristic reaction with phosphine.[19] HNO is known to undergo very fast self-reaction (K_{dim} = 8 ×10^6 $M^{-1}s^{-1}$) (Eq. 5.3) leading to the formation of N_2O and water.[20]

$$2HNO \longrightarrow N_2O + H_2O \quad \text{----- (Eq. 5.3)}$$

Thus, the presence of N_2O in the reaction vessel serves as an indirect evidence of formation of HNO in the reaction. The headspace gas analysis from the reaction vessel using GC-MS suggests the presence of N_2O (Experimental Section and Appendix IV, Figure A4.5). The yield of the produced N_2O was quantified using GC from a calibration curve with N_2O produced from Piloty's Acid and was found to be *ca.* 60%.

Mn(III)-porphyrin complexes are known to act as HNO/NO sponge. It has been reported earlier that Mn(III)-porphyrins react with HNO in a fast and efficient manner to form $\{Mn(NO)\}^6$ complex.[20b] However, in the present case no reaction between Mn(III)-porphyrin complex, $[Mn^{III}(TMPP^{2-})](BF_4)$ and HNO was evidenced as HNO rapidly converts into N_2O (Eq. 5.3).

It is reported that triarylphosphine (R_3P) reacts selectively with HNO donors to result in the corresponding phosphine oxide (R_3P=O) and aza-ylide (R_3P=NH). This reaction is often used as marker of HNO donation.[21a]

Addition of H^+ (HBF_4) (1 mole equivalent) to the mixture of complex **14** and Ph_3P resulted in an immediate change of colour of the solution. ^{31}P NMR studies of the reaction mixture suggested the presence of Ph_3P=O (δ, 26 ppm), Ph_3P=NH (δ, 21.4 ppm) along with unreacted Ph_3P (δ, −6.4 ppm) (Appendix IV, Figure A4.9). The signal at δ, 43.5 ppm is attributed to Mn(III)-bound PPh_3.[21b] When the Mn(III)-porphyrin complex is made to react with PPh_3 and HBF_4, the signal δ, 43.5 ppm along with that for free PPh_3 was observed. In this reaction, the appearance of the O=PPh_3 signal is attributed to the areal oxidation of

PPh_3 in the presence of HBF_4 (Appendix IV, Figure A4.10). It is worth mentioning here that the complex **14** was found to be not reactive towards Ph_3P. Thus, this result supports the formation of HNO upon addition of H^+ (HBF_4) to complex **14**.

Further, the nitroxyl releasing ability of complex **14** was evidenced through its reaction with $[Fe^{III}(dtc)_3]$. $[Fe^{III}(dtc)_3]$ is well-known nitroxyl (NO^-)/HNO acceptor.[22] Addition of stoichiometric amount of $[Fe^{III}(dtc)_3]$ to the CH_2Cl_2 solution of complex **14** resulted in the formation of $[Fe(dtc)_2(NO)]$ and $[Mn^{III}(TMPP^{2-})]^+$ (Eq. 5.4).

$$[Mn^{II}(TMPP^{2-})(NO)] + [Fe^{III}(dtc)_3] \longrightarrow [Mn^{III}(TMPP^{2-})](dtc^-) + [Fe(dtc)_2(NO)]$$

----- (Eq. 5.4)

The reaction was monitored using UV-visible, FT-IR and X-band EPR spectroscopic studies. In the UV- visible spectrum, upon addition of 1 equivalent of $[Fe^{III}(dtc)_3]$ into the CH_2Cl_2 solution of complex **14**, the intensity of 429 nm band decreases gradually with a concomitant increase of the intensity of a band at 480 nm. This is attributed to the formation of $[Mn^{III}(TMPP^{2-})]^+$ complex (Figure 5.3).

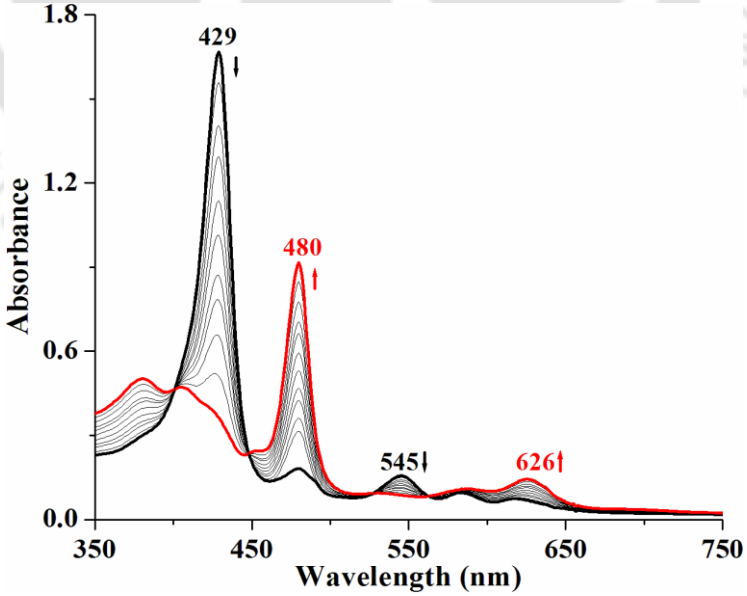

Figure 5.3. UV-visible spectral monitoring of the reaction of complex **14** (black) and $[Fe(dtc)_3]$ to give $[Fe(dtc)_2(NO)]$ and $[Mn(TMPP^{2-})](dtc)$ (red) in CH_2Cl_2 at room temperature.

In FT-IR spectral monitoring, the nitrosyl stretching of complex **14** appears at 1734 cm^{-1} in CH_2Cl_2 solution. It was found to diminish upon addition of $[Fe^{III}(dtc)_3]$ with a simultaneous appearance of a new stretching band at 1708 cm^{-1} (Figure 5.4). In solid state, this band appears at 1690 cm^{-1}. This band is assigned to the nitrosyl frequency of $[Fe(dtc)_2(NO)]$ (Appendix IV).[23] It has been confirmed using a separately prepared authentic sample (Appendix IV).

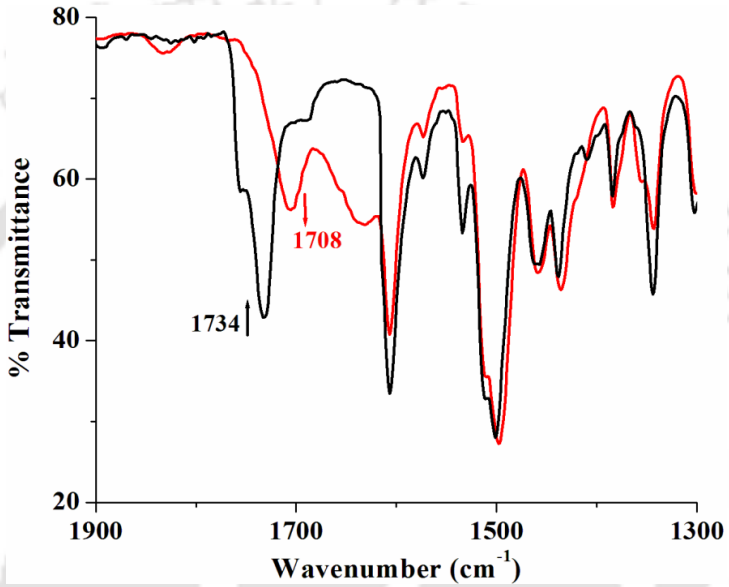

Figure 5.4. FT-IR spectral monitoring of the reaction of complex **14** (black) and $[Fe(dtc)_3]$ to give $[Fe(dtc)_2(NO)]$ (red) in CH_2Cl_2.

Additional evidence of formation of $[Fe(dtc)_2(NO)]$ came from the X-band EPR studies of the reaction mixture. The complex **14** was EPR silent owing to its low-spin $\{Mn(NO)\}^6$ configuration. Addition of $[Fe^{III}(dtc)_3]$ in CH_2Cl_2 solution of complex **14** at 77 K resulted in the appearance of a sharp signal at g, 2.05. The same signal was found to be splitted in DMSO solution as expected (Appendix IV, Figure A4.17).[22] Further, the ESI-Mass spectrum of the reaction mixture shows peak at m/z, 351.976 which matches with the $[Fe(dtc)_2]$ unit formed by the loss of axial NO group (Appendix IV, Figure A4.19). The simulated isotropic distribution pattern matches well with observed one. Thus, all these results strongly suggest the NO^- transfer from complex **14** to $[Fe^{III}(dtc)_3]$. It is to be noted

that this reaction was not observed with $[Fe^{II}(dtc)_2]$, as expected.

It is evident that complex **14** behaves differently in the presence of the H^+ (HBF_4) or $[Fe^{III}(dtc)_3]$ compared to that in the presence of $[Co^{II}(TMPP^{2-})]$. As mentioned earlier, in case of NO ligand transfer reaction from complex **14** to $[Co^{II}(TMPP^{2-})]$, the existence of $[Mn^{II}(TMPP^{2-})]$ and NO in equilibrium is responsible.[17]. On the other hand, it produces HNO in the presence of HBF_4 and donates nitroxyl (NO^-) in the presence of $[Fe^{III}(dtc)_3]$. The redox potential for the corresponding Mn^{III}/Mn^{II} couple rules out the possibility of initial electron transfer from complex **14** to reduce $[Fe^{III}(dtc)_3]$ followed by NO transfer (Appendix IV).[19] It is worth mentioning here that in nitrosyl complexes of Mn(II)-porphyrinates, the oxidation is less favourable as it leads to the formation of a 15-electron system from a 16-electron one and it involves the π-bonding effects.[24]

In addition, the redox potential of the Mn^{III}/Mn^{II} couple suggests that the direct reduction of the NO group by the Mn(II) moiety through an outer-sphere mechanism is also not feasible. However, an inner-sphere electron transfer from the metal ion to the coordinated NO group in the presence of electron rich ligand (as sixth ligand) will consequently increase the electron density on the central metal ion which, in turn, stabilizes Mn(III) form of the complex and contributes to the HNO/NO^- donation.[25] In case of HBF_4, it acts as the H^+ source to polarize the NO group as well as the BF_4^- donates electron density to the metal center to get stabilized in Mn(III) form (Scheme 5.1).

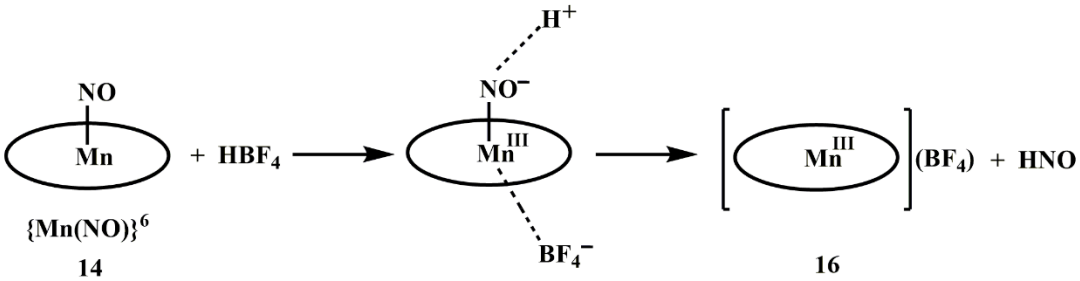

Scheme 5.1. Plausible reaction mechanism.

Indeed, the UV-visible and X-band EPR studies also indicate the formation of the Mn(III) intermediate species after addition of HBF_4. As mentioned above, the thermal instability precludes the characterization of the intermediate using FT-IR spectroscopy.

On the other hand, $[Fe^{III}(dtc)_3]$ is known to equilibrate between $[Fe^{III}(dtc)_2]^+$ and dtc^- in solution. dtc^- unit provides the extra electron density to stabilize the corresponding Mn(III) form of the complex whereas the positively charged $[Fe(dtc)_2]^+$ helps in polarizing the coordinated NO group and the cooperative effect of these two results in NO^- release from complex **14**.

Further, one common yet sensitive test for the HNO/NO^- involves the reaction with Fe(III)-porphyrins to results in the coreesponding $\{Fe(NO)\}^7$ complexes.[19a] It has been reported that $[Fe^{III}(TPP^{2-})(Cl)]$ can act as trapping agent for NO^- to result in $[Fe^{II}(TPP^{2-})(NO)]$.[19] When the reaction between complex **14** and stoichiometric amount of HBF_4 was carried out in the presence of $[Fe^{III}(TPP^{2-})(Cl)]$ in a degassed CH_2Cl_2 solution, a new stretching frequency at 1698 cm^{-1} corresponding to $\{Fe(NO)\}^7$ appeared with concomitant diminishing of NO stretching frequency for complex **14** at 1755 cm^{-1} (Experimental Section; Appendix IV, Figure A4.30). The yield of the product from this reaction was *ca.* 66%. This observation is also in accord with the conclusion that NO^- transfer takes place from complex **14** in the presence of stoichiometric amount of HBF_4. The possibility of formation of $[Fe(TPP^{2-})(NO)]$ through reduction of $[Fe(TPP^{2-})(Cl)]$ by complex **14** resulting into a $\{Mn(NO)\}^5$ derivative that will release NO to the $[Fe^{II}(TPP^{2-})]$ can be ruled out on the basis of redox potentials (Appendix IV).[19]

The existence of alternate mechanism involving the dissociation of NO from complex **14** in the first step leaving $[Mn^{II}(TMPP^{2-})]$ has been ruled out as (i) no change in the UV-visible spectrum of only complex **14** was observed even after 12 h time (Appendix IV,

Figure A4.31); (ii) addition of HBF_4 leads to the shift of absorption maxima to 475 nm which corresponds to an unstable intermediate and this is characteristics to the Mn(III)-porphyrin complexes.[18] If NO would have been released, that could lead to the corresponding Mn(II)-porphyrin complex coordinated to BF_4^- and the five coordinated Mn(II)-porphyrin complexes are known to show Soret band in the range of 435-450 nm.[26]

5.3 Experimental Section

5.3.1 Materials and Methods

All the reagents were purchased from commercial sources and used as it is without further purification unless specified. CH_2Cl_2 was passed through an alumina column, stored over calcium hydride overnight followed by distillation under N_2. Tetrafluoroboric acid was dried over 4A molecular sieve under Ar. All the reactions were performed under inert atmosphere except mentioned differently. Deoxygenation of solvents and solutions were effected by consecutive vacuum/Ar purge cycles. UV-visible spectra were taken on an Agilent Cary 8454 spectrophotometer. FT-IR spectra were recorded as KBr pellets or in a KBr cell using a PerkinElmer spectrophotometer. ^1H, ^{13}C and ^{31}P NMR studies were done in 400 MHz and 500 MHz Varian FTNMR spectrophotometers. X-band EPR spectra were recorded on a JES-FA200 ESR spectrophotometer with microwave power, 0.998 mW; microwave frequency, 9.14 GHz; and modulation amplitude, 2. Cyclic voltammograms were recorded on CH instrument CHI660A machine with a platinum wire working electrode, a glassy carbon counter electrode, and an Ag/AgCl reference electrode. CH_2Cl_2 solutions of complexes containing 0.10 M $[(^nBu)_4N]ClO_4$ as supporting electrolyte, were used for the measurements. Gas chromatograms were obtained on an Agilent 8860 GC analyzer.

Single crystals were grown from respective chloroform solutions using slow evaporation

technique. The intensity data were collected using a Bruker SMART APEX-II CCD diffractometer, equipped with a fine focus 1.75 kW sealed tube Mo Kα radiation (λ = 0.71073 Å), with increasing ω (width of 0.3° per frame) at a scan speed of 3 s/frame. The SMART software was used for data acquisition. Data integration and reduction were undertaken with SAINT and XPREP software.[27] Multi-scan empirical absorption corrections were employed to the data using the program SADABS. Structures were solved by direct methods using SHELXS-2016 and refined with full-matrix least-squares on F^2 using SHELXL-2016/6.[28a] Structural illustrations were drawn with ORTEP-3 for Windows.[28b]

5.3.2. Syntheses

[$Fe^{III}(dtc)_3$], (dtc = diethyldithiocarbamate). $FeCl_3.6H_2O$ (1 mmol, 0.27 g) was dissolved in 10 mL methanol. A solution of sodium diethyldithiocarbamate trihydrate (3 mmol, ~0.68 g) in 20 mL methanol was added slowly. The reaction mixture was stirred for 2 h and solvent was removed *in vacuo*. The crude product was recrystallized from boiling toluene as dark brown needles of **[$Fe^{III}(dtc)_3$]**. Yield: 0.4 g (*ca.* 80%). Elemental analyses for $C_{15}H_{30}N_3S_6Fe$, Calcd. (%): C, 35.99; H, 6.04; N, 8.39, found (%): C, 36.01; H, 6.03; N, 8.35. UV-visible (CH_2Cl_2): 345 nm (ε/$M^{-1}cm^{-1}$, 1.42 × 10^4), 387 nm (ε/$M^{-1}cm^{-1}$, 1.16 × 10^4), 510 nm (ε/$M^{-1}cm^{-1}$, 3.50 × 10^3) and 590 nm (ε/$M^{-1}cm^{-1}$, 2.85 × 10^3). FT-IR (in KBr): 1493, 1458, 1450, 1432, 1374, 1353, 1296, 1269, 1208, 1145, 1134, 1074, 993, 912, 845 and 783 cm^{-1}. ESI-mass (m/z): Calcd: 500.011, found: 499.971 (molecular ion peak).

[$Fe^{III}(TPP^{2-})(Cl)$], ($TPPH_2$ = 5,10,15,20-tetraphenylporphyrin). $FeCl_3.6H_2O$ (5mmol, 1.35 g) and $TPPH_2$ (0.5 mmol, 0.31 g) were dissolved in 20 mL DMF and refluxed for 4 hours. The reaction mixture was cooled to room temperature and water was added to obtain precipitate of the crude solid. This precipitate was then isolated and subjected to

column chromatography to get purple solid of **[Fe^{III}(TPP^{2-})(Cl)]**. Yield: 0.18 g (*ca.* 50%). Elemental analyses for $C_{44}H_{28}N_4ClFe$, Calcd. (%):C, 75.07; H, 4.01; N, 7.96, found (%): C, 75.01; H, 4.03; N, 7.95. UV-visible (CH_2Cl_2): 416 nm ($\varepsilon/M^{-1}cm^{-1}$, 1.33×10^5), 508 nm ($\varepsilon/M^{-1}cm^{-1}$, 1.32×10^4), 572 nm ($\varepsilon/M^{-1}cm^{-1}$, 5.28×10^3) and 690 nm ($\varepsilon/M^{-1}cm^{-1}$, 1.90×10^3). FT-IR (in KBr): 1596, 1485, 1440, 1339, 1200, 1174, 1070, 1002, 995, 805, 750 and 702 cm^{-1}.

5.3.3. Reaction of complex 14 with complex 6

Complex **14** (0.1 mmol, 0.08 g) was taken in a Schlenk flask and made air free *via* several vacuum/Ar purge cycles. A dry and degassed solution of complex **6** (0.1 mmol, 0.08 g) in 5 mL dichloromethane was added to it and stirred vigorously. Reaction was continued until complete disappearance of nitrosyl stretching of **14** in FT-IR spectroscopy.

5.3.4. Reaction of complex 14 with HBF_4

Complex **14** (0.05 mmol, 0.04 g) was dissolved in 5 mL of dry and degassed dichloromethane. 8 μL of tetrafluoroboric acid diethyl ether complex was added to this solution. The reaction mixture was allowed to stand for several hours to get dark green crystalline precipitate of complex **16**. Elemental analyses for $C_{48}H_{40}N_4O_6BF_4Mn$, Calcd. (%):C, 63.31; H, 4.43; N, 6.15, found (%): C, 63.28; H, 4.45; N, 6.14. FT-IR (in KBr): 1604, 1511, 1496, 1462, 1342, 1292, 1250, 1176, 1083, 1035, 1006, 805, 604 and 534 cm^{-1}. UV-visible (CH_2Cl_2): 452 nm ($\varepsilon/M^{-1}cm^{-1}$, 0.90×10^5), 575 nm ($\varepsilon/M^{-1}cm^{-1}$, 0.78×10^4), 613 nm ($\varepsilon/M^{-1}cm^{-1}$, 1.01×10^4) and 690 nm ($\varepsilon/M^{-1}cm^{-1}$, 1.47×10^4). ESI-mass (m/z): Calcd: 787.211, found: 787.181 for $[Mn(TMPP^{2-})]^+$.

5.3.5. Determination of yield of N_2O

Different amounts of N-hydroxybenzenesulfonamide were taken in four 25 mL round bottom flask and degassed with vacuum/Ar purge. Each flask was then treated with 10 mL

0.1 M NaOH solution under sealed condition. At the end of the reaction 1mL of headspace gas was subjected to GC. From there, a calibration curve between concentration of N-hydroxybenzenesulfonamide and peak intensity at 0.78 min (corresponding to N_2O) was generated (Appendix IV, Figure A4.32).

Complex **14** (0.2 mmol, 0.16 g) dissolved in 10 mL dry and degassed CH_2Cl_2 was taken in a 25 mL round bottom flask and 32 μL of $HBF_4.Et_2O$ was added to it under anaerobic condition. After the completion of the reaction 1 mL of headspace gas was subjected to GC and amount of N_2O was measured from the calibration curve. Yield. ~60%.

5.3.6. Reaction of complex 14 with HBF_4 in presence of triphenylphosphine

A mixture of Complex **14** (0.025 mmol, 0.02 g) and PPh_3 (0.062 mmol, 0.016 g) was dissolved in 0.2 mL of dry and degassed CH_2Cl_2 under anaerobic conditions. 4 μL of tetrafluoroboric acid diethyl ether complex was added to this solution and ^{31}P NMR of the reaction mixture was recorded in CD_3CN. ^{31}P NMR (202 MHz, CD_3CN): δ_{ppm}, 43.5, 26.0 ($Ph_3P=O$) and 21.4 ($Ph_3P=NH$).

5.3.7. Reaction of complex 14 with $[Fe^{III}(dtc)_3]$

To a dry and degassed solution of complex **14** (0.1 mmol, 0.08 g) in 5 mL CH_2Cl_2, another dry and degassed solution of $[Fe^{III}(dtc)_3]$ (0.1 mmol, 0.05 g) in 3 mL dichloromethane was added. The reaction mixture was stirred vigorously and progress of the reaction was monitored in FT-IR spectroscopy. The reaction was stopped after complete disappearance of the nitrosyl stretch at 1755 cm^{-1} corresponding to complex **14**. The final products were isolated and characterized separately. Moreover, the reaction was monitored separately in UV-visible, X-band EPR and solution phase FT-IR spectroscopy.

$[Fe(dtc)_2(NO)]$. Yield: 0.03 g (*ca.* 75%). Elemental analyses for $C_{10}H_{20}N_3OS_4Fe$, Calcd. (%): C, 31.41; H, 5.27; N, 10.99, found (%): C, 31. 40; H, 5. 25; N, 10.96. FT-IR (in KBr):

ν_{NO}=1690 cm^{-1}, also 1505, 1492, 1457, 1436, 1419, 1382, 1354, 1273, 1202, 1147, 1091, 1075, 1005, 970, 914 and 818 cm^{-1}. FT-IR (in CH_2Cl_2): ν_{NO}=1708 cm^{-1}. UV-visible (CH_2Cl_2): 365, 470 and 635 nm. ESI-mass (m/z): Calcd: 351.986, found: 351.976 (M−NO).

[$Mn^{III}(TMPP^{2-})$](dtc). Yield: 0.08 g (*ca.* 85%). Elemental analyses for $C_{53}H_{46}N_5O_4S_2Mn$, Calcd. (%):C, 68.01; H, 4.95; N, 7.48, found (%): C, 68.04; H, 4. 93; N, 7.46. FT-IR (in KBr): 1604, 1572, 1511, 1495, 1462, 1440, 1342, 1288, 1250, 1175, 1006, 806 and 603 cm^{-1}. UV-visible (CH_2Cl_2): 480 nm ($\varepsilon/M^{-1}cm^{-1}$, 1.0 × 10^5), 535 nm ($\varepsilon/M^{-1}cm^{-1}$, 0.81 × 10^4), 585 nm ($\varepsilon/M^{-1}cm^{-1}$, 1.02 × 10^4) and 626 nm ($\varepsilon/M^{-1}cm^{-1}$, 1.33 × 10^4). ^{1}H NMR (600 MHz, $CDCl_3$): δ_{ppm}, 7.71 (br, 16H), 4.08 (br, 12H), 1.55 (br, 4H), 1.30 (br, 3H) and 0.75 (br, 3H). ESI-mass (m/z): Calcd: 958.227, found: 958.306 (M+Na).

5.3.8. Reaction of complex 14 with HBF_4 in presence o [$Fe^{III}(TPP^{2-})(Cl)$]

Complex **14** (0.1 mmol, 0.08 g) was taken in a Schlenk flask in inert condition. A dry and degassed solution of [$Fe^{III}(TPP^{2-})(Cl)$] (0.1 mmol, 0.07 g) in 5 mL CH_2Cl_2 followed by 15 μL of tetrafluoroboric acid diethyl ether complex was added to it and stirred vigorously. Reaction was discontinued after 2 h and dried under Ar atmosphere. FT-IR spectrum of the final reaction mixture was recorded in KBr.

5.4 Conclusion

In conclusion, the nitrosyl complex of Mn(II)-porphyrin, **14** has been found to release HNO in the presence of HBF_4. This has been evidenced by the characteristic reaction of HNO with triarylphosphine and by isolation of [$Mn^{III}(TMPP^{2-})(H_2O)_2$]($BF_4$). It is attributed to the fact that H^+ from HBF_4 polarizes the NO group whereas the BF_4^- interacts with metal ion to stabilize the Mn(III) form. These two effects cooperatively result in the

release of HNO from complex **14**. In addition, complex **14** behaves as a nitroxyl (NO^-) donor in the presence of $[Fe^{III}(dtc)_3]$ to result in $[Fe(dtc)_2(NO)]$. In this case, the cooperative interaction of $[Fe(dtc)_2]^+$ with the coordinated NO group and dtc^- with the manganese center, results in the transfer NO^- to $[Fe(dtc)_2]^+$. The NO^- transfer from complex **14** to $[Fe^{III}(TPP^{2-})(Cl)]$ has also been demonstrated. Thus, these results demonstrate an example where a nitrosyl complex of Mn(II)-porphyrin having $\{Mn(NO)\}^6$ can act as HNO/nitroxyl donor.

5.5 References

1 (a) Doctorovich, F.; Bikiel, D. E.; Pellegrino, J.; Suárez, S. A.; Martí, M. A. *Acc. Chem. Res.* **2014**, *47*, 2907. (b) Suarez, S. A.; Neuman, N. I.; Munoz, M.; Alvarez, L.; Bikiel, D. E.; Brondino, C. D.; Ivanovic-Burmazovic, I.; Miljkovic, J. L.; Filipovic, M. R.; Marti, M. A.; Doctorovich, F. *J. Am. Chem. Soc.* **2015**, *137*, 4720.

2 Doctorovich, F.; Bikiel, D.; Pellegrino, J.; Suárez, S. A.; Larsen, A.; Martí, M. A. *Coord. Chem. Rev.* **2011**, *255*, 2764.

3 Cline, M. R.; Tu, C.; Silverman, D. N.; Toscano, J. P. *Free Radical Biol. Med.* **2011**, *50*, 1274.

4 Reisz, J. A.; Zink, C. N.; King, S. B. *J. Am. Chem. Soc.* **2011**, *133*, 11675.

5 Donzelli, S.; Espey, M. G.; Flores-Santana, W.; Switzer, C. H.; Yeh, G. C.; Huang, J.; Stuehr, D. J.; King, S. B.; Miranda, K. M.; Wink, D. A. *Free Radical Biol. Med.* **2008**, *45*, 578.

6 Dobmeier, K. P.; Riccio, D. A.; Schoenfisch, M. H. *Anal. Chem.* **2008**, *80*, 1247.

7 Rosenthal, J.; Lippard, S. J. *J. Am. Chem. Soc.* **2010**, *132*, 5536.

8 Zhou, Y.; Liu, K.; Li, J.-Y.; Fang, Y.; Zhao, T.-C.; Yao, C. *Org. Lett.* **2011**, *13*,

1290.

9 Miao, Z.; King, S. B. *Nitric Oxide* **2016**, *57*, 1.

10 Walter, M. R.; Dzul, S. P.; Rodrigues, A. V.; Stemmler, T. L.; Telser, J. C.; Ghosh, A.; Harrop, T. C. *J. Am. Chem. Soc.* **2016**, *138*, 12459.

11 (a) Goodrich, L. E.; Roy, S.; Alp E. E.; Zhao, J.; Hu, M. Y.; Lehnert, N. *Inorg. Chem.* **2013**, *52*, 7766. (b) Speelman, A. L.; Lehnert, N. *Acc. Chem. Res.* **2014**, *47*, 1106.

12 (a) Farmer, P. J.; Kumar, M. R.; Almaraz, E. *Comments Inorg. Chem.* **2010**, *31*, 130. (b) Farmer, P. J.; Sulc, F. *J. Inorg. Biochem.* **2005**, *99*, 166. (c) Patra, A. K.; Dube, K. S.; Sanders B. C.; Papaefthymiou G. C.; Conradie, J.; Ghosh, A. *Chem. Sci.* **2012**, *3*, 364.

13 (a) Khin, C.; Heinecke, J. L.; Ford, P. C. *J. Am. Chem. Soc.* **2008**, *130*, 13830. (b) Heinecke, J. L.; Khin, C.; Pereira, J. C. M.; Suarez, S. A.; Iretskii, A. V.; Doctorovich, F.; Ford, P. C. *J. Am. Chem. Soc.* **2013**, *135*, 4007. (c) Miljkovic, J. L.; Kenkel, I.; Ivanovic-Burmazovic, I.; Filipovic, M. R. *Angew. Chem. Int. Ed.* **2013**, *52*, 12061.

14 (a) Merkle, A. C.; Fry, N. L.; Mascharak, P. K.; Lehnert, N. *Inorg. Chem.* **2011**, *50*, 12192-12203. (b) Kumar, M. R.; Fukuto, J. M.; Miranda, K. M.; Farmer, P. J. *Inorg. Chem.* **2010**, *49*, 6283.

15 Franz, K. J.; Lippard, S. J. *J. Am. Chem. Soc.* **1998**, *120*, 9034.

16 Bari, S. E.; Olabe, J. A.; Slep, L. D.; *Advances in Inorganic Chemistry*; van Eldik, R.; Olabe, J. A. Eds.; Elsevier: Amsterdam; **2015**, *67*, 87.

17 Zavarine, I. S.; Kini, A. D.; Morimoto, B. H.; Kubiak, C. P. *J. Phys. Chem. B* **1998**, *102*, 7287.

18 (a) Galinato, M. J. I.; Brocious, E. P.; Paulat, F.; Martin, S.; Skodack, J.; Harl-

and, J. B.; Lehnert, N. *Inorg. Chem.* **2020**, *59*, 2144. (b) Mondal, B.; Borah, D.; Mazumdar, R.; Mondal, B. *Inorg. Chem.* **2019**, *58*, 14701.

19 (a) Bari, S. E.; Marti, M. A.; Amorebieta, V. T.; Estrin, D. A.; Doctorovich, F. *J. Am. Chem. Soc*. **2003**, *125*, 15272. (b) Rhine, M. A.; Rodrigues, A. V.; Bieber Urbauer, R. J.; Urbauer, J. L.; Stemmler, T. L.; Harrop, T. C. *J. Am. Chem. Soc.* **2014**, *136*, 12560.

20 (a) Shafirovich, V.; Lymar, S. V. *Proc. Natl. Acad. Sci. U.S.A.* **2002**, *99*, 7340. (b) Marti, M. A.; Bari, S. E.; Estrin, D. A.; Doctorovich, F. *J. Am. Chem. Soc.* **2005**, *127*, 4680.

21 (a) Reisz, J. A.; Klorig, E. B., Wright, M. W., King S. B. *Org. Lett.* **2009**, 11, 2719. (b) Rentsch, D.; Hany, R.; von Philipsborn, W. Magn. Reson. Chem. **1997**, *35*, 832.

22 Komarov, A. M.; Reef, A.; Schmidt, H. H. H. W.; *Methods in Enzymology*; Cadenas, E.; Packer, L. Eds.; Academic Press, **2002**, *359*, 18.

23 Ileperuma, O. A.; Feltham, R. D. *Inorg. Chem.* **1977**, *16*, 1876.

24 Kelly, S.; Lancon, D.; Kadish, K. M. Inorg. Chem. **1984**, *23*, 1451.

25 Ivanovic-Burmazovic, I.; *The Chemistry and Biology of Nitroxyl (HNO)*; Doctorovich, F.; Farmer, P. J.; Marti, M. A. Eds.; Elsevier, **2017**, 67.

26 Jones, R. D.; Summerville, D. A.; Basolo F. *J. Am. Chem. Soc.* **1978**, *100*, 4416.

27 SMART, SAINT and XPREP, Siemens Analytical X-ray Instruments Inc., Madison, Wisconsin, USA, **1995**.

28 (a) Sheldrick, G. M. SHELXS-2014, University of Gottingen, Germany. (b) Farrugia, L. J. ORTEP-3 for Windows - a version of ORTEP-III with a Graphical User Interface (GUI) *J. Appl. Crystallogr.* **1997**, *30*, 565.

Conclusion

This thesis broadly covers our endeavor to comprehend some interesting reactivity of nitrosyl complexes of Co(II) and Mn(II) porphyrinates. A series of these complexes were synthesized by varying the substitutions at the *meso* positions of the porphyrin ring (e.g. phenyl, pentafluorophenyl and 4-methoxyphenyl) and central metal ion (e.g. Co^{2+} and Mn^{2+}). The reactivity of these complexes towards reduced oxygen species (O_2^- and O_2^{2-}) was explored following an attempt to mimic the mechanism of the nitric oxide dioxygenase (NOD) enzyme, which has been discussed in the chapters 2 to 4. In every instance formation of a putative PN intermediate was observed. Tedious efforts to identify and characterize the associated intermediates that form during its formation and decomposition led to some significant findings. For instance, in chapter 2, the formation of a [$Co^{II}(NO)(O_2^-)$] species was evidenced spectroscopically prior to the formation of a [Co(II)-PN] intermediate. In chapter 3, a Co(III) porphyrin cation radical species has been detected in the decomposition of a [Co(III)-PN], which in turn confirms the involvement of a [Co(IV)=O] intermediate in the reaction. In chapter 4, we could prove the involvement of [Mn(IV)=O] in the decomposition of an [Mn(III)-PN] intermediate both spectroscopically and chemically. A [$Mn^{III}(NO)(O_2^-)$] species was also observed prior to the formation of the [Mn(III)-PN]. We believe that these findings will contribute crucially to our existing knowledge of NOD chemistry and extensively to the field of metalloenzyme chemistry. However, despite our best efforts, the characterization of the PN complex itself was not very successful because of its highly unstable nature.

In chapter 5, the HNO donation ability of a nitrosyl of Mn(II)-porphyrin complex was investigated in presence of HBF_4. Previously, $\{Mn(NO)\}^6$ complexes were not considered as HNO/NO^- donors due to their [$Mn(I)\text{-}NO^+$] nature. However, we have shown that

presence of electron donating ligand environment along with an electron rich sixth ligand may induce [Mn(III)-NO^{-}] character and result in release of HNO. This is a new type of reactivity for such complexes and definitely needs more investigation in future. The mechanism of the process needs further experimental support which may be achieved by tuning the ligand framework with appropriate electron donating groups.

Appendix I

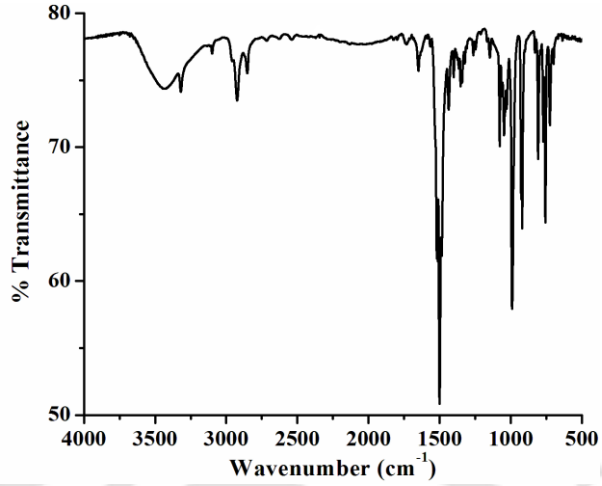

Figure A1.1. FT-IR spectrum of ligand **F_{20}TPPH$_2$** in KBr.

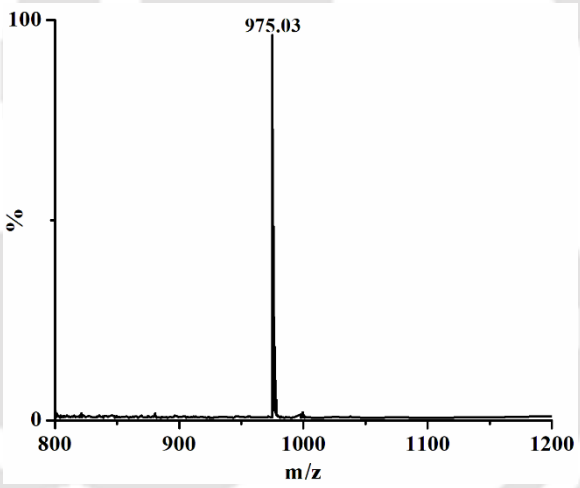

Figure A1.2. ESI-mass spectrum of ligand **F_{20}TPPH$_2$** in CH_3CN [Calcd. m/z 975.06 (M+1)].

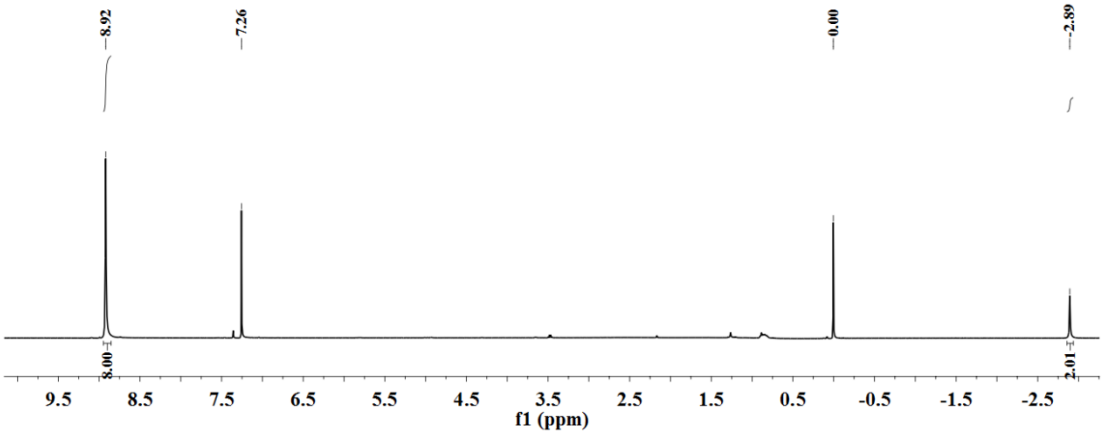

Figure A1.3. ^{1}H NMR spectrum of ligand **F_{20}TPPH$_2$** in $CDCl_3$.

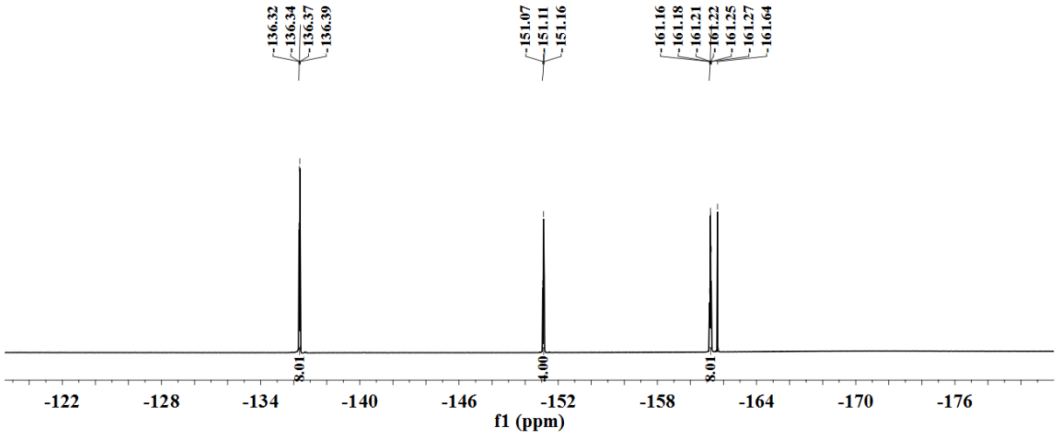

Figure A1.4. ^{19}F NMR spectrum of ligand $\mathbf{F_{20}TPPH_2}$ in $CDCl_3$.

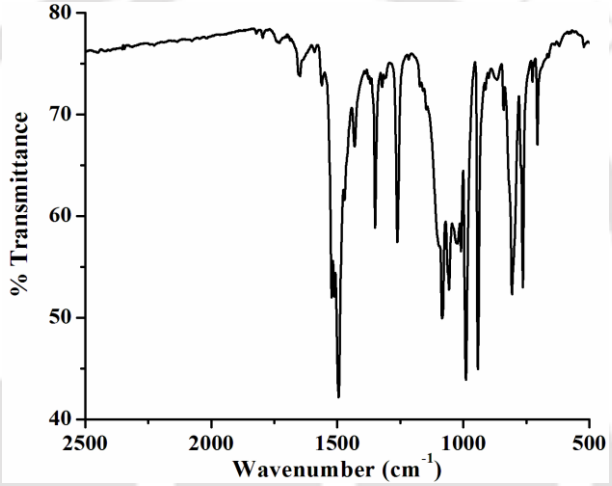

Figure A1.5. FT-IR spectrum of complex **1** in KBr.

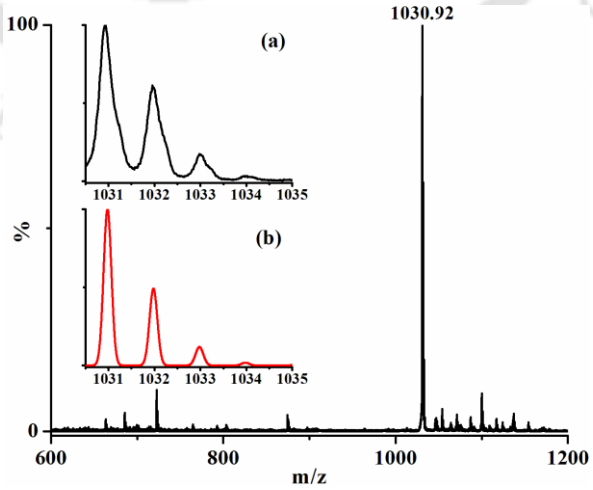

Figure A1.6. ESI-mass spectrum of complex **1** in CH_3CN [Calcd. m/z 1030.98 (M+1); Inset: (a) experimental and (b) simulated isotopic distribution pattern].

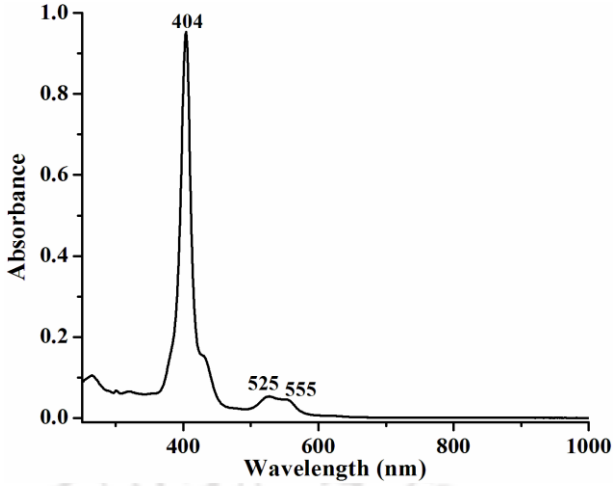

Figure A1.7. UV-visible spectrum of complex **1** in CH_2Cl_2 at room temperature (4.5 μM).

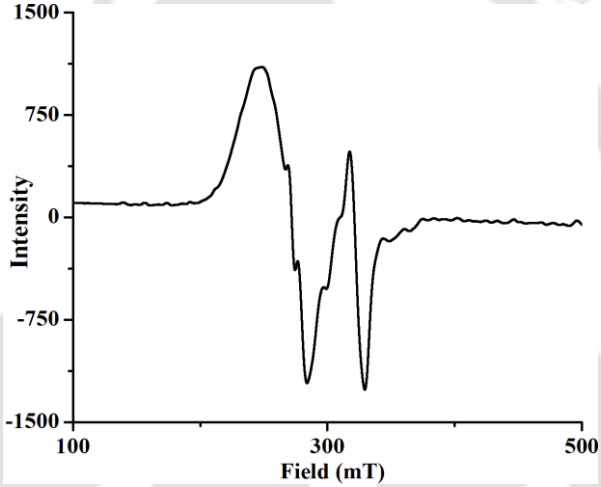

Figure A1.8. X-band EPR spectrum of complex **1** in CH_2Cl_2 at 77K.

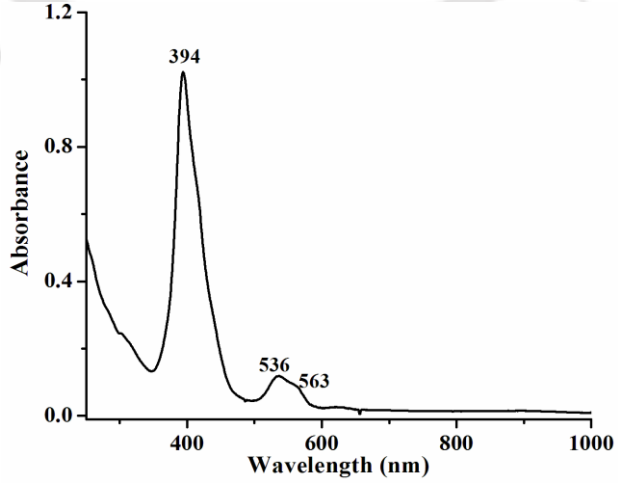

Figure A1.9. UV-visible spectrum of complex **2** in CH_2Cl_2 at −40 °C (9 μM).

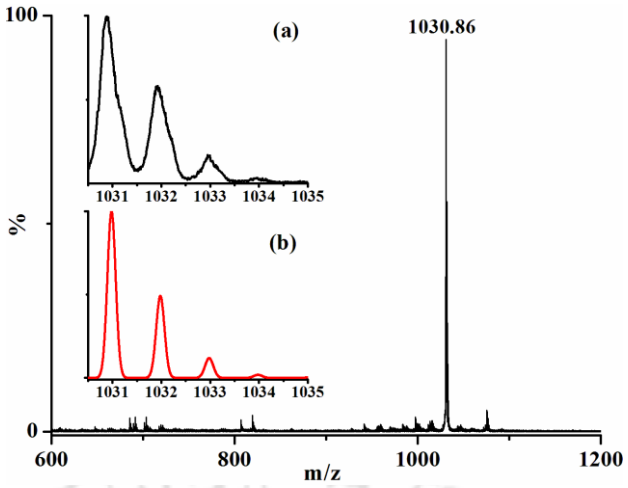

Figure A1.10. ESI-mass spectrum of complex **2** in CH_3CN [Calcd. m/z 1030.98 (M−NO); Inset: (a) experimental and (b) simulated isotopic distribution pattern].

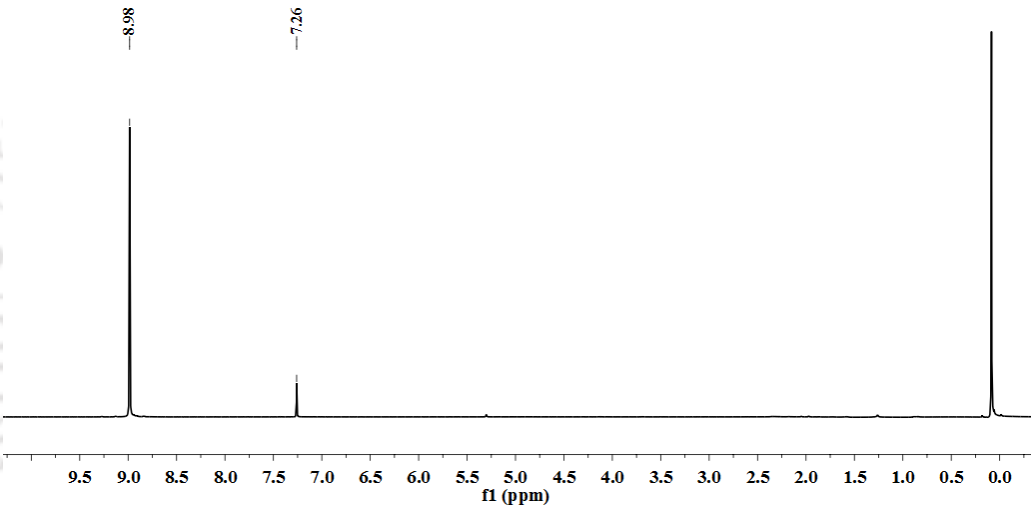

Figure A1.11. ^1H NMR spectrum of complex **2** in $CDCl_3$.

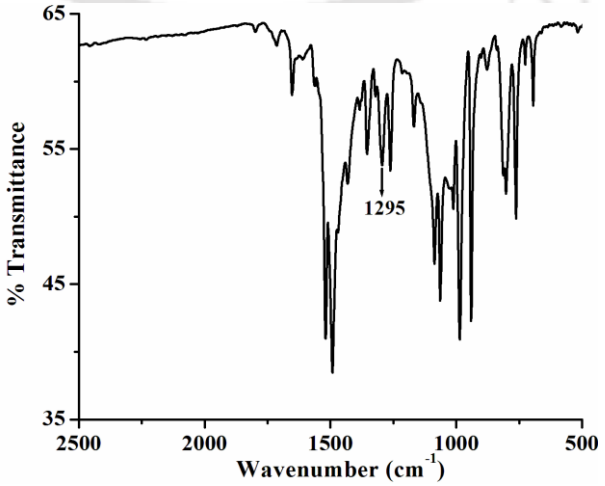

Figure A1.12. FT-IR spectrum of complex **3** in KBr.

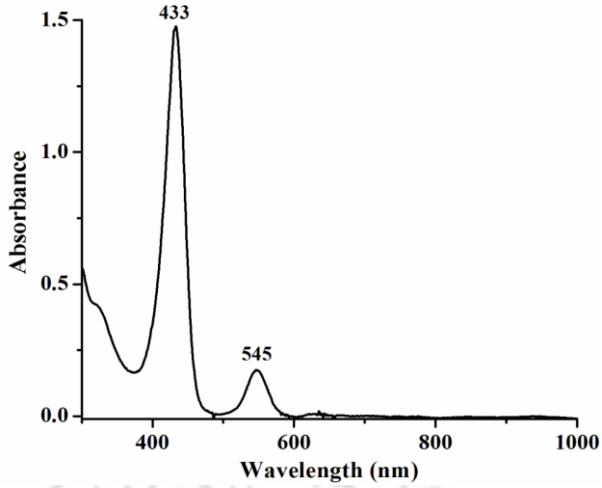

Figure A1.13. UV-visible spectrum of complex **3** in CH_2Cl_2 at room temperature (10 μM).

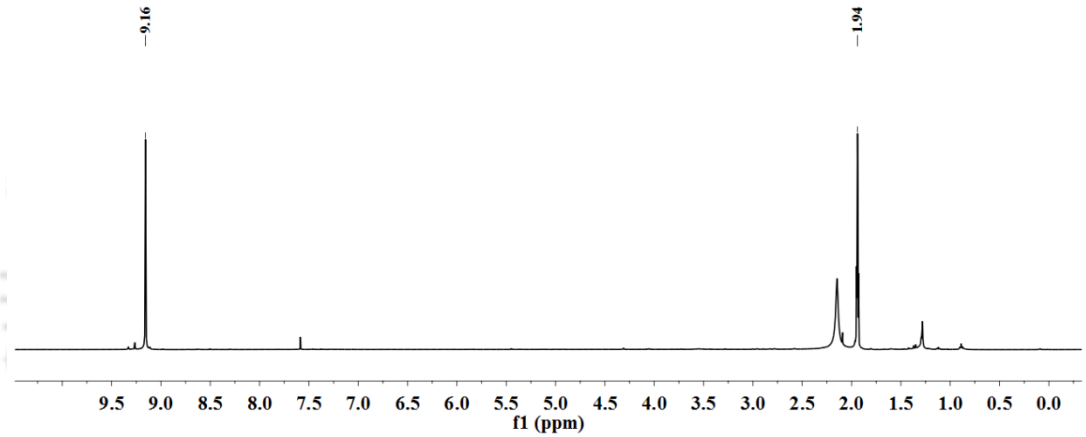

Figure A1.14. ^1H NMR spectrum of complex **3** in CD_3CN.

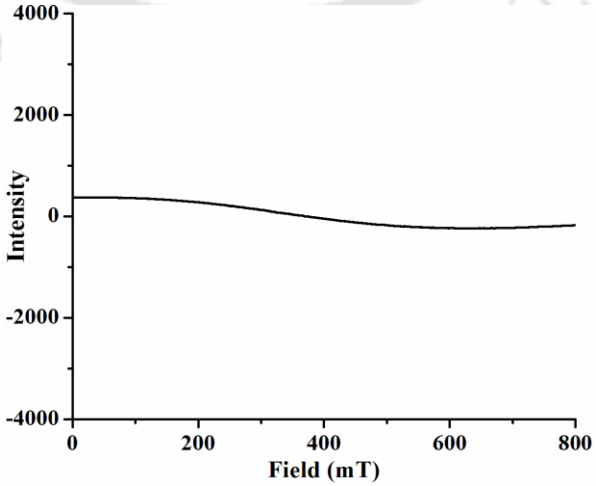

Figure A1.15. X-band EPR spectrum of complex **3** in CH_2Cl_2 at 77K.

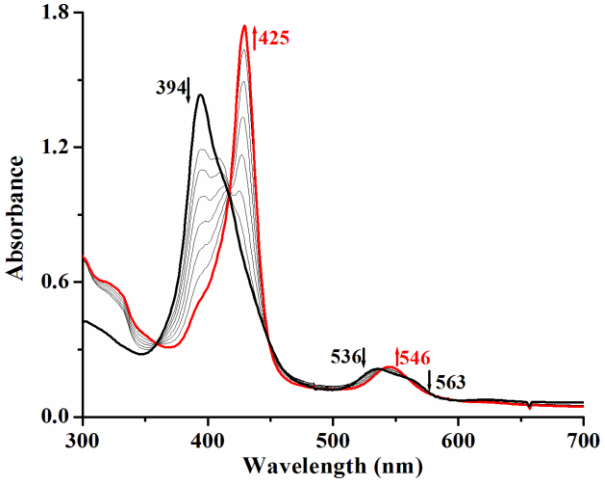

Figure A1.16: UV-visible spectral monitoring of complex **2** (black) and after addition of imidazole (red) in CH_2Cl_2 at room temperature.

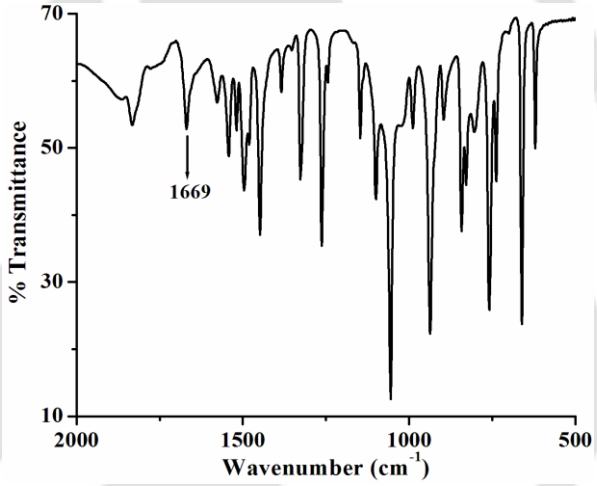

Figure A1.17. FT-IR spectrum of the reaction mixture of complex **2** and imidazole in KBr.

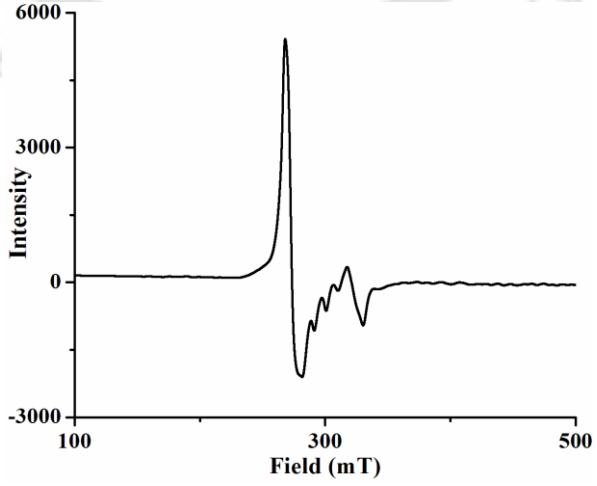

Figure A1.18. X-band EPR spectrum of reaction mixture of complex **2** and KO_2 in CH_2Cl_2 at 77K.

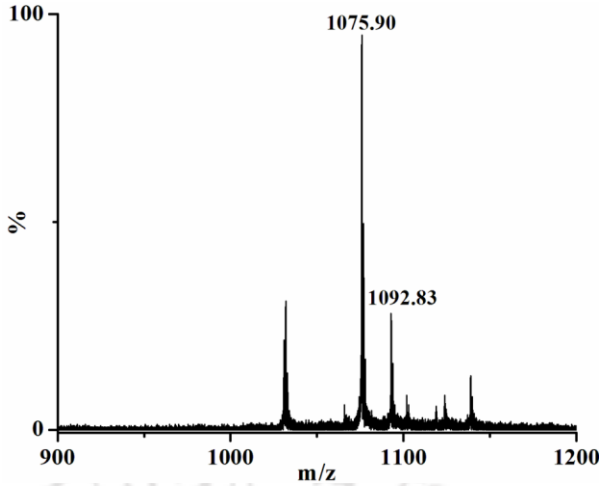

Figure A1.19. ESI-mass spectrum of reaction mixture of complex **2** and KO_2 (in CH_2Cl_2) in CH_3CN.

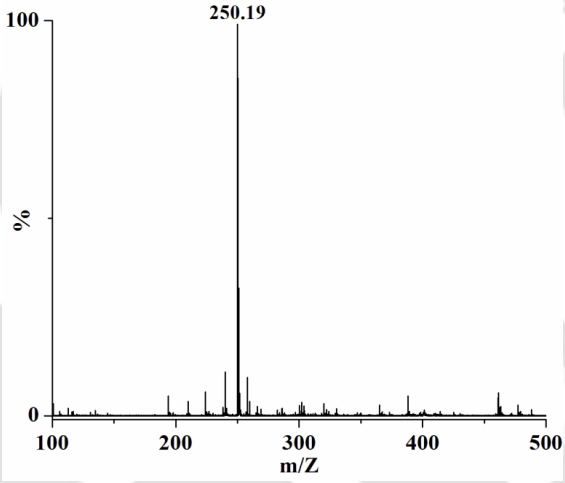

Figure A1.20. ESI-mass spectrum of 2,4-di-*tert*-butyl-6-nitrophenol in CH_3CN [Calcd. m/z 250.15 (M−1)].

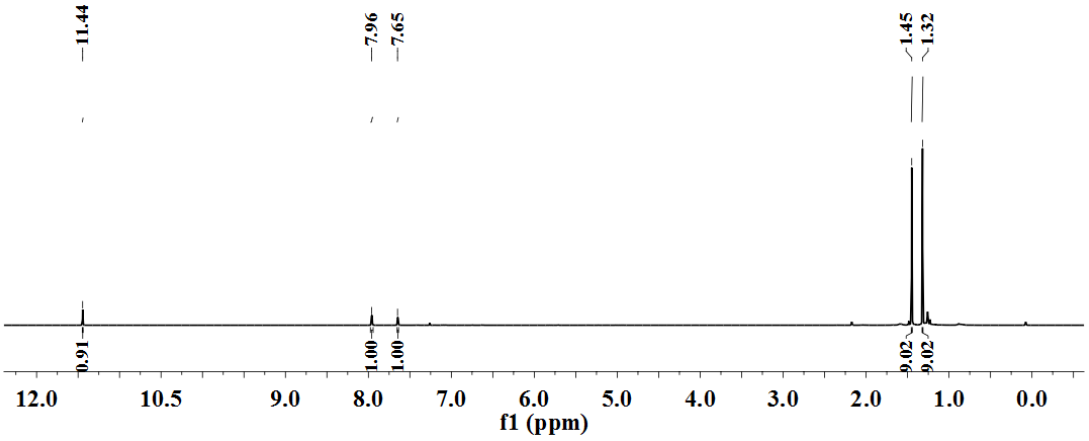

Figure A1.21. ^1H NMR spectrum of 2,4-di-*tert*-butyl-6-nitrophenol in $CDCl_3$.

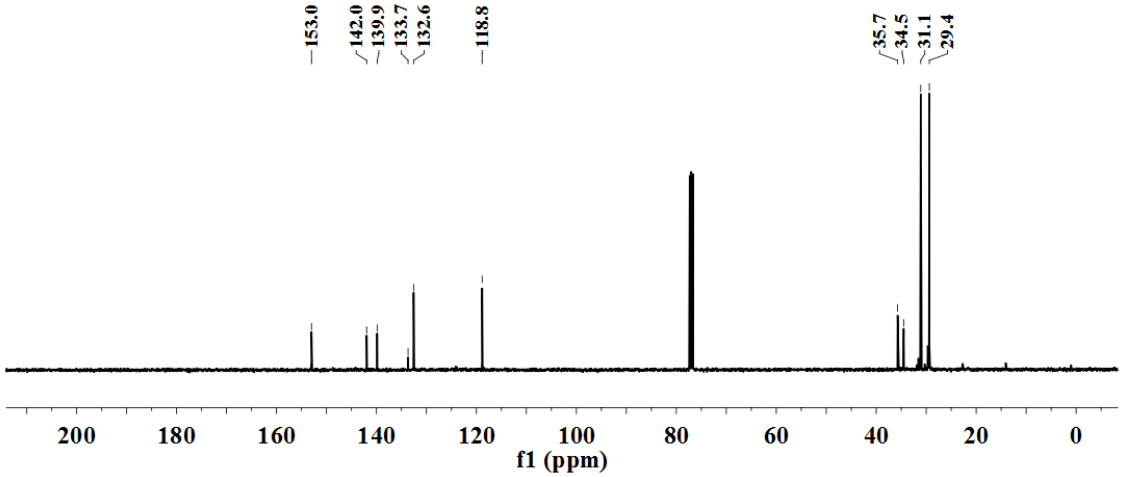

Figure A1.22. ^{13}C NMR spectrum of 2,4-di-*tert*-butyl-6-nitrophenol in $CDCl_3$.

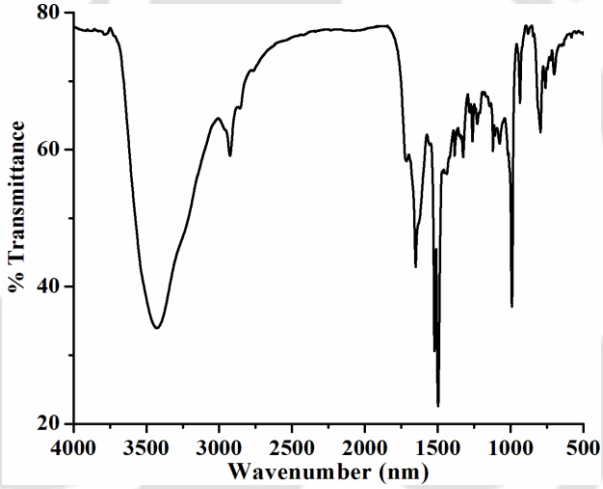

Figure A1.23. FT-IR spectrum of complex **4** in KBr.

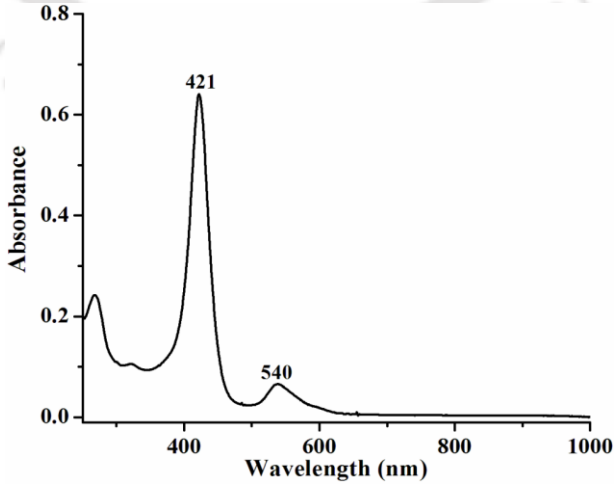

Figure A1.24. UV-visible spectrum of complex **4** in CH_2Cl_2 at room temperature.

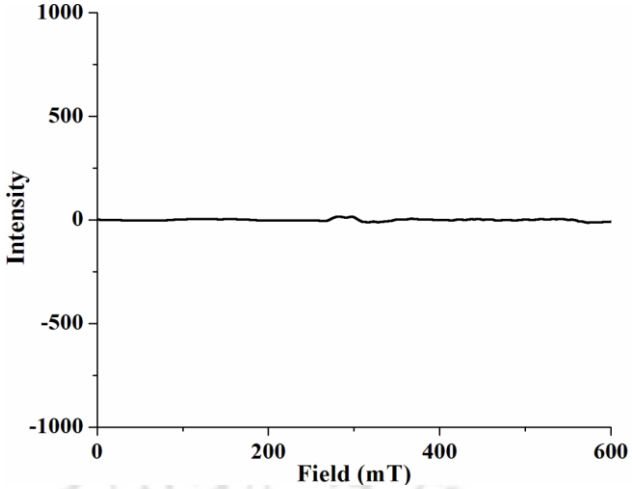

Figure A1.25. X-band EPR spectrum of complex **3** in CH_2Cl_2 at 77K.

Table A1.1. Crystallographic data for complexes **1**, **2** and **3**.

	1	**2**	**3**
Formulae	$C_{44}H_8CoF_{20}N_4$	$C_{60}H_{40}CoF_{20}N_5O_5$	$C_{49}H_{17}C_{l3}CoF_{20}N_5O_3$
Mol. wt.	1031.47	1349.90	1268.96
Crystal system	Trigonal	Tetragonal	Monoclinic
Space group	R -3 :H	I 4/m	P 21/n
Temperature /K	293(2)	293(2)	293(2)
Wavelength /Å	0.71073	0.71073	0.71073
a /Å	20.3537(13)	17.598(2)	12.6854(10)
b /Å	20.3537(13)	17.598(2)	31.185(3)
c /Å	24.165(2)	9.462(3)	13.3739(13)
α/°	90	90	90
β/°	90	90	113.089(10)
γ/°	120	90	90
V/ $Å^3$	8669.9(14)	2930.5(13)	4866.9(8)
Z	9	2	4
Density/Mgm^{-3}	1.778	1.530	1.732
Abs. Coeff. /mm^{-1}	0.584	0.411	0.645
Abs. correction.	Multi-scan	Multi-scan	Multi-scan
F(000)	4563	1364	2512
Total no. of reflections	3391	1376	8551
Reflections, $I > 2\sigma(I)$	2224	945	4184
Max. 2θ/°	24.989	24.995	25.000
Ranges (h, k, l)	$-20 \le h \le 12$ $-12 \le k \le 20$ $-11 \le l \le 6$	$-20 \le h \le 12$ $-12 \le k \le 20$ $-11 \le l \le 6$	$-15 \le h \le 15$ $-35 \le k \le 37$ $-15 \le l \le 12$
Complete to 2θ (%)	0.998	0.996	0.999
Refinement method	Full-matrix least-squares on F^2	Full-matrix least-squares on F^2	Full-matrix least-squares on F^2
Goof (F^2)	0.958	0.987	1.054

R indices [$I > 2\sigma(I)$]	0.0549	0.0717	0.0693
R indices (all data)	0.0911	0.1017	0.1527

Table A1.2. Selected bond lengths (Å) of complexes **1**, **2** and **3**.

Atoms	**1**	**2**	**3**
Co1-N1	1.962(3)	1.97(2)	1.895(5)
Co1-N2	1.963(3)	1.968(4)	1.973(4)
N1-O1		1.01(3)	1.194(6)
N1-O2			1.216(6)
N1-C1	1.382(5)		
C1-C2	1.382(6)	1.343(8)	1.437(7)
C2-C3	1.499(5)	1.433(8)	1.372(8)
C4-C5	1.368(7)	1.490(8)	1.393(7)
C5-C6	1.330(9)	1.378(6)	1.369(8)
C6-C7	1.359(9)		1.351(9)
C4-F1	1.332(6)		
C5-F1			1.335(7)
C6-F1		1.329(6)	

Table A1.3. Selected bond angles (˚) of complexes **1**, **2** and **3**.

Atoms	**1**	**2**	**3**
N1-Co1-N2	89.98(13)	90.000(2)	90.2(2)
Co1-N1-O1		123(2)	119.0(5)
Co1-N1-O2			119.7(4)
O1-N1-O2			121.3(5)
N1-C1-C2	124.4(4)		
C1-C2-C3	117.4(4)	107.4(5)	125.1(5)
C2-C3-C4	120.6(4)	124.5(5)	118.2(5)
C4-C5-C6	120.5(6)	122.1(3)	122.6(6)
C3-C4-F1	119.6(4)		
C5-C6-F1		119.0(4)	
C4-C5-F1			118.7(5)

Appendix II

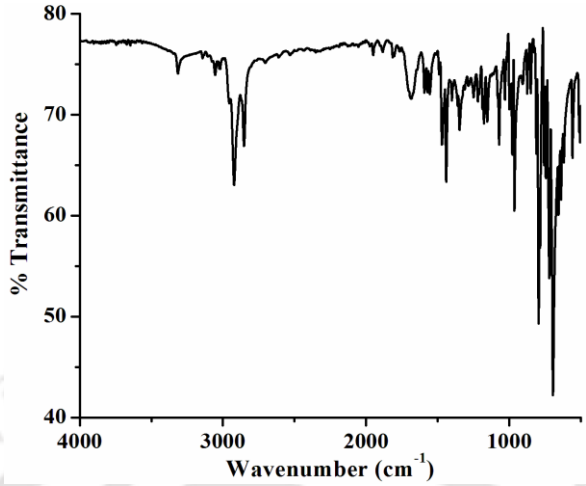

Figure A2.1. FT-IR spectrum of ligand **MPTPPH$_2$** in ATR.

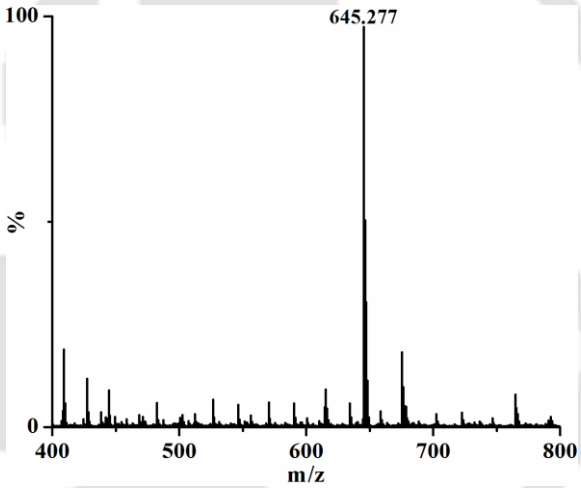

Figure A2.2. ESI-mass spectrum of ligand **MPTPPH$_2$** in CH_3CN [Calcd. m/z 644.258 (M+1)].

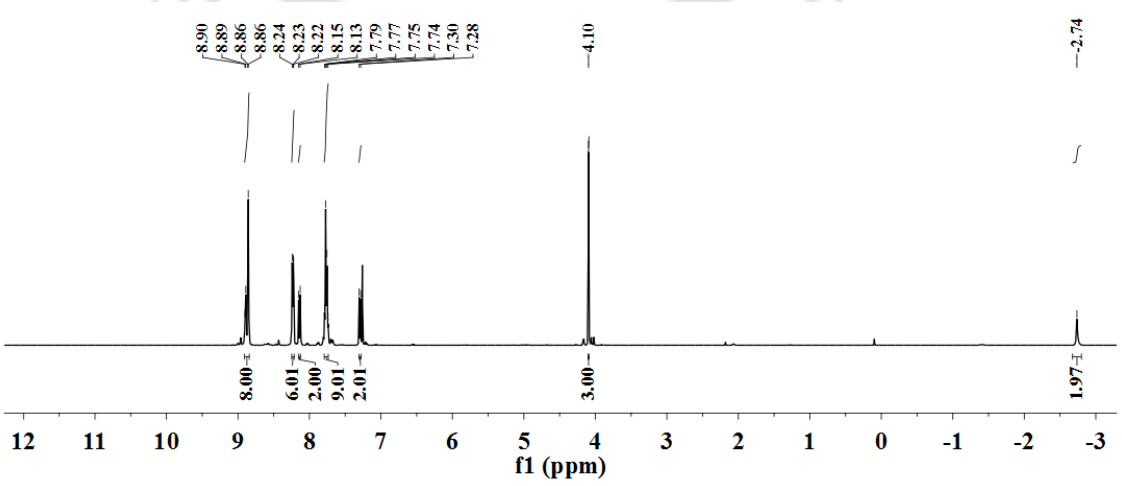

Figure A2.3. ^{1}H NMR spectrum of ligand **MPTPPH$_2$** in $CDCl_3$.

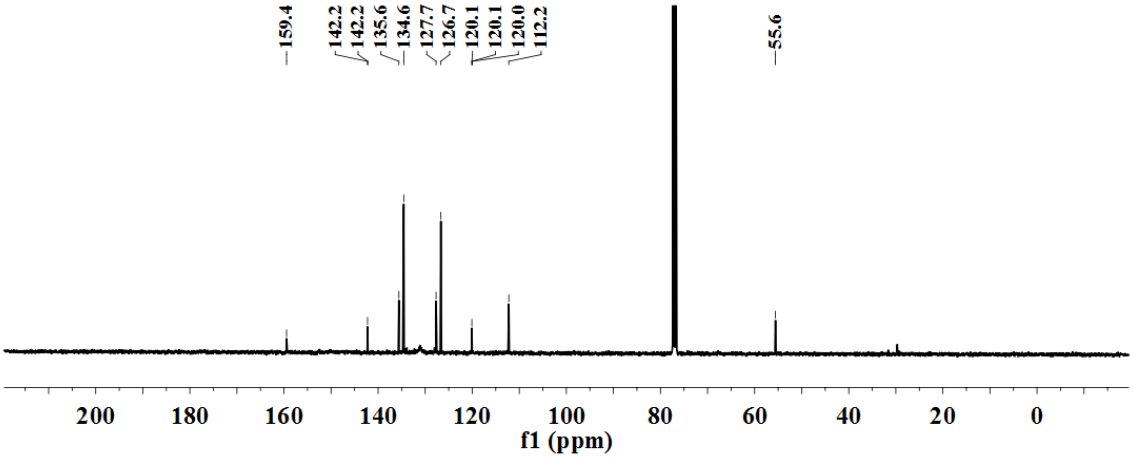

Figure A2.4. ^{13}C NMR spectrum of ligand **MPTPPH$_2$** in $CDCl_3$.

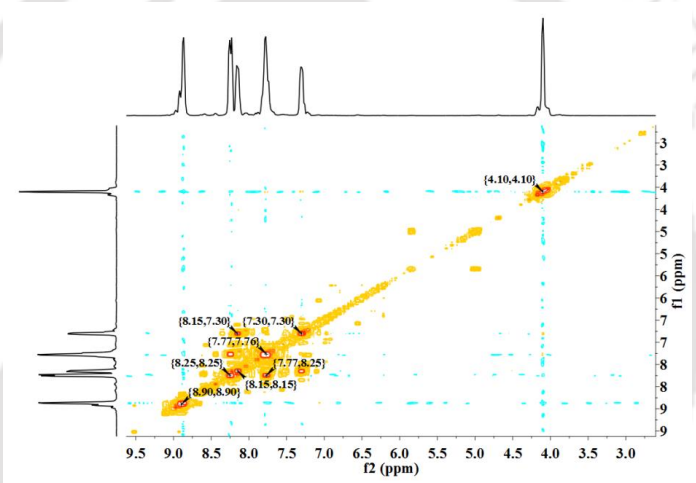

Figure A2.5. COSY spectrum of ligand **MPTPPH$_2$** in $CDCl_3$.

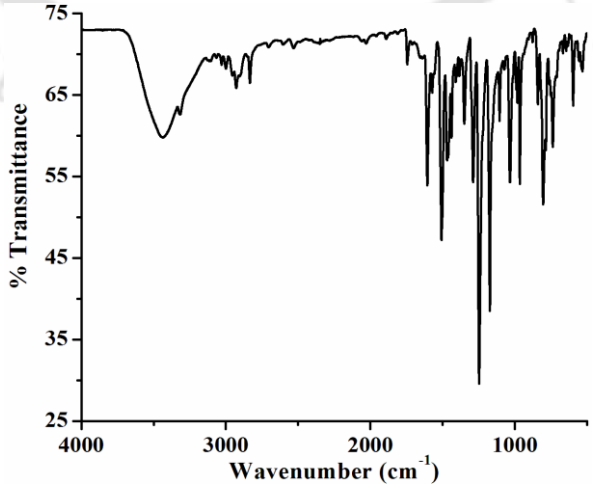

Figure A2.6. FT-IR spectrum of ligand **TMPPH$_2$** in KBr.

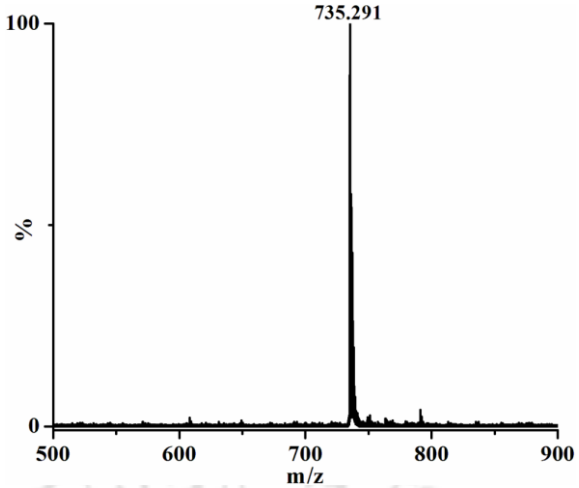

Figure A2.7. ESI-mass spectrum of ligand **TMPPH$_2$** in CH_3CN [Calcd. m/z 734.289 (M+1)].

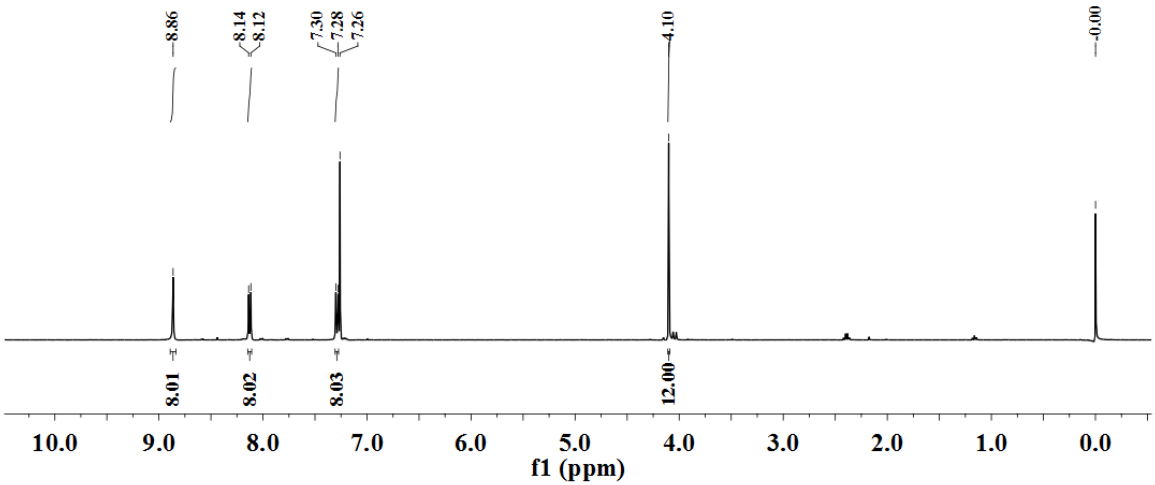

Figure A2.8. ^{1}H NMR spectrum of ligand **TMPPH$_2$** in $CDCl_3$.

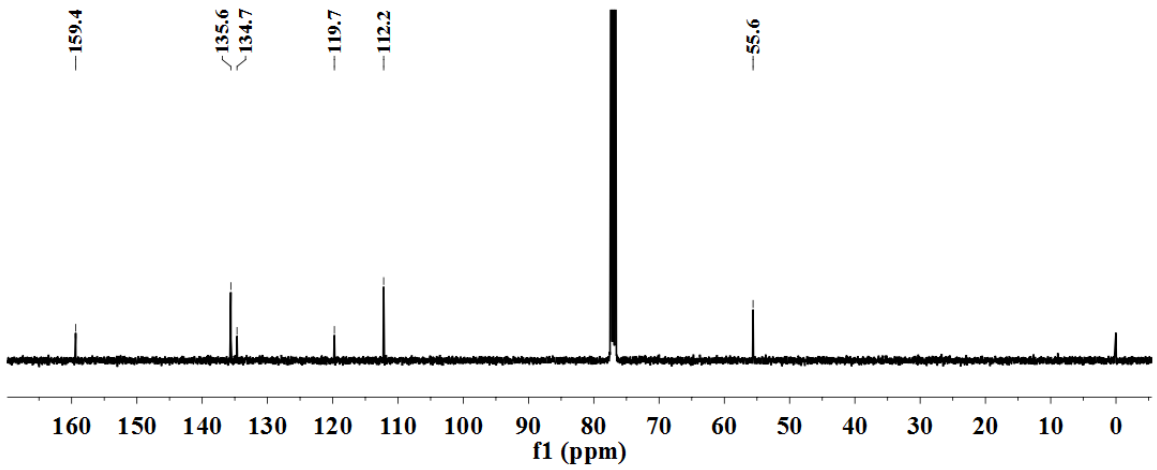

Figure A2.9. ^{13}C NMR spectrum of ligand **TMPPH$_2$** in $CDCl_3$.

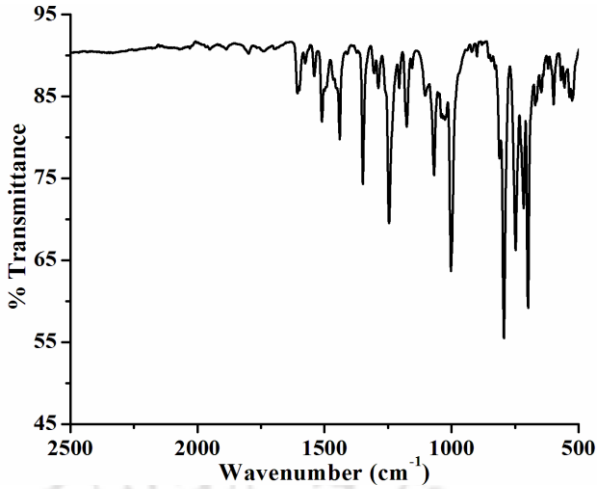

Figure A2.10. FT-IR spectrum of complex **5** in KBr.

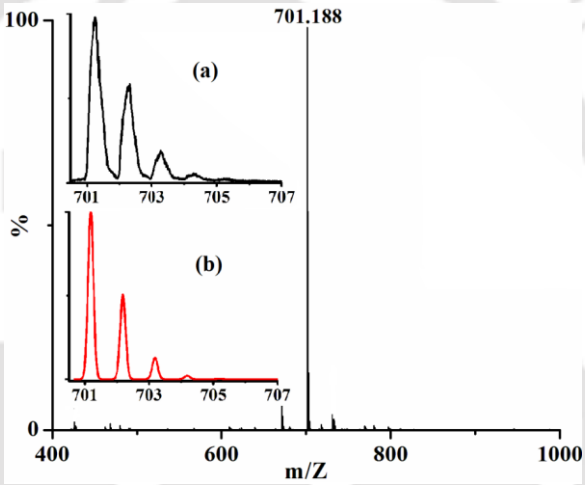

Figure A2.11. ESI-mass spectrum of complex **5** in CH_3CN [Calcd. m/z 701.175 (molecular ion peak); Inset: (a) experimental and (b) simulated isotopic distribution pattern].

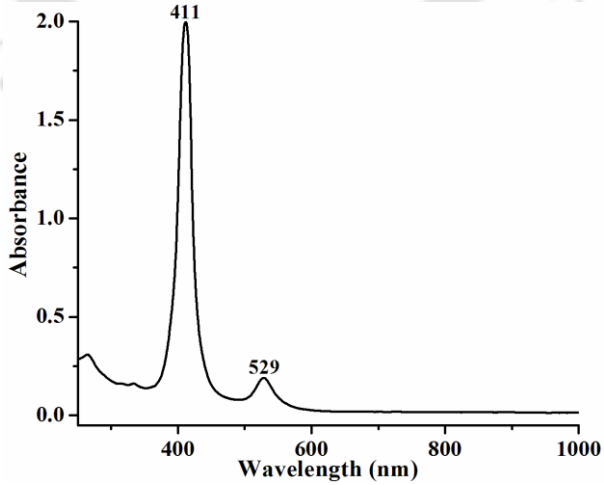

Figure A2.12. UV-visible spectrum of complex **5** in CH_2Cl_2 at room temperature (17 μM).

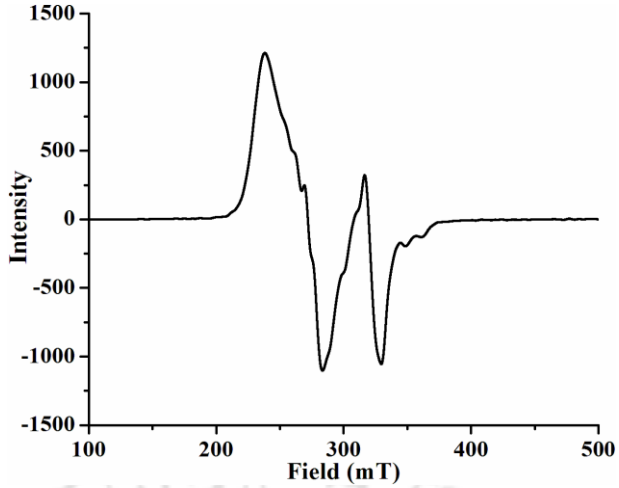

Figure A2.13. X-band EPR spectrum of complex **5** in CH_2Cl_2 at 77 K.

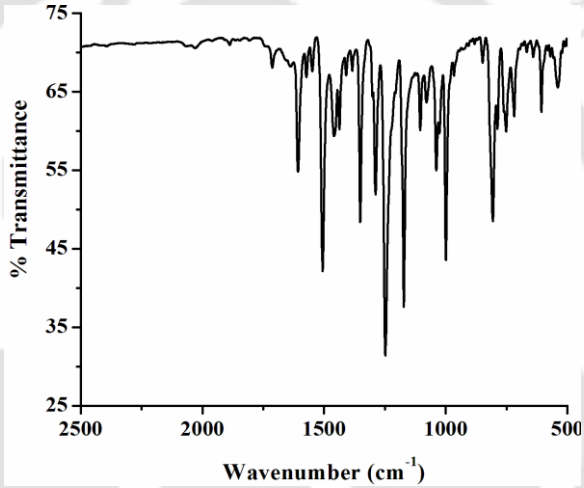

Figure A2.14. FT-IR spectrum of complex **6** in KBr.

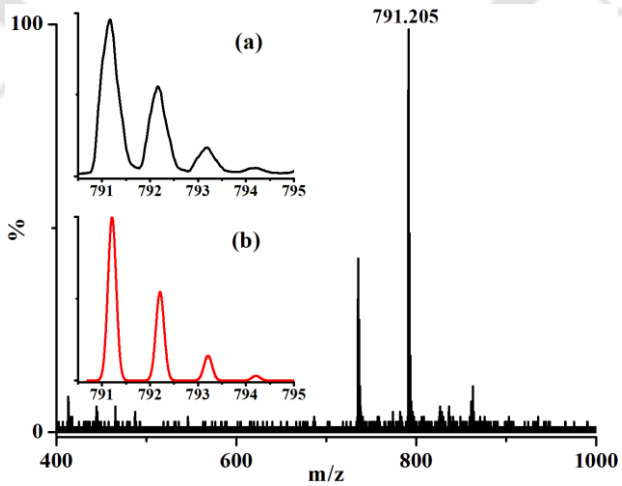

Figure A2.15. ESI-mass spectrum of complex **6** in CH_3CN [Calcd. m/z 791.207 (molecular ion peak); Inset: (a) experimental and (b) simulated isotopic distribution pattern].

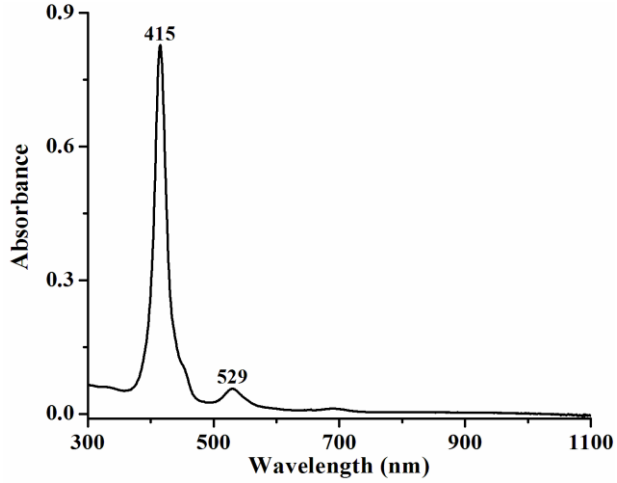

Figure A2.16. UV-visible spectrum of complex **6** in CH_2Cl_2 at room temperature (4 μM).

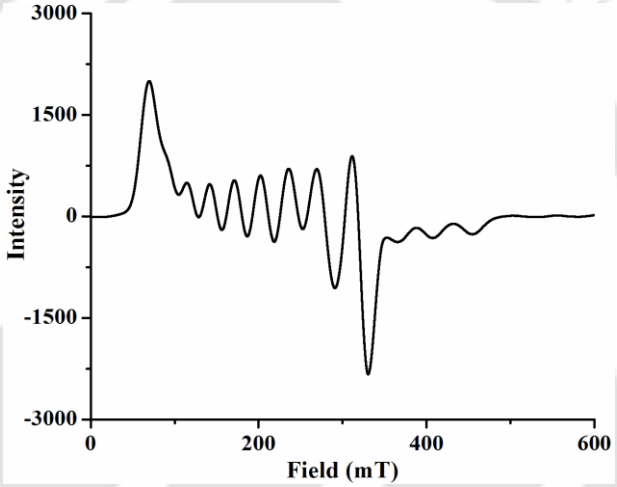

Figure A2.17. X-band EPR spectrum of complex **6** in CH_2Cl_2 at 77 K.

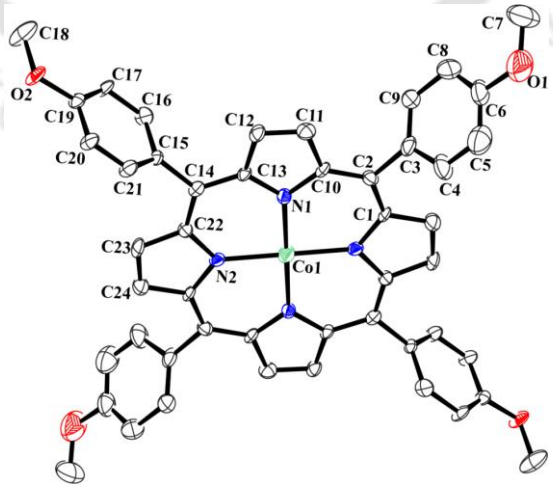

Figure A2.18. ORTEP diagram of complex **6** (30% thermal ellipsoid plot, H-atoms are omitted for clarity).

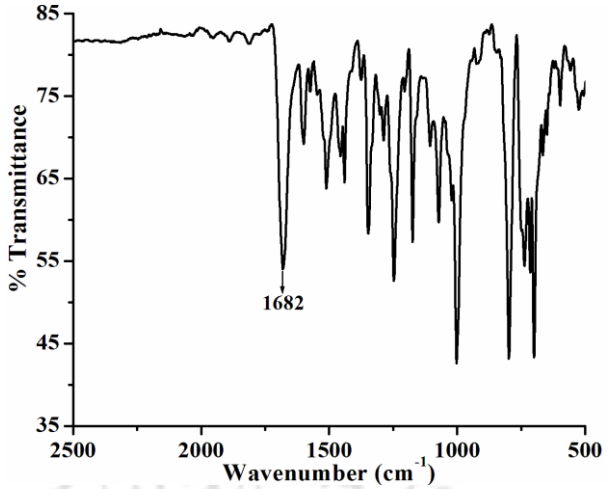

Figure A2.19. FT-IR spectrum of complex **7** in KBr.

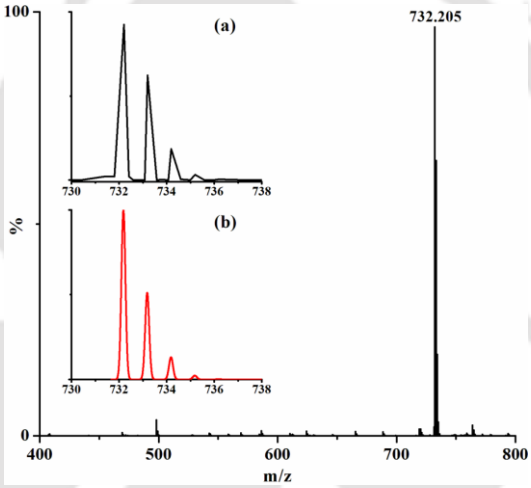

Figure A2.20. ESI-mass spectrum of complex **7** in CH_3CN [Calcd. m/z 731.173 (M+1); Inset: (a) experimental and (b) simulated isotopic distribution pattern].

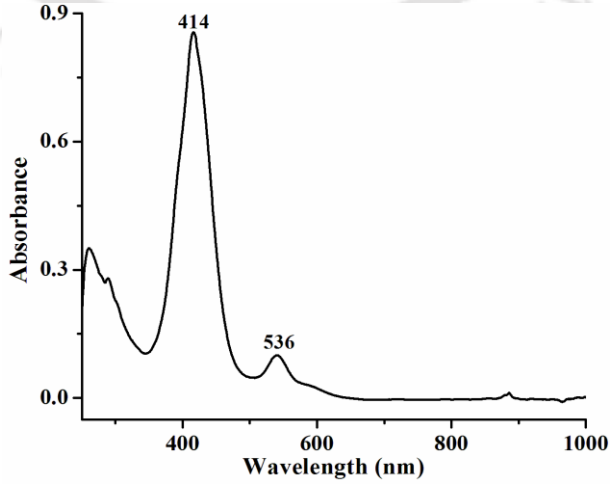

Figure A2.21. UV-visible spectrum of complex **7** in CH_2Cl_2 at −40 °C (10 μM).

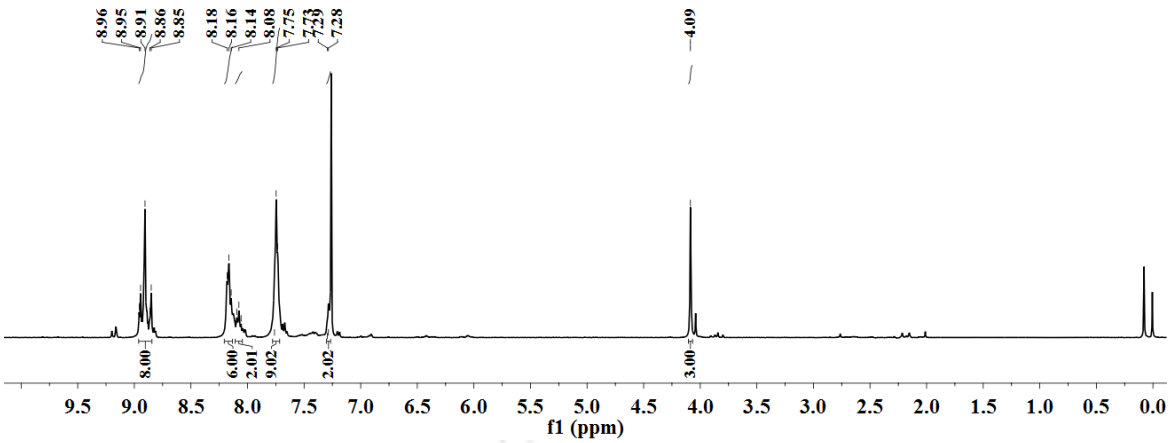

Figure A2.22. ^{1}H NMR spectrum of complex **7** in $CDCl_3$.

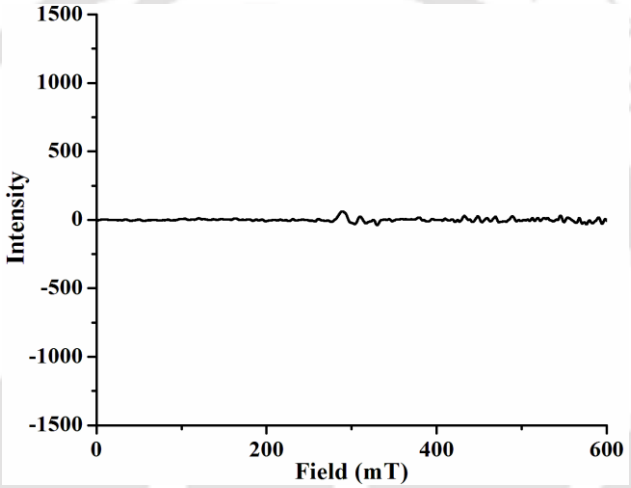

Figure A2.23. X-band EPR spectrum of complex **7** in CH_2Cl_2 at 77K.

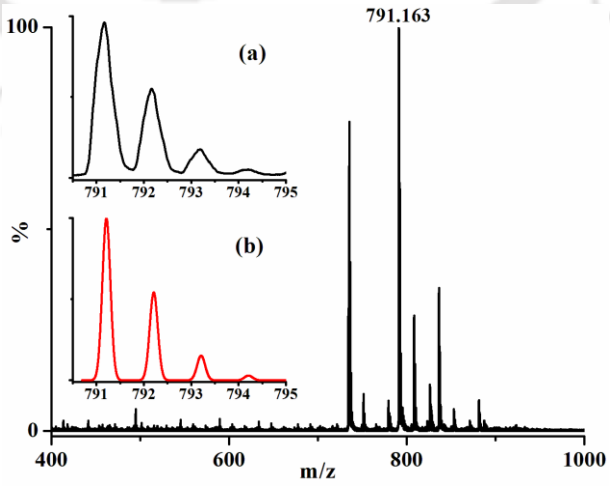

Figure A2.24. ESI-mass spectrum of complex **8** in CH_3CN [[Calcd. m/z 791.207 (M−NO); Inset: (a) experimental and (b) simulated isotopic distribution pattern].

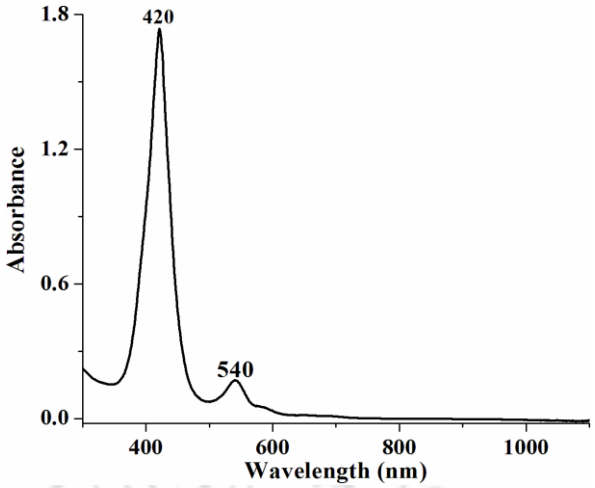

Figure A2.25. UV-visible spectrum of complex **8** in CH_2Cl_2 at −40 °C (13 μM).

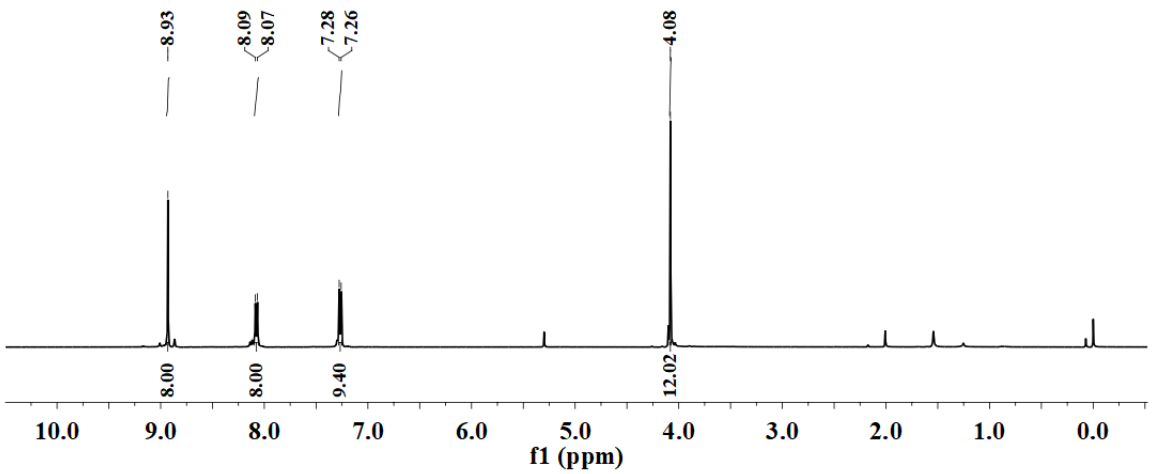

Figure A2.26. ^1H NMR spectrum of complex **8** in $CDCl_3$.

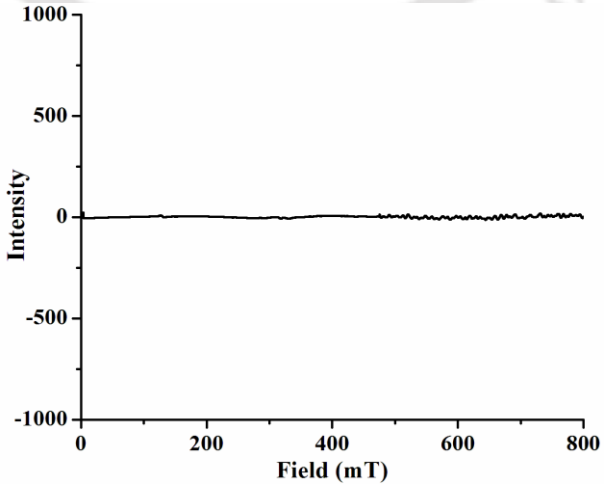

Figure A2.27. X-band EPR spectrum of complex **8** in CH_2Cl_2 at 77K.

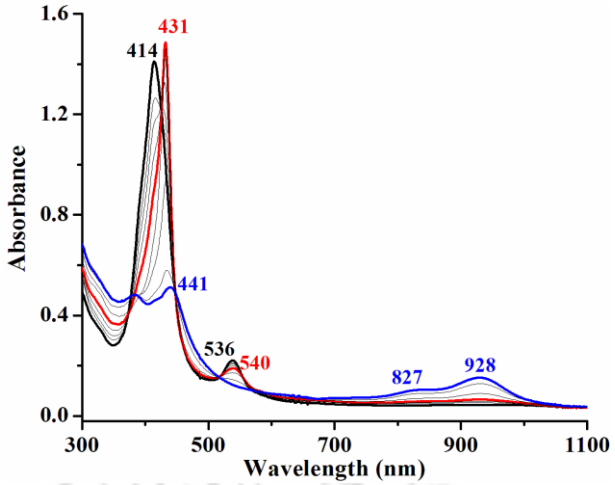

Figure A2.28. UV-visible spectral monitoring of complex **7** (black) and after addition of H_2O_2 (red) to result in complex **9** (red) in CH_2Cl_2 at −80 °C.

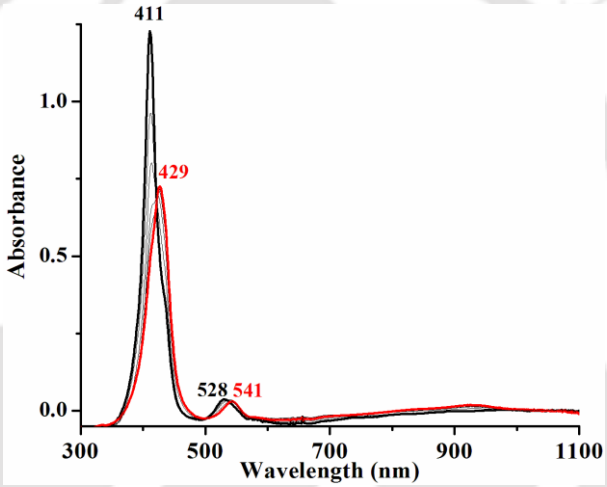

Figure A2.29. UV-visible spectra of complex **5** (black) and after addition of *m*CPBA (red) in CH_2Cl_2 at −40 °C.

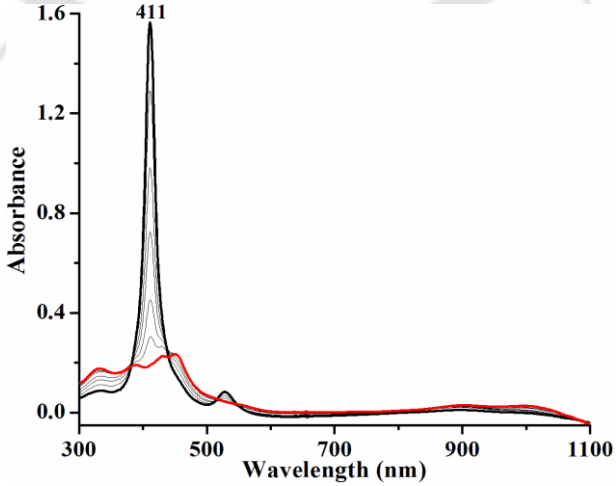

Figure A2.30. UV-visible spectra of complex **5** (black) and after addition of H_2O_2 (red) in CH_2Cl_2 at −40 °C.

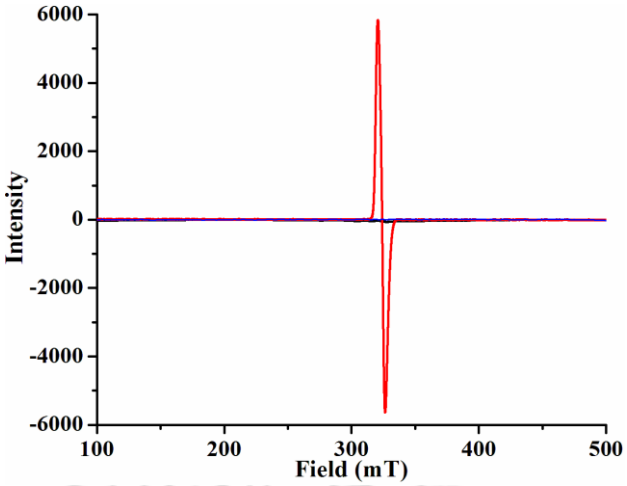

Figure A2.31. X-band EPR spectra of complex **7** (black), the intermediate (red) formed in the reaction of complex **7** and H_2O_2 and complex **9** (blue) in CH_2Cl_2 at 77K.

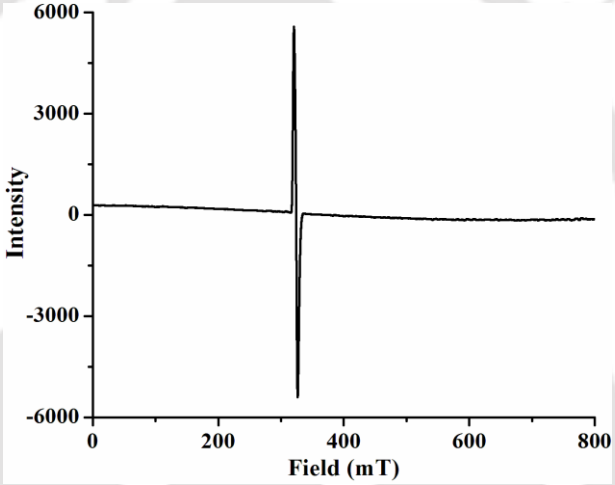

Figure A2.32. X-band EPR spectrum of the reaction of complex **5** and *m*CPBA in CH_2Cl_2 at 77K.

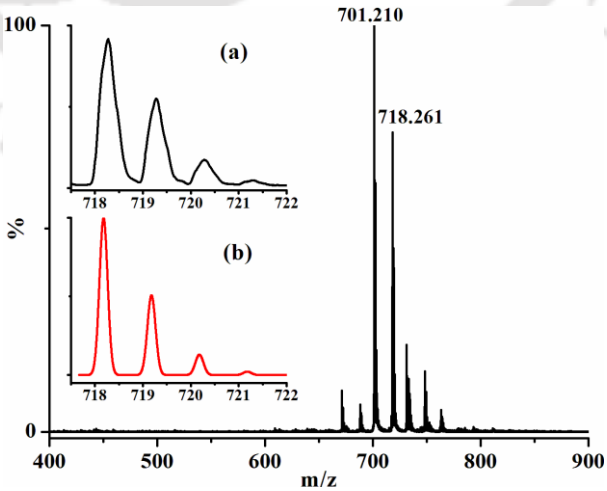

Figure A2.33. (ii) ESI-mass spectrum of the reaction mixture obtained from the reaction of complex **7** and H_2O_2 (in CH_2Cl_2 at −40 °C) in CH_3CN. [Inset: (a) experimental and (b) simulated isotopic distribution pattern].

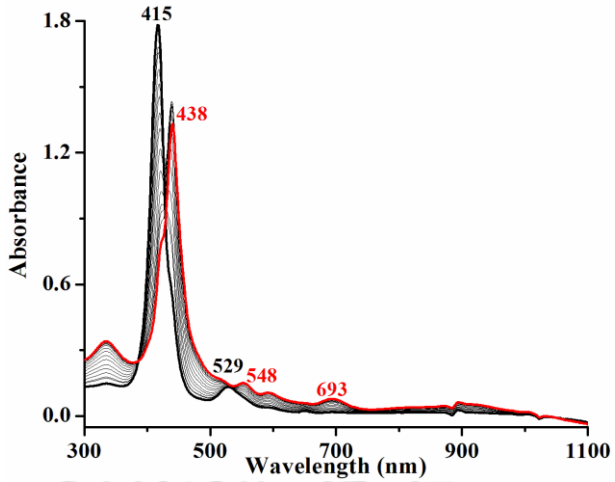

Figure A2.34. UV-visible spectra of **6** (black) and after addition of *m*CPBA (red) in CH_2Cl_2 at −40 °C.

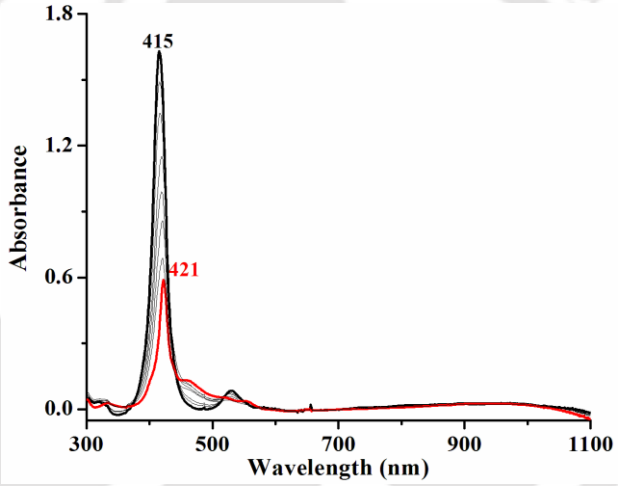

Figure A2.35. UV-visible spectra of **6** (black) and after addition of H_2O_2 (red) in CH_2Cl_2 at −40 °C.

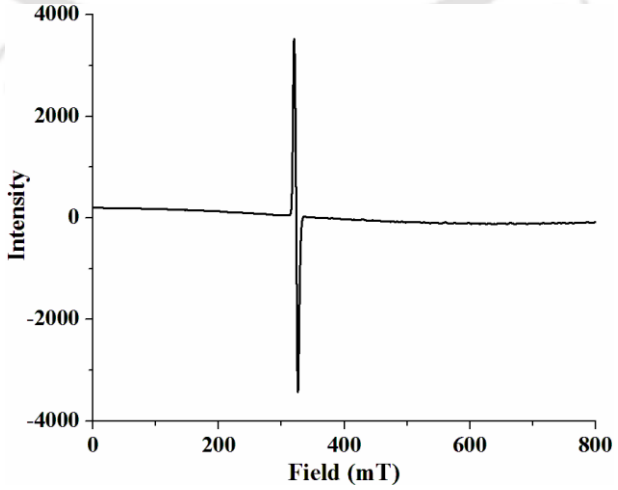

Figure A2.36. EPR spectrum of the reaction of **6** and *m*CPBA in CH_2Cl_2 at 77K.

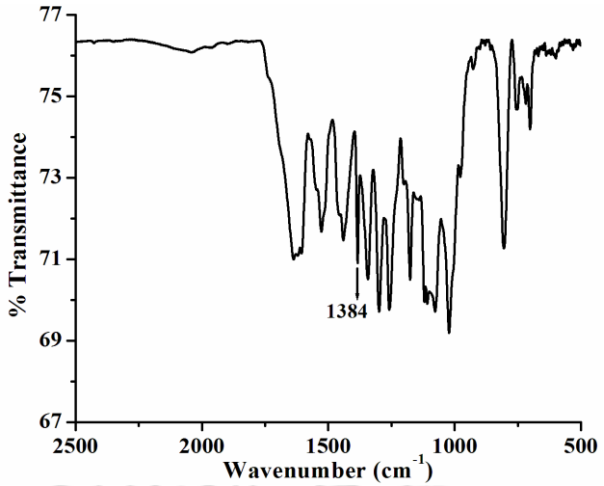

Figure A2.37. FT-IR spectrum of complex **9** in KBr.

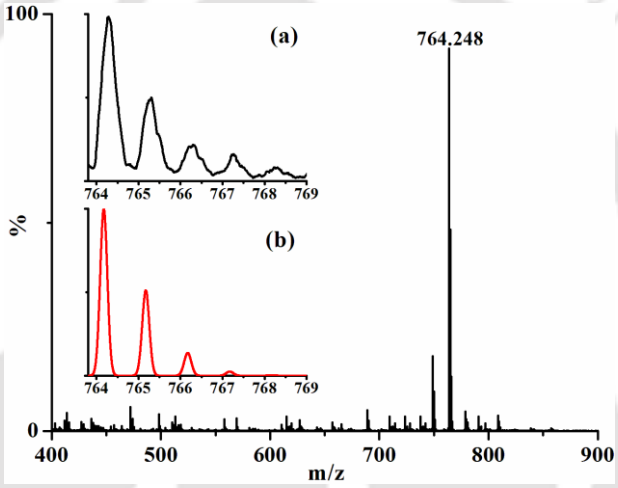

Figure A2.38. ESI-mass spectrum of complex **9** in CH_3CN [Calcd. m/z 763.163 (M+1); Inset: (a) experimental and (b) simulated isotopic distribution pattern].

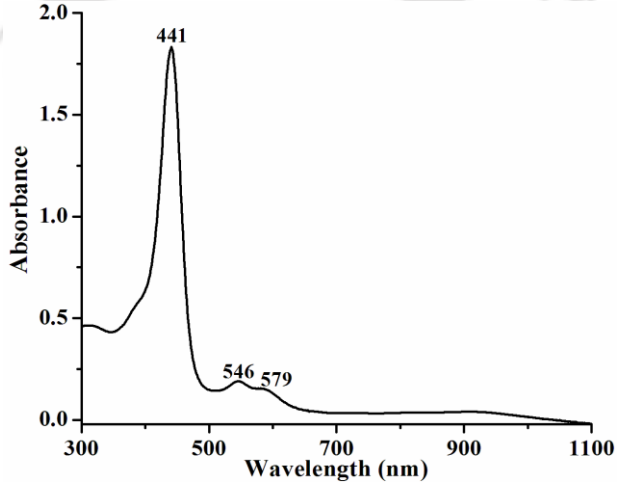

Figure A2.39. UV-visible spectrum of complex **9** in CH_2Cl_2 at room temperature (60 μM).

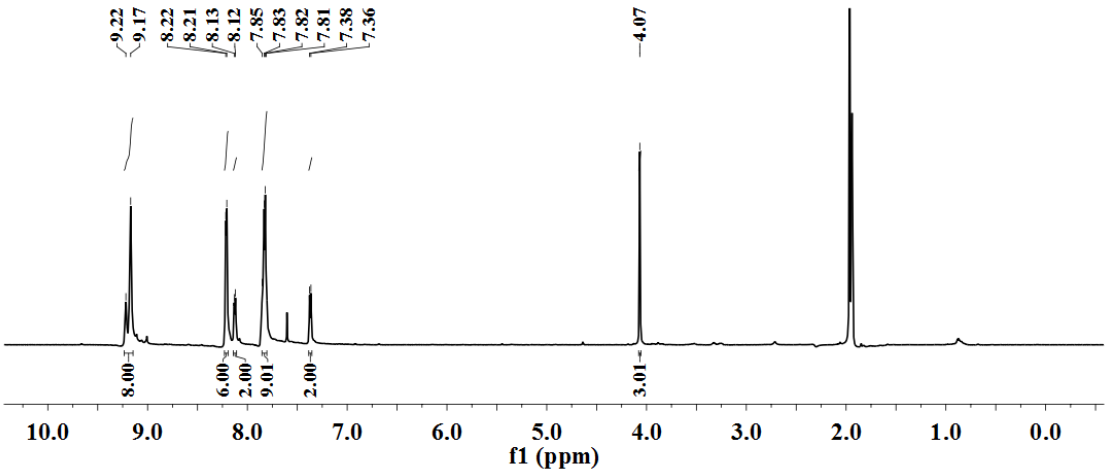

Figure A2.40. ^{1}H NMR spectrum of complex **9** in CD_3CN.

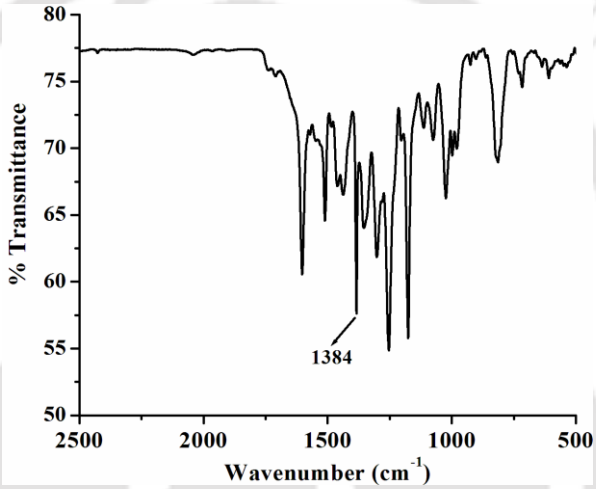

Figure A2.41. FT-IR spectrum of complex **10** in KBr.

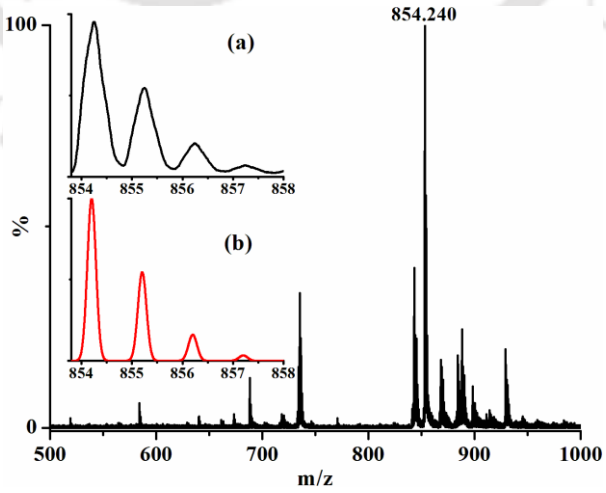

Figure A2.42. ESI-mass spectrum of complex **10** in CH_3CN [Calcd. m/z 853.195 (M+1); Inset: (a) experimental and (b) simulated isotopic distribution pattern].

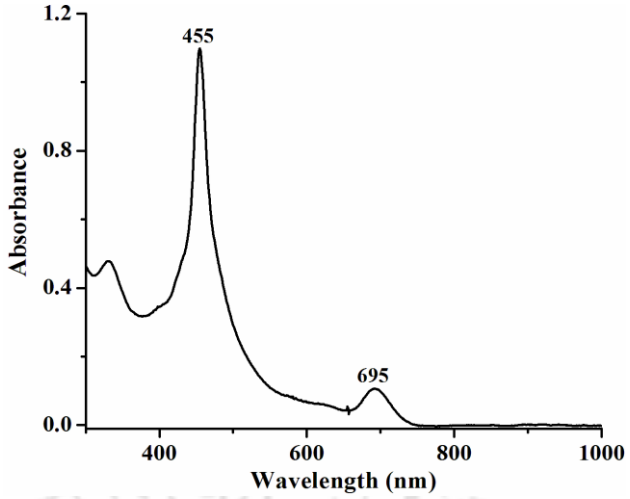

Figure A2.43. UV-visible spectrum of complex **10** in CH_2Cl_2 at room temperature (10 μM).

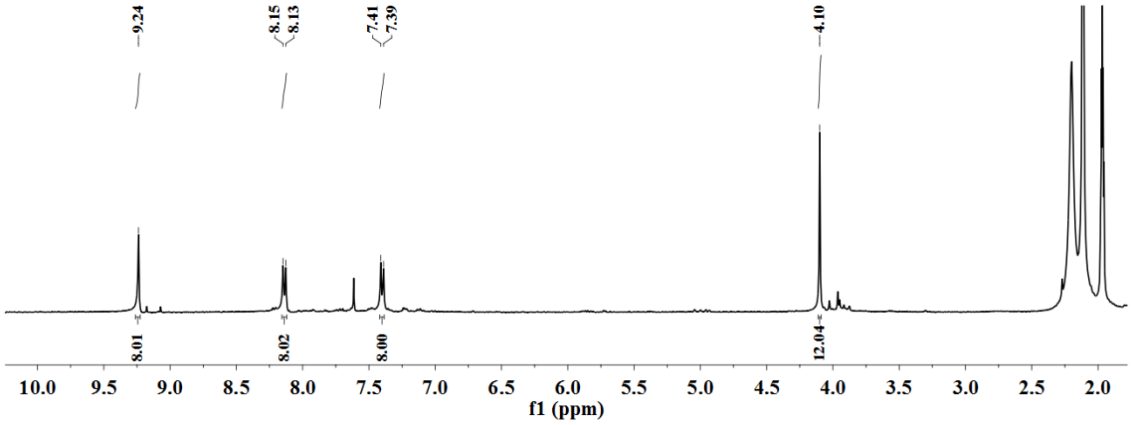

Figure A2.44. ^1H NMR spectrum of complex **10** in CD_3CN.

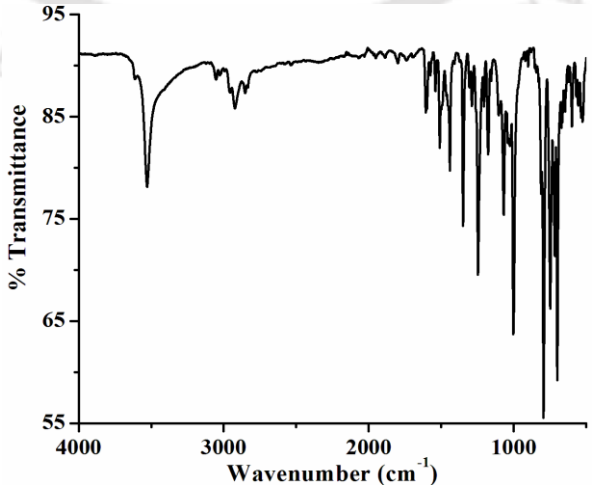

Figure A2.45. FT-IR spectrum of complex **11** in ATR.

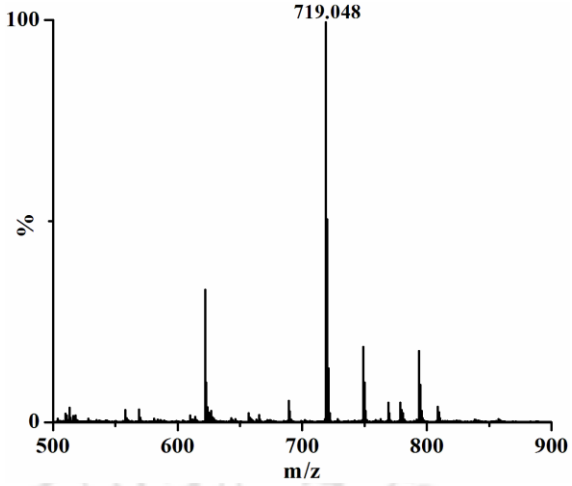

Figure A2.46. ESI-mass spectrum of complex **11** in CH_3CN [Calcd. m/z 718.178 (M+1)].

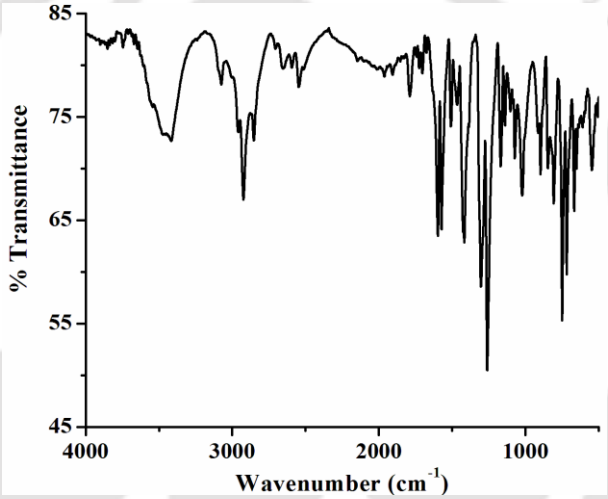

Figure A2.47. FT-IR spectrum of complex **12** in KBr.

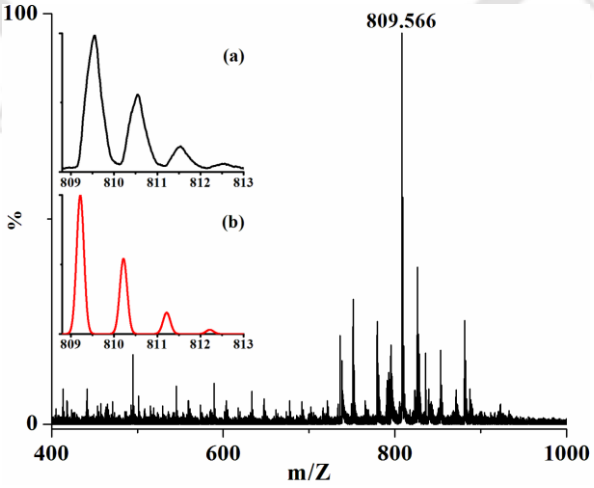

Figure A2.48. ESI-mass spectrum of complex **12** in CH_3CN [Calcd. m/z 808.210 (M+1)].

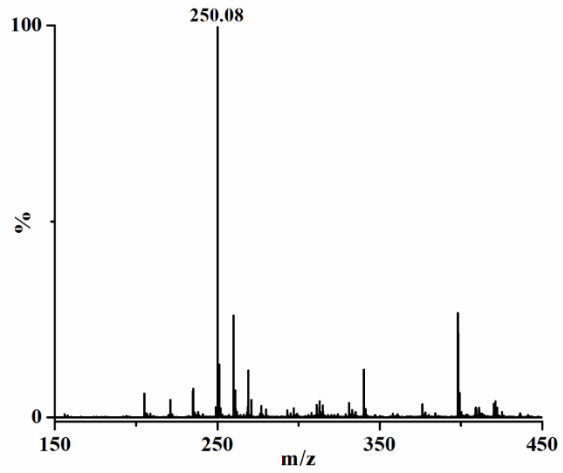

Figure A2.49. ESI-mass spectrum of **2,4-di-*tert*-butyl-6-nitrophenol** in CH_3CN [Calcd. m/z 251.15 (M−1)].

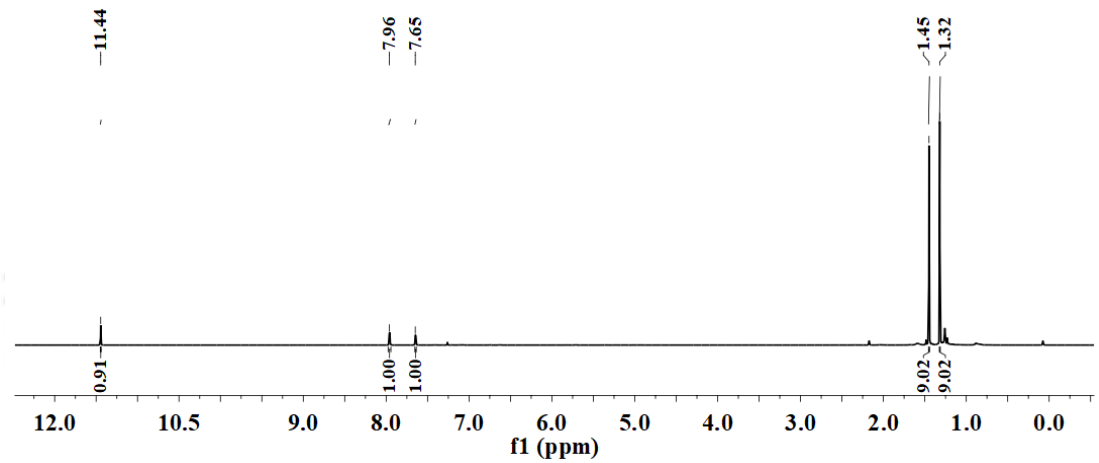

Figure A2.50. ^{1}H NMR spectrum of **2,4-di-*tert*-butyl-6-nitrophenol** in $CDCl_3$.

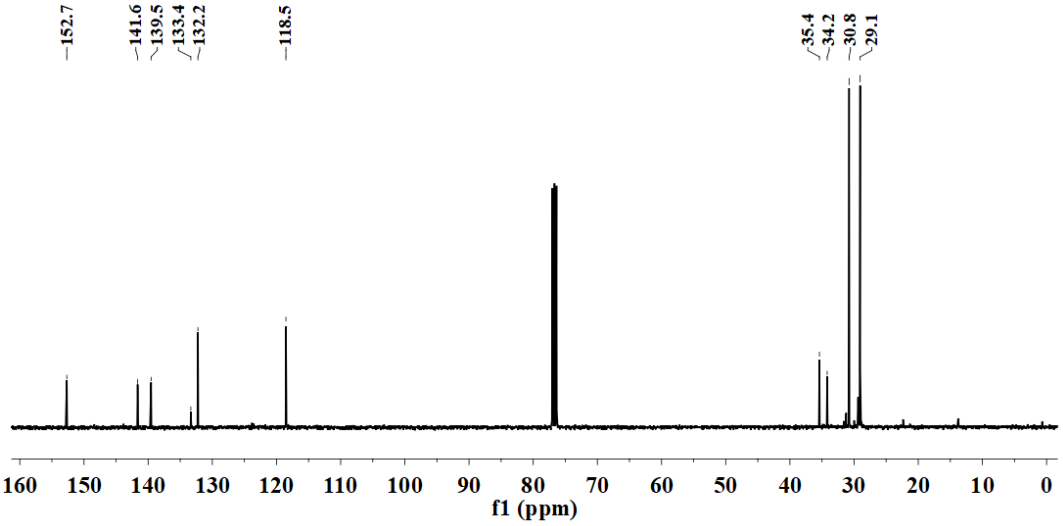

Figure A2.51. ^{13}C NMR spectrum of **2,4-di-*tert*-butyl-6-nitrophenol** in $CDCl_3$.

Table A2.1. Crystallographic data for complexes **6** and **8**.

	6	**8**
Formulae	$C_{48}H_{36}N_4O_4Co$	$C_{48}H_{36}N_5O_5Co$
Mol. wt.	791.74	821.75
Crystal system	Monoclinic	Orthorhombic
Space group	P 21/c	I b c a
Temperature /K	296(2)	293(2)
Wavelength /Å	0.71073	0.71073
a /Å	14.5454(14)	15.349(3)
b /Å	9.5684(9)	18.464(3)
c /Å	15.5717(15)	30.444(4)
α/°	90.00	90.00
β/°	99.547(4)	90.00
γ/°	90.00	90.00
V/ Å^3	2137.2(4)	8628(2)
Z	2	8
Density/Mgm^{-3}	1.230	1.265
Abs. Coeff. /mm^{-1}	0.449	0.449
Abs. correction	none	Multi-scan
F(000)	822	3408
Total no. of reflections	3770	3804
Reflections, $I > 2\sigma(I)$	3045	1662
Max. 2θ/°	24.998	24.998
Ranges (h, k, l)	$-17 \le h \le 17$ $-11 \le k \le 11$ $-18 \le l \le 18$	$0 \le h \le 18$ $0 \le k \le 21$ $0 \le l \le 36$
Complete to 2θ (%)	1.000	0.999
Refinement method	Full-matrix least-squares on F^2	Full-matrix least-squares on F^2
Goof (F^2)	1.097	0.905
R indices [$I > 2\sigma(I)$]	0.0913	0.0966
R indices (all data)	0.1178	0.1706

Table A2.2. Selected bond lengths (Å) of complexes **6** and **8**.

Atoms	**6**	**8**
Co1-N1	1.981(4)	1.962(5)
Co1-N2	1.985(4)	1.961(5)
Co1-N3		1.859(8)
N3-O3		1.166(6)
N1-C1	1.389(6)	1.400(8)
C1-C2	1.439(7)	1.432(8)
C2-C3	1.329(8)	1.324(9)
C4-C5	1.383(7)	1.392(9)
C5-C6	1.491(6)	1.511(9)

C6-C7	1.370(7)	1.316(11)
C9-O1	1.372(6)	1.434(10)
O1-C10	1.404(8)	1.385(14)

Table A2.3. Selected bond angles (˚) of complexes **6** and **8**.

Atoms	**6**	**8**
N1-Co1-N2	89.93(16)	89.30(19)
N1-Co1-N3		93.89(14)
Co1-N3-O3		119.1(9)
Co1-N1-C1	127.1(3)	126.7(4)
N1-C1-C2	109.9(4)	109.6(6)
C1-C2-C3	107.0(5)	108.0(7)
C2-C3-C4	108.1(5)	107.6(6)
C4-C5-C6	118.1(4)	118.1(6)
C9-O1-C10	117.6(5)	119.6(10)

Appendix III

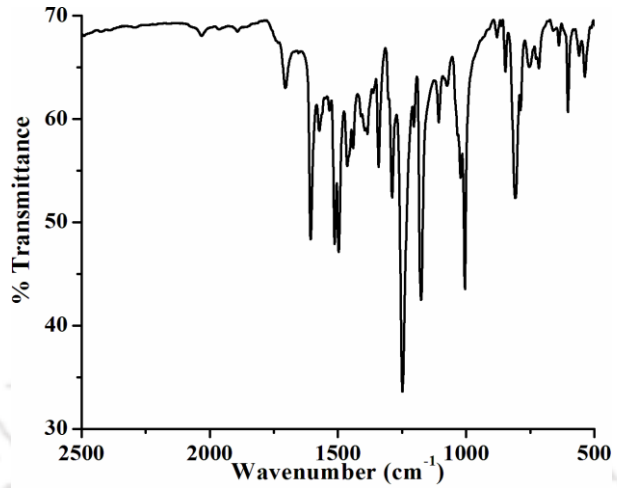

Figure A3.1. FT-IR spectrum of complex **13** in KBr.

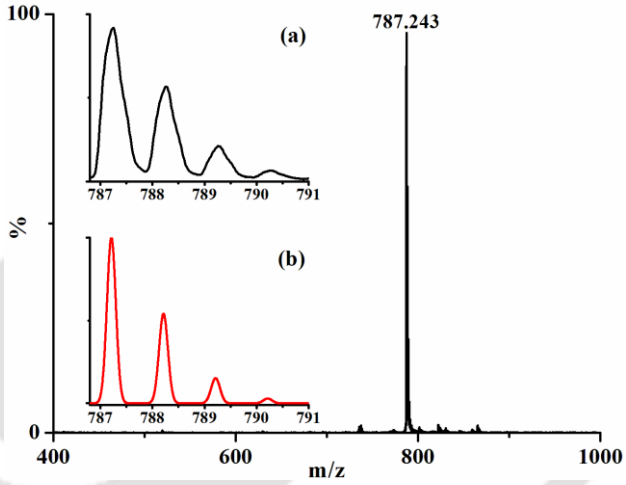

Figure A3.2. ESI-mass spectrum of complex **13** in CH_3CN. [Calcd. m/z 787.211 for $[(TMPP^{2-})Mn]^+$; Inset: (a) experimental and (b) simulated isotopic distribution pattern].

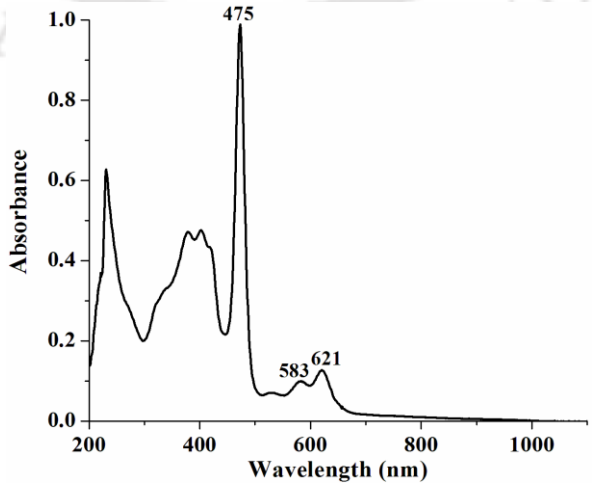

Figure A3.3. UV-visible spectrum of complex **13** in CH_2Cl_2 at room temperature (10 μM).

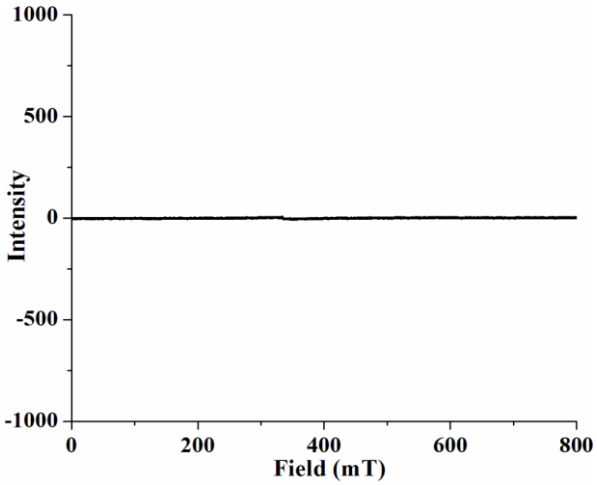

Figure A3.4. X-band EPR spectrum of complex **13** in CH_2Cl_2 at 77K.

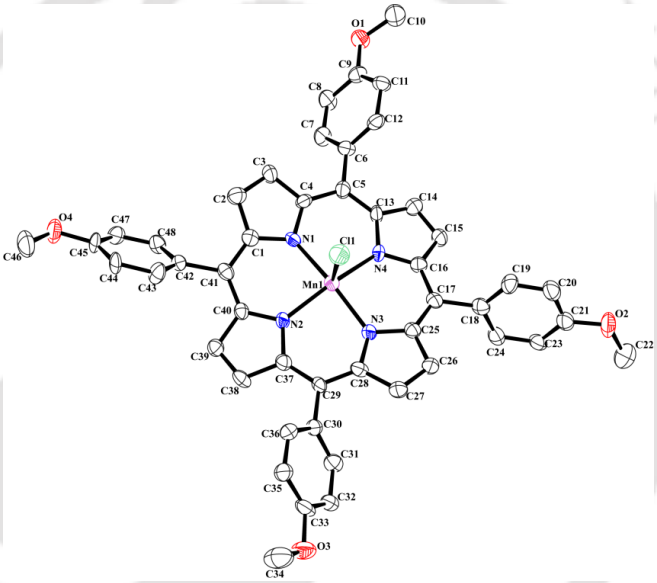

Figure A3.5. ORTEP diagram of complex **13** (30% thermal ellipsoid plot, H-atoms are omitted for clarity).

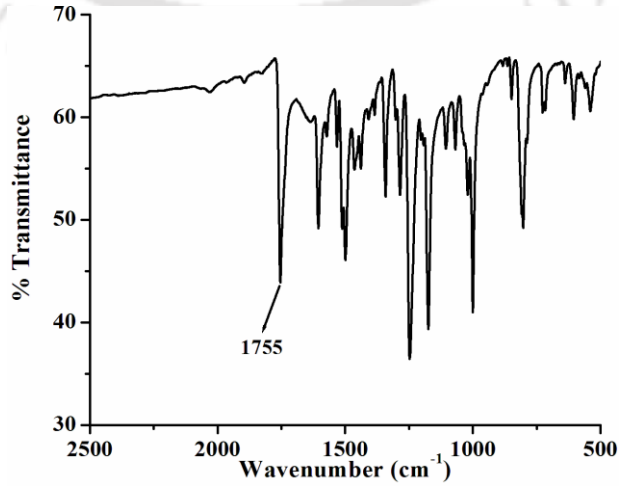

Figure A3.6. FT-IR spectrum of complex **14** in KBr.

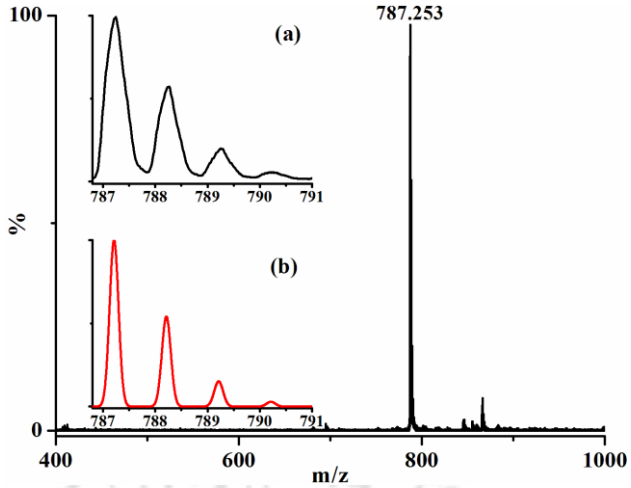

Figure A3.7. ESI-mass spectrum of complex **14** in CH_3CN. [Calcd. m/z 787.211 (M−NO); Inset: (a) experimental and (b) simulated isotopic distribution pattern].

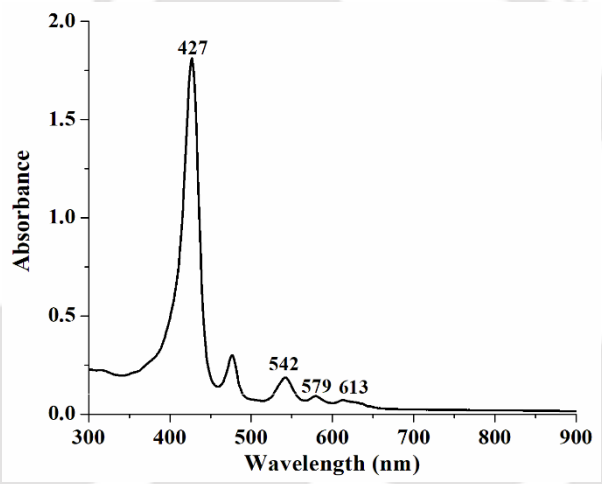

Figure A3.8. UV-visible spectrum of complex **14** in THF at room temperature (10 μM).

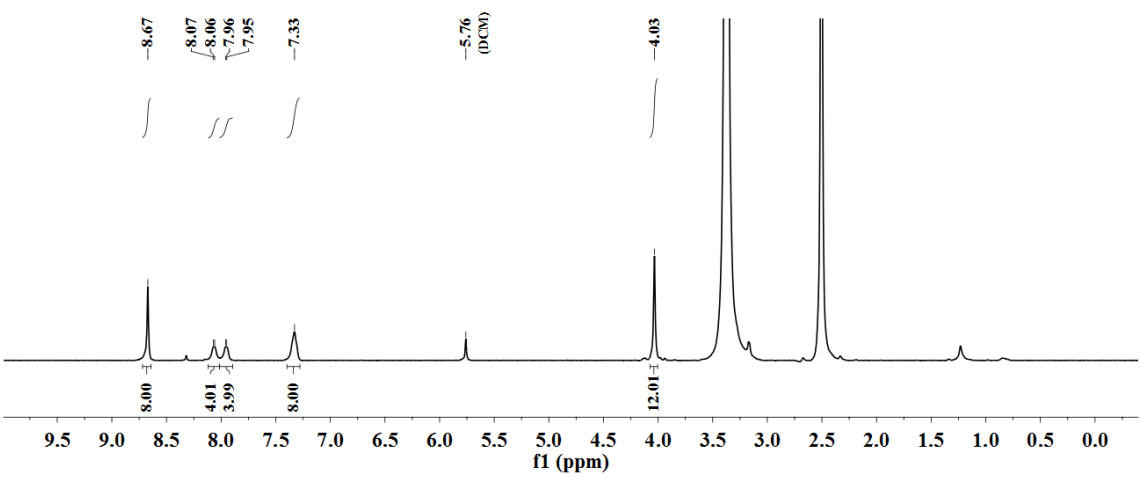

Figure A3.9. ^1H NMR spectrum of complex **14** in DMSO-d_6.

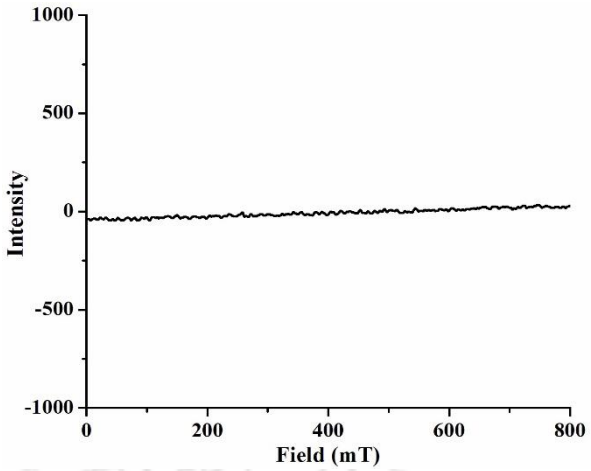

Figure A3.10. X-band EPR spectrum of complex **14** in THF at 77K.

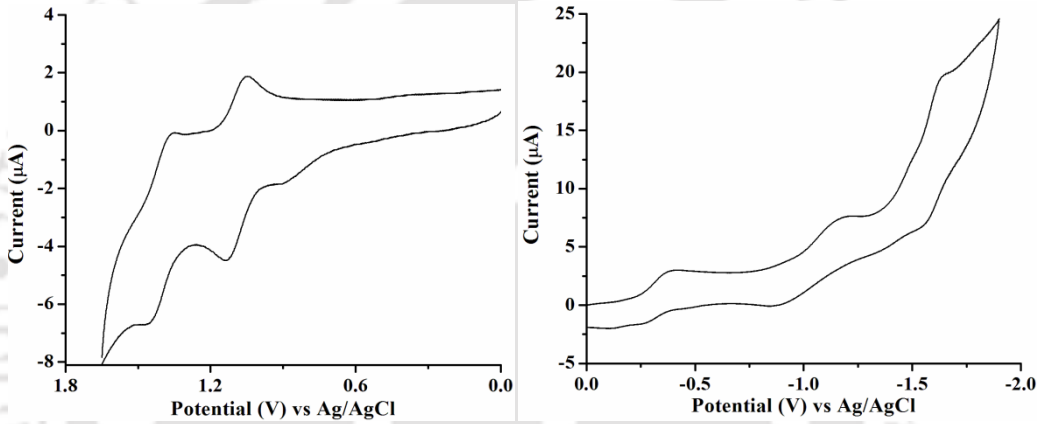

Figure A3.11. Cyclic voltammograms of complex **14** in CH_2Cl_2 *vs.* Ag/AgCl, supporting electrolyte 0.1 M TBAP, Scan rate 0.1 v/s.

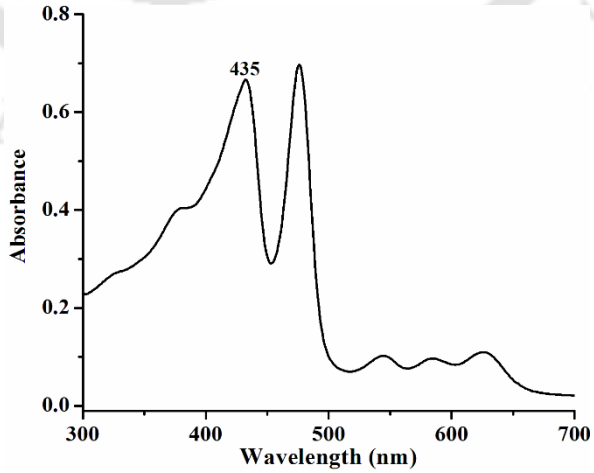

Figure A3.12: UV-visible spectrum of the reaction mixture of complex **13** and *t*BuOOH at −40 °C in THF.

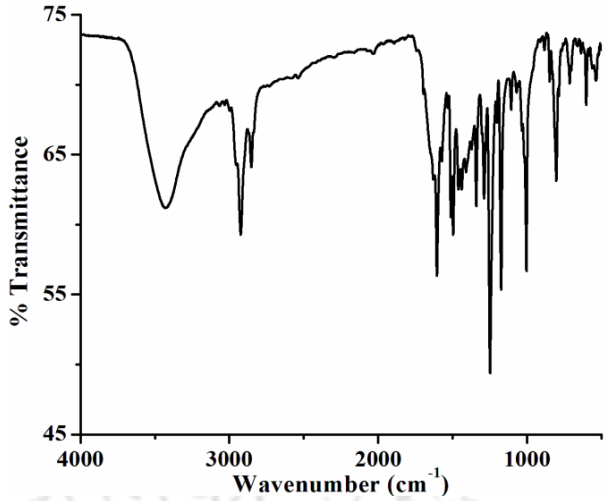

Figure A3.13. FT-IR spectrum of complex **15** in KBr.

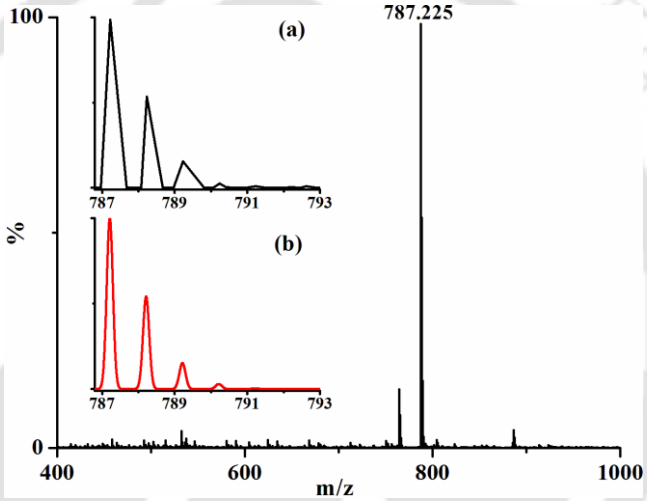

Figure A3.14. ESI-mass spectrum of complex **15** in CH_3CN. [Calcd. m/z 787.211 for $[(TMPP^{2-})Mn]^+$; Inset: (a) experimental and (b) simulated isotopic distribution pattern].

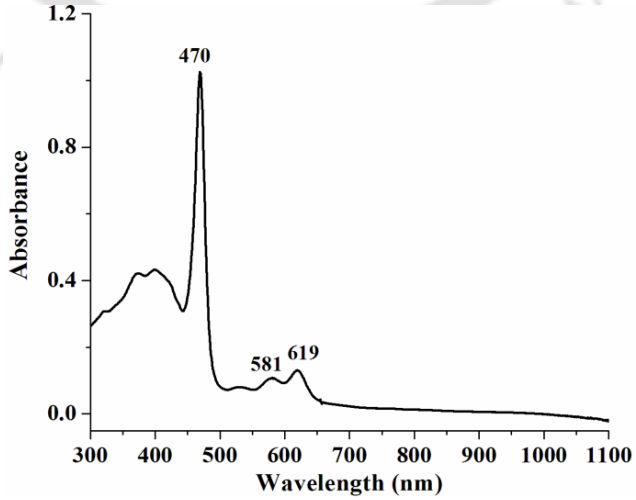

Figure A3.15. UV-visible spectrum of complex **15** in THF (10 μM).

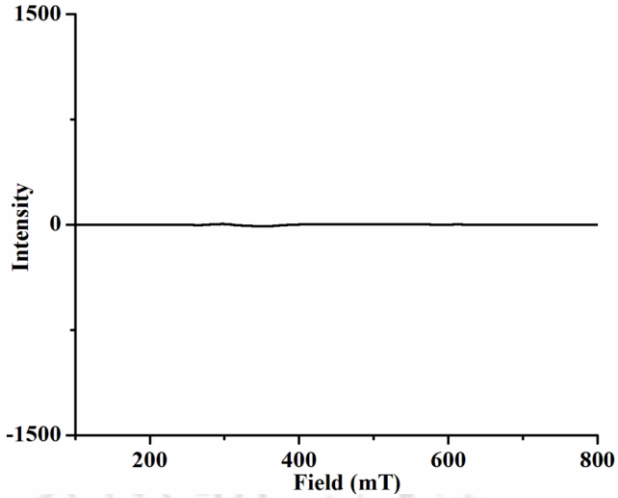

Figure A3.16. X-band EPR spectrum of complex **15** in THF at 77K.

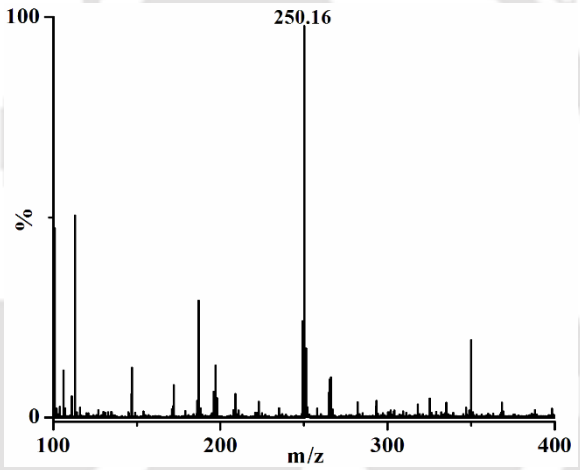

Figure A3.17. ESI-mass spectrum of **2,4-di-*tert*-butyl-6-nitrophenol** in CH_3CN [Calcd. m/z 251.15 (M−1)].

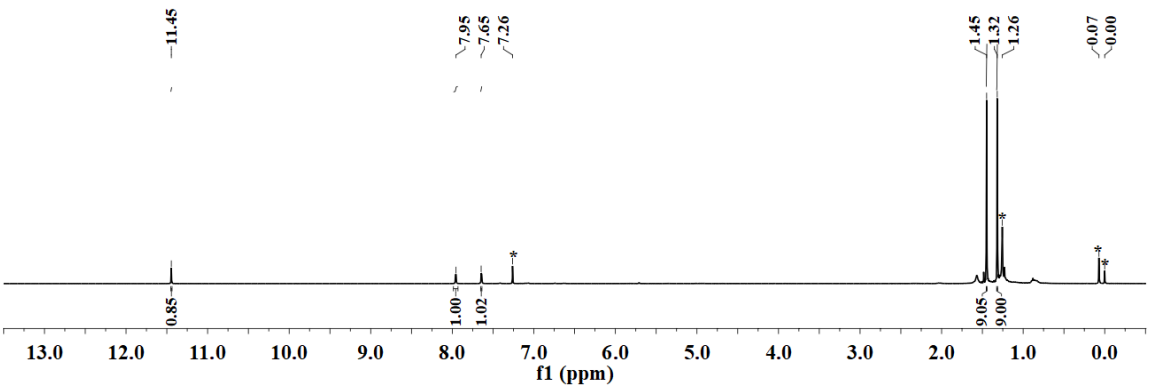

Figure A3.18. ^1H NMR spectrum of **2,4-di-*tert*-butyl-6-nitrophenol** in $CDCl_3$.

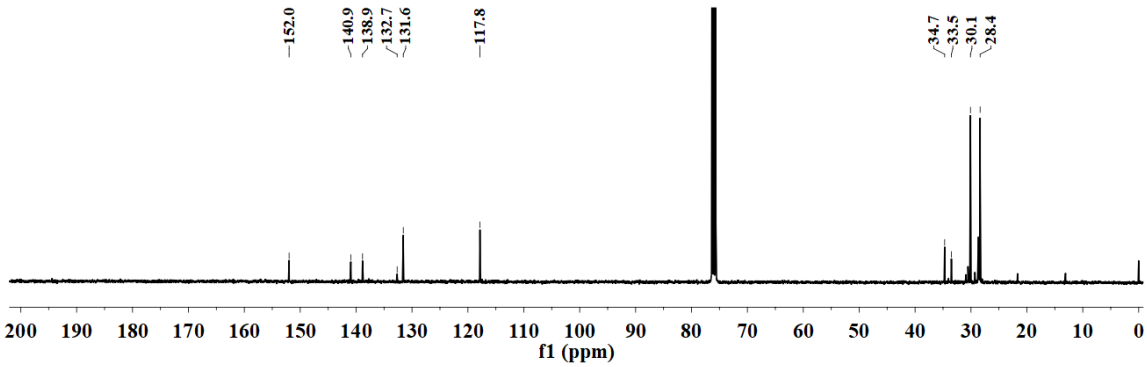

Figure A3.19. ^{13}C NMR spectrum of **2,4-di-*tert*-butyl-6-nitrophenol** in $CDCl_3$.

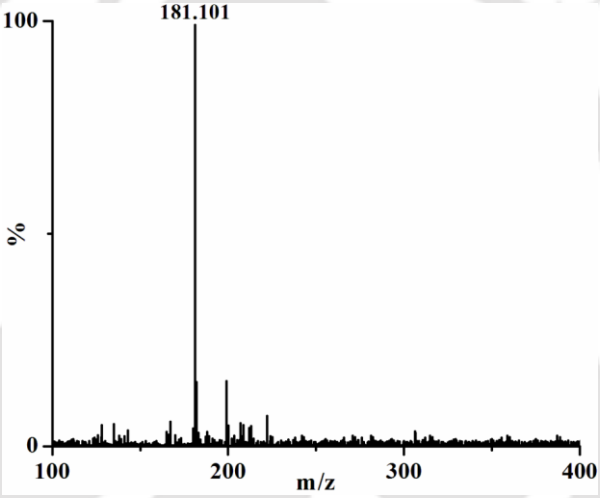

Figure A3.20. ESI-mass spectrum of **9-fluorenone** in CH_3CN [Calcd. m/z 180.057 (M+1)].

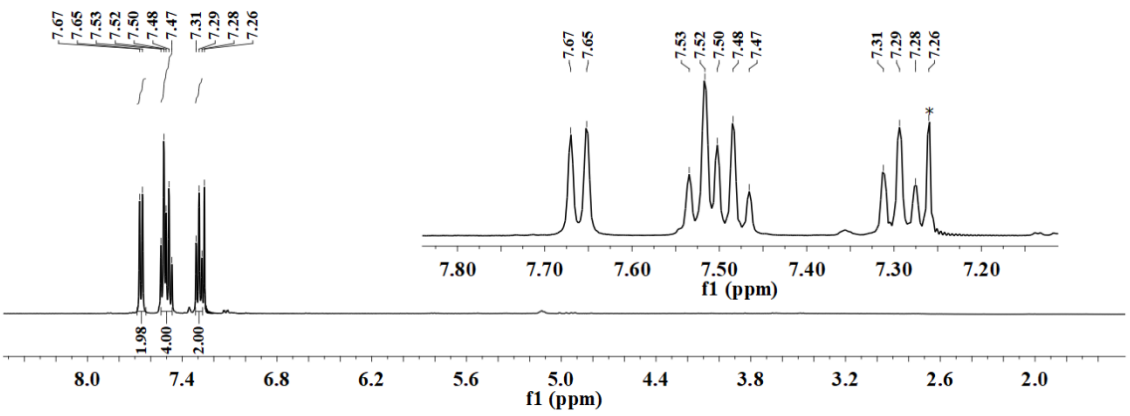

Figure A3.21. ^{1}H NMR spectrum of **9-fluorenone** in $CDCl_3$.

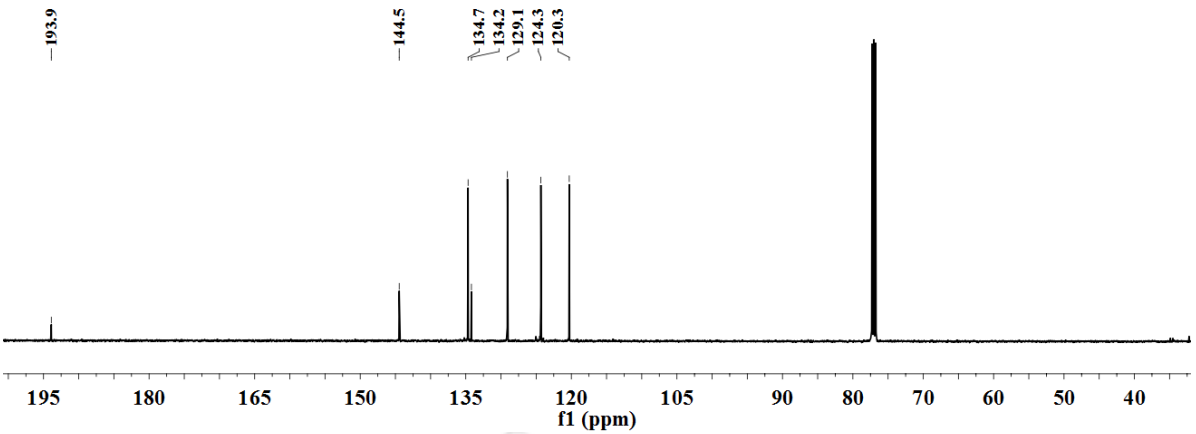

Figure A3.22. ^{13}C NMR spectrum of **9-fluorenone** in $CDCl_3$.

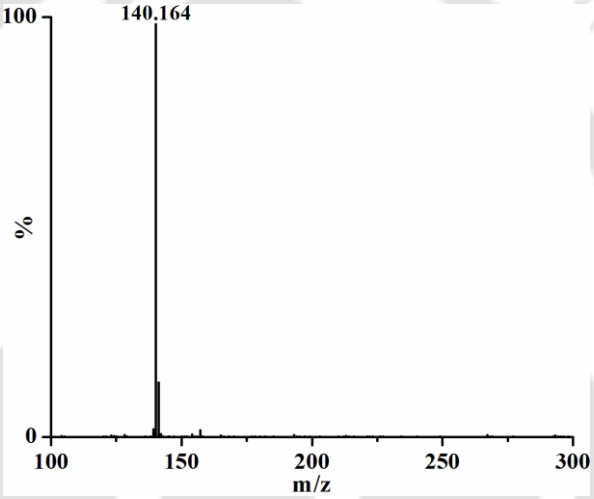

Figure A3.23. ESI-mass spectrum of **tmpNO$_3$** in CH_3CN [Calcd. m/z 140.144 for tmp^+].

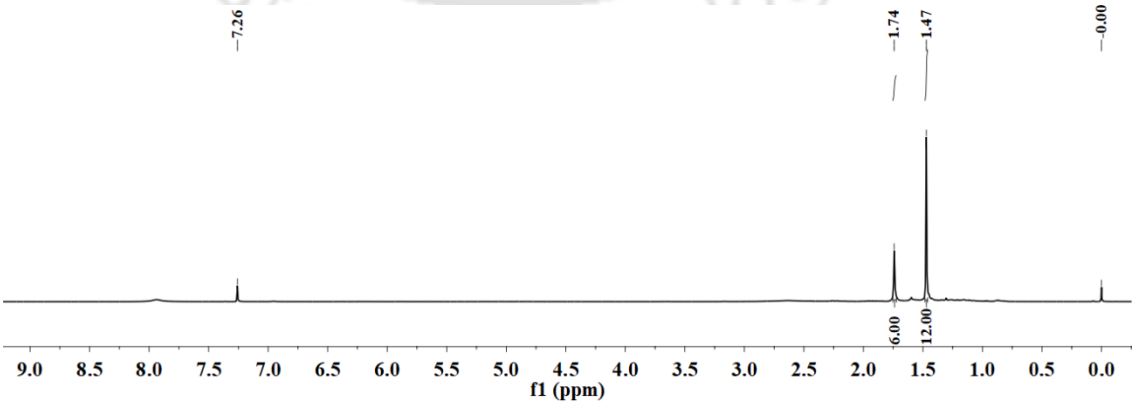

Figure A3.24. ^1H NMR spectrum of **tmpNO$_3$** in $CDCl_3$.

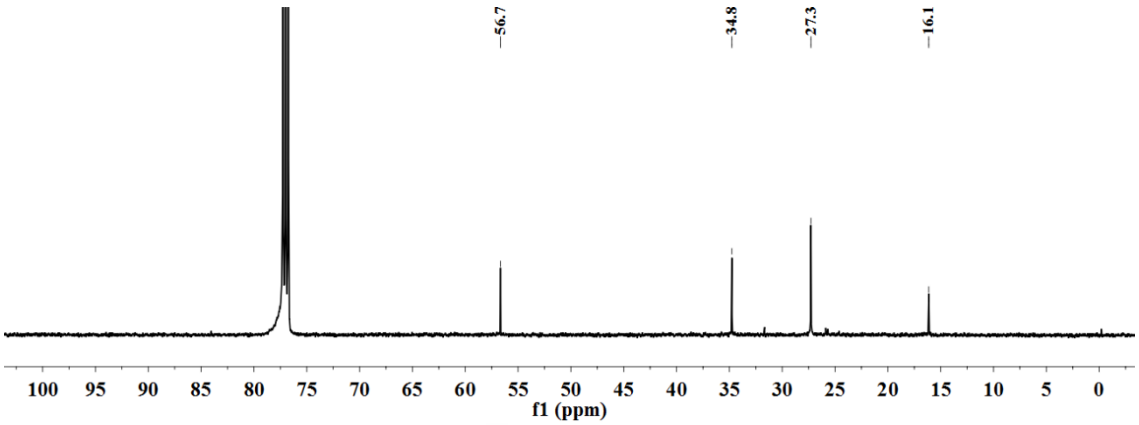

Figure A3.25. ^{13}C NMR spectrum of **tmpNO$_3$** in $CDCl_3$.

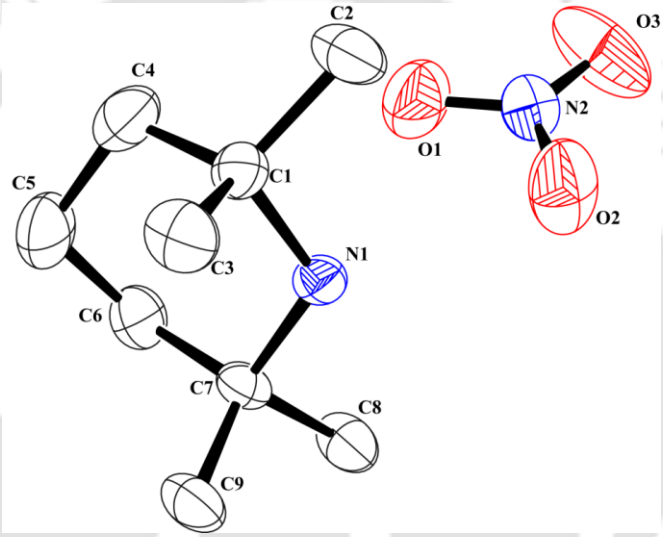

Figure A3.26. ORTEP diagram of **tmpNO$_3$** (30% thermal ellipsoid plot, H-atoms are omitted for clarity).

Table A3.1. Crystallographic data for complexes **13**, **15** and $tmpNO_3$.

	13	**15**	**tmpNO$_3$**
Formulae	$C_{48}H_{36}N_4O_4ClMn$	$C_{48}H_{38}N_4O_6Mn$	$C_9H_{18}N_2O_3$
Mol. wt.	823.20	821.76	202.25
Crystal system	Triclinic	Monoclinic	Orthorhombic
Space group	P-1	P 21/c	P c a 21
Temperature /K	296(2)	100(2)	293(2)
Wavelength /Å	0.71073	0.71073	0.71073
a /Å	14.993(3)	9.8(2)	15.56(4)
b /Å	15.017(4)	10.4(2)	9.90(2)
c /Å	22.655(5)	21.2(4)	15.75(4)

α/°	80.082(9)	90	90
β/°	70.695(6)	111.6(7)	90
γ/°	60.110(5)	90	90
V/ Å^3	4173.6(17)	2009(68)	2426(10)
Z	4	2	8
Density/Mgm^{-3}	1.310	1.358	1.107
Abs. Coeff. /mm^{-1}	0.429	0.385	0.083
Abs. correction	none	none	none
F(000)	1704	854	880
Total no. of reflections	13799	3524	4260
Reflections, $I > 2\sigma(I)$	4526	1310	2394
Max. 2θ/°	24.998	24.995	24.990
Ranges (h, k, l)	-16 ≤ h ≤ 17 -16 ≤ k ≤ 17 -26 ≤ l ≤ 26	-11 ≤ h ≤ 11 -12 ≤ k ≤ 12 -11 ≤ l ≤ 25	-18 ≤ h ≤ 18 -11 ≤ k ≤ 11 -18 ≤ l ≤ 18
Complete to 2θ (%)	0.940	0.998	1.000
Refinement method	Full-matrix least-squares on F^2	Full-matrix least-squares on F^2	Full-matrix least-squares on F^2
Goof (F^2)	0.986	0.841	1.175
R indices [$I > 2\sigma(I)$]	0.0906	0.0904	0.0790
R indices (all data)	0.2311	0.1702	0.1430

Table A3.2. Selected bond lengths (Å) of complexes **13**, **15** and $tmpNO_3$.

Atoms	**13**	**15**	**$tmpNO_3$**
Mn1-N1	1.999(7)	1.91(3)	
Mn1-N2	2.012(6)	1.95(3)	
Mn1-Cl1	2.355(3)		
Mn1-O1		2.13(3)	
N1-C1	1.399(10)		1.552(10)
C1-C2	1.449(11)	1.28(2)	1.549(11)
C2-C3	1.347(10)	1.37(3)	
C4-C5	1.401(11)	1.49(2)	1.563(13)
C5-C6	1.523(10)	1.32(2)	1.533(14)
C6-C7	1.349(10)	1.37(2)	1.511(11)
N2-O1			1.226(8)
N2-O2			1.250(9)

Table A3.3. Selected bond angles (˚) of complexes 1**3, 15** and $tmpNO_3$.

Atoms	**13**	**15**	**$tmpNO_3$**
N1-Mn1-N2	89.1(3)	86.8(12)	
N1-Mn1-N3	166.9(3)		
N1-Mn1-Cl1	96.0(2)		
Mn1-N1-C1	124.6(5)		

N1-Mn1-O1		90.5(14)	
C1-C2-C3	105.7(9)	105.2(11)	
C2-C3-C4	109.3(8)		
C5-C6-C7		119.3(14)	
C8-O2-C9		119.8(7)	
N1-C1-C4			107.8(7)
C1-C4-C5			112.8(8)
C4-C5-C6	116.7(8)		109.9(8)
O1-N2-O2			124.0(9)
O1-N2-O3			119.0(9)

Appendix IV

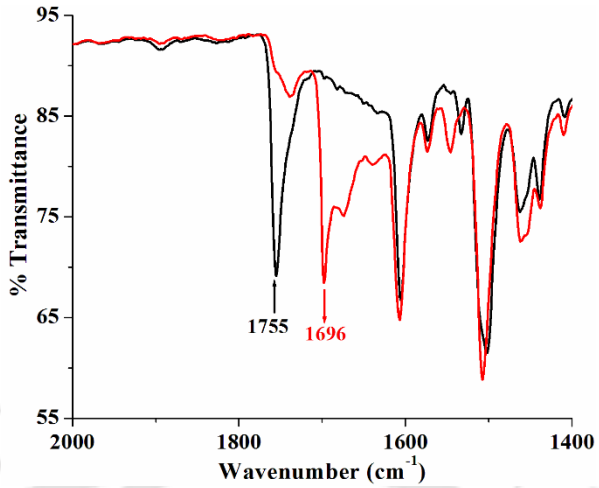

Figure A4.1. FT-IR spectra of the reaction of complex **14** (black) and complex **6** to give complex **8** (red) in KBr.

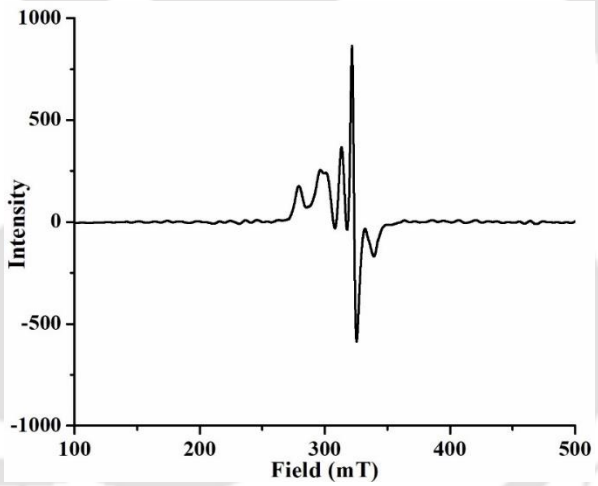

Figure A4.2. X-band EPR spectrum of the reaction mixture of complex **14** and HBF_4 at 77K.

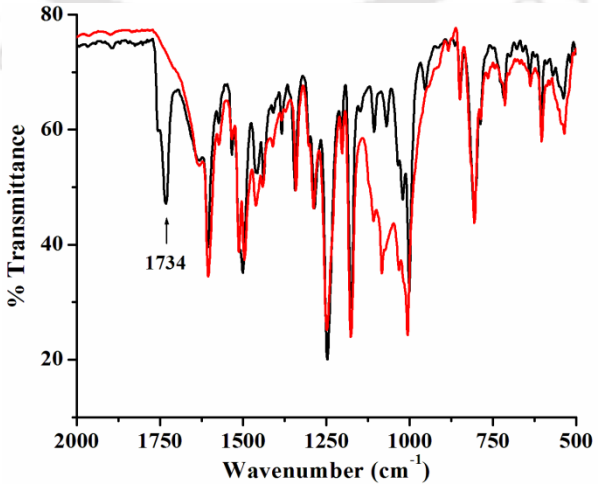

Figure A4.3. FT-IR spectra of complex **14** (black) and after addition of HBF_4 (red) in CH_2Cl_2.

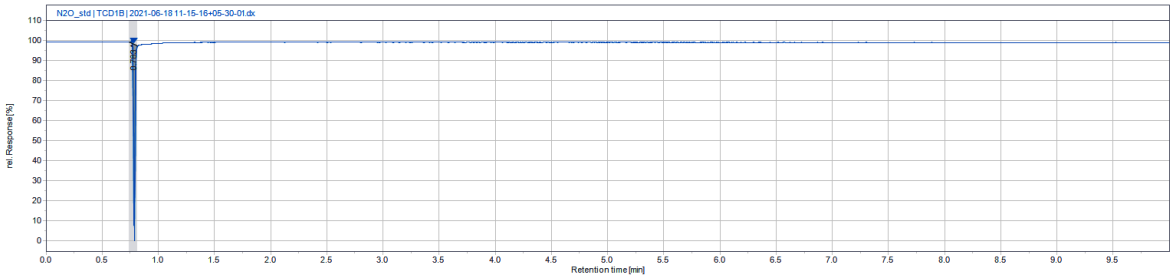

(a)

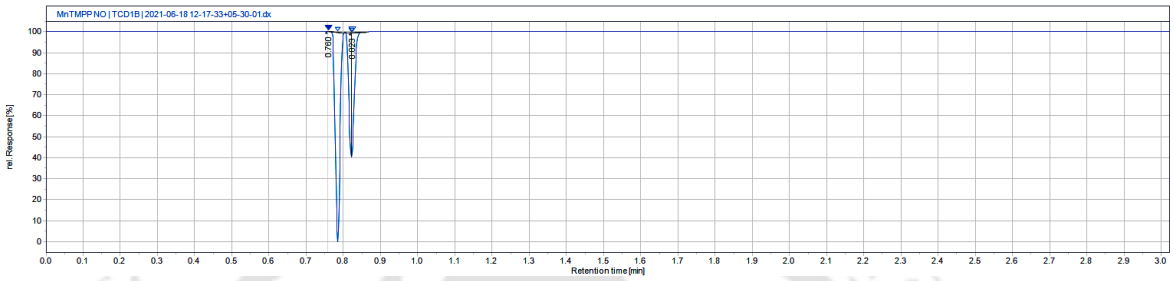

(b)

Figure A4.4. Gas chromatograms for (a) standard N_2O. (retention time = 0.78 min) and, (b) the headspace gas of the reaction mixture of complex **14** and HBF_4. (retention time = 0.78 and 0.82 min)

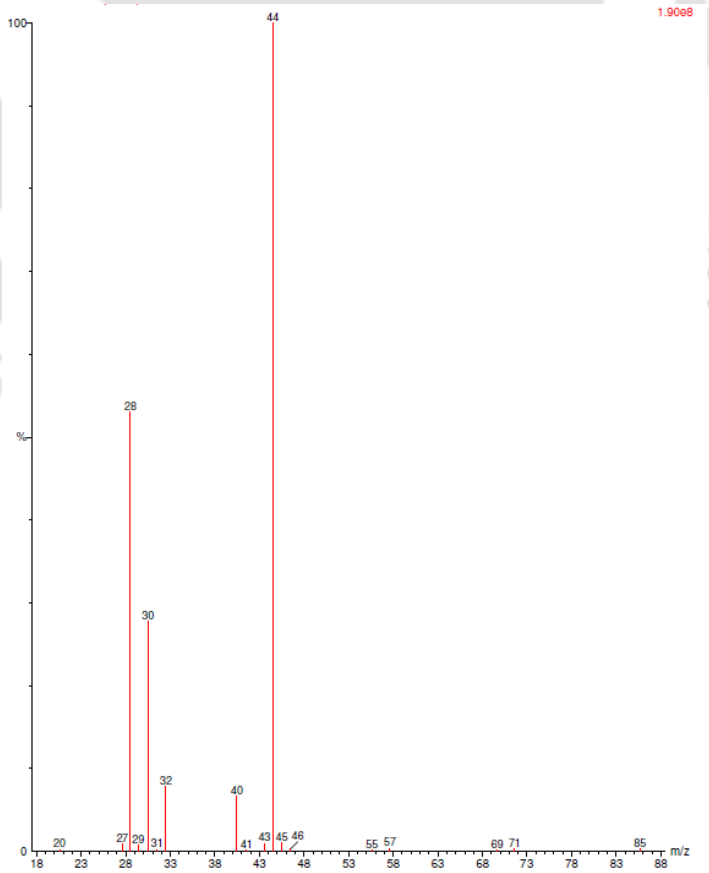

Figure A4.5. GC-mass spectrum of the headspace gas of the reaction mixture of complex **14** and HBF_4.

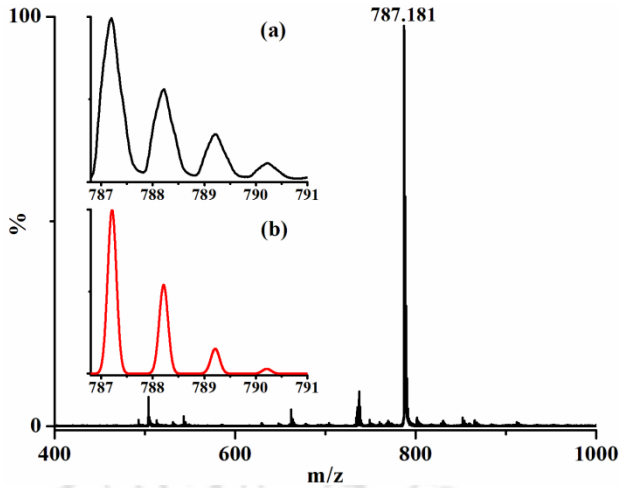

Figure A4.6. ESI-mass spectrum of complex **16** in acetonitrile. [Calcd. m/z 787.211 for $[Mn(TMPP^{2-})]^{+}$; Inset: (a) experimental and (b) simulated isotopic distribution pattern].

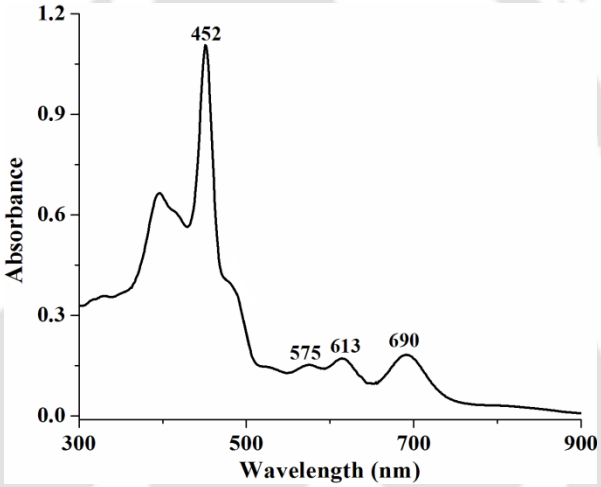

Figure A4.7. UV-visible spectrum of complex **16** in CH_2Cl_2 at room temperature (12 μM).

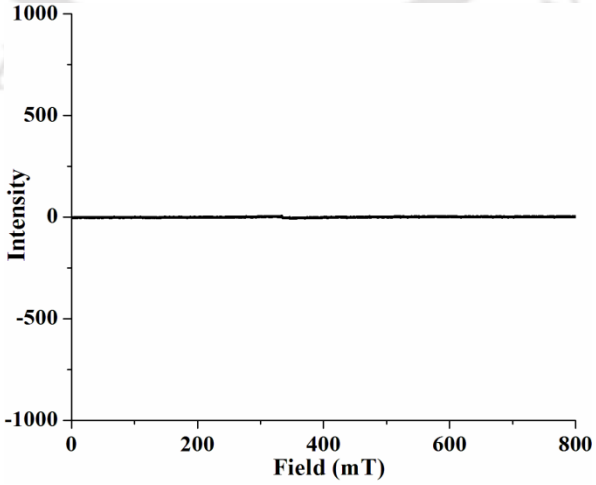

Figure A4.8. X-band EPR spectrum of complex **16** in CH_2Cl_2 at 77K.

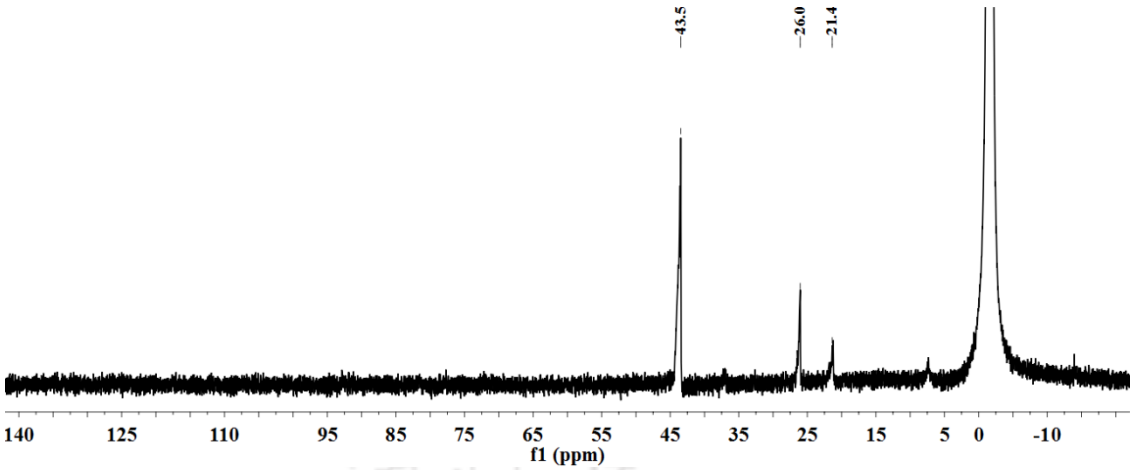

Figure A4.9. ^{31}P NMR spectrum of reaction mixture from the reaction of complex **14**, HBF_4 and Ph_3P in CD_3CN.

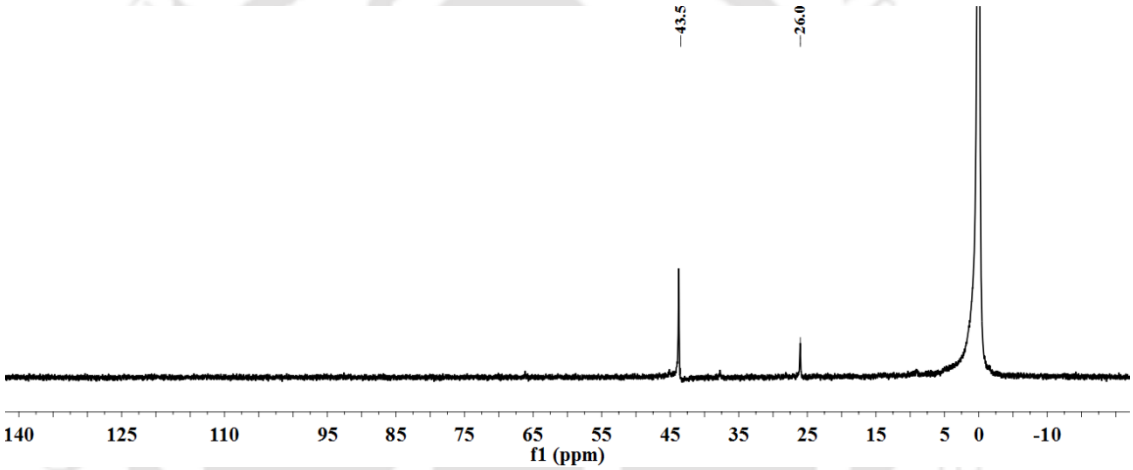

Figure A4.10. ^{31}P NMR spectrum of reaction mixture from the reaction of complex **13**, HBF_4 and Ph_3P in CD_3CN.

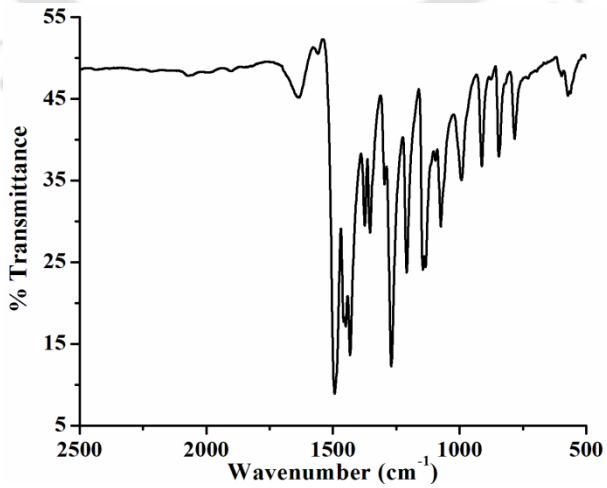

Figure A4.11. FT-IR spectrum of **$[Fe^{III}(dtc)_3]$** in KBr.

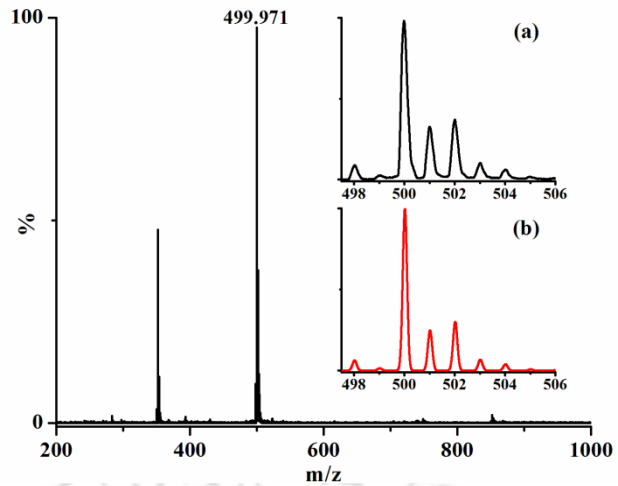

Figure A4.12. ESI-mass spectrum of **[Fe^{III}(dtc)$_3$]** in acetonitrile. [Calcd. m/z 500.011 (molecular ion peak); Inset: (a) experimental and (b) simulated isotopic distribution pattern].

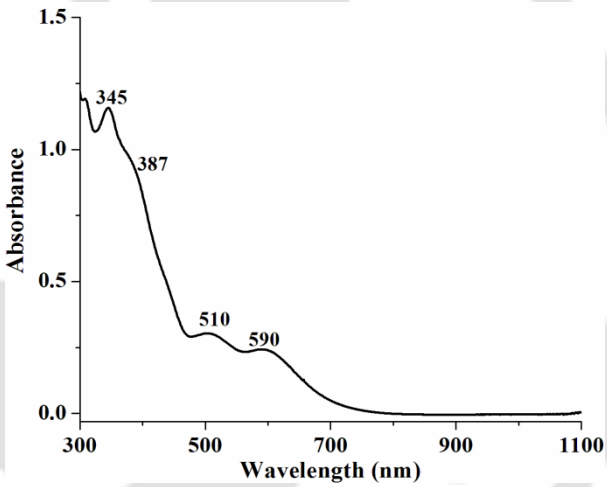

Figure A4.13. UV-visible spectrum of **[Fe^{III}(dtc)$_3$]** in CH_2Cl_2 at room temperature (80 μM).

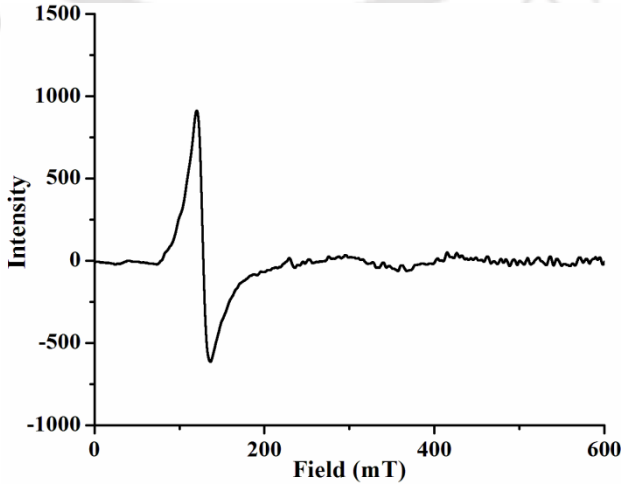

Figure A4.14. X-band EPR spectrum of **[Fe^{III}(dtc)$_3$]** in CH_2Cl_2 at 77K.

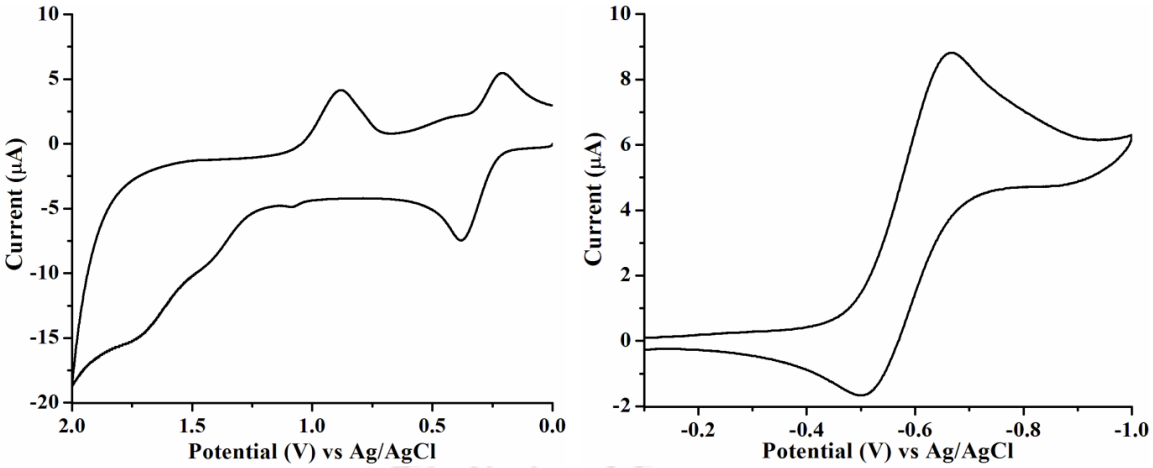

Figure A4.15. Cyclic voltammograms of **[Fe^{III}(dtc)$_3$]** in CH_2Cl_2 *vs.* Ag/AgCl, 0.1 M TBAP, Scan rate 0.1 V/s.

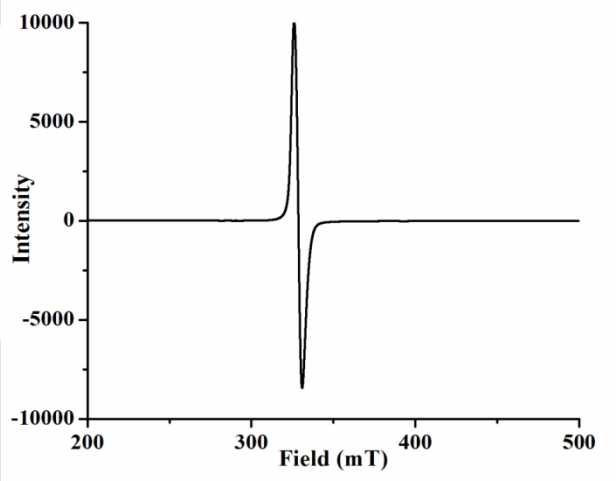

Figure A4.16. X-band EPR spectrum of reaction mixture from the reaction of complex **14** and **[Fe^{III}(dtc)$_3$]** in CH_2Cl_2 at 77K.

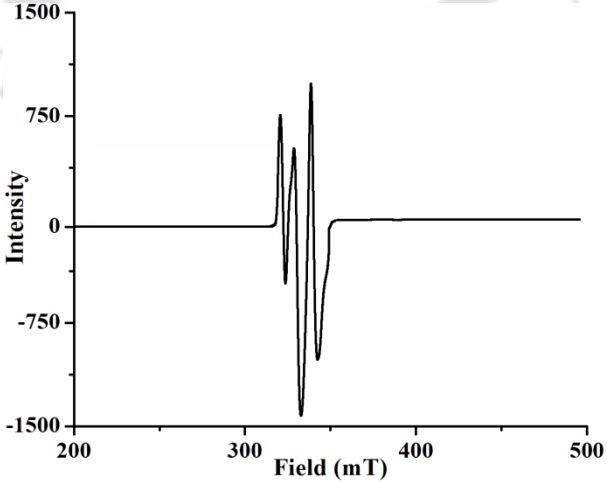

Figure A4.17. X-band EPR spectrum of reaction mixture from the reaction of complex **14** and **[Fe^{III}(dtc)$_3$]** in DMSO at room temperature.

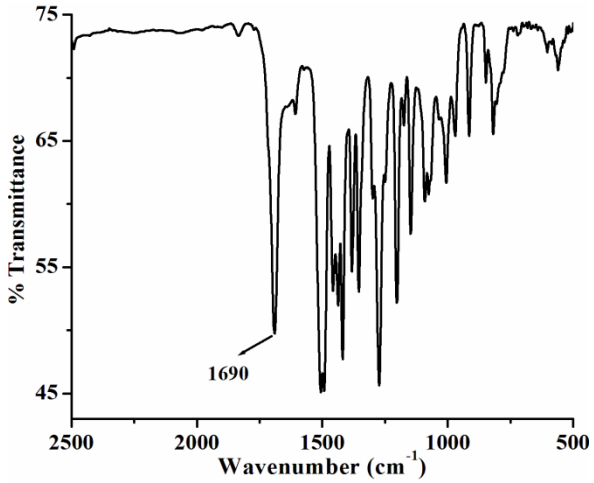

Figure A4.18. FT-IR spectrum of **[Fe(dtc)$_2$(NO)]** in KBr.

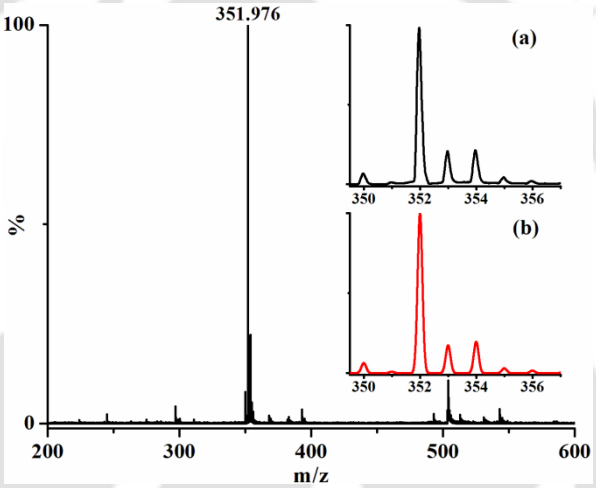

Figure A4.19. ESI-mass spectrum of **[Fe(dtc)$_2$(NO)]** in acetonitrile. [Calcd. m/z 351.986 (M−NO); Inset: (a) experimental and (b) simulated isotopic distribution pattern].

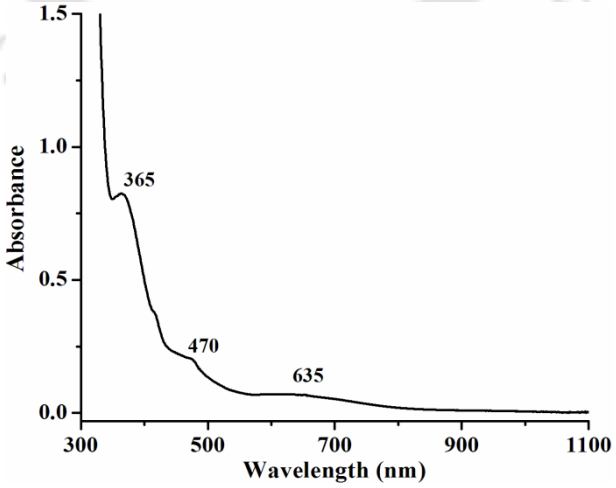

Figure A4.20. UV-visible spectrum of **[Fe(dtc)$_2$(NO)]** in CH_2Cl_2 at room temperature.

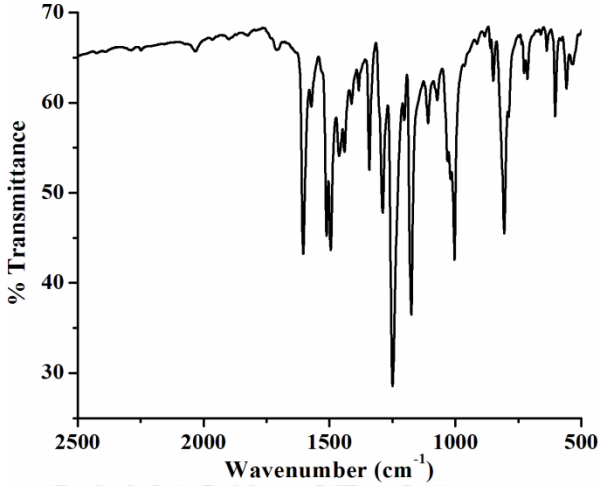

Figure A4.21. FT-IR spectrum of **[Mn^{III}($TMPP^{2-}$)](dtc)** in KBr.

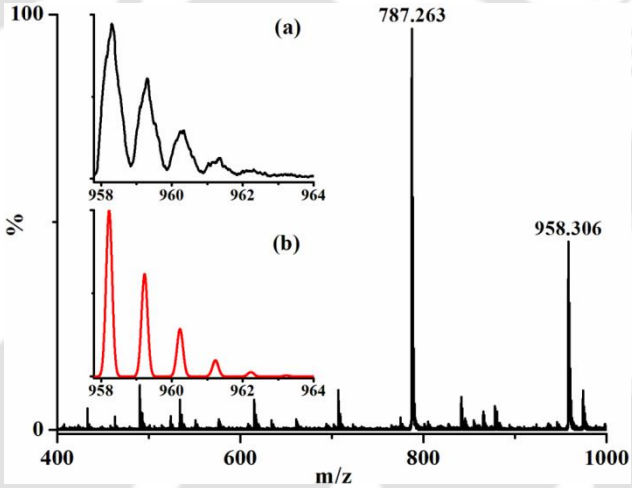

Figure A4.22. ESI-mass spectrum of **[Mn^{III}($TMPP^{2-}$)](dtc)** in methanol. [Calcd. m/z 958.227 (M+Na); Inset: (a) experimental and (b) simulated isotopic distribution pattern].

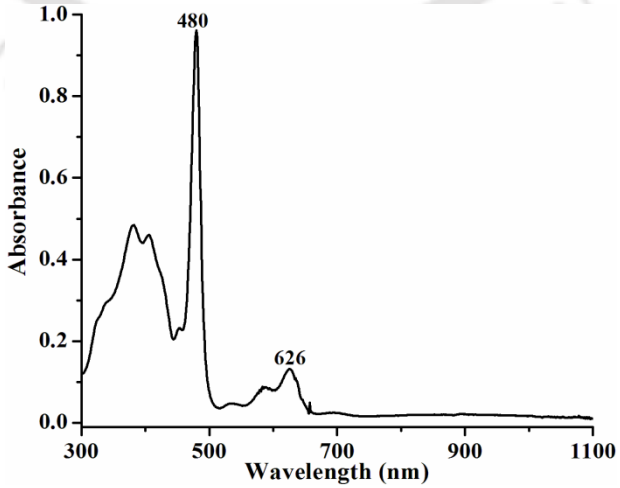

Figure A4.23. UV-visible spectrum of **[Mn^{III}($TMPP^{2-}$)](dtc)** in CH_2Cl_2 at room temperature (10 μM).

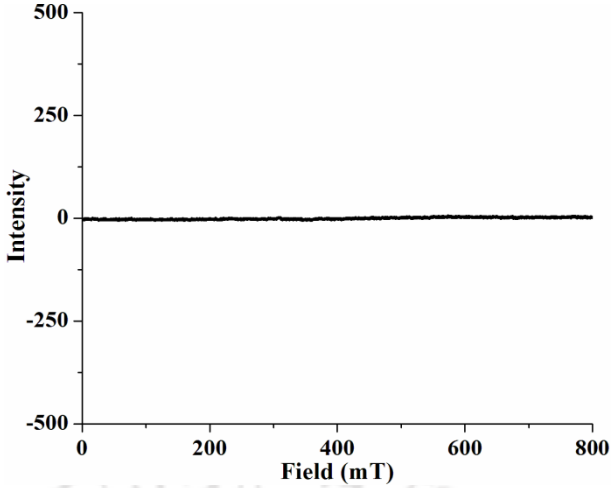

Figure A4.24. X-band EPR spectrum of **[Mn^{III}($TMPP^{2-}$)](dtc)** in CH_2Cl_2 at 77K.

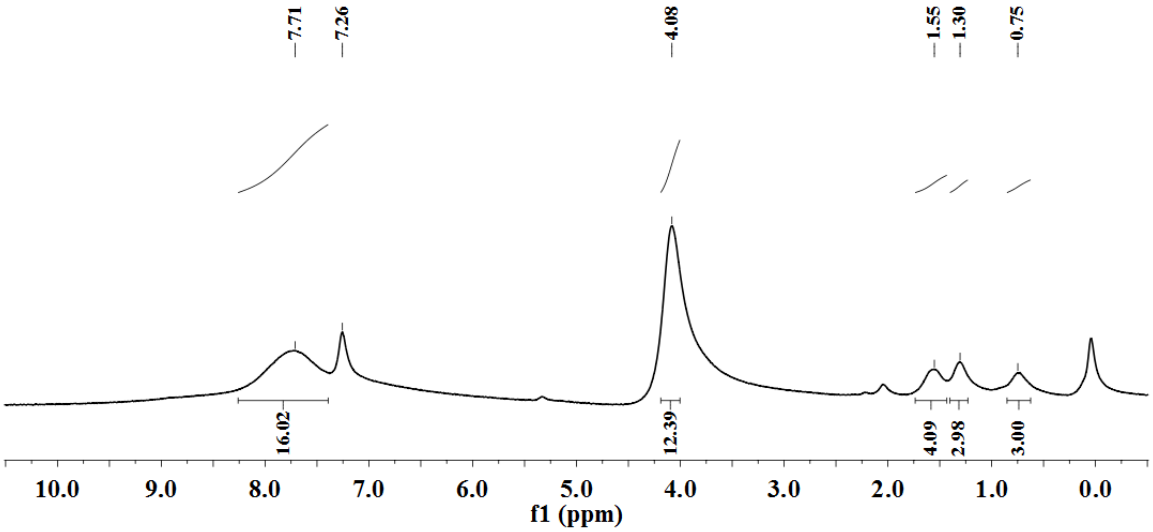

Figure A4.25. ^1H NMR spectrum of **[Mn^{III}($TMPP^{2-}$)](dtc)** in $CDCl_3$.

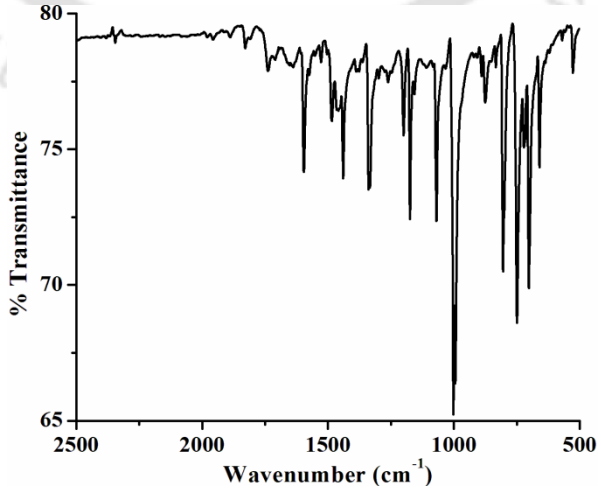

Figure A4.26. FT-IR spectrum of **[Fe^{III}(TPP^{2-})(Cl)]** in KBr.

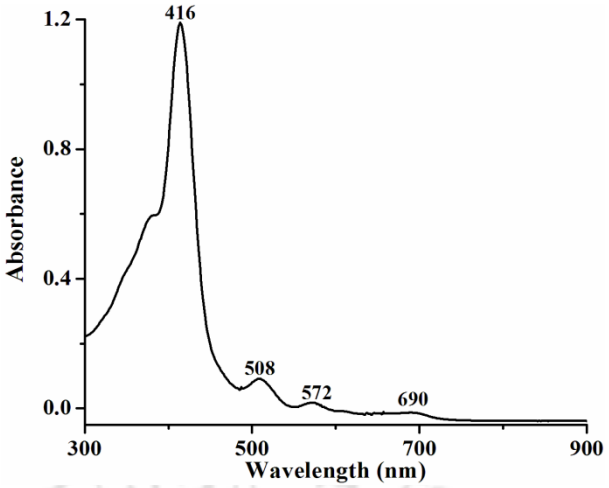

Figure A4.27. UV-visible spectrum of **[$Fe^{III}(TPP^{2-})(Cl)$]** in CH_2Cl_2 at room temperature (9 μM).

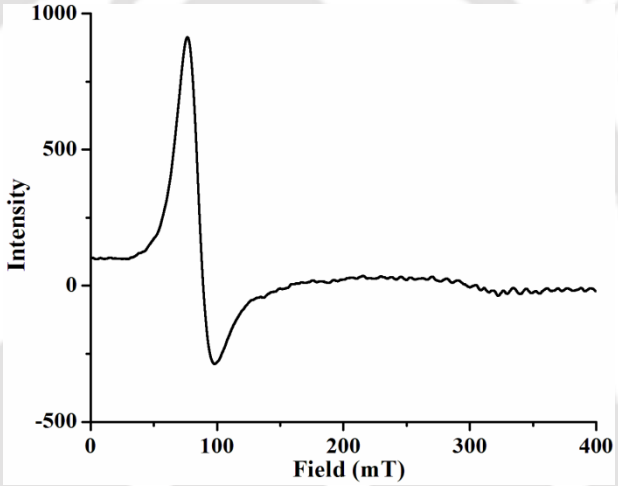

Figure A4.28. X-band EPR spectrum of **[$Fe^{III}(TPP^{2-})(Cl)$]** in CH_2Cl_2 at 77K.

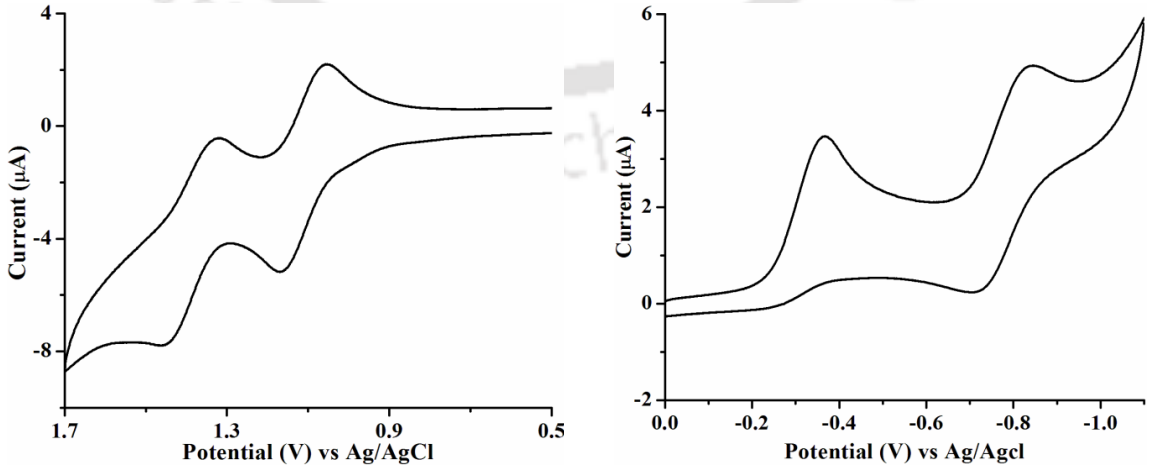

Figure A4.29. Cyclic voltammograms of **[$Fe^{III}(TPP^{2-})(Cl)$]** in CH_2Cl_2 *vs.* Ag/AgCl, 0.1 M TBAP, Scan rate 0.1 V/s.

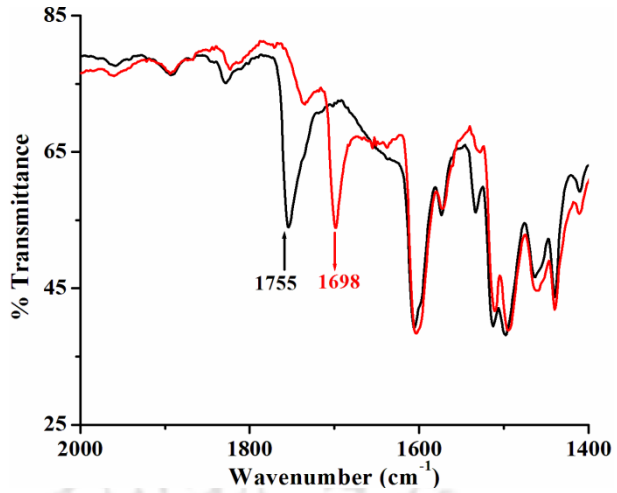

Figure A4.30. FT-IR spectra of the reaction of complex **14** (black), HBF_4 and **[(TPP)Fe^{III}(Cl)]** to give **[(TPP)Fe(NO)]** (red) in KBr.

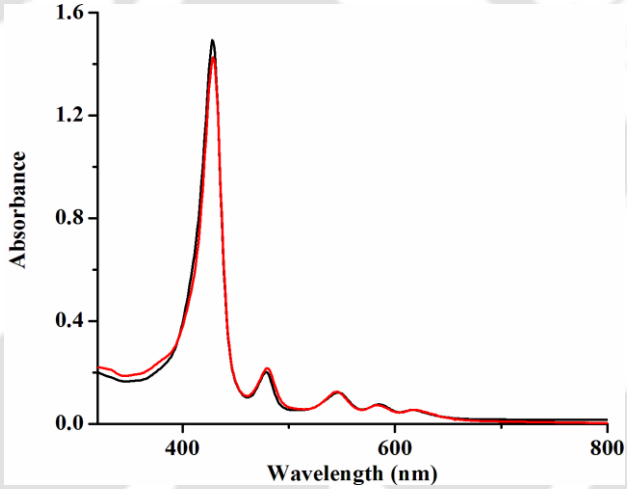

Figure A4.31. UV-visible spectra of complex **14** in CH_2Cl_2 (black) and the same solution after 12 h (red).

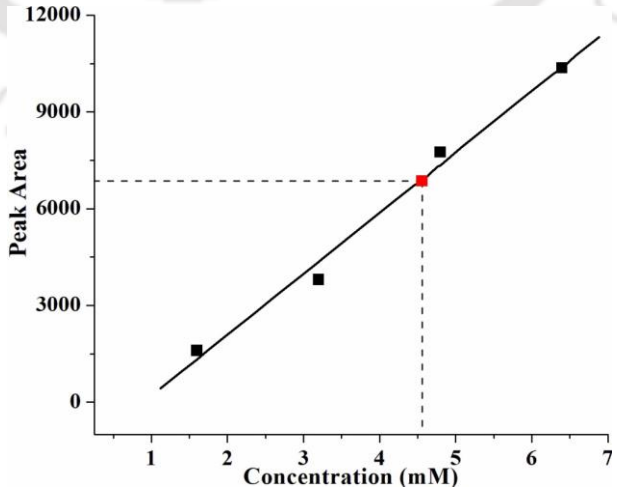

Figure A4.32. GC calibration curve for determination of amount of N_2O (red dot corresponds to the reaction mixture of complex **14** and HBF_4).

Table A4.1. Crystallographic data for complex **16**.

Formulae	$C_{48}H_{40}BF_4N_4O_6Mn$
Mol. wt.	910.59
Crystal system	Triclinic
Space group	P-1
Temperature /K	100(2)
Wavelength /Å	0.71073
a /Å	10.23(4)
b /Å	10.88(4)
c /Å	20.98(7)
α/°	89.93(4)
β/°	77.95(4)
γ/°	89.99(4)
V/ Å^3	2284(14)
Z	2
Density/Mgm^{-3}	1.324
Abs. Coeff. /mm^{-1}	0.357
Abs. correction	none
F(000)	940
Total no. of reflections	7977
Reflections, $I > 2\sigma(I)$	2385
Max. 2θ/°	24.999
Ranges (h, k, l)	$-11 \le h \le 12$ $-12 \le k \le 12$ $0 \le l \le 24$
Complete to 2θ (%)	0.991
Refinement method	Full-matrix least-squares on F^2
Goof (F^2)	0.710
R indices [$I > 2\sigma(I)$]	0.0978
R indices (all data)	0.2360

Table A4.2. Selected bond lengths (Å) of complex **16**.

Mn1-N1	2.032(8)
Mn1-N2	2.030(8)
Mn1-O3	2.272(8)
N1-C1	1.409(11)
C1-C2	1.439(12)
C2-C3	1.363(12)
C4-C5	1.387(11)
C5-C6	1.548(12)
C6-C7	1.402(12)
C9-O1	1.401(10)
O1-C10	1.442(12)

B1-F1	1.35(3)

Table A4.3. Selected bond angles (˚) of complex **16**.

N1-Mn1-N2	89.9(3)
N1-Mn1-O3	89.9(3)
Mn1-N1-C1	126.3(6)
N1-C1-C2	108.8(8)
C1-C2-C3	107.8(8)
C2-C3-C4	108.0(8)
C4-C5-C6	117.9(8)
C9-O1-C10	116.9(7)
F1-B1-F2	108(2)

List of Publications

(1) Nitric Oxide Dioxygenase Activity of a Nitrosyl Complex of Cobalt(II) Porphyrinate in the Presence of Hydrogen Peroxide *via* Putative Peroxynitrite Intermediate

Baishakhi Mondal, Soumen Saha, Dibyajyoti Borah, **Rakesh Mazumdar**, and Biplab Mondal*

Inorg. Chem. **2019**, *58*, 1234.

(2) Nitric Oxide Dioxygenase Activity of a Nitrosyl Complex of Mn(II)-Porphyrinate in Presence of Superoxide: Formation of a Mn(IV)-oxo Species through a Putative Peroxynitrite Intermediate

Baishakhi Mondal, Dibyajyoti Borah, **Rakesh Mazumdar**, and Biplab Mondal*

Inorg. Chem. **2019**, *58*, 14701.

(3) Can a Nitrosyl of a Mn(II)-Porphyrin Complex Release Nitroxyl/HNO?

Rakesh Mazumdar, Shankhadeep Saha, Bapan Samanta, and Biplab Mondal*

Inorg. Chem. **2021**, *60*, 18024.

(4) Reaction of a $\{Co(NO)\}^8$ complex with superoxide: Formation of a six coordinated $[Co^{II}(NO)(O_2^{\cdot-})]$ species followed by peroxynitrite intermediate

Rakesh Mazumdar, Baishakhi Mondal, Shankhadeep Saha, Bapan Samanta, and Biplab Mondal*

J. Inorg. Biochem. **2022**, *228*, 111698. (*Invited Article*)

(5) Reaction of a non-heme iron-nitrosyl with dioxygen: Self-killing through NOD-like activity

Riya Ghosh, **Rakesh Mazumdar**, Bapan Samanta, Shankhadeep Saha, and Biplab Mondal*

(*Under Revision*)

(6) Reaction of a Nitrosyl Complex of Mn(II)-porphyrinate with Superoxide: NOD Activity is More Favorable Over SOD Activity

Rakesh Mazumdar, Shankhadeep Saha, Bapan Samanta, Riya Ghosh, Sayani Maity and Biplab Mondal*

(*Communicated*)